Universidad de Salamanca

Departamento de Física, Ingeniería y Radiología Médica

Tesis Doctoral

Quantum wires in one dimension: disorder, electronic transport and dissipation

Alberto Rodríguez González

Dirigida por el
Dr. José María Cerveró Santiago

Memoria que presenta Alberto Rodríguez González, en el departamento de Física, Ingeniería y Radiología Médica de la Facultad de Ciencias para optar al Grado de Doctor en Físicas

Universidad de Salamanca, Julio 2005

A mi familia

Agradecimientos

En primer lugar vaya mi más sincero agradecimiento para el Dr. Jose María Cerveró, por su sabia dirección a largo de estos casi cinco años. Gran parte de mi interés por la investigación se debe a su persona, ya desde que era alumno suyo durante la carrera, hace algún tiempo. La relación con él durante este período no ha hecho más que alimentar ese interés. Sin su consejo y guía esto no hubiera sido posible.

No quiero olvidarme de Pilar García y el resto del grupo de Física Matemática No Lineal, siempre dispuestos a echar una mano.

Una persona que merece especial mención es el Dr. Enrique Diez, que me ha prestado ayuda desinteresada siempre que la he requerido y me ha dado sabios consejos. No me cabe la más mínima duda de que este trabajo no sería lo que es si no le hubiese conocido. Por todo esto creo que siempre estaré en deuda con él. Gracias también al Dr. Francisco Domínguez-Adame por su interés y su sincera disposición. Fue en parte gracias a Enrique y a Francisco que caí en los *"International workshop on disordered systems"* en los que tanto he aprendido y a tanta gente interesante he conocido.

Gracias a mi familia —a los que nunca olvido— por dejarme decidir libremente mi camino y procurarme lo necesario en todos los aspectos de la vida. A Olga le guardo un sitio especial, por saber entenderme y animarme en los momentos difíciles, que siempre los hay.

Al final de mi tesis me doy cuenta de la cantidad de personas con las que estoy en deuda de una u otra manera. A todos ellos, gracias de todo corazón.

Salamanca, julio 2005

"The principles of physics, as far as I can see, do not speak against the possibility of maneuvering things atom by atom. It is not an attempt to violate any laws; it is something, in principle, that can be done..."

Richard P. Feynman[†]

Introduction

The dreamt idea of being able to make and control systems at the atomic scale has fascinated scientists since the middle of the past century. Nowadays, the wish to carry on the race of miniaturization of the electronic devices along with the development and improvement of different techniques for seeing and altering the microscopic nature of matter, have made it possible to manufacture semiconductor devices for which one can choose at will their electrical, optical or magnetic properties, and whose reduced dimensions can include only a few tens of atoms. This technology is now a part of our Everyday Life, appearing in different systems ranging from semiconductor lasers to memory chips and microprocessors of computers, cellular phones and other digital appliances.

Semiconductor heterostructures can be designed to change the dimensionality of the confinement of the carriers [95] (two-dimensional electron gas, quantum wires (1-D), quantum dots (0-D)) and this quality has been used to observe different physical phenomena such as the Quantum Hall Effect or the electronic localization in disordered potentials. Other structures in Nature can also exhibit features of low-dimensional systems such as certain configurations of carbon nanotubes [187] or pieces of DNA [156], whose main electronic properties can be understood by describing the system in terms of a 1-D potential.

[†]Excerpt from the talk *"There's plenty of room at the bottom"* that Richard Feynman gave on December 29th 1959 at the annual meeting of the American Physical Society at Caltech.

The study of the physics underlying these low-dimensional systems requires of a proper theoretical approach different from the one used at the macroscopic scale, since at the former level matter exhibits a behaviour completely determined by quantum mechanical rules. In particular a detailed characterization of the electronic properties of these systems is essential not only for the development of practical applications but also to look into the principles of physics which are revealed at this scale. For this characterization one important element to be considered is the presence of disorder in the structures: roughness of interfaces in the semiconductor layers, dislocations, vacancies and impurities in the lattices or substitutional and structural disorder in the system. In low-dimensional structures, disorder plays a key role in the transport processes and it can strongly alter the properties of the system, giving rise to phenomena such as electronic localization and other particular features which are specially noticeable at this scale and in the low temperature regime. The main aim of this work is to contribute to the understanding of the electronic properties of one-dimensional structures and more specifically to analyse the effects of the presence of disorder. Then, since disorder is a key ingredient of our recipe, let us discuss some basic concepts about the theory of disordered systems.

1.1 Diving in the physics of disordered systems

1.1.1 What do you mean by 'disordered'?

In solid state physics the notion of order has always been tied to periodic structures and translational symmetry. This definition establishes a well-defined border in the classification of matter between crystalline materials, exhibiting translational invariance and several rotational symmetries, and amorphous materials. Hence, periodicity is regarded as a paradigm of order and thus other aperiodic arrangements could be labelled as *disordered* configurations. However, this choice is not useful since it is possible to differentiate well-defined groups of aperiodic sequences, each one characterized by its own properties [137]. One can roughly speak of:

- Incommensurate potentials: those formed from two or more interpenetrated periodic chains whose periods are incommensurate, that is, their ratio cannot be expressed as a ratio of integer numbers.

- Sequential arrangements: those aperiodic sequences which are built following a set of well-defined substitutional rules, like the Fibonacci or Thue-Morse series.

- Other arrangements that do not obey the previous patterns.

Within the context of this work, the disordered sequences will be the members of the latter group. And two different types of elements must be distinguished, namely uncorrelated and correlated disordered sequences. The first one obeys a completely random generating process while in the correlated case the generation of the nth element of the sequence is affected by the values previously assigned. Depending on the range of this influence one can speak of long-range or short-range correlated sequences. Hence, from our point of view, correlations must be defined in a strictly statistical sense from the sequence.

The construction of a one-dimensional disordered array of atomic potentials requires the following elements:

1. Set of configurational variables: the physical parameters of the potentials (atomic species, interatomic distances, concentrations, ...) along with the distributions that such variables must obey.

2. Disordered sequence: a disordered sequence must be generated according to the number of variables and their distributions.

3. Physical mapping: a one-to-one correspondence between the elements of the disordered sequence and the physical variables of the configurational set.

Depending on the parameters constituting the configurational set one can differentiate between two main types of disorder. If one chooses different atomic species with a certain distribution as configurational parameters but the interatomic distances are fixed to form a regular lattice, then the system is said to have substitutional disorder, also known as alloy-type disorder. On the contrary, if the interatomic distances are the configurational parameters to be mapped onto the disordered sequence while only one atomic species is allowed, then we have structural or topological disorder.

Let us remark that we say that the one-dimensional disordered potential exhibits correlations only when the distributions of the configurational variables of the system give rise to disordered sequences possessing correlations in a statistical sense. To clarify this concept let us consider a simple case in which one builds a disordered binary system including two atomic species, namely A and B, with equal concentrations and each species being followed by a characteristic distance d_A and d_B respectively. Then a disordered sequence for two variables with equal concentrations must be generated. Since no further requirements concerning the distributions of the different species have been imposed, the generation of the disordered sequence will be completely random, and therefore we say that such a disordered system does not possess correlations, that is, it is completely random. Notice that A, B and d_A, d_B could take

any values, they even can be chosen to satisfy strange relations or to ensure certain properties of the system, but in all cases the disordered sequence will be random, and then from our point of view the system does not exhibit correlations. This is of course a personal criterion but we understand that helps to avoid confusions.

1.1.2 Effects of disorder: Localization

In a periodic structure all the electronic states have the same probability of finding themselves in any primitive cell of the crystal, as it follows from the Bloch theorem. These states are completely extended over the system. Will the properties of the system and the nature of the eigenstates change in the presence of disorder? An approach to the problem of disorder was originally made in one-dimensional systems (see reference [135] for a collection of the first works on one-dimensional disordered systems). And it was Anderson in 1958 who described one of the most important physical consequences of disorder: localization [9]. Anderson studied the electronic diffusion in a three-dimensional tight-binding model in which the energies of the different sites are randomly assigned from a given interval according to a constant probability distribution. He showed that above a critical degree of disorder, which he quantifies as the width of the site-energy distribution, diffusion in the system is suppressed due to the spatial localization of all the electronic eigenstates. After the work of Anderson localization was regarded as one of the main effects stemming from the absence of periodicity in the systems. Localization of eigenstates implies that their probability density does not vanish only in a limited spatial region. Moreover if the envelope of the state decreases exponentially from a given point inside the localization region, the state is said to be exponentially localized. The **localization length** is a measure of the spatial extension of the localized state. Localization is tightly tied to electronic transport and it is a fundamental concept to understand the existence of metals and insulators and in particular to explain the **metal-insulator transition** (MIT) of matter. Let us suppose that the Fermi energy (E_F) of a certain material at zero temperature lies in a region of the spectrum populated by localized states. In this situation since the conducting properties of the system are mainly determined by the states around E_F, the material behaves as an insulator because the electronic states around the Fermi level are not able to move throughout the system and thus they will not carry any current. On the contrary if the eigenstates near E_F are extended, the material will exhibit good conducting properties because these states contribute actively to the transport through the system. Localization is the result of coherent interference phenomena and that means that its significance goes beyond the field of condensed matter and it can be observe for example studying the propagation of waves in classical systems as

well as in other contexts. Localization in quantum random systems can be connected to classical analogues [183, 114], in particular to chaotic systems of oscillators where quantum localization can be understood in terms of energetic stability of phase-space orbits of the classical system [177].

Anderson proved for his model (the Anderson model) that the system in 3-D registers a MIT with the strength of the disorder. It was also subsequently proved that the Anderson model in 2-D and 1-D does not exhibit such transition because all the electronic states are exponentially localized whatever the magnitude of the disorder is [1, 11, 155, 55]. These results were completely understood and explained by the Scaling theory of localization [1, 11], which we shall briefly describe later on. Scaling theory was intended to derive the different asymptotic regimes of the system, namely the ohmic and the insulating regime, analysing the disorder on a microscopic scale. According to this theory a MIT is only possible in 3-D structures and it is absent in 2-D and 1-D systems, for which all states must be localized in the presence of disorder. By the eighties, Scaling theory seemed to close the problem of localization and its relation with the dimensionality of the system. However, in the nineties, several experimental works on two-dimensional electron and hole systems, directly related with the Quantum Hall Effect, were reported in which a MIT was observed as a function of the carrier density or as a result of an applied magnetic field [123, 168, 189]. These observations were not compatible with the Scaling theory and they meant a reopening of the localization and the MIT problem. A similar process (perhaps even more dramatic) has happened in 1-D systems, as we shall see in the following sections.

Localization in 1-D

After Anderson, many works have concluded that localization also appears in different disordered one-dimensional systems.

In 1961 Mott and Twose showed for a particular 1-D model, consisting of square barriers of the same height placed at arbitrary distances from one another obeying a continuous distribution, that all electronic states are exponentially localized [148] (confirmed by Mott in 1967 [147]). They conjectured that perhaps the same thing occurs for other 1-D models, however it can be read in their work: *"we have not been able to extend the proof to a more general case"*. In 1963, Borland was led to the same conclusion for a 1-D chain composed of equal potentials of finite range and arbitrary shape separated by zones of zero potential assigned randomly according to a continuous distribution [27]. It was later specified by Tong (1970) than for the Borland model extended states could exist for any structural disorder if the individual potential unit exhibits resonances of the transmission [182]. A study on localization

in different models of one-dimensional random potentials can be found in a review by Ishii [109].

Only for particular models and for certain types of disorder it has been analytically proved that all eigenstates are exponentially localized in one dimension. However, probably because localization has been consider as a central tenet of the theory of disordered systems and also due to a naive extension of the properties of the 1-D Anderson model to other potentials, one can frequently find in the literature (even nowadays!) assertions like: "it has been proved that in one-dimensional disordered random systems all sates are localized", which must be interpreted quite carefully.

Correlated disorder on stage

It was then believed for a long time that one-dimensional disordered systems could not exhibit complex features like a metal-insulator transition. However further research has shown that a large variety of different situations can occur in 1-D. For example, deterministic quasi-periodic potentials were considered that can generate localized or extended electronic states depending on their parameters [19, 162, 90].

On the other hand at the beginning of the nineties the works by Flores [81] and Dunlap and co-workers [73] introduced different 1-D models in which the disorder showed short-range correlations, a feature absent from the original Anderson model. The short-range correlations were able to include in the spectrum of the system isolated extended states, in particular the **random-dimer model** (RDM) proposed by Dunlap and co-workers was used to try to explain the anomalous high conductivity observed in certain organic polymers that should behave as insulators [154]. Since then, the RDM has been extensively treated in the literature both from a theoretical viewpoint [29, 83, 161, 160, 111, 107, 167, 87] and also with a view to make practical implementations in semiconductors superlattices [64, 71, 65]. And other models of one-dimensional disordered systems with short-range correlations have appeared: the diluted Anderson model [104, 131, 130, 50], symmetrical impurities in a pure chain [108, 188], short-range correlations with classical analogues [110, 121], and more [77, 103, 68, 178, 190]. In all models considered the effect of short-range correlations is to include in the spectrum of the disordered chain isolated extended states that constitute a set of null measure. In 1999 the first experimental evidence that short-range correlations delocalize the electronic states at certain energies and thus improve the transport properties of the system, was observed in semiconductor superlattices [18].

The role of long-range correlations has also been analysed. Moura and Lyra considered a 1-D tight-binding disordered model with long-range correlations in the se-

quence of site-energies [46, 47]. They observed numerically the emergence of a continuum of extended states and mobility edges for the carriers, marking the transition between phases of localized states and extended states. An important contribution to the understanding of the effect of long-range correlations was made by Izrailev and Krokhin who established an analytical relation between localization length and potential pair correlators and showed how long-range correlations lead to the appearance of mobility edges in 1-D [112]. However their results are only valid in the approximation of weak disorder and to second-order perturbation theory. Tessieri has extended the perturbative approach to fourth-order to show that in fact the apparently extended states are still exponentially localized but on much larger scale than the states of the localized phase [176]. Upon crossing the 'mobility edges' the inverse of the localization length changes from a quadratic to a quartic dependence on the disorder strength, and for weak disorder it means that the increase of the spatial extension of the electrons can be huge. Therefore qualitatively this change can be regarded as a MIT. Similar conclusions have also been reported for other disordered models with long-range correlations [159, 45, 170]. The long-range correlation effects predicted have been experimentally confirmed in microwave transmission through single-mode waveguides with a linear array of long-range correlated scatterers [125, 124].

Therefore correlations of the random potentials can deeply affect the structure of electronic states and endow 1-D disordered models with far richer transport properties than it was previously thought.

...and more

Nowadays, the significance of the appearance of phases of extended states in one-dimensional disordered systems keeps growing and interesting dynamical phenomena such as Bloch oscillations have been theoretically described in disordered systems [69, 48]. On the other hand the influence of correlated disorder on the transport properties is also becoming apparent in 2-D structures [105, 99]. It has recently been shown that delocalization in 1-D systems with completely random disorder can also take place due to the existence of long-range interactions [157, 138, 49].

Almost half a century after the work of Anderson, the problem of localization can be understood in different ways (see for example reference [70] for a quite pedagogical approach to Anderson localization) and the corresponding field of research is still becoming larger and larger.

1.1.3 Conductance in 1-D systems

The study of the quantum-mechanical probability of transmission of 1-D systems is essential since it is directly related to the conductance of the system, which is a measurable quantity, hence establishing a bridge between theory and experiment. A fundamental approach to the characterization of conductance in one-dimensional systems was first made by Landauer in 1957 [126] and also in subsequent works in 1970 [127] and 1988 [128]. Landauer concluded that the conductance of a one-dimensional guide in which the carriers are scattered by static obstacles is given by

$$\mathcal{G} = \frac{e^2}{2\pi\hbar}\frac{T}{R},\tag{1.1}$$

where T and $R = 1 - T$ are the probabilities of transmission and reflection of the whole structure respectively. Moreover, taking into account multiple scattering processes, Landauer established that the resistance of the system grows exponentially with the number of obstacles. He also thought that such a behaviour could be related to the exponential decrease of the wave functions in disordered systems. By that time these results were not considered to be fully correct mainly because they were not based on the widely accepted linear response theory. It was Economou and Soukoulis [75] and also Langreth and Abrahams [129] who faced the conductance problem using the linear response theory. Both works lead to similar results: that conductance strongly depends on the nature of the leads. On the one hand if the leads are considered to be perfect one-dimensional conductors, then conductance should obey

$$\mathcal{G} = \frac{e^2}{2\pi\hbar}T.\tag{1.2}$$

On the other hand if the leads are considered to behave classically as a current source, then Landauer expression would be obtained. The authors conclude that both situations are idealizations and that the connection with real experimental situations is not clear. Later, Engquist and Anderson tackled the question in the context of real experimental situations [76]. In particular they point out that together with the leads supplying the current, the voltage difference in the sample is usually measured via two additional contacts, what is known as a four-probe measurement. For this experimental set-up they obtained a general expression for the conductance of the sample which reduces to the Landauer formula in the case of zero temperature. Then, the different physical situations in which the Landauer formula (four-probe measurement) and the Economou and Soukoulis formula (1.2) (two-probe measurement) hold were established. For two and three-dimensional systems, the conductance formalism is similar to the one described in 1-D. The expressions show a significant resemblance

with the above equations and the role played by the transmission probability in 1-D is performed by the scattering matrix connecting the different transmission channels in a system with a higher dimensionality. For example, the two-probe conductance for a quasi-one-dimensional system including an arbitrary number of transmission channels N, reads —as stated by Fisher and Lee [79]—

$$\mathcal{G} = \frac{e^2}{2\pi\hbar}\text{Tr}\left(\mathbf{t}\mathbf{t}^\dagger\right), \tag{1.3}$$

where $\mathbf{t}$ is the $N \times N$ transmission matrix connecting the incident flux in the various channels on one side of the disordered region to the outgoing flux on the other side. Subsequently, Büttiker generalized the expressions for the conductance in the case of multichannel and multiprobe measurements [31, 34]. A nice discussion on the historical development of the conductance formalism and the physical meaning and implications of the different formulae, is given in reference [174].

The characteristic coefficient e^2/h appearing in the above definitions is the quantum of conductance and equivalently its inverse is the quantum of resistance $h/e^2 = 25\,812.8\ \Omega$. Quantization of conductance and resistance was revealed in the measure of the Integer Quantum Hall Effect [184], where the value of the Hall resistance obeys $R_H = \frac{1}{j}h/e^2$ for integer j, thus producing the plateau structure. The quantized Hall resistance is known to an extremely high accuracy and it is one of the most accurate ways to determine the atomic fine-structure constant. Quantization of conductance has also been experimentally observed in the ballistic regime of electronic transport through low-dimensional systems such as quantum point contacts [185], and the significance of the elemental unit e^2/h has been also established in the universal conductance fluctuations observed in mesoscopic systems [133, 98].

1.1.4 Universality and Scaling

Landauer described that disorder should cause an exponential increase of the resistance of the system with its length, which has been rigorously proved later for certain disordered models [117, 120]. Then he was somehow a precursor of the scaling theory, whose origin is also directly related to quantum phase transitions and critical phenomena [172]. Initially, scaling theory —as proposed by Abrahams, Anderson, Liciardello and Ramakrishnan— tried to understand localization by considering the behaviour of an 'average' or 'scaling' dimensionless conductance g as a function of the system size or of other scale variables [1]. The theory was intended to derive the different asymptotic regimes for g, the ohmic metal regime on the one hand and the insulator regime in which g must decrease exponentially with the system size on the other hand, from the value g_0 of the conductance on a mean free path scale, which is

a measure of the microscopic disorder. And it gave a successful explanation of why a MIT is possible in 3-D disordered systems while it is absent in 2-D and 1-D structures (see reference [132] by Lee and Ramakrishnan for a thorough description of scaling theory and its consequences). However it was later remarked by Anderson and co-workers that since resistance of a 1-D sample varies exponentially with its length, its value can fluctuate wildly and its distribution function becomes increasingly broad as the length increases. Consequently the average resistance can be very different from the typical resistance and thus the choice of a scaling variable requires some care. They concluded that the variable $-\log(T)$ is well-behaved as the length of the system goes to infinity [11, 10]. Therefore scaling must be understood in a wider sense, since a complete scaling description must necessarily include the behaviour of the distributions of the proper quantities. Let us discuss in some detail the aspects of scaling theory that are more relevant for our work.

Universality and scaling stem from the insensitivity of macroscopic laws to microscopic details. In the context of disordered systems, universality means that probability distributions for various (macroscopic) transport-related quantities are largely universal an do not depend on the details specifying the microscopic Hamiltonian. Consider, for instance, the dimensionless resistance $\rho \equiv g^{-1}$ of a 1-D disordered system. The value of ρ will depend upon the particular realization of the disorder. Then it is natural to define the probability distribution for the resistance $P_L(\rho)$ of different realizations of the system with a given length. For large L one can expect that the microscopic details will become irrelevant and the distribution will approach some universal shape. Then, only a few parameters will be needed to specify the distribution completely. Single-parameter scaling in these terms means that the large-scale distribution is specified by just one parameter Δ_L which obeys a scaling law,

$$\frac{\mathrm{d}\log\Delta_L}{\mathrm{d}\log L} = \beta(\Delta_L). \tag{1.4}$$

Let us try to outline the general situation concerning the distribution functions of the proper quantities for a 1-D disordered system. In the most general case, it seems that as $L \to \infty$ and in the strong localization regime, when L is much greater that the localization length (ξ), the distribution of the variable $u_L \equiv -\log T_L$ approaches a Gaussian, which is determined by two parameters: the mean value $\langle u_L \rangle$ and the variance $\mathrm{var}(u_L)$. However if one assumes the phase randomization hypothesis, which was initially proposed by Anderson and co-workers [11], scaling can be different. The phase randomization hypothesis assumes that phases of individual scatterers (i.e. the phases of the individual complex scattering amplitudes) can be considered to vary randomly on a length scale l_{ph}, such that $l_{ph} \ll \xi$, and hence the cumulative phase
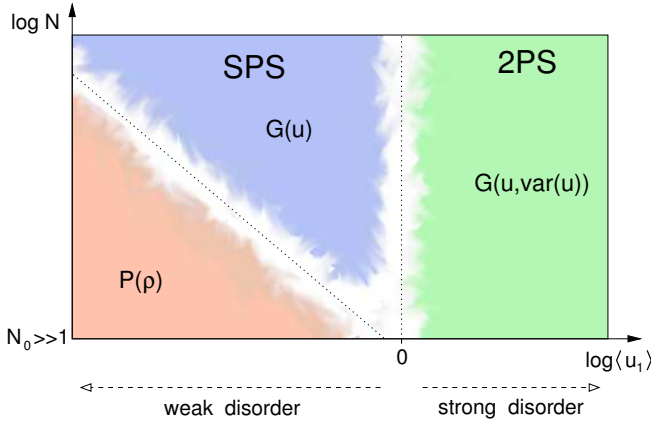
Figure 1.1. Universality diagram for 1-D disordered systems within the phase randomization hypothesis. N means the length of the system and $u = -\log T$, G means a Gaussian distribution and $P(\rho)$ is the exponential distribution for the dimensionless resistance. Different colours highlight the ranges of validity of the different scaling regimes.

appearing in the composite transmission of the system can be considered to spread uniformly in the interval $[0, 2\pi]$. In this case in the limit $L \to \infty$ and in the strong localization regime ($L \gg \xi$) a Gaussian distribution for u_N is recovered, for which the mean value satisfies $\langle u_N \rangle = N\langle u_1 \rangle$, where N is the number of scatterers or sites of the system and $\langle u_1 \rangle$ means the average of the quantity $-\log T_1$ over all possible configurations of an individual scatterer. However in the weak disorder approximation, that is $\langle u_1 \rangle \ll 1$, the variance of the Gaussian distribution turns out to be determined by the mean value according to $\text{var}(u_N) = 2\langle u_N \rangle$. Therefore single parameter scaling (SPS) holds[1]. On the contrary for strong disorder ($\langle u_1 \rangle \gg 1$) the variance cannot be written in terms of the mean only and thus two parameter scaling (2PS) is obtained. In the weak disorder approximation and within the weak localization regime ($L \ll \xi$) a universal exponential distribution for the dimensionless resistance ρ is also found, that reads $P_L(\rho) = \frac{\xi}{2L} \exp(-\rho \frac{\xi}{2L})$. Notice that the concept of weak or strong disorder is defined from a microscopic criterion and it must not be confused with the regime of strong or weak localization that is decided from the comparison of the length of the system and the localization length. The physical situation within the phase randomization hypothesis is summarized in the diagram of figure 1.1 and the details are very well described in the works of Shapiro and co-workers [169, 37], Mello [141] and Flores and co-workers [80].

Scaling theory is still evolving nowadays. In fact it has been recently questioned whether the phase randomization hypothesis is a necessary condition to have SPS [62]. And it seems that the emergence of SPS is governed by a new length scale which is related to the integrated density of states [59, 60, 57] and also that different

---

[1]Alternatively it is also very common to define the universal Gaussian distribution using the variable $\lambda_L = -\frac{1}{2L} \log T_L$ instead of u_L. Therefore the SPS requirement is usually written as $\text{var}(\lambda_L) = \langle \lambda_L \rangle / L$. The variable λ_L is known as the Lyapunov exponent and it will be introduced in the following chapter.

SPS regimes can be found when correlations in the disorder are introduced [58].

1.1.5   Decoherence mechanisms: Delocalization

Decoherence mechanisms can be very relevant in disordered systems. Since localization is a coherent interference effect, the different phenomena introducing decoherence in the system —which are generally enhanced at non-zero temperature— such as inelastic scattering events, electron-electron or electron-phonon interaction, non-linear effects,… can give rise to the break of electronic localization in certain energetic regimes and thus improving the transport properties of disordered systems (see reference [142] for a description on decoherence measurements). The coherent transport regime, the mesoscopic regime, in which the system size is comparable to the coherence length of the carriers, is characterized by quantum interference patterns that can be altered by applying external fields, giving rise to the well-known universal conductance fluctuations [116]. Therefore decoherence also entails the lost of this universal regime in which conductors cannot be characterized by materials constants.

As described by Büttiker, the effect of inelastic scattering events inducing phase-randomization on barrier tunnelling can increase the off-resonant transmission [33]. Similar results on barrier tunnelling have been found as a consequence of non-linear effects [63]. It has also been shown that in the strong localization regime the conductance of a one-dimensional disordered system can be improved due to electron-electron interaction [186, 166], inelastic scattering events modelled by parametrized scatterers [140, 102] or complex extensions of the potential [173, 41], and also non-linear effects [67]. Additionally it has been recently described how delocalization can take place as a result of the decoherence induced by iterative measurements on the disordered system [93, 82]. The analysis and modelling of delocalization mechanisms is important to evaluate to which extent they can alter the transport properties of disordered systems.

1.2   Objectives and outline of the work

Once some basic concepts about one-dimensional disordered systems have been introduced and the present situation of the research in the field has been briefly described, let us shortly discuss the main purposes of this work.

Our fundamental premise to study the electronic properties of one-dimensional disordered systems is to consider non-interacting spinless carriers within the independent particle approximation. Also our approach focuses on the characterization of the static transport properties of these structures. Within this framework, probably the

most important aim of this work is to generalize, extend and compile a set of tools that can be used for all one-dimensional systems in order to analyse their electronic properties (distribution of states, nature of states, ...). In particular, we derive an ensemble of universal functional equations which characterize the thermodynamic limit of all one-dimensional models (within the approximations made above) and that are useful to obtain relevant quantities of the system such as density of states or localization length in that limit. Therefore a great part of our efforts are aimed at contributing to the growth of a general methodology that can be applied to all potential models in one-dimension. Our approach is analytical up to a point from which numerical techniques are necessary to obtain the desired solutions. These methods are used to perform a systematic study of different models of quantum wires in one dimension. The effects that disorder induces upon the distribution of states is studied in detail and the existence or not of extended states in the spectrum is thoroughly examined. Correlated disorder is also treated via a new model of short-range correlations whose influence on the transport properties of finite 1-D structures is revealed. Finally, imaginary potentials are introduced in the linear arrays to include dissipative processes in the wire.

The contents of the work are divided in different chapters according to the following scheme:

- Chapter 2 is devoted to the description and development of the theory underlying the different methods used to characterize disordered 1-D systems.

- In chapter 3 the well-known delta model is used to build one-dimensional chains. The properties of these wires are studied in detail.

- In chapter 4 a new type of 1-D disordered system based on Pöschl-Teller-like potentials is built. The interesting features that compositions of these potentials exhibit are analysed.

- Chapter 5 comprises quantum wire models with imaginary potentials. Two different tasks are carried out: the building of $\mathcal{PT}$-symmetric periodic chains and the modelling of dissipative processes.

- Chapter 6 includes a summary of the concluding remarks and a final discussion.

Let us finally remark that some intricate calculations and extensive analysis of certain subjects have been included in several appendices at the end of the manuscript. It has been done so in order to make the reading as easy as possible. However the information contained in some of the appendices is essential for a full understanding of the work.

Theory and methodology

Unlike the case of ordered matter, for disordered systems there is a lack of a general theory describing in a compact form their physical properties. Nevertheless a large ensemble of different techniques exists that can be used to unravel some features of this kind of structures. The aim of this chapter is to build a general methodology that can be applied to all one-dimensional potential models. We give a detailed description of the tools used in this work to characterize several models of disordered wires, regarding mainly their electronic properties.

2.1 The canonical equation

We shall be considering one-dimensional atomic wires within the independent particle approximation. The electron-electron interaction is not considered and also the carriers are supposed to be spinless. Then, the Hamiltonian of the system only includes the potential of a linear array of different atomic units. From the solutions of the one-particle Schrödinger equation it is always possible to derive an expression with the following canonical form[1] [137, 161]

$$\Psi_{j+1} = J(\gamma_{j-1}, \gamma_j)\Psi_j - \frac{K(\gamma_j)}{K(\gamma_{j-1})}\Psi_{j-1}, \tag{2.1}$$

where Ψ_j means the amplitude of the electronic state at the jth site of the wire, γ_j denotes the parameters of the potential at the jth site (jth sector) and the functions

---

[1]The meaning of the coefficients appearing in the canonical equation depends on the particular Hamiltonian. For a tight-binding model they have a straightforward interpretation in terms of the on-site energies and the transfer integrals, thus the equation is usually written in the form $\alpha_j \Psi_j = t_{j,j+1}\Psi_{j+1} + t_{j,j-1}\Psi_{j-1}$. For other models that comparison may not be so clear, so we keep a more general expression.
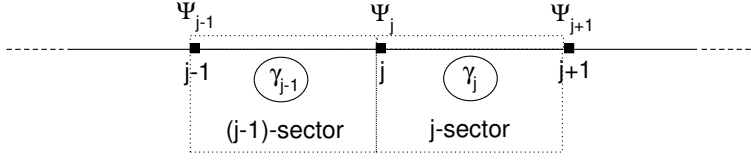
Figure 2.1. Sites and sectors of a linear chain

$J(\gamma_{j-1}, \gamma_j)$, $K(\gamma_j)$, which depend on the potential and the energy, rule the spreading of the state from one site to its neighbours, as shown in figure 2.1. The canonical equation can be systematically obtained for a given solvable Hamiltonian and it contains the same information as the Schrödinger equation. It is not hard to see that $J(\gamma_{j-1}, \gamma_j)$ and $K(\gamma_j)$ are real functions provided the potential is real, so that the state amplitudes can be considered to be real. Equation (2.1) determines also the behaviour of other elementary excitations inside 1-D structures, thus it appears in different physical contexts such as the study of vibrational states (phonons), electron-hole pairs (excitons), ...

Although the applicability of the canonical equation is not restricted by the ordering of the sequence in the wire, it is a key ingredient to study non-periodic arrangements of potentials, for which the Bloch theorem is not valid. For certain boundary conditions, one can numerically obtain the permitted levels and the form of the envelope of the wave functions inside the system using equation (2.1). Apart from being useful from a numerical viewpoint, the canonical form also provides some analytical results concerning the gaps of the system's spectrum. For this purpose, the equation must be written as a two-dimensional mapping, originally proposed in reference [110], that permits establishing analogies between the quantum problem and classical dynamical systems [114]. The matrix form of (2.1) with the definitions $x_{j+1} = \Psi_{j+1}$, $y_{j+1} = \Psi_j$, reads

$$\begin{pmatrix} x_{j+1} \\ y_{j+1} \end{pmatrix} = \begin{pmatrix} J(\gamma_{j-1}, \gamma_j) & -\frac{K(\gamma_j)}{K(\gamma_{j-1})} \\ 1 & 0 \end{pmatrix} \begin{pmatrix} x_j \\ y_j \end{pmatrix}, \qquad (2.2)$$

which in polar coordinates $x_j = \rho_j \cos\theta_j$, $y_j = \rho_j \sin\theta_j$, leads to the following transmission relations for the phase and the moduli:

$$\theta_{j+1} \equiv \mathcal{T}(\theta_j; \gamma_{j-1}, \gamma_j) = \arctan\left\{ \left(J(\gamma_{j-1}, \gamma_j) - \frac{K(\gamma_j)}{K(\gamma_{j-1})} \tan\theta_j \right)^{-1} \right\}, \qquad (2.3)$$

$$\left(\frac{\rho_{j+1}}{\rho_j} \right)^2 \equiv \mathcal{F}(\theta_j; \gamma_{j-1}, \gamma_j) = \cos^2\theta_j + \left(J(\gamma_{j-1}, \gamma_j) \cos\theta_j - \frac{K(\gamma_j)}{K(\gamma_{j-1})} \sin\theta_j \right)^2. \qquad (2.4)$$

Now let us impose hard-wall boundary conditions in our wire composed of N atoms. That means $\Psi_0 = \Psi_{N+1} = 0$. Using the mapping it is clear that the initial point is $\{x_1, y_1\} = \{\Psi_1, 0\}$ placed on the x axis. Thus for an eigenenergy, after all the

steps the final point must be of the form $\{x_{N+1}, y_{N+1}\} = \{0, \Psi_N\}$ lying on the y axis. That means the whole transformation acts rotating the initial point. Therefore the permitted levels must be clearly contained in the ranges of energy for which the sequence of mappings generates a rotating trajectory (generally open) around the origin, which is the only fixed point independently of the parameters of the mapping. This behaviour guarantees that after an arbitrary number of steps the final boundary condition could still be satisfied. However if all mappings have real eigenvalues the behaviour described is not possible (see for example reference [175]). And it follows that permitted levels cannot lie inside the energy ranges satisfying

$$J^2(\gamma_{j-1}, \gamma_j) > 4\frac{K(\gamma_j)}{K(\gamma_{j-1})}, \qquad \forall\, \gamma_j,\, \gamma_{j-1}. \tag{2.5}$$

Note that this conclusion does not depend upon the sequence of the chain, thus it holds for ordered and disordered structures.

In the following sections it will become clear that obtaining the canonical equation is essential when treating one-dimensional disordered systems.

2.2 Continuous transmission matrix formalism

The time-independent scattering process in one dimension can be described using the well-known continuous transfer matrix method,

$$\begin{pmatrix} A_R \\ B_R \end{pmatrix} = \begin{pmatrix} M_{11} & M_{12} \\ M_{21} & M_{22} \end{pmatrix} \begin{pmatrix} A_L \\ B_L \end{pmatrix} \equiv \mathbf{M} \begin{pmatrix} A_L \\ B_L \end{pmatrix}, \tag{2.6}$$

where A_L, $B_L(A_R,\ B_R)$, mean the amplitudes of the asymptotic travelling plane waves e^{ikx}, e^{-ikx}, at the left (right) side of the potential. The peculiarities of the transmission matrix $\mathbf{M}$ and its elements depend on the nature of the potential. A detailed analysis on this subject can be found in appendix A. As a summary let us say that for real potentials $\mathbf{M}$ belongs to the group $\mathcal{SU}(1,1)$ and that the property $\det \mathbf{M} = 1$ holds for all kind of potentials whether they are real or complex.

The transmission and reflection scattering amplitudes read

$$t = \frac{1}{M_{22}}, \quad r^L = -\frac{M_{21}}{M_{22}}, \quad r^R = \frac{M_{12}}{M_{22}}, \tag{2.7}$$

where the superscripts L, R, stand for left and right incidence. The insensitivity of the transmission amplitude to the incidence direction is a universal property. In general the reflection amplitudes will differ, although $|r^L| = |r^R|$ for real potentials and complex ones with parity symmetry [7].

Obtaining the transmission matrix is specially easy for discontinuous short-range potentials such as deltas or square well/barriers, for which the asymptotic limit is not necessary to satisfy (2.6). In these cases the effect of a composition of N different potential units can be considered through the product of their transmission matrices,

$$\mathbb{M} = \mathbf{M}_N \mathbf{M}_{N-1} \cdots \mathbf{M}_2 \mathbf{M}_1, \tag{2.8}$$

therefore obtaining analytically or numerically the exact scattering probabilities of the whole structure. This formalism can also be used to obtain the bound states from the poles of the complex transmission amplitude. An intuitive and general interpretation of the composition procedure can be given in the following form. Let us consider two finite range potentials $V_1(x)$, $V_2(x)$, characterized by the amplitudes t_1, r_1^L, r_1^R, t_2, r_2^L, r_2^R, and joined at a certain point. Then, the scattering amplitudes of the composite potential can be obtained by considering the coherent sum of all the multiple reflection processes that might occur at the connection region [17],

$$t \equiv t_1 \left\{ \sum_{n=0}^{\infty} (r_2^L r_1^R)^n \right\} t_2 = \frac{t_1 t_2}{1 - r_2^L r_1^R}, \tag{2.9a}$$

$$r^L \equiv r_1^L + t_1 r_2^L \left\{ \sum_{n=0}^{\infty} (r_2^L r_1^R)^n \right\} t_1 = r_1^L + \frac{r_2^L t_1^2}{1 - r_2^L r_1^R}, \tag{2.9b}$$

$$r^R \equiv r_2^R + t_2 r_1^R \left\{ \sum_{n=0}^{\infty} (r_2^L r_1^R)^n \right\} t_2 = r_2^R + \frac{r_1^R t_2^2}{1 - r_2^L r_1^R}. \tag{2.9c}$$

Replacing the scattering amplitudes with the elements of the corresponding transmission matrices $\mathbf{M}_1$, $\mathbf{M}_2$, one can trivially check that in fact the latter formulae are the equations of the matrix product $\mathbf{M}_2 \mathbf{M}_1$. Thus, the composition rules given by (2.9) are not restricted to the convergence interval of the series $\sum_{n=0}^{\infty} (r_2^L r_1^R)^n$. They provide an explicit relation of the global scattering amplitudes in terms of the individual former ones and can be easily used recurrently for numerical purposes.

In the case of continuous potentials the calculation of the transfer matrix is more complex. After solving the Schrödinger equation for positive energies, one has to take the limits $x \to \pm\infty$ to recover the free particle states and identify the matrix elements. Hence equation (2.6) is strictly satisfied only asymptotically. However depending on the decay of the potential one could neglect its effects outside a certain length range. If the asymptotic transmission matrix $\{\mathcal{M}_{ij}\}$ of the potential in figure 2.2 is known, then the matrix for the cut-off potential contained between the dashed lines is simply (see appendix A)

$$\mathbf{M}_{\text{cut}} = \begin{pmatrix} \mathcal{M}_{11}\, \mathrm{e}^{\mathrm{i}k(d_2+d_1)} & \mathcal{M}_{12}\, \mathrm{e}^{\mathrm{i}k(d_2-d_1)} \\ \mathcal{M}_{21}\, \mathrm{e}^{-\mathrm{i}k(d_2-d_1)} & \mathcal{M}_{22}\, \mathrm{e}^{-\mathrm{i}k(d_2+d_1)} \end{pmatrix}. \tag{2.10}$$
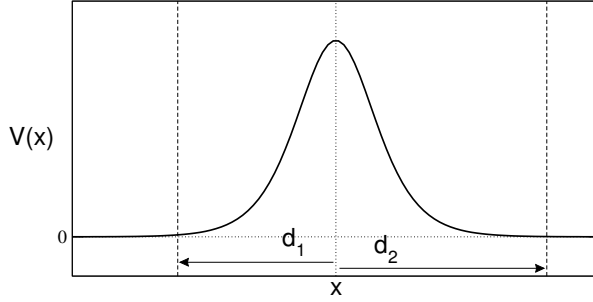
Figure 2.2. A continuous potential

The cut-off matrix is the same as the asymptotic one plus an extra phase term in the diagonal elements that accounts for the total distance $(d_1 + d_2)$ during which the particle feels the effect of the potential, and also an extra phase term in the off-diagonal elements measuring the asymmetry of the cut-off $(d_2 - d_1)$. Doing such approximation one gets matrices suitable to be composed in linear arrays.

Once the transmission matrix of the potential is known one can obtain the canonical equation applying to the electronic states in the one-dimensional composite chain. Let us consider $\mathbf{M}_j$ to be the continuous transmission matrix of the jth potential,

$$\begin{pmatrix} A_{j+1} \\ B_{j+1} \end{pmatrix} = \mathbf{M}_j \begin{pmatrix} A_j \\ B_j \end{pmatrix}, \tag{2.11}$$

where the coordinates of the electronic wave function in the different sectors of the chain are chosen to satisfy that the value of the state at all sites is simply given by the sum of the complex amplitudes of the travelling plane waves, that is $\Psi_j = A_j + B_j$ for all j. Then the canonical equation of the system can generally be written as (see appendix A)

$$\Psi_{j+1} = \left(\overline{S}_j + S_{j-1} \frac{K_j}{K_{j-1}} \right) \Psi_j - \frac{K_j}{K_{j-1}} \Psi_{j-1}, \tag{2.12}$$

where for a real potential

$$\overline{S}_j = \text{Re}\left[(\mathbf{M}_j)_{11} \right] + \text{Re}\left[(\mathbf{M}_j)_{12} \right], \tag{2.13a}$$

$$S_j = \text{Re}\left[(\mathbf{M}_j)_{11} \right] - \text{Re}\left[(\mathbf{M}_j)_{12} \right], \tag{2.13b}$$

$$K_j = \text{Im}\left[(\mathbf{M}_j)_{11} \right] - \text{Im}\left[(\mathbf{M}_j)_{12} \right]. \tag{2.13c}$$

Then, the canonical equation can be easily calculated from the continuous transmission matrix of the compositional potentials of the system.

2.3   Discrete transmission matrix formalism

The problem of a one-dimensional quantum wire can also be treated via a composition procedure of another type of transfer matrices, when one obtains a discretized version

of the Schrödinger equation. An analytical discretized form of this equation is given by the canonical expression (2.1), that can be written as

$$\begin{pmatrix} \Psi_{j+1} \\ \Psi_j \end{pmatrix} = \begin{pmatrix} J(\gamma_{j-1}, \gamma_j) & -\frac{K(\gamma_j)}{K(\gamma_{j-1})} \\ 1 & 0 \end{pmatrix} \begin{pmatrix} \Psi_j \\ \Psi_{j-1} \end{pmatrix} \equiv \mathbf{P}_j(\gamma_{j-1}, \gamma_j) \begin{pmatrix} \Psi_j \\ \Psi_{j-1} \end{pmatrix}. \tag{2.14}$$

The properties of the system can then be calculated from the product $\mathbf{P}_N \mathbf{P}_{N-1} \cdots \mathbf{P}_1$ imposing appropriate boundary conditions.

If the solutions of the differential equation are not known, one can always take a spatial discretization, translating the original equation

$$\psi''(x) = \left[V(x) - k^2 \right] \psi(x), \tag{2.15}$$

into

$$\psi_{n+1} = \left\{ \left[V_n - k^2 \right] (\Delta x)^2 + 2 \right\} \psi_n - \psi_{n-1}, \tag{2.16}$$

where we have defined $\psi_n \equiv \psi(n \cdot \Delta x)$, $V_n \equiv V(n \cdot \Delta x)$ and Δx being the spatial step. And the corresponding matrix representation is

$$\begin{pmatrix} \psi_{n+1} \\ \psi_n \end{pmatrix} = \begin{pmatrix} \left[V_n - k^2 \right] (\Delta x)^2 + 2 & -1 \\ 1 & 0 \end{pmatrix} \begin{pmatrix} \psi_n \\ \psi_{n-1} \end{pmatrix} \equiv \mathbf{Q}_n \begin{pmatrix} \psi_n \\ \psi_{n-1} \end{pmatrix}. \tag{2.17}$$

Then, the scattering probabilities of the system can be numerically obtained by constructing $\mathbb{Q} = \mathbf{Q}_n \mathbf{Q}_{n-1} \cdots \mathbf{Q}_1$, considering a large enough distance $n \cdot \Delta x$ so that the correct asymptotic form of the state $\psi(x) = e^{ikx} + r\, e^{-ikx}$ and $\psi(x) = t\, e^{ikx}$ can be imposed at the extremes. The transmission and reflection probabilities are then given by

$$T = \frac{4 \sin^2(k \cdot \Delta x)}{\left| \mathbb{Q}_{21} - \mathbb{Q}_{12} + \mathbb{Q}_{22} e^{ik \cdot \Delta x} - \mathbb{Q}_{11} e^{-ik \cdot \Delta x} \right|^2}, \tag{2.18}$$

$$R = \left| \frac{\mathbb{Q}_{11} - \mathbb{Q}_{22} + \mathbb{Q}_{12} e^{-ik \cdot \Delta x} - \mathbb{Q}_{21} e^{ik \cdot \Delta x}}{\mathbb{Q}_{21} - \mathbb{Q}_{12} + \mathbb{Q}_{22} e^{ik \cdot \Delta x} - \mathbb{Q}_{11} e^{-ik \cdot \Delta x}} \right|^2. \tag{2.19}$$

2.4 Characterizing electronic localization

The localized nature of the electronic states inside a disordered wire can be analyzed using different tools (see for example reference [122]). Let us see some reliable parameters which can be used as a probe of the localized or extended character of the carriers inside the system.

2.4.1 Lyapunov exponents

Lyapunov exponents emerge from random matrix theory [38], and they are used to characterize the asymptotic behaviour of systems determined by products of such matrices. They are a key element in chaotic dynamics [175] and play an important role in the study of disordered systems.

For a full understanding of the meaning of the Lyapunov exponents and their expressions it is mandatory to recall Oseledet's multiplicative ergodic theorem (MET) (a complete analysis can be found in reference [12]), which in its deterministic version and without full mathematical rigour[2] reads as follows. Let be $\{\mathbf{M}_n\}$ a sequence of $d \times d$ matrices and be $\mathbb{M}_N = \mathbf{M}_N \mathbf{M}_{N-1} \cdots \mathbf{M}_1$. Then the following matrix exists as a limit

$$\lim_{N\to\infty} \left(\mathbb{M}_N^t \mathbb{M}_N\right)^{\frac{1}{2N}} \equiv \Gamma \geqslant 0, \tag{2.20}$$

so that its eigenvalues can be written as $e^{\lambda_1} < e^{\lambda_2} < \cdots < e^{\lambda_d}$ and the corresponding eigenspaces $U_1, \ldots, U_d$. And for every vector $\mathbf{x}$ of this d-dimensional space the following quantity exists as a limit

$$\lambda(\mathbf{x}) \equiv \lim_{N\to\infty} \frac{1}{N} \log \|\mathbb{M}_N \mathbf{x}\|, \tag{2.21}$$

that verifies $\lambda(\mathbf{x}) = \max(\lambda_i, \ldots, \lambda_j)$ where $\{U_i, \ldots, U_j\}$ is the set of spaces in which $\mathbf{x}$ has a non-zero projection. The set $\{\lambda_i\}$ are the Lyapunov characteristic exponents (LCE) of the asymptotic product $\mathbb{M}_N$. Therefore this theorem implies that the asymptotic exponential divergence of any spatial vector $\mathbf{x}$ under the action of the product of matrices $\mathbb{M}_N$ is determined by the LCE. More precisely, the divergence will be dominated by the component of $\mathbf{x}$ on $\{U_i\}$ with the fastest growing rate.

Now let us consider our one-dimensional quantum wires, which as already known can be described through products of different type of 2×2 matrices, namely the discrete transfer matrices $\mathbf{P}_j$ defined from the canonical equation in (2.14) and the continuous transmission matrices $\mathbf{M}_j$ defined in equation (2.6). It can be proved that for one-dimensional Hamiltonian systems the two LCE come in a pair of the form $\{\lambda, -\lambda\}$ (see appendix B). Considering the discrete transfer matrices we have

$$\mathbf{x}_{N+1} = \mathbf{P}_N \mathbf{P}_{N-1} \cdots \mathbf{P}_1 \mathbf{x}_1, \tag{2.22}$$

where $\mathbf{x}_{N+1} = \begin{pmatrix} \Psi_{N+1} \\ \Psi_N \end{pmatrix}$ and $\mathbf{x}_1 = \begin{pmatrix} \Psi_1 \\ \Psi_0 \end{pmatrix}$. Therefore applying the MET

$$\lambda(\mathbf{x_1}) = \lim_{N\to\infty} \frac{1}{N} \log \sqrt{\Psi_N^2 + \Psi_{N+1}^2}. \tag{2.23}$$

---

[2]Several conditions must be satisfied by the set $\{\mathbf{M}_n\}$ and its products that we suppose to be fulfilled in meaningful physical situations.

Imposing hard-wall boundary conditions $\lambda(\mathbf{x_1}) = \lim_{N\to\infty} \frac{1}{N} \log|\Psi_N|$ which is straightforwardly equivalent to

$$\lambda = \lim_{N\to\infty} \frac{1}{N} \sum_j \log \frac{|\Psi_{j+1}|}{|\Psi_j|}, \tag{2.24}$$

a common expression found in the literature for the Lyapunov exponent, and that always provides the largest LCE [175], in our case the positive one.

On the other hand the same physical system can be realized using the continuous transmission matrix formalism, that must yield asymptotically the same values for the Lyapunov exponents if they have physical sense at all. Therefore,

$$\mathbf{x}_{N+1} = \mathbf{M}_N \mathbf{M}_{N-1} \cdots \mathbf{M}_1 \mathbf{x}_1, \tag{2.25}$$

where $\mathbf{x}_{N+1} = \begin{pmatrix} A_{N+1} \\ B_{N+1} \end{pmatrix}$ and $\mathbf{x}_1 = \begin{pmatrix} A_1 \\ B_1 \end{pmatrix}$ corresponding to the amplitudes of the travelling plane waves. If we impose the initial conditions $A_1 = 1$, $B_1 = r(E)$, then the final result will be $A_{N+1} = t(E)$, $B_{N+1} = 0$, where $r(E)$ and $t(E)$ are the scattering amplitudes. Thus the MET implies

$$-\lambda = \lim_{N\to\infty} \frac{1}{2N} \log T(E), \tag{2.26}$$

where $T(E)$ is the transmission probability of the system, and obviously the negative Lyapunov exponent is obtained. The above expression was first obtained by Kirkman and Pendry [120]. It implies that for a given energy, the transmission of a one-dimensional disordered structure decreases asymptotically exponentially with the length of the system $T_N(E) \sim e^{-2\lambda(E)N}$ [117]. This is a consequence of the same asymptotic exponential decreasing behaviour exhibited by the electronic states for that energy. From this fact we define the localization length $\xi(E)$ of the electronic state with energy E, if it exists, as the inverse of the rate of the asymptotic exponential decrease of the transmission amplitude with the length of the system for that energy,

$$\xi(E) \equiv \lambda(E)^{-1}. \tag{2.27}$$

This definition is also a measure of the spatial extension of the exponentially localized state inside the system, and it has a clear physical meaning.

Although the Lyapunov exponent and therefore the localization length defined can only be strictly obtained asymptotically, it makes also sense to characterize the electronic localization in a long enough finite system through

$$\xi(E)^{-1} = -\frac{1}{2N} \log T(E), \tag{2.28}$$

because the Lyapunov exponent is a self-averaging quantity [122], thus it agrees with the most probable value (its mean value) in the thermodynamic limit, for every energy. Therefore expression (2.28) gives relevant information of the localization length for finite N, since it will show a fluctuating behaviour around the asymptotic value.

Finally let us say that a complex extension of the Lyapunov exponent is possible,

$$\lambda_c = \lim_{N \to \infty} \frac{1}{N} \sum_j \log \left(\frac{\Psi_{j+1}}{\Psi_j} \right), \qquad (2.29a)$$

$$-\lambda_c = \lim_{N \to \infty} \frac{1}{N} \log t(E), \qquad (2.29b)$$

being Ψ_j the complex amplitudes of the state and $t(E)$ the complex transmission amplitude. The real part of this extension is related to the localization length whereas its imaginary part turns out to be π times the integrated density of states $n(E)$ per length unit of the system [120].

2.4.2 Inverse participation ratio

Alternatively, localization is also usually characterized by the inverse participation ratio (IPR) [35], which is defined in terms of the amplitudes of the electronic state at the different sites of the system as

$$\text{IPR} = \frac{\sum_{j=1}^{N} |\Psi_j|^4}{\left(\sum_{j=1}^{N} |\Psi_j|^2 \right)^2}. \qquad (2.30)$$

For an extended state the IPR takes values of order N^{-1} whereas for a state localized in the vicinity of only one site it goes to 1. The inverse of the IPR means the length of the portion of the system in which the amplitudes of the state differ appreciably from zero.

2.5 Obtaining the density of states

The density of states (DOS) $g(E)$ gives the distribution of permitted energy levels and it is specially important for calculating some macroscopic properties of the structures which are usually obtained from averages over the electronic spectrum. Strictly speaking $g(E)$ is the function such that $g(E)\mathrm{d}E$ is the number of eigenvalues of the energy inside the interval $(E, E + \mathrm{d}E)$, and it is usually defined per length unit of the system. The integrated density of states $n(E)$ is defined as

$$n(E) \equiv \int_{-\infty}^{E} g(E')\mathrm{d}E', \qquad (2.31)$$

and measures the number of permitted energies below the value E. For a one-dimensional wire the integrated DOS can be determined from the imaginary part of the complex Lyapunov exponent. From (2.29b) one can write [137, 161]

$$n(E) = \frac{1}{\pi N} \arg[t^*(E)], \qquad n(E) = \frac{i}{2\pi N} \log\left(\frac{t(E)}{t^*(E)}\right). \tag{2.32}$$

The electronic DOS can also be numerically determined using the negative eigenvalue theorem proposed by Dean for the phonon spectrum [52], however this method cannot be applied for all potential models. It is possible to build a generalization of Dean's method to obtain the DOS for finite chains. This technique shows some relevant computational advantages comparing with the one involving the complex transmission amplitude. The whole derivation can be found in appendix C. Defining $s_{j,j+1} = \Psi_{j+1}/\Psi_j$ the canonical equation (2.1) reads

$$s_{j,j+1} = J(\gamma_{j-1}, \gamma_j) - \frac{K(\gamma_j)}{K(\gamma_{j-1})} \frac{1}{s_{j-1,j}}. \tag{2.33}$$

Now let us consider a wire composed of different atomic species $\{\alpha\}$ and let be $\mathcal{N}_\alpha(E)$ the number of negative $s_{j,j+1}$ whenever $\gamma_j = \alpha$, divided by the number of sites of the chain. That is, $\mathcal{N}_\alpha(E)$ is the concentration of α atoms after which the envelope of the electronic wave function with energy E changes its sign. Then the DOS can be obtained as

$$g(E) = \left| \sum_\alpha \text{sgn}[K(\alpha)] \frac{d\mathcal{N}_\alpha(E)}{dE} \right|. \tag{2.34}$$

Thus using the recursion relation (2.33), one has to calculate the concentrations of changes of sing for the different atomic species, which must then be added or subtracted according to the sign of the functions $K(\alpha)$ for the corresponding energy. Finally a numerical differentiation with respect to the energy must be performed.

2.6   The functional equation: the thermodynamic limit

The description of the properties of a system in the thermodynamic limit (TL) reveals the fundamental physics underlying the different problems, removing any accidental finite size effects. The TL tells us which observations are a consequence of a general physical principle. With this purpose scaling theory is intended to obtain different magnitudes in the TL by figuring out how they scale with the size of the system. Apart from scaling theory, a few authors have been in pursuit of obtaining analytically several quantities of an infinite one-dimensional disordered system. Dyson (1953) [74] and Schmidt (1957)[164] derived analytically a type of functional equations for

certain distribution functions containing information about the integrated density of states in the TL, for the phonon spectrum of a system of harmonic oscillators with random masses and the electronic spectrum of a delta potential model with random couplings, respectively. Although some efforts were made to solve numerically these equations [3, 28, 51, 4, 91], this approach was almost completely forgotten probably because of its cumbersome mathematics and the lack of analytical solutions.

We assert that it is possible to derive a set of universal functional equations describing the TL of one-dimensional systems. In this way one can build a formalism which can be applied to a large variety of potential models. The solution of these equations can be used to obtain relevant magnitudes of the system such as the DOS or the localization length. A complete derivation of the equations can be found in appendix D. Let our one-dimensional problem be governed by the canonical equation

$$\Psi_{j+1} = J(\gamma_{j-1}, \gamma_j)\Psi_j - \frac{K(\gamma_j)}{K(\gamma_{j-1})}\Psi_{j-1}. \tag{2.35}$$

Using the mapping technique described in section 2.1, one can define a phase θ and radius ρ satisfying the transmission relations (2.3) and (2.4). Assuming that the chain is composed of different species (denoted by Greek letters) $\{\gamma\}$ the following equations hold in the thermodynamic limit,

$$W_\gamma(\theta) = \sum_\beta p_{\gamma\beta} \left| W_\beta \left(\mathcal{T}^{-1}(\theta; \beta, \gamma) \right) - W_\beta \left(\frac{\pi}{2} \right) + \delta(\beta, \gamma) \right|, \tag{2.36a}$$

$$W_\gamma(\theta + n\pi) = W_\gamma(\theta) + n, \qquad \theta \in [0, \pi), \ n \in \mathbb{Z}, \tag{2.36b}$$

where $p_{\gamma\beta}$ is the probability of finding a β atom besides a γ atom, $\delta(\beta, \gamma) = 1$ if $[K(\gamma)/K(\beta)] > 0$ and $\delta(\beta, \gamma) = 0$ otherwise, and $\mathcal{T}^{-1}(\theta; \beta, \gamma)$ is the inverse transmission function for the phase,

$$\mathcal{T}^{-1}(\theta; \beta, \gamma) = \arctan\left\{ \frac{K(\beta)}{K(\gamma)} \left(J(\beta, \gamma) - \frac{1}{\tan\theta} \right) \right\}, \qquad \theta \in [0, \pi). \tag{2.37}$$

$W_\gamma(\theta)$ are the phase distribution functions in the TL for each species γ, that is they mean the probability that the phase modulo π right after a γ atom is included in the interval $[0, \theta)$. Then $\mathrm{d}W_\gamma(\theta)$ is the natural measure of the phase inside the system for the γ species, that is the probability of catching the phase in the interval $(\theta, \theta + \mathrm{d}\theta)$. Therefore this distribution functions can be used to calculate the average in the TL of any quantity of the system that can be written in terms of the phase θ. Using this latter fact one can obtain the inverse of the localization length and the DOS of the

system in terms of the distribution functions as

$$\xi(E)^{-1} = \frac{1}{2} \sum_{\gamma,\beta} c_\gamma p_{\gamma\beta} \log \mathcal{F}(\pi; \gamma, \beta) - \frac{1}{2} \sum_{\gamma,\beta} c_\gamma p_{\gamma\beta} \int_0^\pi W_\gamma(\theta) \frac{\mathcal{F}'(\theta; \gamma, \beta)}{\mathcal{F}(\theta; \gamma, \beta)} d\theta, \quad (2.38)$$

$$g(E) = \left| \sum_\gamma \mathrm{sgn}[K(\gamma)] c_\gamma \frac{dW_\gamma\left(\frac{\pi}{2}\right)}{dE} \right|, \quad (2.39)$$

c_γ being the concentration for the γ species and $\mathcal{F}(\theta; \gamma, \beta)$ the transmission function for ρ defined in (2.4),

$$\mathcal{F}(\theta; \gamma, \beta) = \cos^2\theta + \left(J(\gamma, \beta) \cos\theta - \frac{K(\beta)}{K(\gamma)} \sin\theta \right)^2. \quad (2.40)$$

Let us remark the fact that binary correlations naturally appear in the definition of the distribution functions through the set of probabilities $\{p_{\gamma\beta}\}$, the completely uncorrelated situation would be defined by $p_{\gamma\beta} = c_\beta$ for all species.

Due to the formidable aspect of the functional equations it seems a hard task to obtain analytical solutions, if they exist at all. Nevertheless they might be useful to extract relevant information of the systems in the thermodynamic limit analytically.

2.7   An example: the tight-binding model

To exemplify the study of a quantum wire with the tools described in the previous sections, let us consider a basic one-dimensional model: a tight-binding Hamiltonian with nearest neighbour interactions,

$$\widehat{H} = \sum_k \left(\varepsilon_k \left| k \right\rangle\!\left\langle k \right| + t_{k,k+1} \left| k \right\rangle\!\left\langle k+1 \right| + t_{k,k-1} \left| k \right\rangle\!\left\langle k-1 \right| \right), \quad (2.41)$$

where ε_k are the energies of the on-site orbitals $\left| k \right\rangle$ and $t_{j,j\pm1}$ mean the transfer integrals, which we take equal to 1 for the sake of simplicity. The on-site energies follow a random sequence so that this model is said to have diagonal disorder. The one-dimensional Anderson model consists in choosing ε_j from a finite continuous interval with a constant probability distribution. In our case the composition includes different discrete species $\{\varepsilon_1, \varepsilon_2, \ldots\}$ appearing with concentrations $\{c_1, c_2, \ldots\}$.

Since the orbitals $\{\left| j \right\rangle\}$ constitute an orthonormal basis of the Hilbert space of the system, the eigenstates can be written as $\left| \Psi \right\rangle = \sum_j u_j \left| j \right\rangle$. The Schrödinger equation is then translated into a discrete equation for the coefficients u_j,

$$u_{j+1} = (E - \varepsilon_j) u_j - u_{j-1}, \quad (2.42)$$

showing the desired canonical form of equation (2.1) with $J(\varepsilon_j) = E - \varepsilon_j$ and $K(\varepsilon_j) = 1$ for all j. Using the results of section 2.1 concerning the gaps of the spectrum, it is straightforward to conclude that the energy values satisfying $|E - \varepsilon_j| > 2$ for all j, are not permitted. Therefore the eigenvalues can only be located inside intervals 4 units of energy wide centered at the different on-site energies. In fact each interval corresponds to the allowed band of the pure chain of each species. The simplest mixed system is a binary chain composed of two different species. In this case the spectrum only depends upon the quantity $|\varepsilon_1 - \varepsilon_2|$ thus the on-site energies are usually defined as $\varepsilon_1 = -\varepsilon$, $\varepsilon_2 = \varepsilon$. When $\varepsilon \leqslant 2$ the eigenenergies are all included in the interval $[-2 - \varepsilon, \varepsilon + 2]$. That is the reason why this model is commonly referred to as a one-band model. If $\varepsilon > 2$ a gap appears in the range $[2 - \varepsilon, \varepsilon - 2]$.

From the canonical equation, the two-dimensional mapping defined in section 2.1 is easily built yielding the transmission functions

$$\mathcal{T}^{-1}(\theta; \varepsilon_j) = \arctan\left(E - \varepsilon_j - \frac{1}{\tan\theta}\right), \tag{2.43}$$

$$\mathcal{F}(\theta; \varepsilon_j) = 1 - (E - \varepsilon_j)\sin(2\theta) + (E - \varepsilon_j)^2 \cos^2\theta, \tag{2.44}$$

which only depend on one species at each step. This latter property together with the fact that $K(\varepsilon_j) = 1$ for this model, simplifies considerably the functional equations (2.36) (see appendix D). For a chain with uncorrelated disorder a unique distribution function for the phase can be defined $W(\theta)$ being the solution of

$$W(\theta) = \sum_\gamma c_\gamma W\left(\mathcal{T}^{-1}(\theta; \varepsilon_\gamma)\right) - W\left(\frac{\pi}{2}\right) + 1, \tag{2.45a}$$

$$W(\theta + n\pi) = W(\theta) + n, \qquad \theta \in [0, \pi),\ n \in \mathbb{Z}. \tag{2.45b}$$

Thus only one functional equation needs to be solved. And the DOS per atom as well as the localization length can be obtained in the thermodynamic limit from

$$\xi(E)^{-1} \equiv \lambda(E) = \frac{1}{2}\sum_\gamma c_\gamma \log \mathcal{F}(\pi; \varepsilon_\gamma) - \frac{1}{2}\sum_\gamma c_\gamma \int_0^\pi W(\theta) \frac{\mathcal{F}'(\theta; \varepsilon_\gamma)}{\mathcal{F}(\theta; \varepsilon_\gamma)} \mathrm{d}\theta, \tag{2.46}$$

$$g(E) = \left|\frac{\mathrm{d}W\left(\frac{\pi}{2}\right)}{\mathrm{d}E}\right|. \tag{2.47}$$

Using the discrete transmission matrix formalism, the scattering amplitudes of a finite chain can be obtained. In figure 2.3 the logarithm of the modulus of the transmission amplitude is plotted as a function of the length of the system for different binary chains. The exponential decrease of the transmission is clearly observed and the data for finite chains agrees with the value of the Lyapunov exponent obtained from
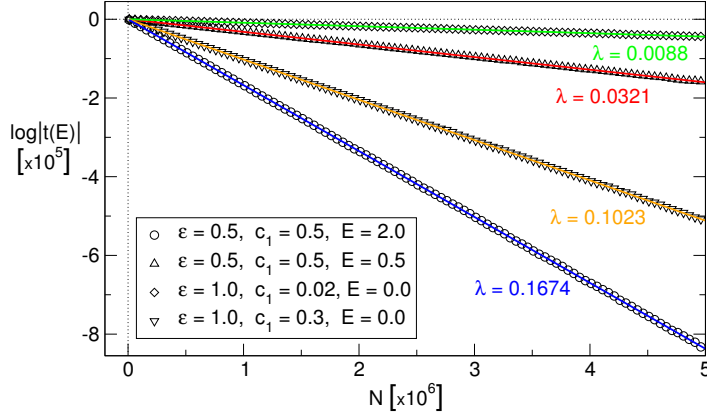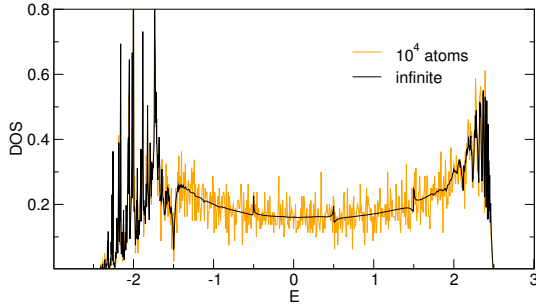
Figure 2.4. Comparison of the DOS for a finite binary sequence with the limiting distribution for the infinite chain with parameters $\varepsilon = 0.5$, $c_1 = 0.3$.
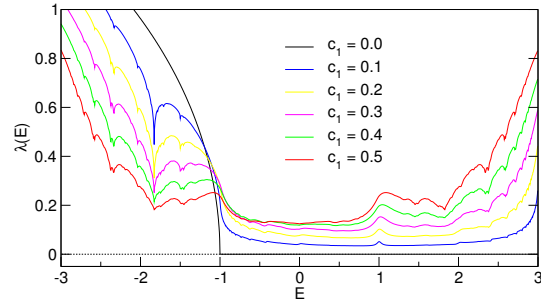

Figure 2.5. Lyapunov exponent for a binary chain with $\varepsilon = 1$ for different concentrations.
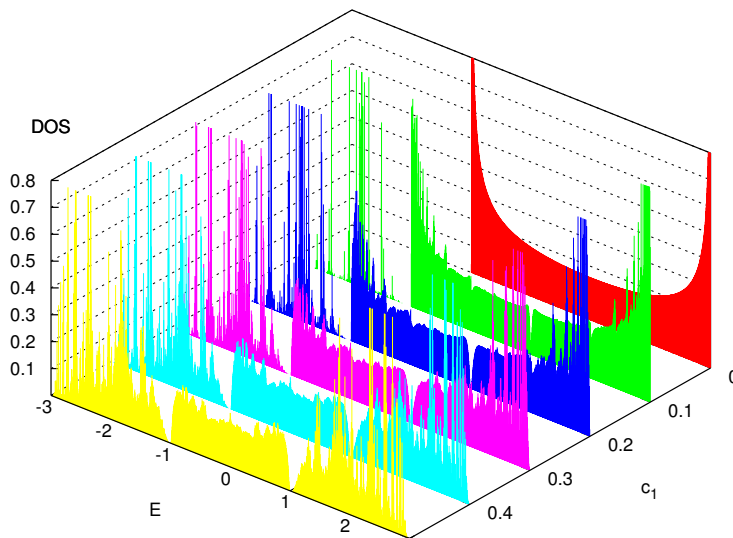

Figure 2.6. DOS for a binary chain with $\varepsilon = 1$ for different concentrations. The distributions for $c_1 > 0.5$ are the same but inverted with respect to the energy due to the symmetry of the Hamiltonian.

the functional equation in the different cases. In figure 2.4 the DOS for a finite chain is plotted, showing a fluctuating behaviour around the distribution corresponding to the thermodynamic limit. The evolution of the DOS and the electronic localization length in the thermodynamic limit for a binary chain as a function of the concentrations can be seen in figures 2.5 and 2.6. It can be observed how the tools used provide the correct results when the chain is composed of only one species: $\lambda(E) = 0$ and $\lambda(E) = \text{arccosh}(|E - \varepsilon|/2)$ inside and outside the allowed energy band respectively and the density of states fits the correct form $g(E) = \pi^{-1} \left[4 - (E - \varepsilon)^2\right]^{-1/2}$.

As can be seen in the analysis of the tight-binding Hamiltonian, taking the canonical equation as a starting point a systematic characterization of the electronic properties of the system can be performed, both for finite arrays via the transmission matrix formalism and in the thermodynamic limit with the functional equations. In the forthcoming chapters, the methods described will be applied to a variety of one-dimensional quantum wire models, trying to reveal the physical properties of this kind of structures and understand their particular features.

Quantum wire with delta chains

3.1 The potential

Let us consider a quantum wire model made up of an array of Dirac delta potentials, each one with its own coupling α_j and placed at equally spaced positions with inter-atomic distance a. Then, the potential energy of an electron inside this linear chain is

$$V(x) = \sum_j \alpha_j \delta(x - ja). \tag{3.1}$$

This model was first introduced by Kronig and Penney in 1931 [44] and since then it has been extensively considered in the literature. Indeed it is nowadays one of the most treated models. In spite of its apparently simplicity, we shall see how it is powerful enough to account for very different schemes containing an unexpected physical richness.

Due to the discontinuous nature of the potential the continuous transmission matrix is easily calculated[1], yielding for the jth delta potential followed by a zero potential zone of length a

$$\mathbf{M}_j = \begin{pmatrix} \left(1 - \frac{\mathrm{i}}{ka_j}\right)\mathrm{e}^{\mathrm{i}ka} & -\frac{\mathrm{i}}{ka_j}\mathrm{e}^{\mathrm{i}ka} \\ \frac{\mathrm{i}}{ka_j}\mathrm{e}^{-\mathrm{i}ka} & \left(1 + \frac{\mathrm{i}}{ka_j}\right)\mathrm{e}^{-\mathrm{i}ka} \end{pmatrix}, \tag{3.2}$$

where $a_j = \hbar^2/m\alpha_j$ means the 'effective range' of the jth delta and $k = \sqrt{2mE}/\hbar$. The transmission probability for a delta potential is a monotonically increasing func-

---

[1] A collection of transmission matrices and canonical equations for different 1-D potentials can be found in appendix F.

tion with the energy. If the delta coupling is negative, then it can host a bound state with energy $k = i/|a_j|$ whose amplitude decreases from the position of the delta as $\exp(-|x/a_j|)$. For positive energies the wave function in the different sectors of the chain is simply a combination of the free particle solutions. Using the transmission matrix one can derive the following relation among the amplitudes of the state at contiguous sites

$$\Psi_{j+1} = 2h_j(\epsilon)\Psi_j - \Psi_{j-1}, \tag{3.3}$$

where Ψ_j is the amplitude of the state at the position of the jth delta and we define

$$h_j(\epsilon) \equiv \cos(\epsilon) + \left(\frac{a}{a_j}\right)\frac{\sin(\epsilon)}{\epsilon}, \tag{3.4}$$

being $\epsilon \equiv ka$ a dimensionless representation of the energy. The canonical form (3.3) leads to the following discrete transmission matrices

$$\mathbf{P}_j = \begin{pmatrix} 2h_j(\epsilon) & -1 \\ 1 & 0 \end{pmatrix}. \tag{3.5}$$

Hence, the effect of a linear array of N deltas can be treated via the product of their transmission matrices or equivalently through the composition rules (2.9). For this model it is possible to write closed expressions for the scattering amplitudes of an arbitrary chain,

$$t_N(\epsilon) = \frac{e^{iN\epsilon}}{f(\epsilon; a_1, \ldots, a_N)}, \tag{3.6}$$

$$r_N^L(\epsilon) = -e^{-2i\epsilon}\frac{g(\epsilon; a_1, \ldots, a_N)}{f(\epsilon; a_1, \ldots, a_N)}, \tag{3.7}$$

with the definitions

$$f(\epsilon; a_1, \ldots, a_N) = 1 + \frac{i}{\epsilon}\sum_{j=1}^{N}\left(\frac{a}{a_j}\right) + \sum_{j=2}^{N}\left(\frac{i}{\epsilon}\right)^j$$
$$\times \left\{ \sum_\sigma \left[\left(\frac{a}{a_{\sigma_1}}\right)\left(\frac{a}{a_{\sigma_2}}\right)\cdots\left(\frac{a}{a_{\sigma_j}}\right)\prod_{r=1}^{j-1}\left(1 - e^{2i\epsilon(\sigma_{r+1}-\sigma_r)}\right)\right] \right\}, \tag{3.8}$$

$$g(\epsilon; a_1, \ldots, a_N) = \frac{i}{\epsilon}\sum_{j=1}^{N}e^{i2j\epsilon}\left(\frac{a}{a_j}\right) + \sum_{j=2}^{N}\left(\frac{i}{\epsilon}\right)^j$$
$$\times \left\{ \sum_\sigma \left[e^{i2\sigma_1\epsilon}\left(\frac{a}{a_{\sigma_1}}\right)\cdots\left(\frac{a}{a_{\sigma_j}}\right)\prod_{r=1}^{j-1}\left(1 - e^{2i\epsilon(\sigma_{r+1}-\sigma_r)}\right)\right] \right\}, \tag{3.9}$$

where for each j the symbol $\sum_\sigma$ means one must sum over the $\binom{N}{j}$ combinations of size j, $\sigma = \{\sigma_1, \sigma_2, \ldots, \sigma_j\}$ from the set $\{1, 2, \ldots, N\}$ with $\sigma_1 < \sigma_2 < \ldots < \sigma_j$. The r^R amplitude up to a phase is obtained from r^L for the reverse chain. The global potential is then characterized by the arranged sequence of the ratios (a/a_j) where the indices label the positions from left to right. In spite of their formidable aspect, the above equations are easy to program for sequential calculations providing the transmittivity and reflectivity of the system with exact analytical expressions.

3.2   Periodic system

Let us briefly discuss the main properties of the periodic arrangement of potentials for this model. According to the Bloch theorem [171] the permitted energies of the infinite periodic system are such that the eigenvalues of the transmission matrix $\mathbf{M}_{pc}$ of the primitive cell with length L, take the form of Bloch phases, $\mathrm{e}^{\mathrm{i}qL}$. Then the allowed bands come from

$$\cos(qL) = \frac{1}{2}\mathrm{Tr}\,\mathbf{M}_{pc}, \tag{3.10}$$

where $q \in [-\pi/L, \pi/L]$ defines the first Brillouin zone (1BZ) in the reciprocal space. The unit cell can be composed of different deltas, thus $\mathbf{M}_{pc}$ is given by a product of matrices of the form (3.2) or equivalently the discrete matrices (3.5) can also be used. For the case in which the primitive cell includes N different potentials it is possible to find a general expression for $\mathrm{Tr}\,\mathbf{M}_{pc}$. The allowed bands obey

$$\cos(Nqa) = \mathcal{B}(\epsilon; a_1, \ldots, a_N), \tag{3.11}$$

where for even N

$$\mathcal{B}(\epsilon; a_1, \ldots, a_N) = (-1)^{\frac{N}{2}} + \sum_{j=1}^{\frac{N}{2}} (-1)^{\frac{N}{2}-j}\, 2^{2j-1}\, \mathrm{Sh}_N(2j), \tag{3.12a}$$

and for odd N

$$\mathcal{B}(\epsilon; a_1, \ldots, a_N) = \sum_{j=1}^{\frac{N+1}{2}} (-1)^{\frac{N+1}{2}-j}\, 4^{j-1}\, \mathrm{Sh}_N(2j-1). \tag{3.12b}$$

And the function $\mathrm{Sh}_N(p)$ is defined as the sum of all possible products of p different $h_j(\epsilon)$ functions $(h_{j_1} h_{j_2} \cdots h_{j_p})$ such that $j_1 < j_2 < \cdots < j_p$ and to an odd index follows

an even one and reciprocally. Let us remark that the indices label the position of each delta inside the primitive cell. The band equation for $N = 1, 2, 3, 4$ as stated by the preceding formulae reads explicitly

$$\cos(qa) = h_1, \tag{3.13}$$

$$\cos(2qa) = 2\,h_1 h_2 - 1, \tag{3.14}$$

$$\cos(3qa) = 4\,h_1 h_2 h_3 - (h_1 + h_2 + h_3), \tag{3.15}$$

$$\cos(4qa) = 8\,h_1 h_2 h_3 h_4 - 2(h_1 h_2 + h_1 h_4 + h_2 h_3 + h_3 h_4) + 1. \tag{3.16}$$

The band structure provided is extremely useful from a computational point of view, due to the systematic use of the combinations of the elementary functions $h_j(\epsilon)$. Once the allowed bands are known the distribution of states can be written in a very simple form. The DOS per atom inside the different permitted bands comes from

$$g(\epsilon) = \frac{1}{N\pi} \left[1 - \mathcal{B}^2(\epsilon)\right]^{-\frac{1}{2}} \left|\frac{\mathrm{d}\mathcal{B}(\epsilon)}{\mathrm{d}\epsilon}\right|. \tag{3.17}$$

The regular oscillatory nature of the bands in the reciprocal space imposes some general characteristic features to the DOS. The distribution of states reaches a minimum at the inflexion point of each band and Van-Hove singularities appear at the band edges, as expected for a one-dimensional system.

It is possible to write a compact analytical expression for the transmission probability of a finite periodic chain by making use of the Cayley-Hamilton theorem, that permits writing the power of a 2×2 matrix in terms of Chebyshev polynomials (see for example reference [89]). As an example the transmittivity for a one species pure chain with m primitive cells can be written as

$$T_m(\epsilon) = \left\{1 + \left(\frac{a}{a_1}\right)^2 \frac{\sin^2\left[m \arccos(h_1(\epsilon))\right]}{\epsilon^2 \left(1 - h_1^2(\epsilon)\right)}\right\}^{-1}. \tag{3.18}$$

In figure 3.1 a characteristic example of the band structure, the DOS and the transmission pattern for a periodic delta chain is shown.

3.3   Short aperiodic sequences

Let us consider now aperiodic arrays of deltas with hard-wall boundary conditions, that is inside an infinite potential well, assuming that the walls are placed at one interatomic distance a before the first potential and after the last one. Then the eigenenergy condition is the vanishing of the wave function at the walls. It can be imposed
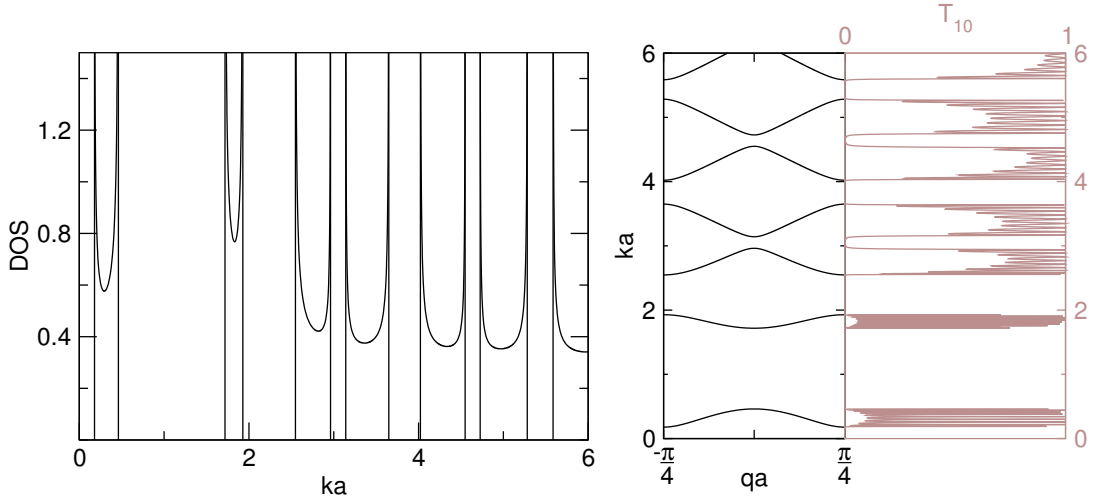
Figure 3.1. DOS (left), band structure in 1BZ (middle) and transmittivity (right) for a periodic chain whose primitive cell includes four deltas with parameters (a/a_j) : $1, -2, -1, 0.6$. The transmission corresponds to a chain with only 10 unit cells.

using the explicit form of the electronic state and the continuous transmission matrices, but the discrete transfer formalism turns out to be specially suitable for this task. For a chain with N potentials the eigenstates satisfy

$$\begin{pmatrix} 0 \\ \Psi_N \end{pmatrix} = \mathbf{P}_N \mathbf{P}_{N-1} \cdots \mathbf{P}_1 \begin{pmatrix} \Psi_1 \\ 0 \end{pmatrix} \equiv \mathbb{P} \begin{pmatrix} \Psi_1 \\ 0 \end{pmatrix}, \tag{3.19}$$

that translates into $\mathbb{P}_{11} = 0$. Apart from these solutions one must take into account also the eigenstates of the infinite square well remaining unperturbed by the delta chain, namely those with energy $\epsilon = n\pi$, $n \in \mathbb{Z}$, which do not feel the delta potentials. For arbitrary N the equation for the energy levels of the system can be written as

$$\sin(\epsilon)\mathcal{A}(\epsilon; a_1, \dots, a_N) = 0, \tag{3.20}$$

where for even N

$$\mathcal{A}(\epsilon; a_1, \dots, a_N) = (-1)^{\frac{N}{2}} + \sum_{j=1}^{\frac{N}{2}} (-1)^{\frac{N}{2}-j} \, 2^{2j} \, \overline{\mathrm{Sh}}_N(2j), \tag{3.21a}$$

and for odd N

$$\mathcal{A}(\epsilon; a_1, \dots, a_N) = \sum_{j=1}^{\frac{N+1}{2}} (-1)^{\frac{N+1}{2}-j} \, 4^{j-1} \, \overline{\mathrm{Sh}}_N(2j-1). \tag{3.21b}$$
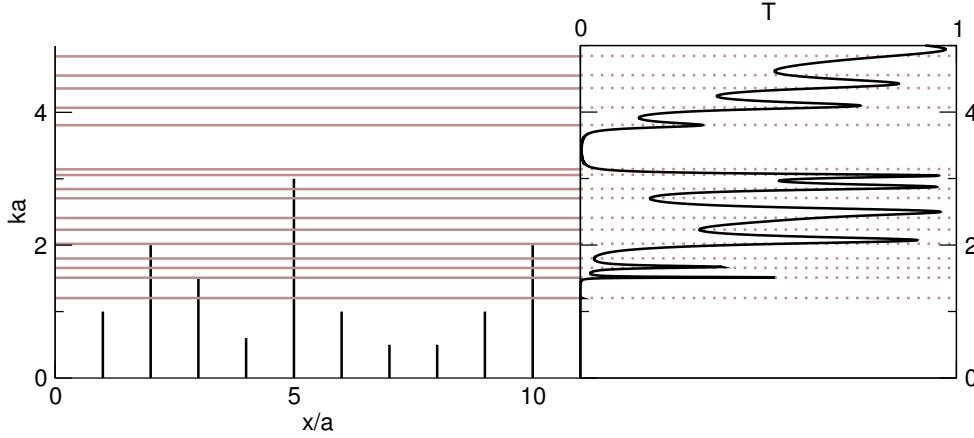
Figure 3.2. (Left) Infinite box including a chain of 10 delta potentials with parameters (a/a_j) : $1, 2, 1.5, 0.6, 3, 1, 0.5, 0.5, 1, 2$. The horizontal lines mark the position of several permitted levels. (Right) Transmission probability of the chain with open boundaries.

The function $\overline{\mathrm{Sh}}_N(p)$ is defined as the sum of all possible products of p different $h_j(\epsilon)$ functions $(h_{j_1} h_{j_2} \cdots h_{j_p})$ such that $j_1 < j_2 < \cdots < j_p$, j_1 is odd and to an odd index follows an even one and reciprocally. The indices mark the position of the different deltas. The eigenvalue condition for $N = 1, 2, 3, 4$ reads

$$\sin(\epsilon) h_1 = 0, \tag{3.22}$$

$$\sin(\epsilon) \left[4\, h_1 h_2 - 1 \right] = 0, \tag{3.23}$$

$$\sin(\epsilon) \left[4\, h_1 h_2 h_3 - (h_1 + h_3) \right] = 0, \tag{3.24}$$

$$\sin(\epsilon) \left[16\, h_1 h_2 h_3 h_4 - 4(h_1 h_2 + h_1 h_4 + h_3 h_4) + 1 \right] = 0. \tag{3.25}$$

In figure 3.2 the position of several eigenlevels of an aperiodic delta sequence with hard-wall boundary conditions is displayed and can be compared with the transmittivity of the system with open boundaries.

3.4 Wires with uncorrelated substitutional disorder

We shall consider the effect of substitutional disorder in this one-dimensional model. The potentials are set out on a regular lattice with parameter a and the delta couplings follow a completely random sequence, yielding a wire composed of a finite number of different atomic species, each one characterized by the parameter (a/a_γ) and its concentration c_γ. And there are not any correlations among the different potentials, hence the probability of finding a certain cluster of atoms is simply given by the product of their concentrations.

The starting point in the study of the electronic properties of this system is the canonical equation described previously,

$$\Psi_{j+1} = 2h_j(\epsilon)\Psi_j - \Psi_{j-1}, \tag{3.26}$$

$h_j(\epsilon)$ being defined in (3.4). The above expression fits the general canonical form (2.1) with $J(a_\gamma) = 2h_\gamma(\epsilon)$ and $K(a_\gamma) = 1$ for all γ. Then from equation (2.5) one obtains that the energy ranges satisfying $|h_\gamma(\epsilon)| > 1$ for all γ are not permitted in the spectrum of the disordered system. This condition can be interpreted using the results from the periodic chains in section 3.2. According to equation (3.13), the previous condition means that the common forbidden bands of the one species pure chains are also forbidden ranges of the mixed system. In fact this conclusion does not depend on the arrangement of atoms in the mixed system. This result means a proof of the generalization of the Saxon and Hutner conjecture [163] concerning the gaps of a binary delta chain that was proved by Luttinger [136].

The limiting distribution of the electronic levels as well as the localization properties in the thermodynamic limit are obtained using the functional equation formalism. The relevant transmission functions for this model read

$$\mathcal{T}^{-1}(\theta; a_\gamma) = \arctan\left(2h_\gamma(\epsilon) - \frac{1}{\tan\theta}\right), \tag{3.27}$$

$$\mathcal{F}(\theta; a_\gamma) = 1 - 2h_\gamma(\epsilon)\sin(2\theta) + 4h_\gamma^2(\epsilon)\cos^2\theta. \tag{3.28}$$

Just like for the tight-binding model, the simple forms of the canonical equation and of the above functions simplify considerably the functional equations. Only one distribution function needs to be known, $W(\theta) \equiv \sum_\gamma c_\gamma W_\gamma(\theta)$ being the solution of

$$W(\theta) = \sum_\gamma c_\gamma W\left(\mathcal{T}^{-1}(\theta; a_\gamma)\right) - W\left(\frac{\pi}{2}\right) + 1, \tag{3.29a}$$

$$W(\theta + n\pi) = W(\theta) + n, \qquad \theta \in [0, \pi), \, n \in \mathbb{Z}. \tag{3.29b}$$

Finally the DOS per atom and the localization length can be numerically obtained from

$$\xi(\epsilon)^{-1} \equiv \lambda(\epsilon) = \frac{1}{2}\sum_\gamma c_\gamma \log \mathcal{F}(\pi; a_\gamma) - \frac{1}{2}\sum_\gamma c_\gamma \int_0^\pi W(\theta)\frac{\mathcal{F}'(\theta; a_\gamma)}{\mathcal{F}(\theta; a_\gamma)}\mathrm{d}\theta, \tag{3.30}$$

$$g(\epsilon) = \left|\frac{\mathrm{d}W\left(\frac{\pi}{2}\right)}{\mathrm{d}\epsilon}\right|. \tag{3.31}$$

In figures 3.3 and 3.4 on pages 38 and 39, several distributions of states and Lyapunov exponents are shown as functions of the energy for disordered chains with different number of atomic species and concentrations.
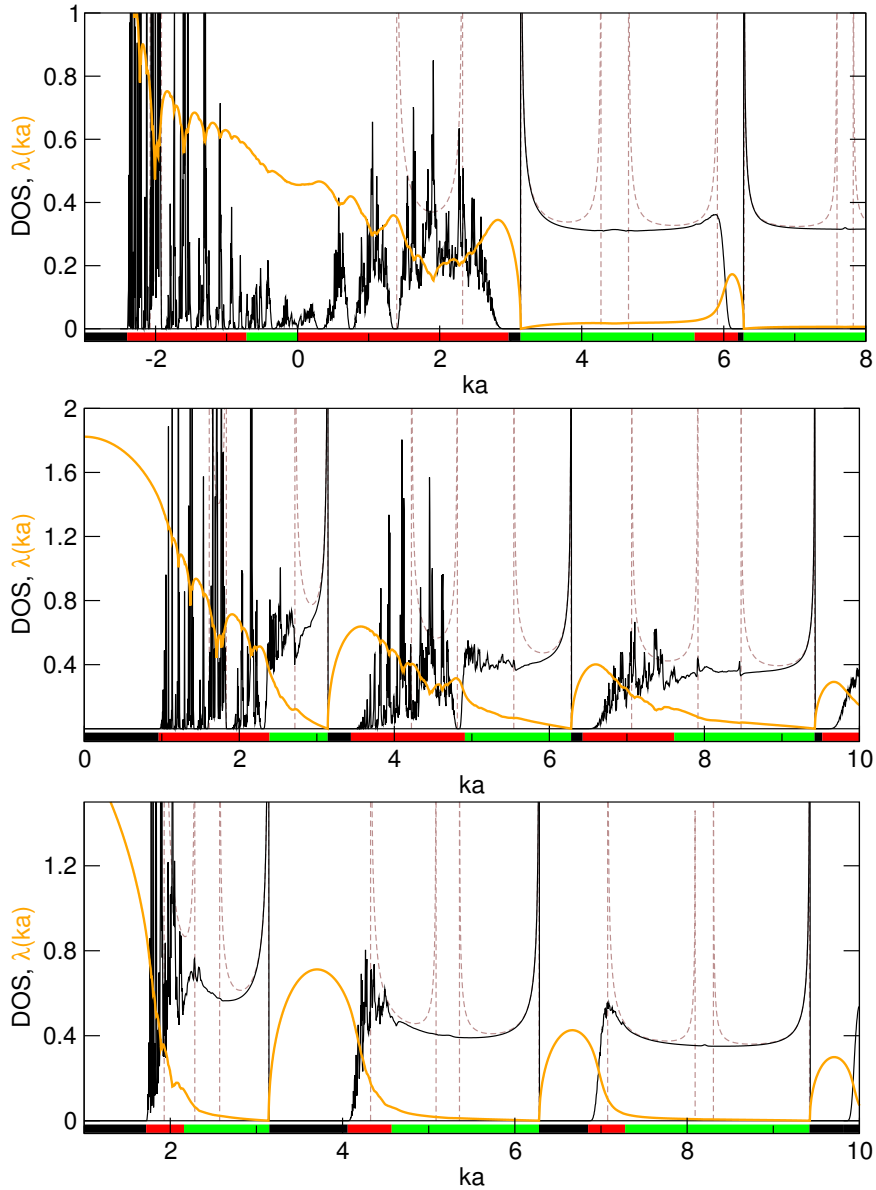
Figure 3.3. DOS (black) and Lyapunov exponent (orange) of several disordered binary wires with parameters $(a/a_\gamma) : -2, -0.25$ (top), $(a/a_\gamma) : 6, 0.5$ (middle) and $(a/a_\gamma) : 2, 4$ (bottom) with equal concentrations. The dashed line corresponds to the density of states of the simplest periodic binary chain in each case. The negative part of the abscissa axis means imaginary values of ka, i.e. negative energies. The different coloured bars on the abscissa axis mean: (black) range forbidden for all species, (red) range forbidden for at least one species, (green) range allowed for all species.
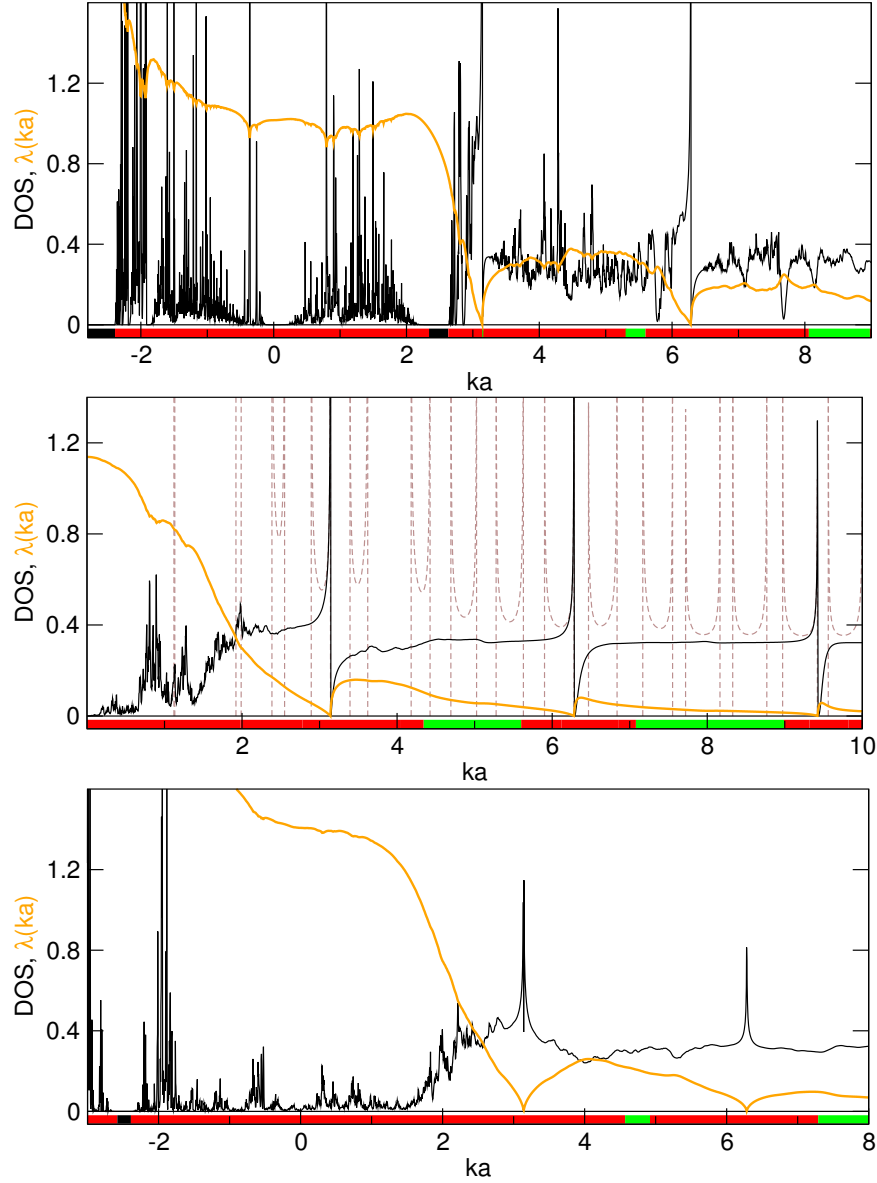
Figure 3.4. DOS (black) and Lyapunov exponent (orange) of several disordered delta wires for three species $(a/a_\gamma)[c_\gamma] : 10[0.3], -1[0.3], -2[0.4]$ (top), five species $(a/a_\gamma)[c_\gamma] : 1[0.2], 2[0.2], 3[0.2], -2[0.2], -0.5[0.2]$ (middle) and eight species $(a/a_\gamma)[c_\gamma] : 1[0.1], -1[0.1], 2[0.1], -2[0.1], 3[0.1], -3[0.1], 4[0.2], -4[0.2]$ (bottom). The dashed line in the middle example shows the DOS for the periodic chain whose primitive cell includes the five species in the order given. The negative part of the abscissa axis means imaginary values of ka, i.e. negative energies. The different coloured bars on the abscissa axis mean: (black) range forbidden for all species, (red) range forbidden for at least one species, (green) range allowed for all species.
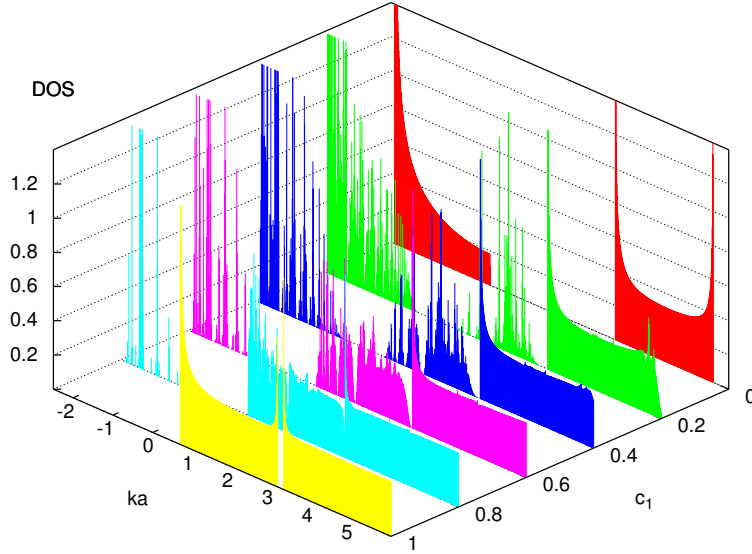
Figure 3.5. DOS of binary wires with species $(a/a_1) = 0.25$ and $(a/a_2) = -2$ for different concentrations.

3.4.1 Features of the distribution of states

Let us comment on the salient features of the density of states of the disordered chains. Firstly let us notice that whenever some of the potential units support bound states, then in the thermodynamic limit a set of permitted levels appears for negative energies, corresponding to pure imaginary values of $\epsilon \equiv ka$, as can be seen in figures 3.3 and 3.4. On the other hand, the higher the energy the less the electrons feel the effect of the potentials and therefore the less they are affected by the disorder. Then, as the energy grows the density of states must approach the free particle distribution of states, that in the variable ϵ is a constant with value $g_{\text{free}}(\epsilon) = 1/\pi \simeq 0.32$. This fact can be observed in the different examples and also it is more clearly seen as the number of atomic species in the wire increases. The distribution of states also shows a particular behaviour for $\epsilon = n\pi$, $n \in \mathbb{Z}$, where independently of the parameters the DOS tends to diverge and resembles the distribution of a periodic chain. This is due to the fact that the multiples of π are permitted levels for all one species pure chains, so that in a mixed system there is always a large number of available states in the vicinity of these energies. But undeniably, the most interesting feature of the spectra of the disordered wires is the irregular and peaky structure appearing in some energy ranges. This strange behaviour is in great contrast with the smooth appearance of the periodic distributions and at first sight it seems a direct consequence of the presence of substitutional disorder in the system. In figure 3.5 the evolution of the DOS of a
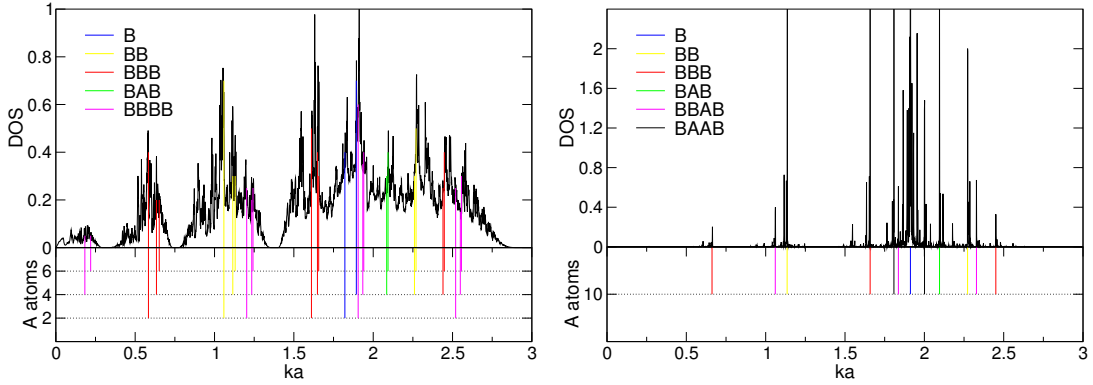
Figure 3.6. DOS for a random binary chain with $(a/a_A) = -2$ and $(a/a_B) = -0.25$ in a range forbidden for the A-type atoms. The concentrations are $c_A = c_B = 0.5$ (left) and $c_A = 0.9$, $c_B = 0.1$ (right). The coloured vertical lines mark the position of eigenstates of different atomic B-clusters surrounded symmetrically by a certain number of A atoms (indicated in the lower ordinate axis), calculated with hard-wall boundary conditions.

pure chain as we dope substitutionally with atoms of a different kind is shown. It can be seen how a sharp-pointed irregular aspect for some energies appears in the disordered configurations. Although this characteristic behaviour of the DOS for this disordered model was more or less distinguished several years ago [4, 91, 92], and it is totally confirmed by the present computational resources, it has not been yet well understood. The general interpretation of the distributions for these systems is non trivial. Nevertheless one can say as a general rule —and following the suggestion of Agacy and Borland [4]— that the peaked regions are more likely to appear in ranges of the spectrum which are forbidden for some of the species involved but not for all of them, since in this latter case the range is also not allowed for the random system. This assertion can be confirmed by studying a random chain composed of two species A and B. In a region forbidden for the A-type chain the allowed energies appearing in the spectrum must be due to atomic clusters involving B atoms. As a result the A atoms surrounding these groups isolate those eigenenergies because this species does not provide any permitted level near the ones introduced by the B atoms, hence inducing a decreasing in the density of states when one moves in a tiny energy region around each of the levels and therefore giving rise to a fluctuating distribution. Thus in principle, one could reproduce the energies where the density of states would be more prominent in this region, from the eigenvalues of certain atomic clusters in which the B species have a substantial contribution. This correspondence can be observed in figure 3.6, where the DOS for a binary random chain within an energy region forbidden for one of the species is compared with the eigenstates of several
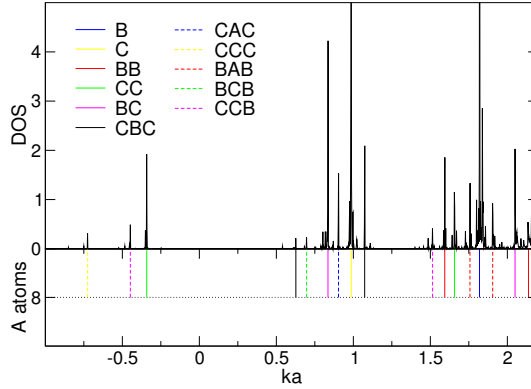
Figure 3.7. DOS for a ternary random chain with $(a/a_A) = 4$, $(a/a_B) = 1$ and $(a/a_C) = -0.5$ and concentrations $c_A = 0.8$ and $c_B = c_C = 0.1$ in a range forbidden for the A-type atoms. The coloured vertical lines mark the position of eigenstates of different atomic clusters surrounded symmetrically by a certain number of A atoms (indicated in the lower ordinate axis), calculated with hard-wall boundary conditions.

atomic clusters calculated with hard-wall boundary conditions using equation (3.20). When the concentrations of both species are equal, it is shown how the eigenstates clusterize around the more peaked regions of the distribution, however one needs to consider a huge number of clusters in order to reproduce all the maxima in this situation. Decreasing the concentration for the species that provides the permitted levels one can see that the sharp points can be quite easily predicted. This behaviour can also be checked when the number of different species increases (figure 3.7).

A cautious investigation of the irregular structure of the distribution of states reveals that this unexpected feature deserves a deeper analysis.

Fractality of the density of states

Let us observe the peaked regions of the distributions in detail. At first sight the apparent roughness make the density of states appear hardly differentiable within those intervals. To decide on the possible lack of differentiability one has to look deeper into the distributions and obtain the DOS in smaller energy ranges, which involves a rigorous and very time-consuming numerical calculation. In figure 3.8 the DOS for a certain random chain is shown for shorter and shorter energy intervals. As can be seen, as the energy domain is made smaller inside the rough region, the distributions reveals a finer structure: new sharp points appear and the density does not evolve smoothly. The existence or not of these irregularities in such a small scale has to be decided by a numerical calculation, thus several technical comments about
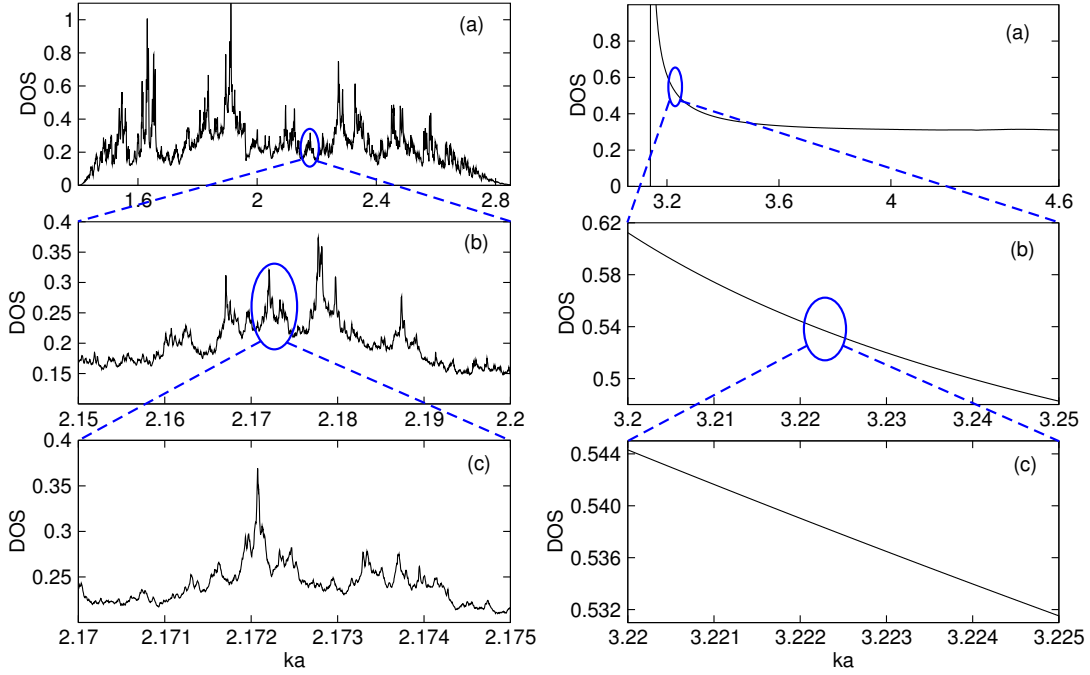
Figure 3.8. DOS for a binary disordered chain with parameters $(a/a_1) = -2$ and $(a/a_2) = -0.25$ and equal concentrations. The left column corresponds to an irregular region and the right one to a smooth region. A global plot of the distribution is shown in figure 3.3

the numerical algorithm seem mandatory here. The functional equation satisfied by the distribution function for the phase $W(\theta)$, is solved with a previous discretization of the phase $\theta \in [0, \pi)$ with a certain number of points, using a self-consistent algorithm that permits knowing $W(\theta)$ up to an error of 10^{-15} in each of the discretized points. Then a numerical differentiation of $W(\pi/2)$ with a sufficiently small step of the energy $\Delta\epsilon$ is performed to obtain the density of states. For a global plot of the DOS, such as those of figures 3.3 and 3.4, taking 5000 points for the discretization and a step of $\Delta\epsilon = 4 \cdot 10^{-3}$ is more than enough and yields very precise results. For the calculation of figure 3.8 we proceeded doubling the number of points for the discretization and checking the convergence of the DOS at each step until the desired accuracy. In all cases the average variation of $g(\epsilon)$ in the last step relative to the domain of the ordinate axis was less than 0.75%. The final parameters were:

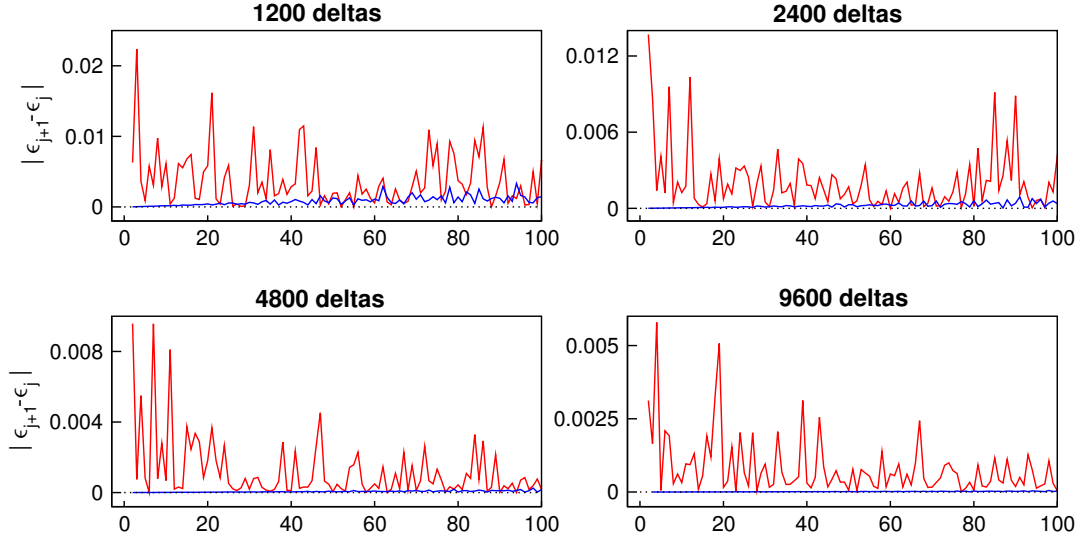|	points for θ	$\Delta\epsilon$
Fig. 3.8 (a)	5001	$7.5 \cdot 10^{-4}$
Fig. 3.8 (b)	35001	$2.5 \cdot 10^{-5}$
Fig. 3.8 (c)	150001	$2.5 \cdot 10^{-6}$

Figure 3.9. Energy spacings for the first 100 eigenlevels appearing inside an irregular zone ($\epsilon > 1.4$, red) and inside a smooth zone ($\epsilon > \pi$, blue) of the spectrum of binary chains with different lengths composed of species $(a/a_1) = -2$ and $(a/a_2) = -0.25$ with equal concentrations (see DOS in figure 3.8). The ordinate corresponding to a point n on the abscissa axis represents the energy distance between the $(n-1)$ and the n level. For a fixed length all the states calculated belong to the same random sequence. The eigenenergies were obtained by carrying out the transmission of the wave function through the system imposing hard-wall boundary conditions.

As a final check we performed the same calculation for the same random chain, with the same parameters but inside an apparently smooth region of the density of states, obtaining the results shown in the right column of figure 3.8 corresponding to a perfectly differentiable function. It seems that the irregular behaviour is not due to numerical errors of the computation and that there exist ranges of the spectrum in which the DOS of the disordered chain is not differentiable. The differentiability of the DOS is a consequence of a regular —almost homogeneous— distribution of the permitted levels inside a small energy interval. A clear view of the differences between the way in which eigenlevels appear inside an irregular region and inside a smooth region of the DOS can be obtained by plotting the energy distances between adjacent permitted levels. In figure 3.9 these spacing distributions are shown for the first 100 permitted levels that appear inside an irregular region of the density of states and inside a smooth zone for several finite length chains. As the length of the array grows the first 100 levels are included in a smaller energy interval, i.e. the energy scale decreases. Following this procedure one sees how the spacing distribution in the smooth region becomes more and more homogeneous, and the energy distance be-

tween neighbouring levels tends regularly to zero which ensures the differentiability of the DOS in that region. On the other hand, the spacing distribution for the levels inside the irregular zone does not show a defined tendency nor a homogeneous aspect as the length of the system increases. In fact this latter distribution exhibits the same aspect whatever the scale in energy is. It is clear that differentiability cannot be reached for the DOS in these irregular ranges.

The results presented strongly support the idea that the density of states for these systems may be fractal in certain energy ranges. Let us analyse rigorously this possibility. First a few words about fractals are in order. Two different type of fractals can be distinguished, namely self-similar fractals and self-affine fractals [16]. The formers are those structures invariant under isotropic scale transformations, i.e. objects such that a part of them enlarged vertically and horizontally by the same factor overlaps exactly the original pattern. An example of this kind is the Cantor set or the Sierpinsky gasket. Self-affine fractals are those invariant under anisotropic scale transformations. For example, a part of a self-affine function $h(x)$ has to be scaled by a factor b according to $h(x) \rightarrow b^{\alpha} h(bx)$ in order to recover the original pattern. If $\alpha = 1$ the scaling would be isotropic and the function would be self-similar. The exponent α is called the Hölder exponent and gives a quantitative measurement of the roughness of the function $h(x)$. When the fractal object emerges from the iteration of a certain rule, it is said to be deterministic. However there exist fractals which are random. In this case the self-similar or self-affine character is decided in a statistical sense, that is when an isotropically or anisotropically enlarged portion of it retains the same statistical properties of the original object. The coastline of a continent is an example of a random fractal.

In our case the DOS seems to behave as a self-affine random fractal in certain energy ranges. To decide on the fractality let us calculate the fractal dimension of the distribution of states within these irregular regions. This task is accomplished by analysing the semivariance of the series of values of the DOS. Let $f(x_i)$ be a value of a discrete series at the point x_i belonging to a certain fixed interval. Then, the semivariance with step s of the series is defined as

$$\Delta_s = \frac{1}{N_s} \sum_{i=1}^{N_s} \left[f(x_{i+s}) - f(x_i) \right]^2, \tag{3.32}$$

where N_s is the number of segments with length s covering the x interval. It can be proved that for a self-affine fractal and sufficiently small values of s the semivariance scales as

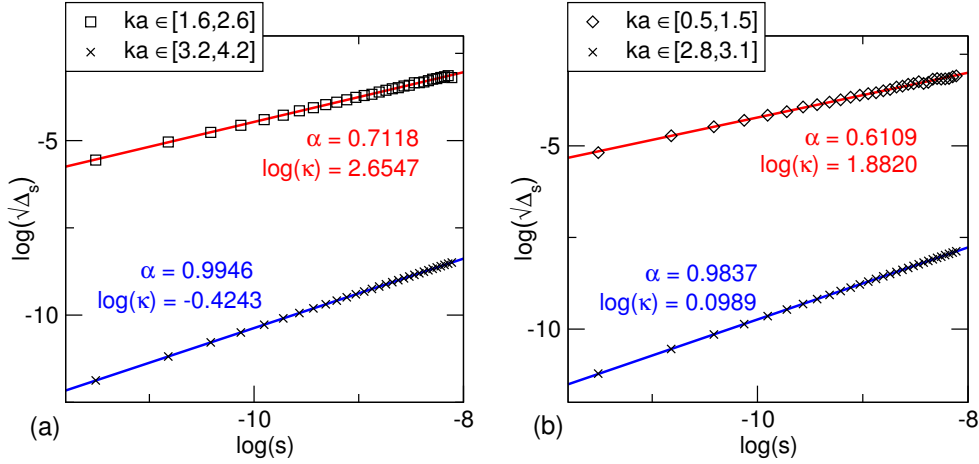$$\sqrt{\Delta_s} = \kappa \cdot s^{\alpha}, \tag{3.33}$$

Figure 3.10. $\log(\sqrt{\Delta_s})$ vs $\log(s)$ for disordered chains in different energy intervals. (a) binary chain with parameters $(a/a_1) = -2$ and $(a/a_2) = -0.25$ and equal concentrations (see DOS in figure 3.3). (b) a five-species chain with parameters $(a/a_\gamma) : 1, 2, 3, -2, -0.5$ and equal concentrations (see DOS in figure 3.4). The legends show the energy interval considered to calculate the semivariance. In all cases s ranges from 10^{-5} to $3 \cdot 10^{-4}$. α and $\log(\kappa)$ mean respectively the slope and the ordinate at the origin of the linear fits.

where κ is a constant and the Hölder exponent satisfies $\alpha = 2 - d_f$ and d_f is the fractal dimension of the series in the interval considered. Then the value of the fractal dimension can be obtained from a linear fit of pairs of values $(\sqrt{\Delta_s}, s)$ in a log-log plot. For our purpose, we proceed considering a fixed energy interval in which the DOS is calculated with a short enough step in energy which is the initial smallest value of s, to obtain subsequently the semivariance of the distribution in the interval given for gradually larger values of the step s. In figure 3.10 the log-log plot of the semivariance and the corresponding linear fit are shown for two disordered infinite chains in different energy ranges corresponding to smooth and irregular regions of their distributions of states. In the case of figure 3.10(a) a binary chain is considered whose DOS can be characterized by a fractal dimension $d_f = 1.2881$ in the range $\epsilon \in [1.6, 2.6]$ whereas in the range $\epsilon \in [3.2, 4.2]$ the fractal dimension changes to $d_f = 1.0054$ which equals the topological dimension of a curve. Then in the latter interval the DOS is not fractal and evolves smoothly. The same thing occurs considering a five species chain in figure 3.10(b) and one can measure $d_f = 1.3891$ for $\epsilon \in [0.5, 1.5]$ and $d_f = 1.0163$ for $\epsilon \in [2.8, 3.1]$.

From this rigorous analysis one is led to the conclusion that fractality in certain energy ranges is a feature of the density of states of delta chains with substitutional disorder. It appears independently of the chain parameters and although further in-

vestigation for other potential models would be needed, the fractal behaviour is probably a universal effect in the sense that it seems a consequence of disorder and the dimensionality of the system only.

Understanding the reason why the distribution of states behaves in a such a peculiar way does not seem trivial. In a previous explanation, the irregular fluctuating aspect of the DOS was justified in terms of permitted levels included in the spectrum by certain atomic clusters, inside energy ranges forbidden for some of the atomic species composing the system. Fractality could also be understood in the following manner. Let us consider a certain piece of the disordered chain. Then, at other positions of the array there certainly exist other pieces with the same length and including the same number of atoms of each species as our initial portion of the system. But all these pieces will differentiate from one another at least in a transposition of two atoms, so that the minimum change from one piece to another is a discrete finite transformation consisting in the interchange of the position of two atoms, due to the structural constraint of the potential. Now if we consider the eigenlevels introduced by one of these pieces of the system, then the permitted levels introduced by the rest of these same length parts cannot be located arbitrarily near the former levels, because of the discretized character of the minimum transformation from one piece to another. In other words, this discretized character of the change among different pieces of the chain, could be possibly translated into an impossibility for the levels introduced in the spectrum by one of these pieces to lay arbitrarily close in energy to the levels introduced by another piece. As a consequence of this effect the energy spacing distribution could not be regularized homogeneously and the density of states would show a fractal behaviour. However, if this was completely correct one would expect a fractal behaviour for all energies and that is not true. There are some energy ranges for which the distribution of states is regular and smooth for the disordered systems. The non-fractal character is more likely to appear in ranges of the spectrum permitted for all the species composing the chain (see figures 3.3 and 3.4). Somehow the fact that a given energy interval is allowed for all the species permits the distribution to become smooth and regular, although the regularization is only strictly reached when the chain is infinite and for a finite array the DOS shows and irregular behaviour inside these energy zones also, as can be seen in figure 3.11.

As a summary the emergence of fractality could be probably due to a combination of the effects described: the discrete character of the minimum change among different portions of the system, together with the existence of ranges forbidden for some of the atomic species involved. The border between fractal and non-fractal zones is not very clear and also it might not be possible to describe the fractal character of a
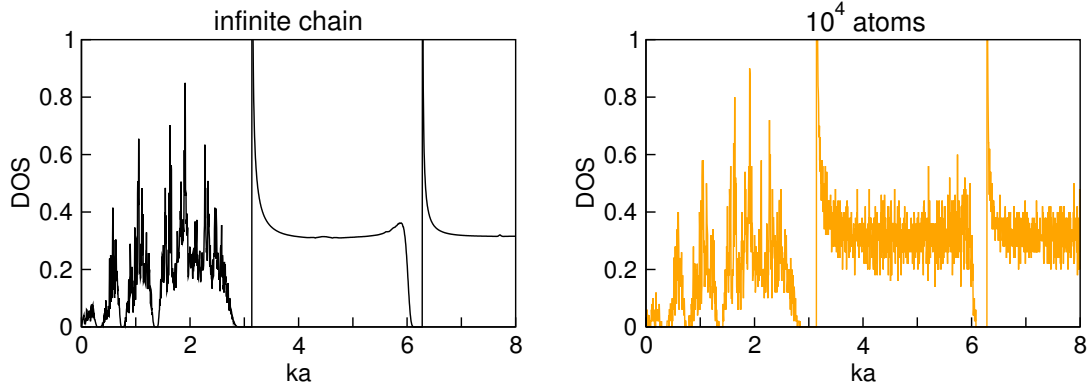
Figure 3.11. Comparison of the DOS for a finite chain (right) with the distribution corresponding to the thermodynamic limit (left). The system is a binary random chain with parameters $(a/a_1) = -2$ and $(a/a_2) = -0.25$ and equal concentrations.

distribution by a single fractal dimension. The density of states for this disordered model shows a highly complex, unexpected and non-trivial behaviour.

3.4.2 Electronic localization

For a one-dimensional system with completely random disorder one generally expects to find the spatial localization of the electronic states. In our case the system exhibits random substitutional disorder together with an underlying structural ordering that surely affects the electronic properties. In figures 3.3 and 3.4 it can be observed how for the different configurations considered in the thermodynamic limit the Lyapunov exponent takes finite non-zero values for all energies, indicating the exponential spatial localization of the states, except for the discrete set $\epsilon = n\pi$, $n \in \mathbb{Z}$, for which the inverse localization length vanishes. Before discussing the nature and the implications of the π-resonances in detail, let us first comment on the general features of the Lyapunov exponent. As the energy grows the Lyapunov exponent shows a tendency to decrease, corresponding to the natural approach to the free particle behaviour, and also the localization length seems to be related to the distribution of states. As can be seen in the examples of pages 38 and 39, the Lyapunov exponent tends to decrease in the peaks of the DOS and increase in the troughs. It seems that the state is less localized when it lies on a range containing a large number of permitted levels close to its energy, whereas on the contrary an isolated energy shows always a stronger localization. The localization length at a given energy depends on the value of the DOS for the rest of the spectrum as stated by Thouless [179, 180]. It is also remarkable that inside the smooth regions of the DOS the Lyapunov exponent takes lower values than inside the fractal ranges of the distribution, which are apparently connected with
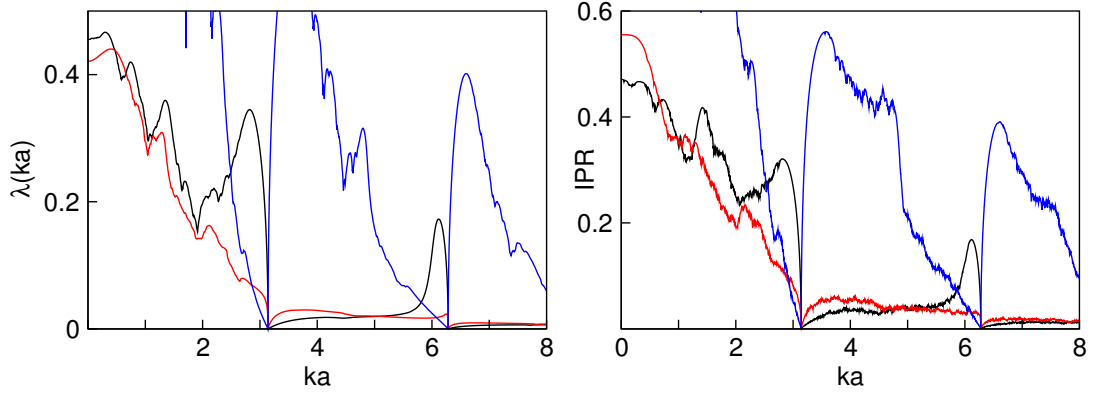
Figure 3.12. Comparison of the Lyapunov exponent and the inverse participation ratio as functions of the energy, for different binary disordered chains. The parameters for the different chains are $(a/a_\gamma)[c_\gamma]$: $-2[0.5], -0.25[0.5]$ (black), $1[0.4], -1[0.6]$ (red), $6[0.5], 0.5[0.5]$ (blue). The IPR is obtained averaging over 100 realizations of a 1000-atom array.

a strong localization. The localized character of the states can also be quantify by the inverse participation ratio that measures directly the spatial extension of the wave function. In figure 3.12 it is clearly seen how the tendency of the IPR as a function of the energy agrees quite well with the evolution of the Lyapunov exponent in the thermodynamic limit.

Regarding the π-resonances of this model, the first evidence of their existence appears explicitly in a work by Agacy and Borland, however they did not comment on this fact that their computations clearly showed [4]. Later, Ishii describes these special energies of the model [109]. This is one of the first disordered systems in which extended states were found coexisting with localized ones. Let us analyse the reason why these extended states can survive within the disordered system. Recalling the study of short aperiodic sequences with hard-wall boundary conditions in section 3.3, the multiples of π were eigenlevels of the infinite well unperturbed by the delta potentials due to their punctual nature. From this fact, one is tempted to conjecture that the resonances remain in the infinite system because of the punctual character of the potential, and this is not completely true. To understand the appearance of these special energies let us consider first the canonical equation for a free particle. By sampling the wave function at different spatial points placed at arbitrary distances, one obtains the relation

$$\Psi_{j+1} = [\cos(kx_j) + \cot(kx_{j-1})\sin(kx_j)]\Psi_j - \frac{\sin(kx_j)}{\sin(kx_{j-1})}\Psi_{j-1}, \qquad (3.34)$$

that naturally describes extended states, where x_j is the length between the positions corresponding to Ψ_j and Ψ_{j+1}. In the simplest case when the sampling is regularly

taken at distance a this expression reduces to

$$\Psi_{j+1} = 2\cos(ka)\Psi_j - \Psi_{j-1}. \tag{3.35}$$

The canonical equation for the electrons inside the disordered system reads

$$\Psi_{j+1} = 2\left(\cos(ka) + \frac{(a/a_j)}{ka}\sin(ka)\right)\Psi_j - \Psi_{j-1}, \tag{3.36}$$

that in the cases $ka = n\pi$, $n \in \mathbb{Z}$, turns out to be the same for all sites of the system as the free canonical equation

$$\Psi_{j+1} = \pm 2\Psi_j - \Psi_{j-1}. \tag{3.37}$$

Therefore the localization length diverges at those energy values in the thermodynamic limit. Whenever the canonical equation of a system for a certain value of the energy and for all its sites reduces to the free canonical form, an extended state appears. And the punctual nature of the potentials is not a crucial condition in principle for this coincidence to happen.

It is important to know the functional dependence of the localization length on the energy near the resonances, since it determines the role these extended states play in the transport through a finite chain. Azbel and Soven concludes that for certain binary chains the localization length near the π-resonances behaves asymmetrically as $|\epsilon - n\pi|^{-1}$ and $|\epsilon - n\pi|^{-1/2}$ [14, 15, 13]. In fact, from their results it is straightforward to obtain the value of the coefficients for each case. Defining $V = c_1(a/a_1) + c_2(a/a_2)$ and $\overline{V} = (a/a_1) - (a/a_2)$, if $V > 0$ then the Lyapunov exponent obeys

$$\lambda(\epsilon) = \begin{cases} \dfrac{c_1 c_2 \overline{V}^2}{4|V|n\pi}|n\pi - \epsilon| + O\left(|n\pi - \epsilon|^2\right), & \epsilon \leqslant n\pi \\[4mm] \sqrt{\dfrac{2|V|}{n\pi}}|\epsilon - n\pi|^{1/2} + O\left(|\epsilon - n\pi|^{3/2}\right), & \epsilon > n\pi \end{cases} \tag{3.38}$$

and for $V < 0$ the dependence is the same but the energy intervals appear reversed. The above expressions are correct only when the following strange relation holds [14]

$$4\epsilon|2V\cot(\epsilon) - \epsilon| \gg 2|\overline{V}|\left[8c_1 c_2 \overline{V}\epsilon\cot(\epsilon)\right]^{2/3}. \tag{3.39}$$

For the multiples of π both members of the inequality diverge, and the left hand side term increases always faster than the other in a region close enough to the resonance if $V \neq 0$ and for all $\overline{V}$. Then, the above requirement limits the energy interval around the resonance where the behaviour of the Lyapunov exponent can be well approximated by equation (3.38). If this interval is very short then the exponents described
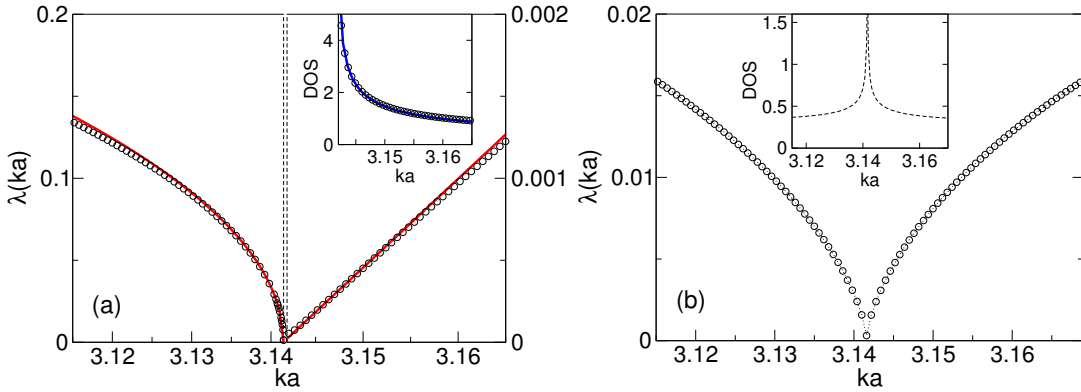
Figure 3.13. Lyapunov exponent for binary disordered chains near the resonance $\epsilon = \pi$. Solid lines correspond to analytical expressions (3.38) for the Lyapunov and (3.40) for the DOS, while circles mark numerical results. (a) Parameters $(a/a_1) = -2$ and $(a/a_2) = -0.25$ with equal concentrations. The inset shows the DOS. Notice that for the Lyapunov exponent the vertical scales are different before and after the resonance to ensure an optimal visualization. (b) Parameters $(a/a_1) = 1$ and $(a/a_2) = -1$ with equal concentrations. The inset shows the numerical DOS. Notice the symmetric behaviour of the quantities.

may not be properly distinguished. Only the binary chains with $V = 0$ show different values for the critical exponents. In figure 3.13(a) the Lyapunov exponent for a binary chain is plotted in the vicinity of $\epsilon = \pi$. The asymmetric structure of the localization length around the resonance is clearly due to the asymmetric behaviour exhibited by the density of states. The exponent $1/2$ for λ corresponds to the side of the resonance showing a gap in the distribution of states and the linear dependence with the energy corresponds to the other side where permitted levels appear. The length of the energy range in which equation (3.38) rules is clearly related to this asymmetry of the DOS: if permitted levels start appearing on the gap side of the resonance then the energy interval for the critical exponents given becomes shorter. In fact for $V = 0$ the DOS is perfectly symmetric around the resonances and coherently the Lyapunov exponent is also symmetric and does not obey (3.38), as can be seen in figure 3.13(b).

The localization length seems to behave in different manners near the resonances depending on the number of species composing the wire and the distribution for their parameters. Ishii found exponents $1/2$ for $\lambda(\epsilon)$ when considering a Cauchy distribution for the species [109].

From the behaviour of the localization length around the critical energies in the thermodynamic limit, one can estimate the effect of the presence of these singular extended states on the transport properties of a finite system. Since the Lyapunov exponent for the finite sample fluctuates around its mean value, corresponding to the

thermodynamic limit value, one can say from equation (3.38) that for a finite system containing N atoms, there is a zone beside the π-resonances of width $|\epsilon_0 - n\pi| \sim N^{-1}$ in which the states have a localization length larger than the system size, where $\lambda(\epsilon_0) = N^{-1}$. And the number of such states can be calculated from the DOS, that near the resonance behaves as the distribution for a periodic chain as discussed in section 3.4.1. From the analytical expression (3.17) one finds

$$g(\epsilon) = \left| \mathrm{Re} \left(\frac{\sqrt{-(a/a_1) - (a/a_2)}}{2\pi\sqrt{n\pi}} [\epsilon - n\pi]^{-1/2} \right) \right| + O\left([\epsilon - n\pi]^{1/2} \right). \qquad (3.40)$$

And therefore the number of states participating actively in the transport through a finite chain for each resonance is

$$\left| \int_{n\pi}^{\epsilon_0} N g(\epsilon) \mathrm{d}\epsilon \right| \sim \sqrt{N}. \qquad (3.41)$$

This is the same scaling exhibited by models with isolated extended states arising from the presence of a correlated disorder such as the random dimer [73, 29, 161] and other correlated schemes [68]. The manner in which these levels whose localization length is larger than the system size, appears near the resonances is very peculiar. Inspecting the vicinity of a multiple of π considering a tiny energy scale for a finite length system, one observes the behaviour shown in figure 3.14. As the length of the system increases, the states corresponding to transmission resonances (marked by a sharp decrease of the Lyapunov exponent) start approaching the exact value of π. The larger the system the more the states squeeze together near $\epsilon = \pi$ (figure 3.14(a)). It may be surprising the fact that the exact value $\epsilon = \pi$ is not a transmission resonance when the length of the chain is finite. This energy becomes a resonance only when the length of the system goes to infinity. The reason for this is clear: the transmission resonances somehow correspond to virtual states of the continuum spectrum of the system, whose nature is absolutely determined by the boundary conditions. Therefore when one considers a finite length system, the resonances arise at the energy values for which the states can satisfy the proper scattering boundary conditions at the extremes of the system with a high value of the transmission, and one expects the fulfilling of the boundary conditions to depend on the length and on the sequence of the chain. Then, the appearance of transmission resonances in the spectrum of a finite disordered system is an agreement between two factors: the spatial extension of the state and the boundary conditions. The former determines the range of energies in which one could find high transmission efficiencies (i.e. a range with low values of the Lyapunov exponent and the IPR) and the latter establishes the precise values of the energies within this range where the resonances occur. Of course this effect only becomes apparent at a very small scale of energies.
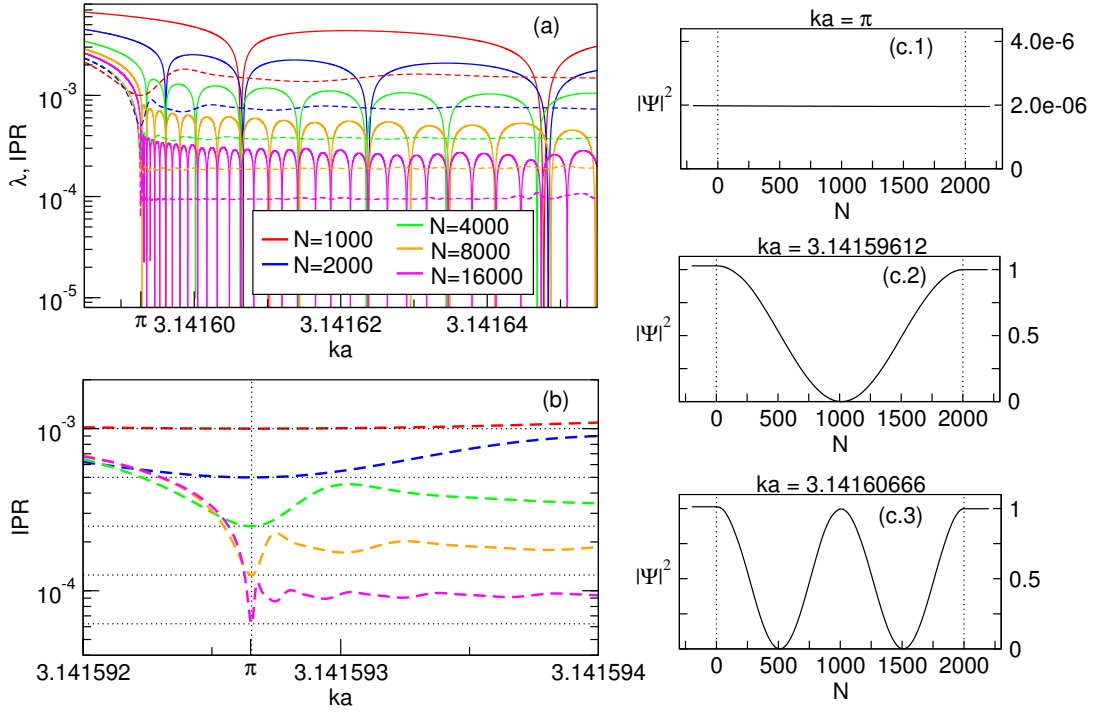
Figure 3.14. (a) Lyapunov exponent and IPR near the resonance $\epsilon = \pi$ for finite length binary chains with parameters $(a/a_1) = -2$, $(a/a_2) = -0.25$ and equal concentrations. The coloured solid lines correspond to the Lyapunov exponent while the dashed lines show the IPR. (b) Magnification of the IPR near the resonance. The horizontal dotted lines mark the inverse of the length of the sample for each case. Graphics on the right column show the envelope of the electronic states for the sequence with $N = 2000$ atoms for three different energies: π and the two first transmission resonances corresponding to the sharp decrease of the Lyapunov exponent. The data of all figures correspond to the same sequence for a given length.

Inspecting the IPR around $\epsilon = \pi$, one finds that for a small scale of energies the inverse participation ratio does not reproduce the behaviour of the Lyapunov exponent, so that the transmission resonances cannot be correctly identified from this quantity. For the different lengths considered the IPR reaches its minimum value N^{-1} exactly at $\epsilon = \pi$ and for higher energies it shows higher values of the same order of magnitude (figure 3.14(b)). The behaviour of the IPR can be understood by observing the explicit form of the envelope of the electronic state at different energies. In figures 3.14(c) the states at $\epsilon = \pi$ and at two transmission resonances for the 2000-atom chain can be seen. The IPR gives us information about the spatial structure of the state, but since it is a normalized quantity it lacks any information about the amplitude of the state, which is essentially the transmission. Hence the IPR does not retain all the information about the boundary conditions. It can be seen in figure 3.14 how the state (c.1)
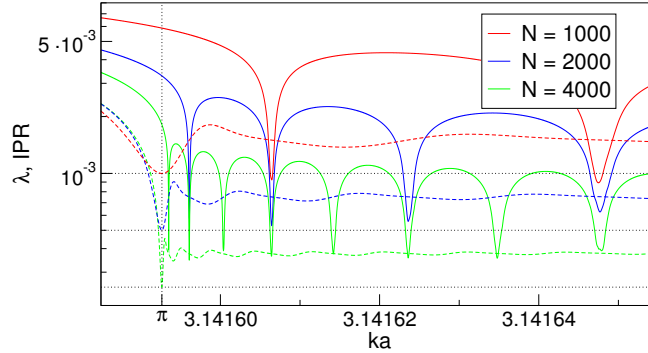
Figure 3.15. Lyapunov exponent (solid lines) and IPR (dashed lines) for binary disordered chains with the same parameters as in figure 3.14. Both quantities have been averaged over 100 realizations of the disorder for each length. The horizontal dotted lines mark the position of the inverse of the length of the system.

is strictly more extended that (c.2) and (c.3) which have valleys with zero amplitude, therefore one expects the IPR in the first case to be smaller than for the other two cases. However, the amplitude for (c.1) is almost zero ($T = 1.96 \cdot 10^{-6}$) while for the other two energies the states live with a transmission coefficient close to unity. If the length of the system grows, the amplitude of the state for $\epsilon = \pi$ would increase so that for an infinite system the state would be perfectly flat with amplitude 1. As a summary, the IPR ignores everything concerning the value of the global amplitude of the state and although open boundary conditions are absolutely necessary to build the state correctly, the information of the transmission coefficient is not contained in the IPR, and this makes it useless for identifying the exact energies of transmission resonances of a finite system within very small ranges of energy. On the other hand this fact means that the IPR retains the information of the thermodynamic limit and as can be seen in figure 3.14(b) the minimum value N^{-1} is reached independently of the length of the system for the energy $\epsilon = \pi$, which we know to be an extended state in the thermodynamic limit. It seems that this behaviour of the IPR is a fingerprint of the existence of a state with a divergent localization length, and in principle it could be useful for identifying such states in other models by studying finite realizations of the systems.

Finally, it can be checked that the behaviour described for the Lyapunov exponent and the IPR for finite chains near the π-resonances depends mainly on the length of the system. In figure 3.15 both quantities are plotted for different lengths of the array after averaging over 100 realizations of the disorder for each length. It can be seen how the hollows of the LE are slightly broadened in energy and shortened in height due to the averaging process, but they are still present manifesting the weak dependence of the
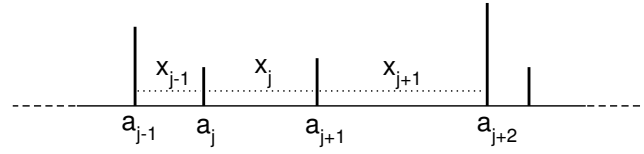
Figure 3.16. Delta chain with structural and substitutional disorder.

transmission resonances upon the particular disordered sequence for a given length. The IPR shows the same aspect as for a single realization of the disorder. This confirms the fact that at this energy scale the IPR contains the information of the system in the thermodynamic limit. This strong dependence on the number of sites explains why when the length of the system is increased proportionally, as in figures 3.14 and 3.15, the transmission resonances appear following a self-similar pattern.

3.5 Wires with uncorrelated structural and substitutional disorder

Besides substitutional disorder one can also include structural disorder as an additional ingredient of the model: the case in which the delta potentials with different couplings following a random sequence are not placed on a regular lattice. The interatomic distances are also random being determined by a certain probability distribution. One-dimensional models with structural disorder for which the distribution of interatomic distances is continuous are known as one-dimensional liquid models. In 1960 the delta model only with structural disorder was studied by Frisch and Lloyd [86] and Borland, who derived and integral equation for obtaining the DOS and the localization length in the thermodynamic limit [25, 26]. This integral equation was later numerically solved showing the effects of structural disorder upon the distribution of a periodic pure chain: as the degree of structural disorder increases the gaps in the spectrum get narrower and the divergences of the DOS at the band edges disappear in a kind of 'melting' process [28]. More recently, the structural disordered delta model has been considered in the approximation of weak disorder with long-range correlations [113] and it has also been used to show how a 1-D disordered conductor in the coherent regime, without considering inelastic collisions, can behave in a metallic way due to thermal smearing and resonant tunnelling [143].

Our system exhibiting structural and compositional disorder is shown in figure 3.16. Now each potential is determined by two parameters: the delta coupling and the distance after the delta. The canonical equation that rules the system takes the

form

$$\Psi_{j+1} = J(x_{j-1}, x_j, a_j)\Psi_j - \frac{K(x_j)}{K(x_{j-1})}\Psi_{j-1}, \tag{3.42}$$

where

$$J(x_{j-1}, x_j, a_j) = \cos(kx_j) + \cot(kx_{j-1})\sin(kx_j) + \frac{2}{ka_j}\sin(kx_j), \tag{3.43}$$

$$K(x_j) = \sin(kx_j). \tag{3.44}$$

The function J depends on the coupling a_j and the distance x_j of the j sector and the distance x_{j-1} of the $(j-1)$ sector while K is determined by the distance of each sector. The system is composed of a discrete number of different species with different concentrations and the interatomic spacings are determined by a continuous distribution which is chosen to satisfy the following requirements:

- It is the same for all atomic species.

- It maximizes at $x_j = a$ for all j. a being the interatomic distance of the regular lattice.

- It is symmetric around the value a and therefore its domain is the interval $(0, 2a]$ in which it must be correctly normalized.

Our distribution for the distances shall be denoted by $P(l, \sigma)$, where $l \equiv x/a$ is a dimensionless variable and σ measures the degree of structural disorder. And it reads

$$P(l, \sigma) = \frac{1}{\mathcal{N}(\sigma)}\frac{1}{\sigma\sqrt{\pi}}e^{-\frac{(l-1)^2}{\sigma^2}}, \tag{3.45}$$

where $\mathcal{N}(\sigma)$ is the normalization factor. $P(l, \sigma)$ is a probability density for the values of the interatomic distances and it satisfies

$$\lim_{\sigma \to 0} P(l, \sigma) = \delta(l - 1), \tag{3.46}$$

$$\lim_{\sigma \to \infty} P(l, \sigma) = \frac{1}{2}. \tag{3.47}$$

The spacing distribution (figure 3.17) is normal for low values of σ and it approaches a constant distribution as σ grows. The most important changes occur in the range $\sigma = 0 - 1$ whereas for higher values the distribution is almost flat. The crossover value above which the Gaussian behaviour is distorted is $\sigma \sim 0.4$.

The properties of this one-dimensional system in the thermodynamic limit are obtained using the functional equation formalism. In terms of the dimensionless variables l and $\epsilon \equiv ka$ the functions of the canonical equation read

$$J\left(\bar{l}, l, a_\gamma\right) = \cos(l\epsilon) + \cot\left(\bar{l}\epsilon\right)\sin(l\epsilon) + \frac{2(a/a_\gamma)}{\epsilon}\sin(l\epsilon), \tag{3.48}$$
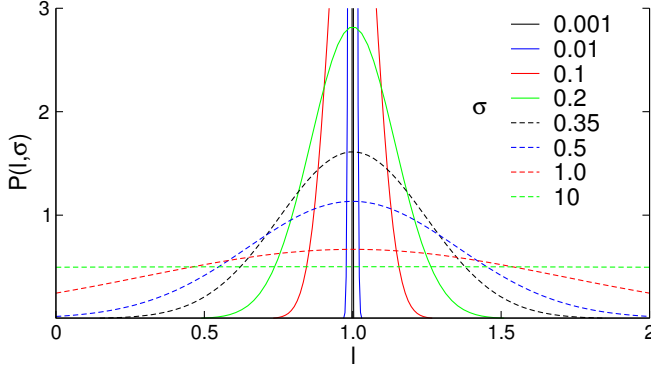
$$K(l) = \sin(l\epsilon). \tag{3.49}$$

Figure 3.17. Probability density function for the interatomic distances.

The relevant functions $\mathcal{T}^{-1}\left(\theta; \bar{l}, l, a_\gamma\right)$ and $\mathcal{F}\left(\theta; \bar{l}, l, a_\gamma\right)$ needed to construct the functional equations are obtained from definitions (2.3) and (2.4). In this case the functional equations take the form (see appendix D),

$$W_l(\theta) = \sum_\gamma c_\gamma \int_0^2 P\left(\bar{l}, \sigma\right) \mathrm{d}\bar{l}\left|W_{\bar{l}}\left(\mathcal{T}^{-1}\left(\theta; \bar{l}, l, a_\gamma\right)\right) - W_{\bar{l}}\left(\frac{\pi}{2}\right) + \delta\left(\bar{l}, l\right)\right|,$$

(3.50a)

$$W_l(\theta + n\pi) = W_l(\theta) + n, \qquad \theta \in [0, \pi), \, n \in \mathbb{Z},$$

(3.50b)

where $\delta\left(\bar{l}, l\right) = 1$ if $[K(l)/K\left(\bar{l}\right)] > 0$ and $\delta\left(\bar{l}, l\right) = 0$ otherwise. A phase distribution function $W_l(\theta)$ is defined for each value of l. A discretization of the spacing distribution must necessarily be taken to carry out the numerical solving. The Lyapunov exponent and the DOS per atom are obtained respectively from

$$\lambda(\epsilon) = \frac{1}{2}\int_0^2 P\left(\bar{l}, \sigma\right) \mathrm{d}\bar{l} \int_0^\pi \mathrm{d}W_{\bar{l}}(\theta)\left[\sum_\gamma c_\gamma \int_0^2 P(l, \sigma)\mathrm{d}l \, \log \mathcal{F}\left(\theta; \bar{l}, l, a_\gamma\right)\right], \quad (3.51)$$

$$g(\epsilon) = \left|\int_0^2 P(l, \sigma)\mathrm{d}l \, \mathrm{sgn}\left[K(l)\right]\frac{\mathrm{d}W_l\left(\frac{\pi}{2}\right)}{\mathrm{d}\epsilon}\right|. \quad (3.52)$$

Let us analyse the effect of structural disorder on the distribution of states. In figure 3.18 the evolution of the DOS versus σ is shown for a binary and a ternary chain. It can be clearly seen how when the structural disorder appears the density of states registers a tendency to smooth down. The gaps close as σ increases, the divergences at the π-resonances disappear and the distribution becomes very homogeneous in the whole energy range approaching the value of the DOS for the free particle. The higher the structural disorder the more regular the distribution becomes independently of the number of species and their concentrations. And what is more interesting, the fractal nature of the DOS in certain ranges due to the substitutional disorder is absolutely removed. In fact the dependence of the fractal behaviour on the
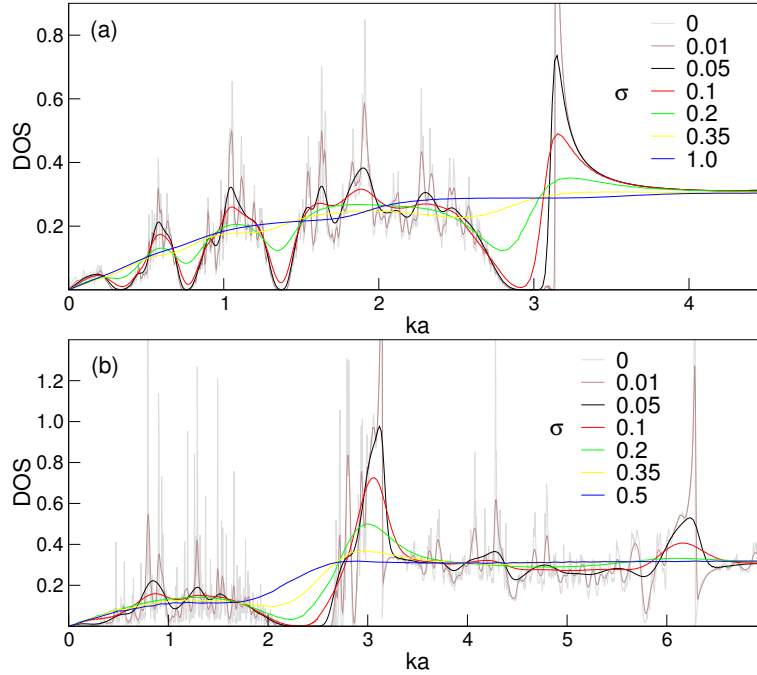
Figure 3.18. Evolution of the DOS vs degree of structural disorder (σ). (a) binary chain with parameters $(a/a_1) = -2$, $(a/a_2) = -0.25$ and equal concentrations. The case $\sigma = 0$ is also shown in figure 3.3. (b) ternary chain with $(a/a_\gamma)[c_\gamma] : 10[0.3], -1[0.3], -2[0.4]$. The case $\sigma = 0$ is also shown in figure 3.4.

structural disorder seems critical. For the binary chain considered in figure 3.18(a) the calculation of the fractal dimension in the range $\epsilon \in [1.6, 2.6]$ yielded $d_f = 1.29$ as discussed in section 3.4.1. Considering a small energy interval $\epsilon \in [1.8, 1.85]$ and a small value for sigma $\sigma = 0.05$ a careful analysis reveals that the fractal dimension has diminished to $d_f = 1.05$. For such a low degree of the structural disorder fractality has almost completely disappeared and the DOS shows the aspect of a differentiable curve. This fact somehow confirms the reasoning of the previous section for explaining the fractality of the distribution, based on the discretized character of the change among different pieces of the chain containing the same number and species of atoms, due to the structural constraint of the regular arrangement. Now the interatomic distances obey a continuous distribution. This means that if we consider a piece of the infinite chain, there certainly exist other pieces with the same length and including the same number and species of atoms which differentiate from the former portion in an infinitesimal displacement of the position of only one atom. So that the spatial changes among substitutionally identical portions of the wire obeys a continuous distribution and they are not discretized. This makes it possible that the permitted levels introduced by one of these pieces can lie arbitrarily close to levels introduced
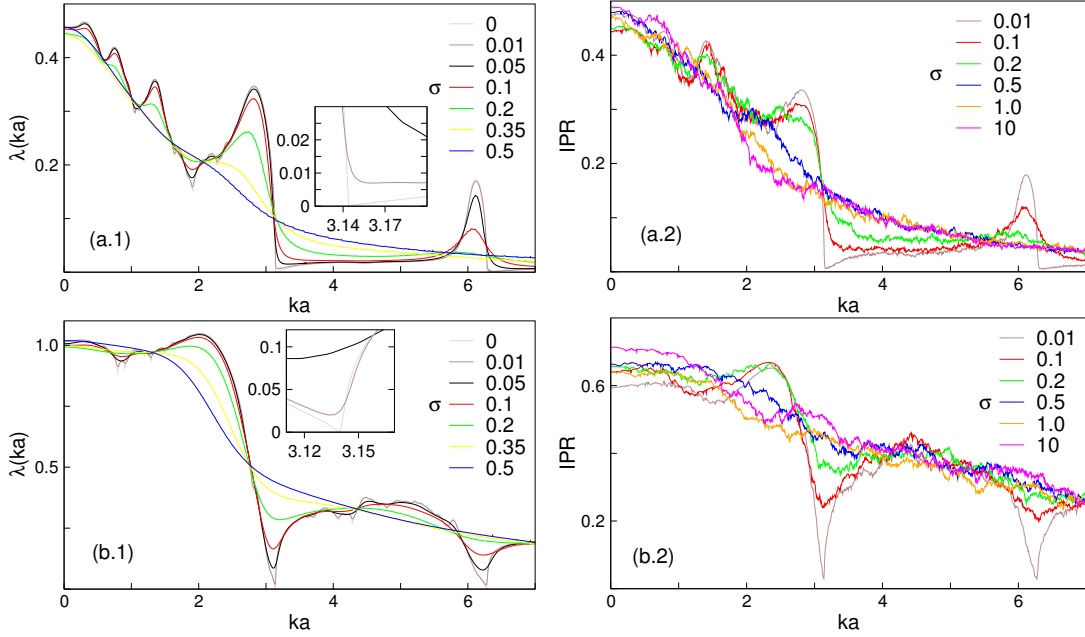
Figure 3.19. Lyapunov exponent (left) and IPR (right) for different degrees of structural disorder for (a) binary chain and (b) ternary chain with the same parameters as in figure 3.18. The insets show a magnification of λ in the vicinity of $\epsilon = \pi$. The IPR corresponds to an average over 100 realizations of a 1000-atom sequence.

by another piece of the system. As a result a regularization of the distribution of states within small energy intervals can be achieved and the differentiability is then guaranteed.

Regarding the effect of structural disorder upon localization of electronic states, the π-resonances must disappear for a non-vanishing σ. This must be expected since these extended states survive in the substitutionally disordered wire due to the regular arrangement of the potentials, as discussed in the previous section. One can check that for $\epsilon = n\pi$ the canonical equation of the system (3.42) is no longer identical to the canonical equation for the free particle (3.34). As σ increases the Lyapunov exponent tends to lose its original structure in a kind of smoothing process until it becomes a monotonically decreasing function with the energy (figure 3.19). This seems a general behaviour independently of the compositional parameters. Structural disorder rearranges the states in such a way that the localization length decreases with σ for some energies and increases for other energies in search of a balance. This effect is also confirmed by the IPR as can be seen in figure 3.19. For $\sigma = 1$ the spacing distribution is quite flat and keeping increasing its value does not mean an essential change in the localization of the carriers. This can be observed comparing the IPR for $\sigma = 1$ and $\sigma = 10$ in the examples given.

To conclude let us say that the presence of structural disorder in the system could be viewed somehow as a result of a finite non-zero temperature. Although temperature effects of course have to be taken into account in terms of electron-phonon interactions and through the Fermi-Dirac distribution modifying the population of active carriers, the thermal vibrations of the atoms are simply a series in time of structurally disordered configurations. Therefore thinking naively one could understand the effects of structural disorder as the effects of temperature on the basic spectrum of the system within the independent particle approximation.

3.6   Wires with correlated substitutional disorder

Once the properties of the completely random system have been analysed, let us consider now the case in which the disorder in the system shows statistical correlations. This means that the values of the parameters characterizing the atomic potentials are not randomly assigned, but the type of potential appearing at a certain site can depend on its neighbours. Correlations can be classified according to the range of this dependence. One roughly speaks of short-range correlations when the length of the system is much larger than the correlation length and long-range correlations when both lengths are comparable. Of course these definitions make sense only for long enough systems. The delta potential model has been treated in the literature with both types of correlations. Short-range correlations in the case of the random-dimer substitutional model [161, 64, 160], consisting in imposing for a binary chain that at least one of the potentials appears always in pairs that are randomly placed. As a result of this correlation new isolated extended states are included in the spectrum together with a set of states close to the resonant one whose localization length is larger than the system size, that participate actively in the transport processes as it has been experimentally verified in semiconductor structures [18]. And long-range correlations, in the approximation of weak disorder, with substitutional [112] and structural disorder [113]. The effect of this type of correlations is the emergence of a continuum set of extended states in the spectrum and mobility edges for the electrons. These predictions have also been experimentally confirmed in microwave experiments [124, 125].

We consider a very natural model of short-range correlations in which for fixed concentrations of the atomic species one can choose the probability of appearance of the different binary clusters composing the system. The system will be characterized by the species concentrations $\{c_i\}_{i=1,...,m}$ where m is the number of different species, and by an additional set of probabilities $\{p_{ij}\}_{i,j=1,...,m}$ where p_{ij} means the probability

for an i-atom to be followed or preceded[2] by a j-atom. Thus the frequency of appearance of binary atomic clusters can be altered by these quantities. The probability of finding at any position the couple $-ij-(-ji-)$ would be $c_i p_{ij}$ or equivalently $c_j p_{ji}$. Then in the thermodynamic limit the physical properties of such a system will depend upon the couplings of the species, the concentrations and the probabilities $\{p_{ij}\}$. This correlated model naturally includes the situation when the disorder in the wire is completely random, that is just defined by the values $p_{ij} = c_j$ for all i, j. The correlations introduced in this way must be the consequence of the existence of an atomic interaction (or the effect of some physical parameter such as the size of the atoms) which might choose certain spatial sequences of the potentials modifying subtly the otherwise chain's purely random character. Thus this procedure seems a natural manner to account for correlations which can be present in nature or even those that can be produced inside a manufactured disordered quantum wire in a non-intentional way, aside from the fact that of course one can always try to construct a wire exhibiting the desired correlations to recover the theoretical results.

Once we have understood the meaning of the correlations, let us check the relations among them. The following equations must be satisfied:

$$c_i p_{ij} = c_j p_{ji}, \tag{3.53a}$$

$$\sum_{j=1}^{m} p_{ij} = 1, \tag{3.53b}$$

$$0 \leqslant p_{ij} \leqslant 1, \qquad i, j = 1, \ldots, m. \tag{3.53c}$$

According to these expressions the correlation matrix $\mathbf{P} \equiv (p_{ij})$ is completely known from the $m(m-1)/2$ above diagonal elements, where m is the number of different species. However these elements are not completely independent due to (3.53c), because when one of the correlations is chosen, the maximum allowed value for some of the others is affected. This fact can be clearly seen in two simple examples:

2 species: the matrix is completely determined by p_{12},

$$p_{11} = 1 - p_{12}, \qquad p_{21} = \frac{c_1}{c_2} p_{12}, \qquad p_{22} = 1 - p_{21},$$

and it must be $p_{21} \leqslant 1 \Rightarrow p_{12} \leqslant \frac{c_2}{c_1}$. Therefore $p_{12} \leqslant \min\left\{1, \frac{c_2}{c_1}\right\}$.

3 species: the matrix is determined by p_{12}, p_{13}, p_{23}. And we choose their values in this order. $p_{12} \leqslant \min\left\{1, \frac{c_2}{c_1}\right\}$ which implies $p_{13} \leqslant \min\left\{1 - p_{12}, \frac{c_3}{c_1}\right\}$. On the

---

[2]This requirement follows from a simple reflection symmetry argument although it is strictly true only for an infinite system.

other hand it must be

$$p_{23} \leqslant 1 - p_{21} \Rightarrow p_{23} \leqslant 1 - \frac{c_1}{c_2}p_{12},$$

$$p_{32} \leqslant 1 - p_{31} \Rightarrow p_{23} \leqslant \frac{c_3}{c_2}(1 - p_{31}) \Rightarrow p_{23} \leqslant \frac{c_3}{c_2} - \frac{c_1}{c_2}p_{13},$$

therefore $p_{23} \leqslant \min \left\{ 1 - \dfrac{c_1}{c_2}p_{12}, \dfrac{c_3}{c_2} - \dfrac{c_1}{c_2}p_{13} \right\}$.

An expression for the general form of the upper bounds can be obtained for arbitrary m. Fixing the above diagonal elements of the correlation matrix from left to right following row order,

$$\mathbf{P} = \begin{pmatrix}
p_{11} & p_{12} & \longrightarrow & \ldots & \longrightarrow & p_{1m} \\
p_{21} & p_{22} & p_{23} & \longrightarrow & \longrightarrow & p_{2m} \\
\vdots & \vdots & \ddots & \ddots & & \vdots \\
\vdots & \vdots & & \ddots & \ddots & \vdots \\
p_{(m-1)1} & p_{(m-1)2} & \cdots\cdots\cdots & & p_{(m-1)(m-1)} & p_{(m-1)m} \\
p_{m1} & p_{m2} & \cdots\cdots\cdots & & p_{m(m-1)} & p_{mm}
\end{pmatrix}, \tag{3.54}$$

then

$$p_{ij} \leqslant \min \left\{ 1 - \frac{1}{c_i}\sum_{k=1}^{i-1} c_k p_{ki} - \sum_{k=i+1}^{j-1} p_{ik}, \; \frac{c_j}{c_i} - \frac{1}{c_i}\sum_{k=1}^{i-1} c_k p_{kj} \right\}, \tag{3.55}$$

where the limits are written in terms of the already chosen correlations.

Once the concentrations and $\mathbf{P}$ are fixed, the characterization of the quantum wire can be given in a compact form using the matrix

$$\mathbf{Q} = (q_{ij}) \equiv (c_i p_{ij}), \tag{3.56}$$

which is symmetric ($\mathbf{Q} = \mathbf{Q}^t$) and it determines uniquely the wire and its correlations,

$$\sum_{j=1}^{m} q_{ij} = c_i, \qquad \sum_{i=1}^{m} q_{ij} = c_j, \qquad p_{ij} = \frac{q_{ij}}{c_i}. \tag{3.57}$$

q_{ij} means the probability of finding the cluster $-ij-(-ji-)$ at any position inside the wire.

In the most general case a wire including m different species is determined by $(m-1)$ independent concentrations and $m(m-1)/2$ independent correlations, which mean a configuration space of dimension $(m+2)(m-1)/2$. The binary case $m = 2$ is the only one for which the entire space can be represented and also the one for which an easy systematic analysis exploring all possible configurations can be carried out.
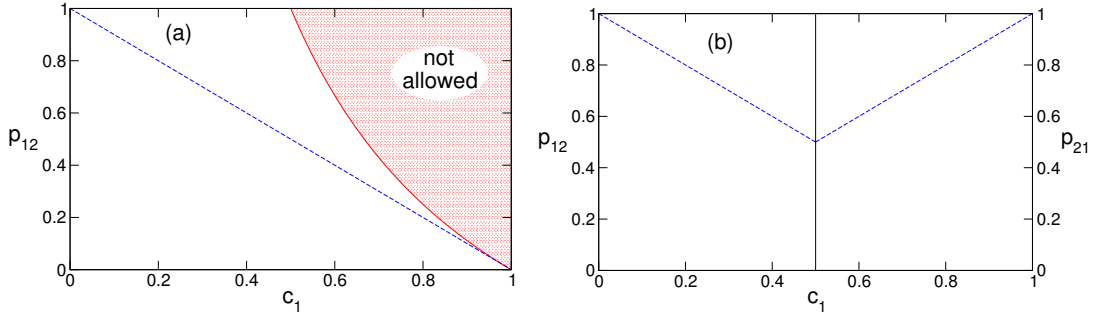
Figure 3.20.   Correlation space for 2 species as a function of the concentration. (a) p_{12} vs c_1. (b) optimal representation: if $c_1 \leqslant 0.5$ then p_{12} vs c_1, if $c_1 > 0.5$ then p_{21} vs c_1. The dashed line corresponds to the completely random configurations.

One usually takes as configuration parameters $\{c_1, p_{12}\}$. The allowed configuration space with these parameters is shown in figure 3.20(a). However one can optimize the representation of this space by choosing the parameters $\{c_1, p_{12}\}$ when $c_1 \leqslant 0.5$ and $\{c_1, p_{21}\}$ when $c_1 > 0.5$, so that the allowed configuration space is expanded and the spatial points can be better differentiated, as shown in figure 3.20(b). Therefore, for a given concentration different values for $p_{12}(p_{21})$ can be chosen, and only one of them corresponds to the completely random chain. When the configuration of the binary chain lies on the dashed lines of figure 3.20 we have a completely random chain, whereas if the configuration lies anywhere else we have a correlated chain. Let us remark that the random dimer binary configuration is not included in this model. Nevertheless, the random dimer model can be viewed as a random chain in which the basic compositional units are couples of identical atoms. With a proper renormalization of the canonical equation, the random dimer model can be solved in the thermodynamic limit using the functional equation formalism.

3.6.1   Effects of the correlations on infinite chains

The effects of the correlations introduced in the wire upon the limiting distribution of states and the localization properties in the thermodynamic limit are obtained by making use of the functional equation formalism. In this case the functional equations read

$$W_\gamma(\theta) = \sum_\beta p_{\gamma\beta} \left\{ W_\beta \left(\mathcal{T}^{-1}(\theta; a_\gamma) \right) - W_\beta \left(\frac{\pi}{2} \right) \right\} + 1, \qquad (3.58a)$$

$$W_\gamma(\theta + n\pi) = W_\gamma(\theta) + n, \qquad \theta \in [0, \pi),\, n \in \mathbb{Z}, \qquad (3.58b)$$

where γ and β run over the different species and the inverse transmission function for the phase is defined in (3.27). The DOS per atom and the inverse localization length
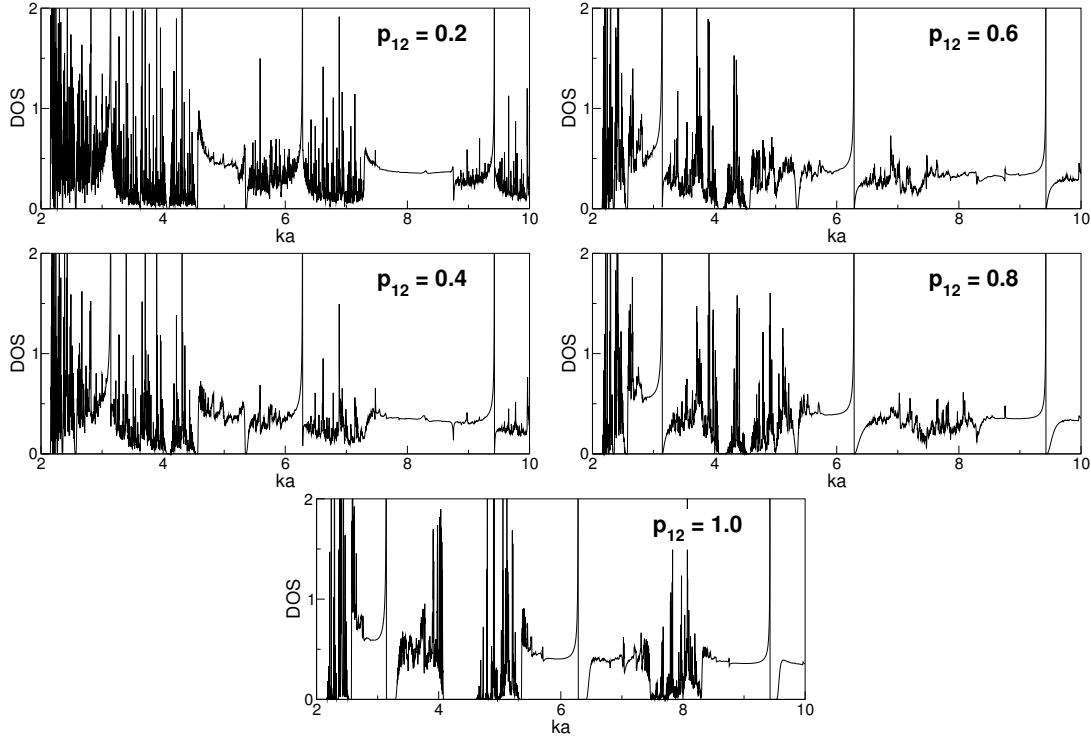
Figure 3.21. DOS for a binary disordered wire with parameters $(a/a_1) = -3$, $(a/a_2) = 4$ and $c_1 = 0.4$ for different values of the correlation p_{12}.

can be numerically obtained respectively from

$$g(\epsilon) = \left| \sum_\gamma c_\gamma \frac{\mathrm{d}W_\gamma\left(\frac{\pi}{2}\right)}{\mathrm{d}\epsilon} \right|, \tag{3.59}$$

$$\xi(\epsilon)^{-1} \equiv \lambda(\epsilon) = \frac{1}{2} \sum_{\gamma,\beta} c_\gamma p_{\gamma\beta} \int_0^\pi \mathrm{d}W_\gamma(\theta) \log \mathcal{F}(\theta; a_\beta), \tag{3.60}$$

where the function $\mathcal{F}(\theta; a_\beta)$ is defined in (3.28).

Once we have built the mathematical framework lying under the model, one can try to answer the physical questions that obviously arise from this new configuration of the disordered quantum wire: how strong is the effect of this short-range correlations?, do they produce a measurable change in the density of states or in the localization of the electrons? Let us analyse in first place the density of states. In figure 3.21 the evolution of the DOS for a binary wire as a function of the correlation p_{12} is shown for a certain value of the concentrations. This distribution of states is drastically changed from the initial situation in which the probability to find the cluster $-12-$ is low, to the final stage when the atoms of species 1 appear always isolated. Note however that the concentrations are the same in all cases. From these
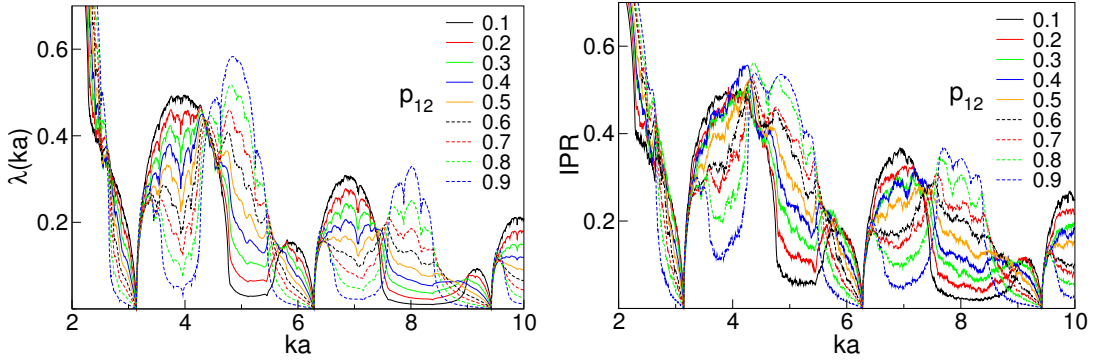
Figure 3.22. Lyapunov exponent (left) and IPR (right) for a binary wire with parameters $(a/a_1) = -2$, $(a/a_2) = 5$ and $c_1 = 0.5$ for different values of the correlations. The IPR in each case is obtained after averaging over 100 realizations of a 1000-atom chain.

graphics we conclude that the correlations can unbalance the spectra of the disorder system quite far from the completely random configuration. In fact the correlation can be tuned to open or close energy gaps, thus modifying the number of available states in a certain energy interval without changing the concentrations of the atomic components. The variation of the DOS with the correlations is of course a function of the concentrations, being the chain with homogenized participation the one whose distribution has the strongest dependence on **P**. Let us also remark that the fractal behaviour of the density of states in certain energy ranges, still manifests itself for the different correlation regimes. Let us have a look at the localization of the electronic states. In figure 3.22 the evolution of the Lyapunov exponent as a function of the correlations is shown for a binary chain with fixed concentrations. The change of the Lyapunov exponent is also faithfully reproduced by the inverse participation ratio. The effective influence of the correlations on the localization of the electrons inside the quantum wires is established. As can be seen, the model of correlations proposed is not able to include in the spectrum new truly extended states in the thermodynamic limit. However an important effect on the localization of the states is shown that seems to act globally in the whole energy range, in contrast to the more restricted effect of others short-range correlated disorder models. In fact for certain energies the Lyapunov exponent can be decreased an 80-90% of its maximum value changing the correlations, at the expense of an increasing behaviour for other energies. The correlations clearly change the distribution of states on both sides of the π-resonances and this causes the behaviour of the localization length close to these energies to change also, as can be seen in figure 3.22. The range of validity of expressions (3.38) or probably the value of the critical exponent itself depends on the correlations.
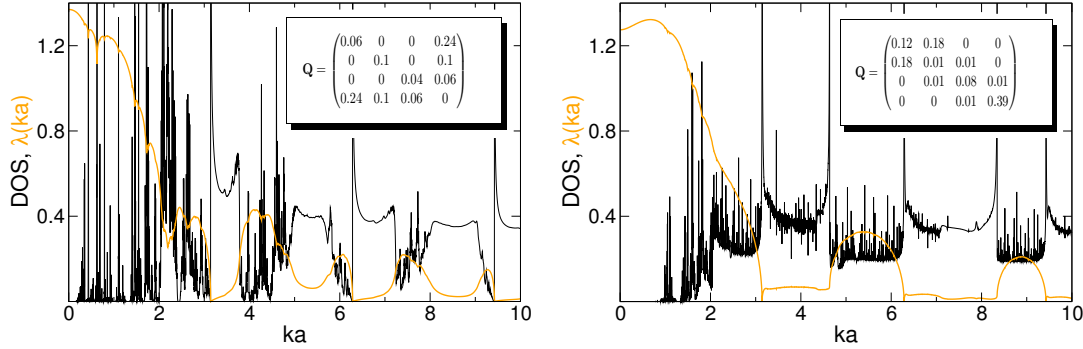
Figure 3.23. DOS (black) and Lyapunov exponent (orange) for a 4-species wire with couplings $(a/a_\gamma) = 1, -1, 3, -5$. The configuration is contained in the characteristic matrix **Q**. Notice that the concentrations are the same in both plots.

As the number of species m increases, similar effects are observed as shown in figure 3.23 for a 4-species wire. The dimension of the configurational space grows as $(m + 2)(m - 1)/2$ ant that makes it more complex to perform a complete analysis in terms of all the independent parameters.

3.6.2 Effects of the correlations on finite wires

Although our model of correlations is not able to include new extended states in the spectrum of the system, this does not mean that the effects upon the transport properties of a real finite wire can be ignored. The electronic localization is altered and it may translate into a measurable change of the macroscopic conductance of these correlated disordered structures. To analyse the effect of the correlations on finite arrays, the transfer matrix formalism described in the previous chapter is used to evaluate the transmission of different samples.

Let us have a look at the transmission patterns of finite binary chains for different configurations of concentrations and correlations. In figure 3.24 the transmission is shown for several chains composed of 1000 atoms, for different values of the couplings and concentrations. In these cases the worst performance corresponds to the completely random configurations, for which the transmission probability only raises near the multiples of π due to the well-known resonances of the model at these energies. However as we move away from the completely random configuration (above or below the dashed line) the transmission is noticeably improved. Notice that this improvement is not necessarily localized around the multiples of π. Although quantitatively this enhancement depends on the values of the couplings, qualitatively it seems a generic behaviour. In order to check whether this effect can be extended over the whole correlation space, we characterize each of its points by an efficiency of
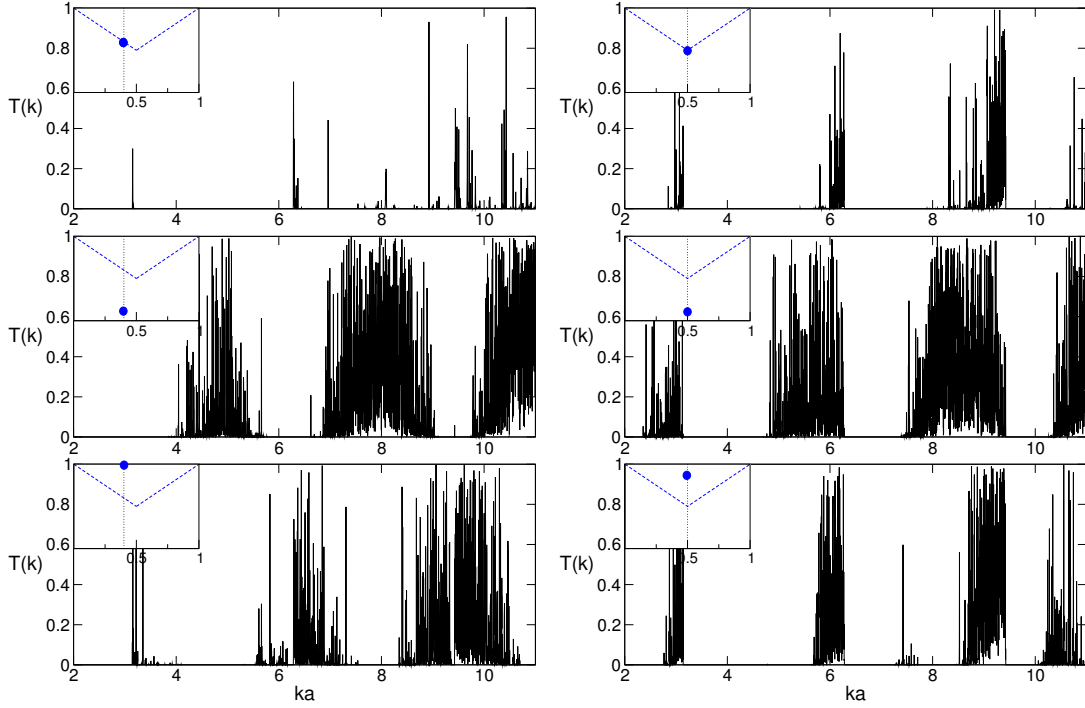
Figure 3.24. Transmission probability vs energy for 1000-atom binary disordered chains in different correlation regimes. The circular point inside the insets marks the configuration on the configurational space. Only one realization of the disorder has been considered for each case. (Left column) couplings $(a/a_1) = 1$, $(a/a_2) = -1$, concentrations $c_1 = 0.4$, $c_2 = 0.6$ and correlation from top to bottom $p_{12} = 0.6, 0.1, 1.0$. (Right column) couplings $(a/a_1) = 2$, $(a/a_2) = 4$, concentrations $c_1 = c_2 = 0.5$ and correlation from top to bottom $p_{12} = 0.5, 0.1, 0.85$.

transmission defined as

$$T_{\text{eff}} = \frac{1}{k_2 - k_1} \int_{k_1}^{k_2} T(k)\mathrm{d}k, \qquad (3.61)$$

which is the area enclosed by the transmission coefficient per energy unit. This definition depends on the integration interval, but qualitatively the results will not be affected as long as a reasonable interval is chosen, generally one of the form $[0, k_2]$. Notice that for very high energies the transmission will saturate for all configurations, thus the contribution to the integral in (3.61) will be the same independently of the $\{c_1, p_{12}\}$ values. We are interested in establishing a qualitative comparison of these efficiencies for different correlations.

For certain values of the couplings and a length of 1000 atoms the evolution of the transmission efficiency over the configuration space is shown in figure 3.25. It is clearly shown that the lowest values for the transmission efficiency are distributed around the completely random configurations, specially when the participation of the
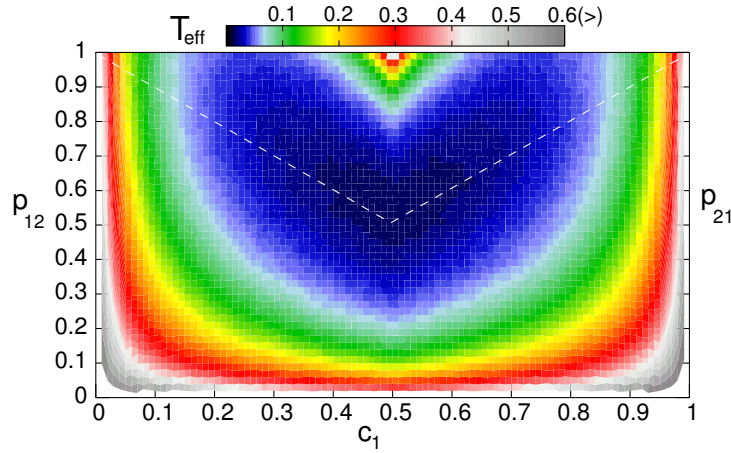
Figure 3.25. Transmission efficiency for different configurations of a binary chain with 1000 atoms and couplings $(a/a_1) = 1$, $(a/a_2) = -1$. For each configuration only one realization of the disorder has been considered. The integration interval for T_{eff} was $[0, 15]$.

species is homogenized ($c_1 \sim 0.5$). High efficiencies can be observed for low and high concentrations of one of the species (and therefore approaching a pure chain) and around the point $\{c_1 = 0.5, p_{12} = 1.0\}$ which corresponds to the periodic binary chain. Nevertheless by looking at the evolution of T_{eff} as a function of p_{12} for a fixed concentration (figure 3.26 on the facing page), we conclude that the minimum efficiency is reached near the completely random configuration and the correlated situations show noticeably higher values. Therefore the electronic transmission through a finite wire is improved by this type of correlations although truly extended states do not appear in the system. The reason for the improvement then must be the existence of states behaving as extended states, that is their localization length being larger than the system size. Let us analyse the behaviour of the Lyapunov exponent. In figure 3.27 the Lyapunov exponent as a function of the energy is shown for a random chain. We can see a very good agreement between the thermodynamic limit distribution and λ for the finite realization of the disorder, that shows a characteristic fluctuating behaviour around the values of the former one. These fluctuations are responsible for the enhancement of transmission. A fine observation of the Lyapunov exponent, in figure 3.28 on the next page, reveals that for a chain with fixed concentrations the number of states whose localization length exceeds the sample length increases dramatically in a correlated configuration with respect to the completely random situation. The correlations induce a decrease of the limiting distribution of the Lyapunov exponent in certain energy ranges, so that for a finite system the fluc-
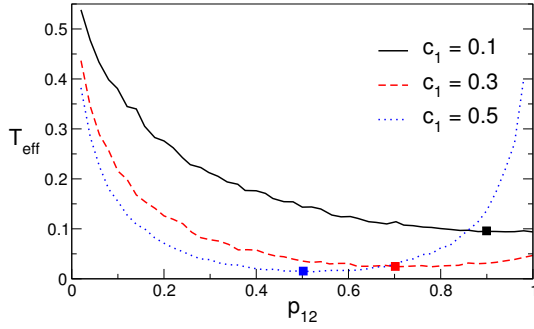
Figure 3.26. T_{eff} vs p_{12} for 1000-atom binary chains with couplings $(a/a_1) = 1$, $(a/a_2) = -1$ and different concentrations. The squares on the lines mark the position of the completely random configuration.
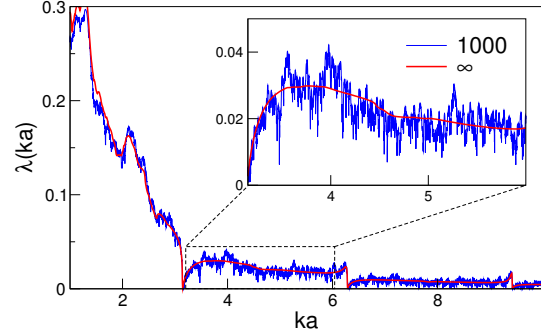

Figure 3.27. Lyapunov exponent vs energy for a binary chain with parameters $(a/a_1) = 1$, $(a/a_2) = -1$, $c_1 = 0.4$, $p_{12} = 0.6$. The blue line corresponds to a 1000-atom realization and the red line to the infinite chain.
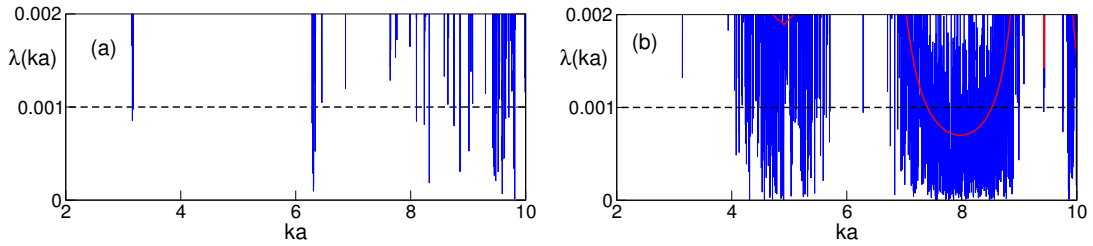

Figure 3.28. Lyapunov exponent vs energy for a 1000-atom binary chain with couplings $(a/a_1) = 1$, $(a/a_2) = -1$ and concentration $c_1 = 0.4$ for (a) completely random configuration $p_{12} = 0.6$ and (b) correlated configuration $p_{12} = 0.1$. The dashed line marks the inverse of the length of the sample. The red line shows the Lyapunov exponent for the infinite chain.

tuations of this quantity around its mean value make the appearance of such states possible. Let us notice that the decreasing of the limiting value of the Lyapunov exponent does occur in different energy ranges depending on the parameters of the chain, so that the improvement of the transmission can take place in different energy intervals, and hence the appearance of states whose localization length (ξ) is larger that the length of the system (L) is not restricted to the vicinity of the resonances located at the multiples of π. This is in sharp contrast to other short-range correlated models such as the random dimer, which is able to improve the transport in finite systems in a similar manner but the states with $\xi > L$ always appear around a resonant extended state ($\xi = \infty$) [161]. Let us remark that although the fluctuating pattern of the Lyapunov exponent is a fingerprint of the particular realization of the disorder, the amplitude of these oscillations does only depend upon the length of the system.
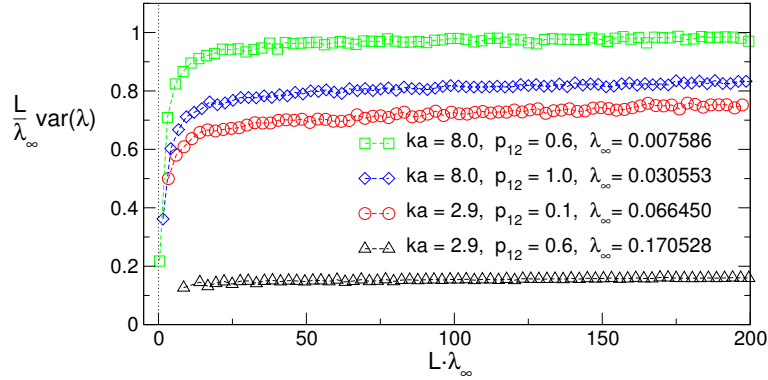
Figure 3.29. Evolution of the fluctuations of the Lyapunov exponent versus the length of the system for a binary chain with parameters $(a/a_1) = 1$, $(a/a_2) = -1$ and concentration $c_1 = 0.4$. The variance times the length of the system divided by the value of the Lyapunov exponent in the thermodynamic limit (λ_∞) is plotted for different energies and correlations. For each length the variance is obtained after averaging over $5 \cdot 10^4$ realizations of the disorder.

Therefore the results are not due to particular unusual realizations of the disorder for a given length. The behaviour described can be clearly observed in all realizations of a certain configuration. The fluctuations of the Lyapunov exponent for finite chains are quantified through the variance $\mathrm{var}(\lambda)$ that according to the central limit theorem must decrease asymptotically with the length of the system as L^{-1} [165]. This asymptotic behaviour of the Lyapunov exponent can be checked in figure 3.29 where the evolution of the variance with the length of the system is analysed for different localization lengths corresponding to different configurations. For a certain value of the energy and the correlations the localization length is obtained from the Lyapunov exponent in the thermodynamic limit λ_∞. Then, different realizations of the disorder for different lengths are considered for calculating the variance of the Lyapunov, $\mathrm{var}(\lambda) = \langle \lambda^2 \rangle - \lambda_\infty^2$, where the average is taken over $5 \cdot 10^4$ sequences for each length. The plot $\mathrm{var}(\lambda) L / \lambda_\infty$ versus $L/\xi \equiv L \lambda_\infty$ clearly shows a saturation when $L \gg \xi$ in all the cases considered. The asymptotic value reached in the strong localization regime ($L\lambda_\infty \gg 1$) depends of course on λ_∞ and the distribution of these asymptotic values for different λ_∞ might correspond to single parameter scaling (SPS) [1, 11]. As we know, SPS implies that the variance of the Lyapunov exponent (LE) scales with the length of the system according to the limiting value of the LE itself, so that the relation $\tau \equiv \mathrm{var}(\lambda) L / \lambda_\infty = 1$ is satisfied. However the regime in which single parameter scaling works is still controversial and new expressions for τ and new requirements for the validity of SPS have recently appeared [59, 57, 58, 72]. Also the exact expression of τ seems to depend on the model and the type of distributions considered. It
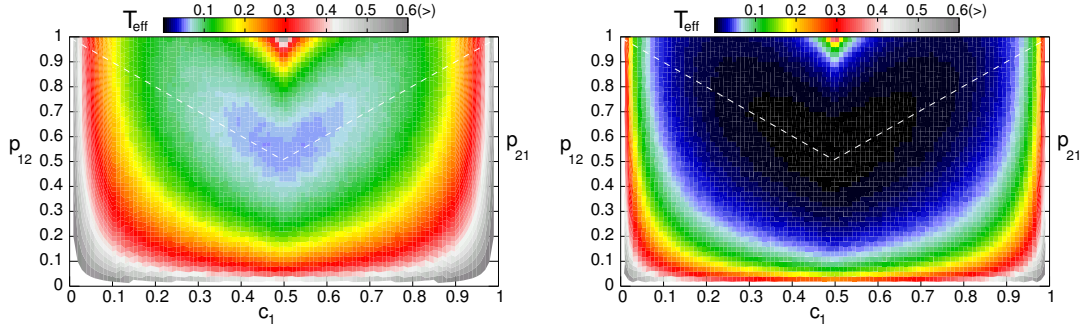
Figure 3.30. Transmission efficiency over configuration space for a binary chain with couplings $(a/a_1) = 1$, $(a/a_2) = -1$ for different lengths: $L = 500$ (left) and $L = 2000$ (right).

would be very interesting to check the applicability of SPS for this correlated model. However this task deserves a thorough and deep analysis.

It must then be clear that taking averages of the Lyapunov exponent over several realizations kills its fluctuating behaviour since that procedure is intended to approach the thermodynamic limit. And on the other hand averaging the values of the efficiency of transmission over several realizations for a given length will not have any effect on the results presented, according to the above discussion.

As expected for a model of short-range correlations, all the effects disappear unavoidably in the thermodynamic limit. Thus as the length of the chain grows the fluctuations of the Lyapunov exponent decrease and the localized character of the electronic states naturally manifests itself for all energies. The lost of the enhancement of transmission can be shown as a function of the evolution of T_{eff} over the configuration space for different lengths. The higher the number of atoms the more the black zones spread from the completely random lines as can be seen in figure 3.30. However the decay of the transmission efficiency with the length of the system depends upon the correlations. In figure 3.31 on the following page it can be seen how the fastest decreasing corresponds to the completely random situation, whereas the correlated chains show always higher efficiencies for all lengths. Plotting for different configurations $\Delta T_{\text{eff}} = T_{\text{eff}} - T_{\text{eff}}(R)$ as a function of the length, where (R) means the completely random situation, we see how the effect of the correlations reaches a maximum which is roughly contained in the region $L \sim 200-500$, apparently independent of the values of the species couplings.

Let us finally remark that although the model of correlations considered is not able to include any new truly extended state in the spectrum, its effects upon the transport of real finite samples are absolutely non-negligible. We believe that the effects described are essentially independent of the potential model so that they may be sig-
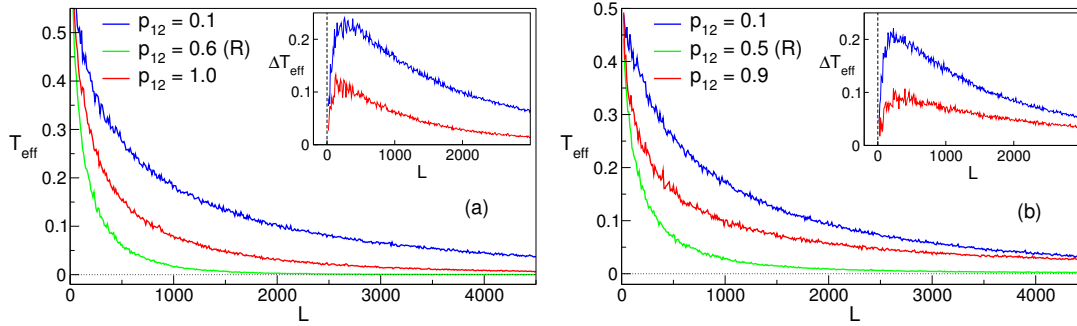
Figure 3.31. Transmission efficiency vs length for different configurations of a 1000-atom binary chain with parameters (a) $(a/a_1) = 1$, $(a/a_2) = -1$, $c_1 = 0.4$ and (b) $(a/a_1) = 2$, $(a/a_2) = 4$, $c_1 = 0.5$. (R) marks the completely random situation. The inset shows the relative differences $\Delta T_{\mathrm{eff}} = T_{\mathrm{eff}} - T_{\mathrm{eff}}(R)$.

nificant in certain experimental devices such as for example superlattices, which have already been used to observe the effect of other models of short-range correlations [18].

3.7 Concluding Remarks

In this chapter we have thoroughly analysed the delta model for a one-dimensional quantum wire. More explicitly:

- Analytical expressions have been built for the band structure of an arbitrary periodic array and for the condition of eigenstates in the case of an aperiodic sequence with hard-wall boundary conditions. The scattering amplitudes for a finite chain with open boundaries have also been described analytically.

- Different disordered configurations have been treated for which the distribution of states and the localization properties in the thermodynamic limit have been numerically obtained by means of the functional equation formalism.

- In the case of substitutional disorder several interesting features of the DOS have been found such as its fractal behaviour in certain energy ranges that has been rigorously demonstrated and interpreted. The existence of extended states at $\epsilon = n\pi$ and the functional dependence of the localization length and the DOS around these energies have been described. The role that the π-resonances play in the spectrum of finite arrays and the importance of the boundary conditions for determining the appearance of transmission resonances have been examined. Within the energy regions of weak localization, the IPR has revealed itself

as a quantity that contains the information of the system in the thermodynamic limit and this makes it useless for certain purposes like identifying correctly the exact energies of transmission resonances in finite chains but very valuable for identifying states with a divergent localization length by studying finite realizations of the system.

- Structural disorder has been included in the system together with the compositional one. The effect of this combination has manifested itself in a smoothing process of the DOS and the complete lost of its fractal character even for very low degrees of structural disorder. The removal of the π-resonances and the global modification of the localization length have been shown. These features might be understood as part of the effects of a non-zero temperature.

- Finally a natural model of short-range correlations have been proposed for substitutional disorder, modifying essentially the distribution of states and the localization properties of the system. Although additional extended states have not been found an important enhancement of the transport properties of finite samples have been observed.

Quantum wire with Pöschl-Teller potentials

So far, in the literature mainly two kind of potentials have been used to build one-dimensional disordered wires, namely the Dirac delta potential and the square well, due to their well-known and easy to manipulate transmission matrices. In this chapter we show how to model a one-dimensional wire using a different potential profile.

4.1 The potential

Let us consider the general Pöschl-Teller potential given by

$$V(x) = \frac{\hbar^2 \alpha^2}{2m} \frac{\mathrm{V}}{\cosh^2(\alpha x)}, \tag{4.1}$$

that is shown in figure 4.1. It resembles the form of an atomic well or barrier depending on the sign of V, a dimensionless parameter that together with α determines the height or depth of the potential. The parameter α, with units of inverse of length, controls the half-width of the potential which reads $d_{1/2} = 2\alpha^{-1}\mathrm{arccosh}\sqrt{2}$. The larger α is the narrower and higher(deeper) the potential becomes. The Schrödinger equation for the Pöschl-Teller potential is analytically solvable and its solutions are well known [84, 118, 40]. The general state for positive energies can be written in terms of Hypergeometric functions. The asymptotic transmission matrix is obtained following the procedure described in appendix A, from the asymptotic forms of the solutions which are collected in appendix E. After some algebra one finds the asymptotic transfer
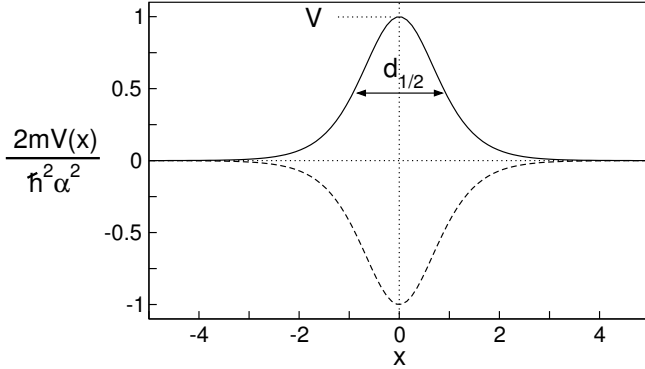
Figure 4.1. Pöschl-Teller potential defined in (4.1).

matrix for positive energies:

$$\mathcal{M} = \begin{pmatrix} \mathrm{e}^{\mathrm{i}\varphi}\sqrt{1+w^2} & -\mathrm{i}w \\ \mathrm{i}w & \mathrm{e}^{-\mathrm{i}\varphi}\sqrt{1+w^2} \end{pmatrix}, \tag{4.2}$$

where

$$w = \frac{\sin(\pi b)}{\sinh(\pi k/\alpha)}, \tag{4.3}$$

$$\varphi = \frac{\pi}{2} + 2\arg\Gamma\left(\mathrm{i}\frac{k}{\alpha}\right) - \arg\left\{\Gamma\left(b+\mathrm{i}\frac{k}{\alpha}\right)\Gamma\left(1-b+\mathrm{i}\frac{k}{\alpha}\right)\right\}, \tag{4.4}$$

$$b = \frac{1}{2} + \sqrt{\frac{1}{4} - \mathrm{V}}, \tag{4.5}$$

and $\Gamma(z)$ is the complex Euler gamma function. The matrix has the symmetries corresponding to a real and parity invariant potential. w is always a real quantity as can be seen in its alternative definition $w = \cosh(\pi\sqrt{\mathrm{V}-1/4})/\sinh(k\pi/\alpha)$. The dimensionless amplitude in terms of b reads $\mathrm{V} = -b(b-1)$ which is the usual form found in the literature. Let us remark that the above expressions are only valid for positive energies since several simplifications have been carried out with the assumption of $k \in \mathbb{R}$. From (4.2) the asymptotic probability of transmission is $T = (1+w^2)^{-1}$. One characteristic feature of this potential is that $T = 1$ for all energies whenever b is a real integer. Hence an absolute resonant transmission occurs for potential holes with $\mathrm{V} = -2, -6, -12, -20, \ldots$ independently of the value of α.

In the case of atomic wells ($\mathrm{V} < 0$) several bound states exist, that can be calculated from the poles of the transmission amplitude by making a proper extension into the complex plane via $k \to \mathrm{i}\eta$, where η can be considered to be positive without loss of generality. The correct form of the transmission matrix for negative energies reads

$$\mathcal{M} = \begin{pmatrix} f(-\eta) & -q \\ q & f(\eta) \end{pmatrix}, \tag{4.6}$$
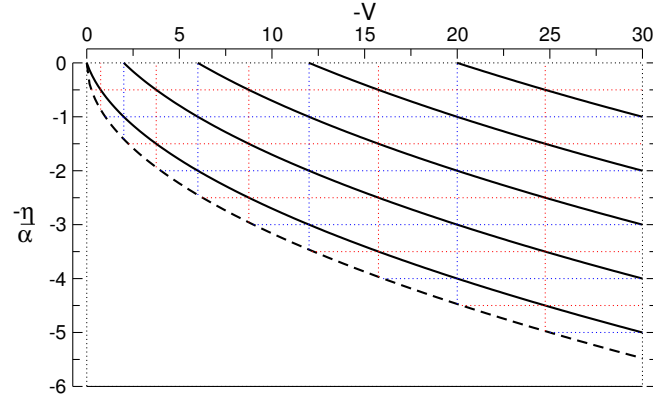
Figure 4.2. Bound states for the Pöschl-Teller hole. The solid curves mark the position of the eigenstates given by equation (4.9). The dashed line mark the position of the bottom of the well ($-\sqrt{|V|}$). The blue dotted grid highlights the integer states and the red dotted grid the half-integers.

where

$$q = \frac{\sin(\pi b)}{\sin(\pi \eta/\alpha)}, \tag{4.7}$$

$$f(\eta) = \frac{\eta/\alpha \, \Gamma^2(\eta/\alpha)}{\Gamma \left(1 - b + \eta/\alpha\right) \Gamma \left(b + \eta/\alpha\right)}. \tag{4.8}$$

The condition for bound states is then $f(\eta) = 0$. Since for potential wells b is real and greater than 1 the eigenstate equation reduces to $\Gamma^{-1}(1 - b + \eta/\alpha) = 0$, which is satisfied whenever the argument of the gamma function equals a negative integer. Finally, the energies of the bound states are

$$\frac{\eta}{\alpha} = b - m, \qquad m = 1, 2, 3, \ldots, [b], \tag{4.9}$$

where $[b]$ reads the integer part of b. Therefore the Pöschl-Teller hole host $[b]$ bound states equally spaced in the variable $\eta = \sqrt{2m|E|}/\hbar$ (figure 4.2). A couple of peculiar cases deserves a comment:

1.- If b is an integer then the energies of the bound states are also integers. $\eta/\alpha = m$, $m = 1, 2, \ldots, b - 1$. This is also the case for which the potential hole behaves as an absolute transparent potential for all energies (resonant well). Example values for the dimensionless amplitude: $V = -2, -6, -12, -20, -30, \ldots$

2.- If b is a half-integer then the energies of the bound states are also half-integers. $\eta/\alpha = m + 1/2$, $m = 0, 1, \ldots, b - 3/2$. In this case the transmission takes the form $T = \tanh^2(\pi k/\alpha)$ independently of b. Some values of the dimensionless amplitude for this situation are $V = -0.75, -3.75, -8.75, -15.75, -24.75, \ldots$

We shall see how due to the characteristic features exhibited by the Pöschl-Teller potential some exciting effects arise when several potential units are connected.

4.2   Building linear chains

To build a chain with the potentials described, one must do the approximation of considering that each potential unit has a finite range. Hence a cut-off must be included in the Pöschl-Teller potential. Using this approximation one obtains matrices suitable to be composed in linear chains, applying the composition technique through equations (2.9). The goodness of this procedure depends on the decay of the potential. Let us suppose that the potential (4.1) is appreciable only inside the interval $[-d^L, d^R]$, where the superindices L, R, stand for the left and right lengths of the interval from the centre of the potential. Outside this interval the wave function is assumed to be a superposition of the free particle solutions. Then, according to chapter 2 and appendix A and from (4.2) and (2.10) the transmission matrix for the cut-off potential reads

$$\mathbf{M}_{\text{cut}} = \begin{pmatrix} e^{i\left[\varphi + k(d^R + d^L)\right]}\sqrt{1+w^2} & -iwe^{ik(d^R - d^L)} \\ iwe^{-ik(d^R - d^L)} & e^{-i\left[\varphi + k(d^R + d^L)\right]}\sqrt{1+w^2} \end{pmatrix}. \tag{4.10}$$

The cut-off matrix is the same as the asymptotic one plus an extra phase term in the diagonal elements that accounts for the total distance $(d^R + d^L)$ during which the particle feels the effect of the potential, and also an extra phase term in the off-diagonal elements measuring the asymmetry of the cut-off $(d^R - d^L)$. These phases are the key quantities since they will be responsible of the interference processes that produce the transmission patterns. In our case due to the rapid decay of the Pöschl-Teller potential the cut-off distance admits very reasonable values. In fact we have seen that for a sensible wide range of the parameters α and V, one can take as a minimum value for the cut-off distance $d_0 = 2d_{1/2} \simeq 3.5/\alpha$ where $d_{1/2}$ is the half-width. Taking $d^{L,R} \geqslant d_0$ the connection procedure works really well, as we have checked in all cases considered by comparing the analytical composition technique versus a numerical integration of the Schrödinger equation for the global potential.

In the case of a symmetric cut-off $d^L = d^R = d$, composing two potentials characterized by the parameters α_1, b_1, d_1, and α_2, b_2, d_2, one finds for the transmission probability, using the previously defined quantities w and φ,

$$T = \frac{1}{w_1^2 w_2^2 + (1+w_1^2)(1+w_2^2) + 2w_1 w_2\sqrt{1+w_1^2}\sqrt{1+w_2^2}\cos\left[\varphi_1 + \varphi_2 + 2k(d_1 + d_2)\right]}. \tag{4.11}$$
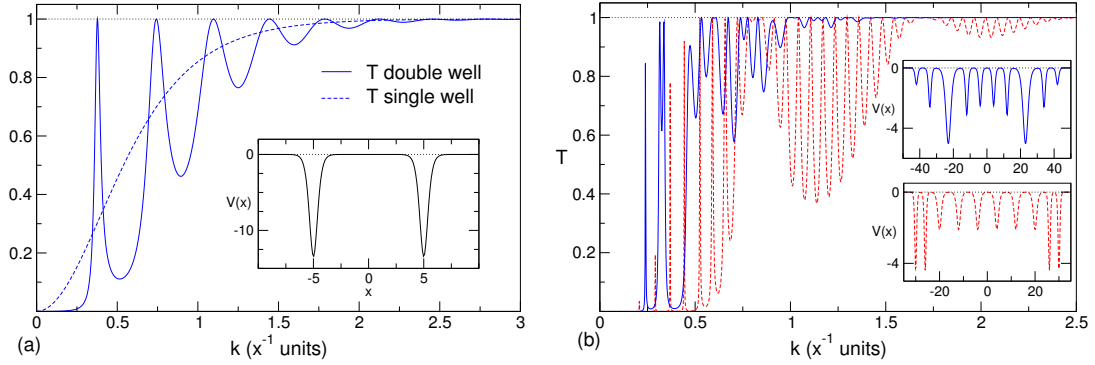
Figure 4.3. Transmission probability for different compositions of Pöschl-Teller holes. (a) double well with parameters: $\alpha_1 = \alpha_2 = 2(x^{-1}$ units), $b_1 = b_2 = 2.4$, $d_1 = d_2 = 5(x$ units). (b) two symmetric compositions with the following parameters for the first five potentials of the sequences: (solid line) $\alpha = 1, 1, 0.5, 1, 1(x^{-1}$ units), $b = 1.66, 2.19, 5.01, 2.3, 2.16$, $d = 4, 4, 7, 4, 4(x$ units) and (dashed line) $\alpha = 2, 2, 1, 1, 1(x^{-1}$ units) $b = 1.66, 1.66, 2.03, 2.03, 2.03$, $d = 2, 2, 4, 4, 4(x$ units). The insets show the potential profiles.

The latter expression clearly shows the interference effect depending on the distance $(d_1 + d_2)$ between the centres of the potentials. An example of transmission is shown in figure 4.3(a).

One important feature of the formulae for the composite scattering probabilities is the fact that they analytically account for the fully transparent behaviour of the whole structure as long as there is resonant forward scattering of the individual potential units, as can be easily checked in equation (4.11). The composition procedure can be applied with a small number of atoms to study the transmittivity of different potential profiles resembling molecular structures, such as those in figure 4.3(b), although our main interest is to consider the transmission matrix (4.10) to make a continuous disordered model in the form of a large chain of these potentials with random parameters.

As it has been shown, using reasonable approximations handy transmission matrices can be obtained for other potentials aside from the delta and the square well.

4.3 Wires with uncorrelated disorder

Once the properties of the potential have been studied and the procedure for constructing linear arrays has been described, let us consider now the effects of uncorrelated disorder upon this particular model. First is obtaining the canonical equation applying to the electronic states inside the system. From the transmission matrix
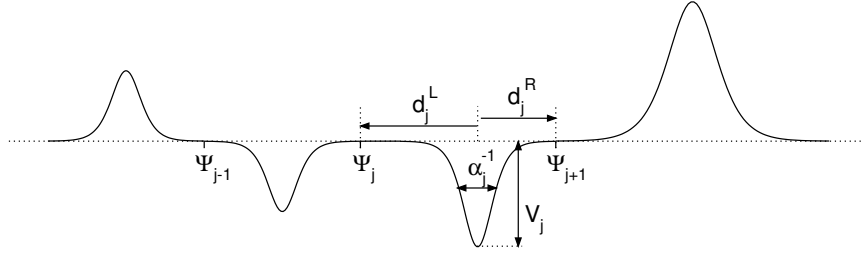
Figure 4.4. Potential of a disordered Pöschl-Teller wire

(4.10) one is led to the following relation

$$\Psi_{j+1} = \left(\overline{S}_j + S_{j-1} \frac{K_j}{K_{j-1}} \right) \Psi_j - \frac{K_j}{K_{j-1}} \Psi_{j-1}, \tag{4.12}$$

where

$$\overline{S}_j \equiv \overline{S}(\alpha_j, V_j, d_j^L, d_j^R) = -w_j \sin \left[k(d_j^L - d_j^R) \right] + \sqrt{1 + w_j^2} \cos \left[k(d_j^L + d_j^R) + \varphi_j \right], \tag{4.13}$$

$$S_j \equiv S(\alpha_j, V_j, d_j^L, d_j^R) = w_j \sin \left[k(d_j^L - d_j^R) \right] + \sqrt{1 + w_j^2} \cos \left[k(d_j^L + d_j^R) + \varphi_j \right], \tag{4.14}$$

$$K_j \equiv K(\alpha_j, V_j, d_j^L, d_j^R) = w_j \cos \left[k(d_j^L - d_j^R) \right] + \sqrt{1 + w_j^2} \sin \left[k(d_j^L + d_j^R) + \varphi_j \right], \tag{4.15}$$

in terms of w and φ defined in (4.3) and (4.4). The amplitudes Ψ_j correspond to the value of the state at the junction points of the potentials as shown in figure 4.4, and in this case each potential is determined by four parameters: $d_j^L, d_j^R, \alpha_j, V_j$. For negative energies the canonical equation reads the same but the functions must be defined as

$$\overline{S}_j = -q_j \sinh \left[\eta(d_j^L - d_j^R) \right] + \frac{1}{2} \left[e^{\eta(d_j^L + d_j^R)} f_j(\eta) + e^{-\eta(d_j^L + d_j^R)} f_j(-\eta) \right], \tag{4.16}$$

$$S_j = q_j \sinh \left[\eta(d_j^L - d_j^R) \right] + \frac{1}{2} \left[e^{\eta(d_j^L + d_j^R)} f_j(\eta) + e^{-\eta(d_j^L + d_j^R)} f_j(-\eta) \right], \tag{4.17}$$

$$K_j = q_j \cosh \left[\eta(d_j^L - d_j^R) \right] + \frac{1}{2} \left[e^{-\eta(d_j^L + d_j^R)} f_j(-\eta) - e^{\eta(d_j^L + d_j^R)} f_j(\eta) \right], \tag{4.18}$$

in terms of q and $f(\eta)$ defined in (4.7) and (4.8). In the case of symmetric cut-off the functions adopt a simpler form and $\overline{S}_j = S_j$.

The properties of the uncorrelated disordered chain in the thermodynamic limit, composed by different species with parameters $\{\vec{p}_\gamma = (d_\gamma^L, d_\gamma^R, \alpha_\gamma, V_\gamma)\}$ and concen-

trations $\{c_\gamma\}$ are obtained from the functional equation formalism:

$$W_\gamma(\theta) = \sum_\beta c_\beta \left| W_\beta\left(\mathfrak{T}^{-1}(\theta; \vec{p}_\beta, \vec{p}_\gamma)\right) - W_\beta\left(\frac{\pi}{2}\right) + \delta(\vec{p}_\beta, \vec{p}_\gamma) \right|, \qquad (4.19\text{a})$$

$$W_\gamma(\theta + n\pi) = W_\gamma(\theta) + n, \qquad \theta \in [0, \pi),\ n \in \mathbb{Z}, \qquad (4.19\text{b})$$

where $\delta(\vec{p}_\beta, \vec{p}_\gamma) = 1$ if $[K(\vec{p}_\beta)/K(\vec{p}_\gamma)] > 0$ and $\delta(\vec{p}_\beta, \vec{p}_\gamma) = 0$ otherwise. The inverse transmission function $\mathfrak{T}^{-1}(\theta; \vec{p}_\beta, \vec{p}_\gamma)$ is constructed from the functions of the canonical equation using definition (2.37). The Lyapunov exponent and the DOS in the thermodynamic limit come from

$$\lambda(\epsilon) = \frac{1}{2} \sum_{\gamma, \beta} c_\gamma c_\beta \int_0^\pi \mathrm{d}W_\gamma(\theta) \log \mathfrak{F}(\theta; \vec{p}_\gamma, \vec{p}_\beta), \qquad (4.20)$$

$$g(\epsilon) = \left| \sum_\gamma \frac{(\alpha_\gamma/\alpha)}{\alpha_\gamma(d_\gamma^L + d_\gamma^R)} \mathrm{sgn}[K(\vec{p}_\gamma)] c_\gamma \frac{\mathrm{d}W_\gamma\left(\frac{\pi}{2}\right)}{\mathrm{d}\epsilon} \right|, \qquad (4.21)$$

where the function $\mathfrak{F}(\theta; \vec{p}_\gamma, \vec{p}_\beta)$ is defined in (2.40). In this case $g(\epsilon)$ corresponds to the density of states per piece of length α^{-1}, where α is a value of reference for the parameters $\{\alpha_\gamma\}$ of the different species. The dimensionless representation of the energy reads $\epsilon \equiv k/\alpha$. These choices are made to get optimal representations of the DOS and also to maintain the value of the density of states for the free particle the same as for the previous models, $g_{\text{free}}(\epsilon) = \pi^{-1}$.

On the one hand the fact that the potentials are determined by four independent parameters gives a high degree of versatility to the model, but on the other hand specifying the configuration of the disordered wire including several species can be really a tedious and repetitive task since one needs to list a large amount of parameters. Therefore, from now on whenever the only configurational parameters of a chain are the dimensionless amplitudes $\{V_\gamma\}$, it is implied that α is equal for all species included in the array and also that the cut-off is symmetric and its distance is set to $d = 4/\alpha$, so that the total length of every potential is $2d = 8/\alpha$.

Several examples of distributions of states and Lyapunov exponents in the thermodynamic limit for different Pöschl-Teller disordered wires can be seen in figure 4.5 on the next page.

4.3.1 General features of the DOS

In the examples given in figure 4.5 the salient features of the distribution of states for this model can be observed. As must be expected, whenever potential wells are included in the disordered chain a group of permitted levels appears for negative energies, which correspond to bound states of the global composite potential. For positive
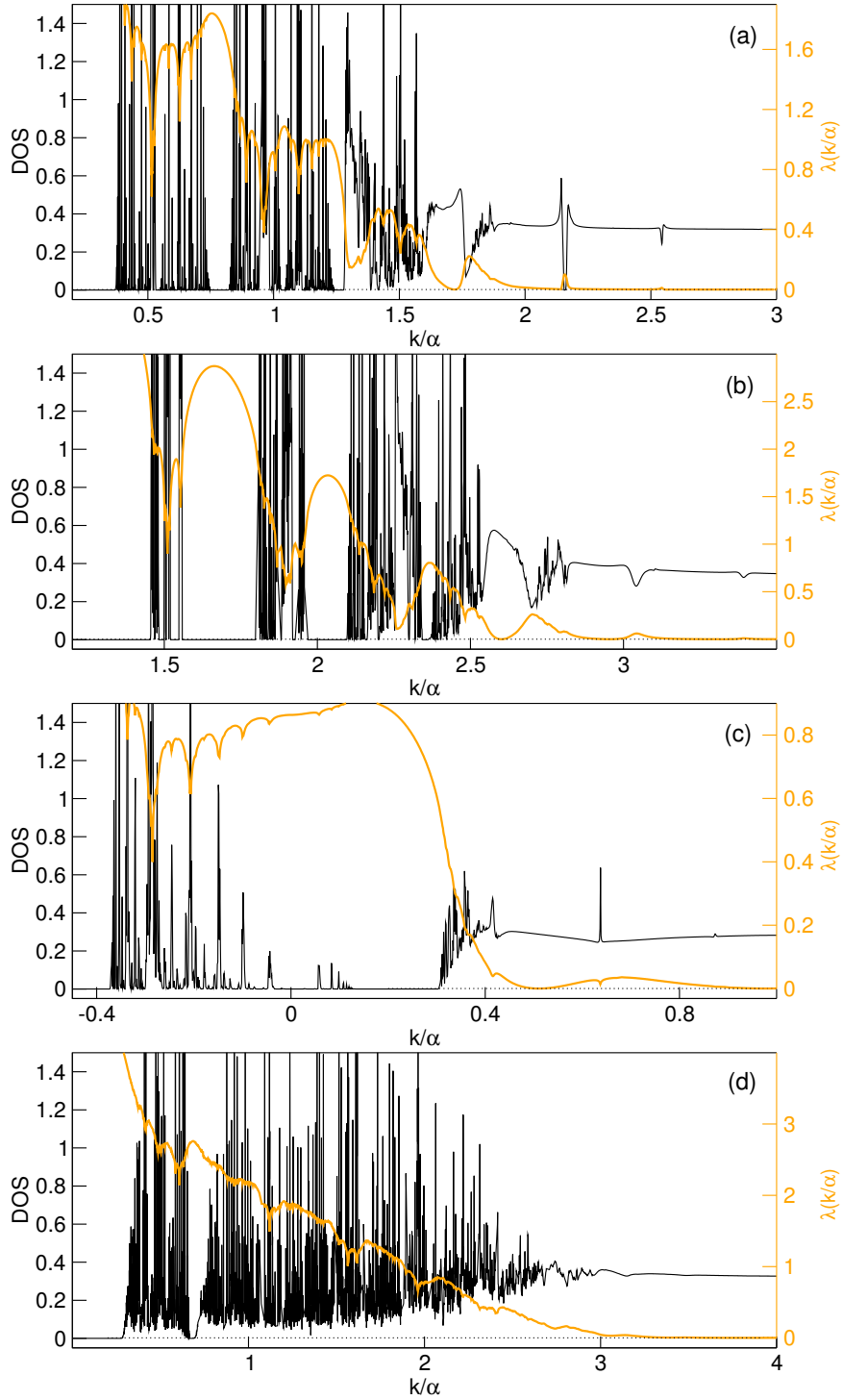
Figure 4.5.   DOS (black) and Lyapunov exponent (orange) for several disordered Pöschl-Teller wires with parameters (a) $V_\gamma[c_\gamma] : -4[0.5], 3[0.5]$, (b) $V_\gamma[c_\gamma] : 5[0.5]$, $7[0.5]$, (c) $V_\gamma[c_\gamma] : -1[0.5], -3[0.5]$ and (d) $V_\gamma[c_\gamma] : 1[0.2], 6[0.2], -5[0.2], -1[0.2]$, $9[0.2]$. Notice the different vertical scales for DOS (left) and λ (right). The negative part of the abscissa axis represents negative energies (-η/α).

Figure 4.6. Semivariance analysis: $\log\left(\sqrt{\Delta_s}\right)$ vs $\log(s)$ for a binary disordered Pöschl-Teller wire with parameters $V_1 = 1$ and $V_2 = -1$ and equal concentrations. The legend s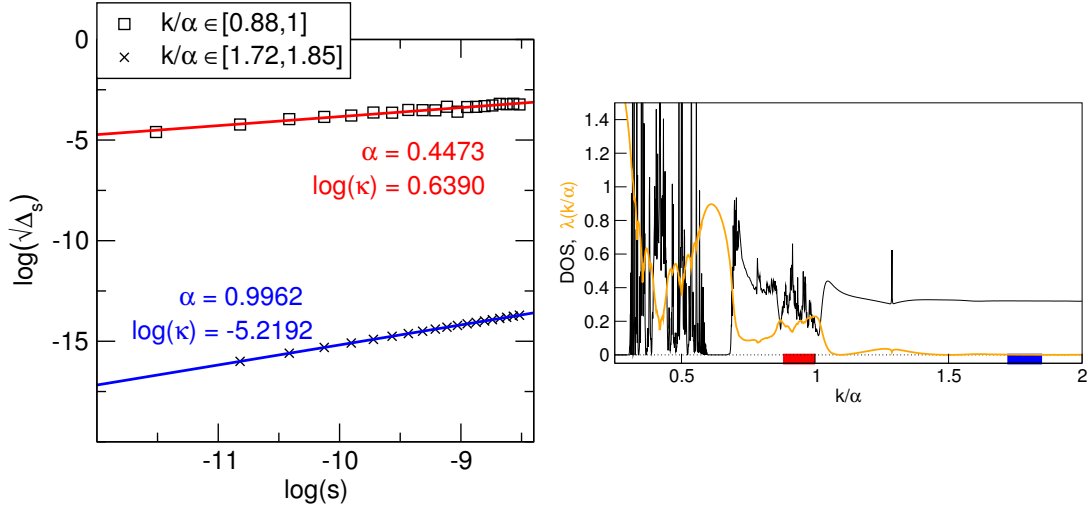hows the intervals considered to calculate the semivariance. α and $\log(\kappa)$ mean respectively the slope and the ordinate at the origin of the linear fits. The graphic on the right shows DOS and λ for the system.

high energies the correct asymptotic value of the free particle distribution is reached in all cases. As for the delta model discussed in the previous chapter, for the Pöschl-Teller disordered wires the density of states also shows an irregular fluctuating behaviour in certain energy ranges. And for this model the location of these energy zones is more predictable than for the delta potentials. The peaky structure lies almost entirely in the energy range below the maximum height of the potential barriers constituting the array. When the energy goes over the top of the potential barriers ($\epsilon \geqslant (\alpha_\gamma/\alpha)\sqrt{V_\gamma}$), the carriers found a regular distribution of states that evolves smoothly towards the value π^{-1} as the energy grows. This description agrees with the intuitive reasoning that for energies exceeding the barriers the effects of the potential and hence of the disorder must drastically decrease. In the cases when the system contains only potential wells, the DOS is regular for almost all the positive spectrum (figure 4.5(c)) and the asymptotic value $g_{\text{free}}(\epsilon)$ is reached for very low energies. The structure of the positive spectrum is naturally much more complex when the chain includes potential barriers.

Regarding the sharp-pointed structure of the DOS, it can be asserted that the distributions for the Pöschl-Teller chains are fractal in certain energy intervals. The semivariance analysis described in chapter 3 clearly reveals the fractal nature of the distributions. In figure 4.6 the linear fit of the log-log plot for pairs of values $(\sqrt{\Delta_s}, s)$ for a binary disordered chain can be seen. For the binary chain considered the anal-

ysis yields a fractal dimension $d_f = 1.5526$ for the irregular interval $\epsilon \in [0.88, 1]$ and $d_f = 1.0038$ for the smooth interval $\epsilon \in [1.72, 1.85]$. This result can be extended to ternary and higher wires for which the fractal behaviour of the distribution of states is noticeable (figure 4.5(d)).

Extensive analysis similar to those performed for the delta potential model, concerning the distribution of spacings of adjacent permitted levels and the description of prominent peaks of the DOS in terms of eigenstates related to the appearance of certain atomic clusters, can also be carried out for the Pöschl-Teller model leading to similar results as those contained in chapter 3.

We conclude that for our one-dimensional wire composed of non-punctual and continuous potentials the DOS exhibits a fractal behaviour as a consequence of the presence of disorder in the system. This result gives strong support to the conjecture made in the previous chapter, that fractality of the distribution of states may be a universal effect independently of the potential model. From the results described in the present chapter and in the previous one, we conclude that fractality seems to be a consequence not of the type of disorder (structural or compositional), but of the nature of the distribution of the parameters in the disordered system. If the distributions of all parameters are discrete, for example the species composing the system are a discrete set, then fractality emerges for the disordered system in the thermodynamic limit. On the other hand if any of the distribution is continuous, for example the one given in section 3.5 to introduce structural disorder or a continuous distribution of compositional species, then fractality must not be generally expected in the thermodynamic limit. Then, this behaviour seems a universal feature of the distribution of states, although probably several matters need to be specified, like for example whether or not there exists a critical width of a continuous distribution of parameters playing a significant role in the appearance of a fractal DOS.

4.3.2　Electronic localization

Let us have a look at the electronic localization for this disordered model. From what can be seen in figures 4.5 and 4.6 the Lyapunov exponent registers globally the localization of the electronic states. As expected, the localization length increases with the energy. When potential barriers are included in the chain, it can be noticed how for energies above the maximum barrier height the electrons become strongly delocalized. If the wire is composed only of potential wells, the Lyapunov exponent takes very low values for almost all the permitted positive spectrum. As discussed for the delta model, the tendency of the Lyapunov exponent to decrease at the energies for which the DOS shows a peak can also be seen. Let us remark that localization
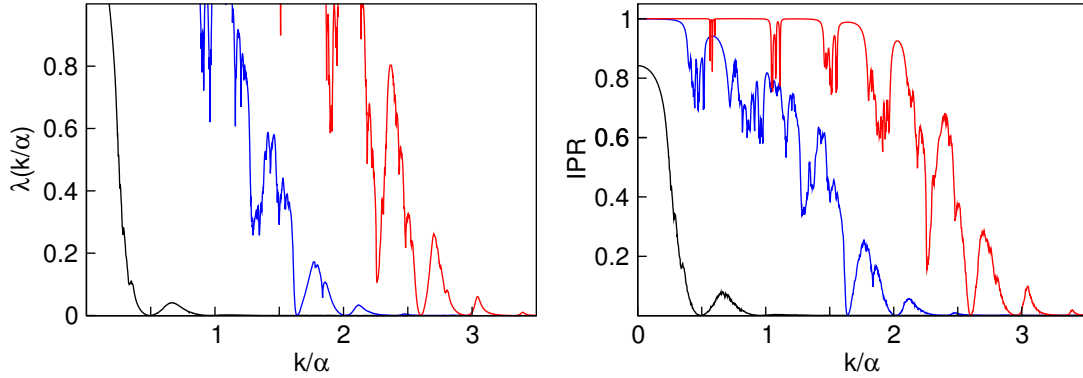
Figure 4.7. Comparison of the Lyapunov exponent and the inverse participation ratio as functions of the energy, for different binary disordered chains. The parameters for the different chains are $V_\gamma[c_\gamma]$: $-1.5[0.5], -4[0.5]$ (black), $1[0.5], 3[0.5]$ (blue), $5[0.5], 7[0.5]$ (red). The IPR is obtained averaging over 100 realizations of a 1000-atom array.

is always weaker inside the non-fractal regions of the spectrum, whereas fractality of the distribution of states seems to be linked to a strong localization.

The most important feature concerning the electronic localization is the presence of isolated energies for which the Lyapunov exponent vanishes (figure 4.5). These critical energies are always located inside non-fractal regions of the spectrum, they appear apparently only for binary chains and their values depend on the compositional species. Before going into a detailed analysis, let us remark that the localization properties deduced from the behaviour of the Lyapunov exponent are also faithfully confirmed by the inverse participation ratio calculated for finite chains after averaging over several realizations of the disordered sequences (figure 4.7).

The isolated resonances of the spectrum seem to be independent of the concentrations of the binary chains, as can be seen in figure 4.8 on the following page, where the evolution of the Lyapunov exponent with the concentration of the disordered wire is shown. Let us notice that when the chain is partially or totally composed of potential barriers the resonances can occur for energies below or above the maximum barrier height as can be checked in the different examples given. Around every resonance there exists a range of energies in which the Lyapunov exponent takes very low values and the higher the energy of the resonance the wider this interval is. In fact, the number of resonances may be infinite but above a certain energy they are indistinguishable since the Lyapunov exponent is almost zero anyway.

The appearance of the extended states shown in the examples given can be explained by the arguments given by Gómez and co-workers for a square barrier model[88], based on the commutativity of the product of the individual transmission matrices of
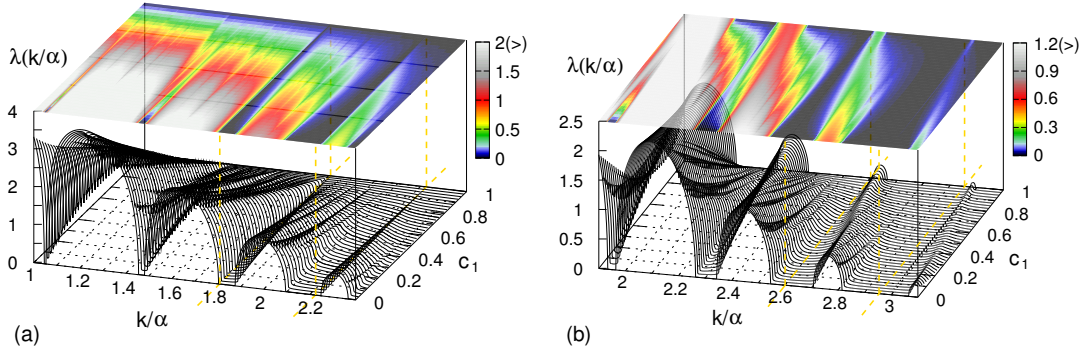
Figure 4.8. Evolution of the Lyapunov exponent vs energy and concentration for disordered binary wires with parameters (a) $V_1 = -2.5$, $V_2 = 5$ with resonances at $\epsilon_c = 1.809$, $\epsilon_c = 2.226$ and (b) $V_1 = 5$, $V_2 = 7$ with resonances at $\epsilon_c = 2.601$, $\epsilon_c = 2.954$. The top mapping shows the Lyapunov exponent in a colour scale. Notice how the resonances are present for all concentrations.

the system, that we shall review here. In the case of a binary chain composed of matrices $\mathbf{M}_1$, $\mathbf{M}_2$, critical energies ϵ_c can be found among those that satisfy $[\mathbf{M}_1, \mathbf{M}_2] = 0$. This is a necessary condition but not a sufficient one. Now since for these energy values the matrices of the two species commute, the disordered sequence can be changed at will and therefore the effects of the disorder disappear. Let us imagine that the atoms are rearranged so that the sequence becomes a juxtaposition of two semi-infinite pure chains. It is clear that the transparency intervals common to both pure chains are also transparent. Therefore if ϵ_c lies on the permitted bands of both species pure chains it will be a resonance of transmission and an extended state in the thermodynamic limit. Let us remark that this reasoning holds for all values of the concentrations in the binary array. To summarize, in a binary disordered system extended states exist at energies ϵ_c fulfilling the following requirements: commutative matrix product ($[\mathbf{M}_1, \mathbf{M}_2] = 0$), and they belong to the permitted spectrum of both species.

Let us analyse these conditions in our particular model. The commutator of the Pöschl-Teller transmission matrix becomes in the more general case

$$[\mathbf{M}_1, \mathbf{M}_2] = \begin{pmatrix} y & z \\ z^* & y^* \end{pmatrix}, \tag{4.22}$$

where

$$y = -\,2\,\mathrm{i}w_1 w_2 \sin\left[k(d_1^L - d_1^R - d_2^L + d_2^R)\right], \tag{4.23}$$

$$z = 2\,\mathrm{e}^{\mathrm{i}k(d_2^R - d_2^L)} w_2 \sqrt{1 + w_1^2}\,\sin\left[k(d_1^L + d_1^R) + \varphi_1\right]$$
$$-\,2\,\mathrm{e}^{\mathrm{i}k(d_1^R - d_1^L)} w_1 \sqrt{1 + w_2^2}\,\sin\left[k(d_2^L + d_2^R) + \varphi_2\right], \tag{4.24}$$

that for the critical energies must be zero. And the condition of belonging to the permitted spectrum of the pure chains can straightforwardly be written from the trace of the transmission matrix,

$$\left|\sqrt{1 + w_j^2}\,\cos\left[k(d_j^L + d_j^R) + \varphi_j\right]\right| \leqslant 1, \qquad j = 1, 2. \tag{4.25}$$

We shall assume that none of the species is a resonant well, hence $w_1 \neq 0$ and $w_2 \neq 0$ in general. Let us begin considering the simplest case, taking the parameter α the same for both species and a symmetric cut-off equal for all potentials to $d = 4/\alpha$. In this case, since y is identically zero the commutative condition reduces to

$$w_2 \sqrt{1 + w_1^2}\,\sin(8\epsilon + \varphi_1) = w_1 \sqrt{1 + w_2^2}\,\sin(8\epsilon + \varphi_2). \tag{4.26}$$

There exist two free parameters corresponding to the dimensionless amplitudes V_1, V_2, and although the above equation cannot be solved analytically, we have found that seemingly for all values of the amplitudes there exist solutions of this equation that also satisfy the requirement (4.25). It can be checked that the extended states observed in figures 4.5, 4.7 and 4.8 correspond to energies meeting these conditions.

Going one step further, one can consider that both species have different α_j, with symmetric cut-off but with different lengths depending on the species, $d_1^R = d_1^L = d_1$ and $d_2^R = d_2^L = d_2$. In this situation y is again identically zero and the commutative constraint is simply

$$w_2 \sqrt{1 + w_1^2}\,\sin(2kd_1 + \varphi_1) = w_1 \sqrt{1 + w_2^2}\,\sin(2kd_2 + \varphi_2). \tag{4.27}$$

And each potential is specified by three parameters α_j, V_j, d_j for $j = 1, 2$. Due to the oscillatory nature of the members of the above equation, there exist many energies satisfying the commutative matrix product, and as the energy grows they appear more easily, in such a manner that some of them always lie in the permitted spectrum of both species. In all the cases we have considered with these three parameters chosen randomly we have always found at least one or two resonant energies perfectly distinguishable. One example can be seen in figure 4.9(a). In fact by modifying the parameters α_j and the cut-off distances one can favour the emergence of resonances for energies below the highest barrier.
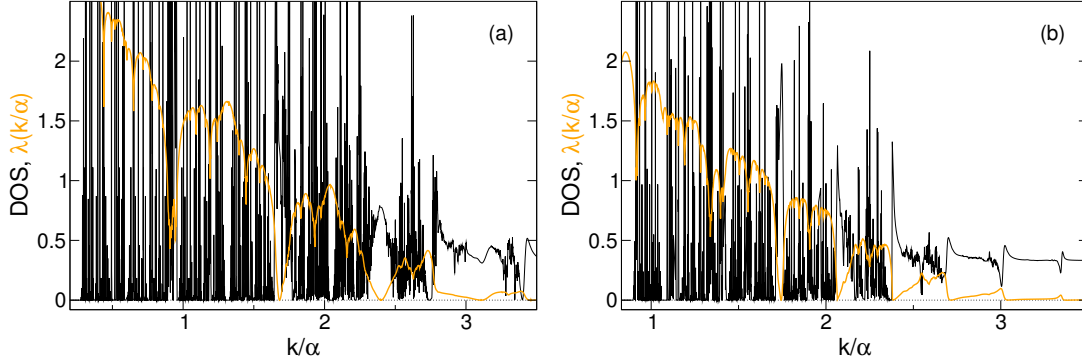
Figure 4.9. DOS and Lyapunov exponent for binary chains. (a) Two species with symmetric cut-off: $\alpha_1 = \alpha$, $V_1 = -1$, $d_1 = 4.5/\alpha_1$ and $\alpha_2 = 1.95\alpha$, $V_2 = 2$, $d_2 = 4.1/\alpha_2$. The three first resonances occur at $\epsilon_c = 1.6818$, $\epsilon_c = 2.3986$ and $\epsilon_c = 3.1064$. Notice that the first two resonances are located below the barrier height $\epsilon_{\max} = 1.95\sqrt{2} \simeq 2.76$. (b) Two species with asymmetric cut-off: $\alpha_1 = \alpha$, $V_1 = 1$, $d_1^L = 5.2/\alpha_1$, $d_1^R = 4.2/\alpha_1$ and $\alpha_2 = 1.5\alpha$, $V_2 = 3$, $d_2^L = 6.8/\alpha_2$, $d_2^R = 5.3/\alpha_2$. The first four resonances occur at $\epsilon_c = 1.7434$, $\epsilon_c = 2.0618$, $\epsilon_c = 2.3865$ and $\epsilon_c = 2.7143$. Notice that the first three resonances are located below the highest barrier $\epsilon_{\max} = 1.5\sqrt{3} \simeq 2.60$.

Things can even be more general by considering asymmetric cut-off satisfying $d_1^R - d_1^L = d_2^R - d_2^L$, that is the asymmetry being the same for both species. In this situation y is again identically zero and the commutation relation can still be written in a simple form

$$w_2\sqrt{1 + w_1^2} \sin\left[k(d_1^L + d_1^R) + \varphi_1\right] = w_1\sqrt{1 + w_2^2} \sin\left[k(d_2^L + d_2^R) + \varphi_2\right]. \qquad (4.28)$$

One can choose freely 7 of the 8 parameters of the system and finally set one of the cut-off distances to satisfy the asymmetry condition, and in all cases considered we have checked the appearance of resonances. An example is shown in figure 4.9(b). It is remarkable that contrary to what one could think at the beginning, these type of resonances appear very easily without doing awkward or very restrictive fits of the parameters of the system.

Of course other particular situations can also be considered, for example one can choose where to place the resonance from the condition $k(d_1^L - d_1^R - d_2^L + d_2^R) = n\pi$, $n \in \mathbb{Z}$, and hence making $y = 0$ and then fit some of the left parameters to fulfill $z = 0$.

As we have seen, this kind of resonances, that we shall refer to as commuting-resonances (according to reference [88]), appear very often and they are very versatile in the sense that their presence seem to be compatible with a wide continuous range of several parameters of the potentials.
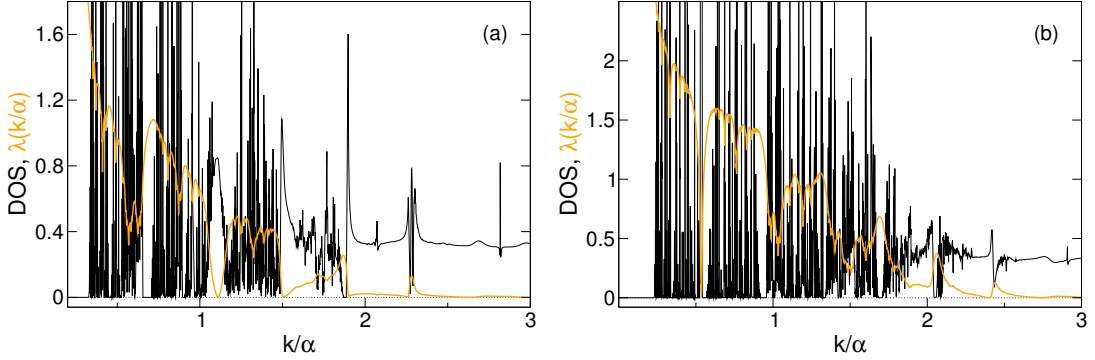
Figure 4.10. DOS and Lyapunov exponent for binary chains with all parameters chosen randomly. (a) $\alpha_1 = \alpha$, $V_1 = -4$, $d_1^L = 4/\alpha_1$, $d_1^R = 5/\alpha_1$ and $\alpha_2 = 1.8\alpha$, $V_2 = 1$, $d_2^L = 6/\alpha_2$, $d_2^R = 4.5/\alpha_2$. (b) $\alpha_1 = \alpha$, $V_1 = -5$, $d_1^L = 4.2/\alpha_1$, $d_1^R = 5.5/\alpha_1$ and $\alpha_2 = 1.5\alpha$, $V_2 = 2$, $d_2^L = 6.1/\alpha_2$, $d_2^R = 4.25/\alpha_2$.

Finally in the case of a binary chain in which the 8 parameters of the system (4 for each species) are chosen at random, one would expect in principle to see no resonances in the spectrum, since in this case it will be more difficult to satisfy all requirements for a critical energy to exist. Let us have a look at the spectra of a couple of such chains in figure 4.10. From what can be seen in the figures it seems that there exist resonances, but they are not indeed. They seem to correspond to energies for which the commutator of the transmission matrices is relatively small and that at the same time these energies belong to the spectrum of both species. For such energies the resonance conditions are close to be satisfied. This kind of energies appears surprisingly very often when choosing the parameters of the binary system at random, and that is due to the nature of the elements of the commutator. The functions y, $\mathrm{Re}\,(z)$ and $\mathrm{Im}\,(z)$ are oscillatory functions whose amplitude decay with the energy, hence even when choosing all the parameters of the chain at random, there exist always some energy intervals within which all the functions crosses zero relatively near from one another. It is impressive that for some of these energies the Lyapunov exponent takes such very low values that make them hardly distinguishable from real extended states. In fact these energies may have a significant effect on the transmission of a finite sample although they are not true resonances in the thermodynamic limit.

Although commuting-resonances naturally emerge for a binary system they could also exist in ternary and higher chains. For N species all the binary commutators must vanish and at the same time the energies must belong to the permitted spectrum of all species. Let us make a simple calculation for the Pöschl-Teller case. Let us consider that the cut-off distances are chosen to satisfy $d_i^R - d_i^L = d_j^R - d_j^L$, for $i, j = 1, \ldots, N$. Then the system is determined by $3N + 1$ variables, and on the other hand

in this situation the conditions of commuting-resonance imply one equation for each commutator plus one inequality for each species. Therefore in the case of an N-species wire we have $3N + 1$ variables to fulfill $N(N + 1)/2$ requirements. This simple calculation shows that for $N \leqslant 5$ is perfectly possible to find commuting-resonances, and in fact we have done so for a ternary chain, although the fit of the parameters is much more restrictive as N grows in comparison with the binary case.

Extended states can also appear in the thermodynamic limit of disordered systems by imposing different conditions in principle, like for example the one introduced by Hilke and Flores to describe extended states in a square barrier/well model [106]. The condition consists in imposing $\Psi_{j+1} = \pm \Psi_j$ for all sites of the system. Clearly if all species of the chain satisfy this constraint for the same energy a transmission resonance arises in the thermodynamic limit. Our Pöschl-Teller disordered wires can also host extended states of this kind. Let us see how one can build them by imposing the specific conditions to the transmission matrices of the individual species included in the system.

Let us consider the transmission matrix of a real potential ranging in the interval $[x_j, x_{j+1}]$. Its tranfer matrix is an element of the group $\mathcal{SU}(1, 1)$ as stated in appendix A and it connects the amplitudes of the travelling plane waves on both sides of the potential (A_j, B_j) and (A_{j+1}, B_{j+1}). The coordinates are chosen to ensure that the state right before the potential Ψ_j, and right after the potential Ψ_{j+1}, is simply given by the sum of the respective complex amplitudes. Then, one can wonder about the form the transmission matrix must adopt to satisfy the condition $\Psi_{j+1} = \pm \Psi_j$. It can be easily calculated that the transmission matrix must fit the expression

$$\mathbf{M} = \begin{pmatrix} \pm 1 - \mathrm{i}a & -\mathrm{i}a \\ \mathrm{i}a & \pm 1 + \mathrm{i}a \end{pmatrix}, \qquad a \in \mathbb{R}. \tag{4.29}$$

Thus whenever the transmission matrix takes this form, the probability distribution of the state does not decay after the individual potential but it remains constant. Trivially, the matrices (4.29) constitute a subgroup of $\mathcal{SU}(1, 1)$. Then a disordered linear array of potentials which can be described in terms of these matrices will give rise to a completely extended state with a flat probability distribution. Imposing the given form to the most general transmission matrix for a real potential

$$\mathbf{M}_j = \begin{pmatrix} \Lambda_j & \beta_j \\ \beta_j^* & \Lambda_j^* \end{pmatrix}, \qquad |\Lambda_j|^2 - |\beta_j|^2 = 1, \tag{4.30}$$

one is led to equations

$$\mathrm{Im}\left(\Lambda_j\right) = \mathrm{Im}\left(\beta_j\right), \tag{4.31a}$$

$$\mathrm{Re}\left(\beta_j\right) = 0, \qquad \forall j, \tag{4.31b}$$

and they straightforwardly guarantee that $\mathrm{Re}\,(\Lambda_j) = \pm 1$. This latter condition implies that the energy is a common band-edge of the periodic spectrum of all species. Therefore, this kind of extended states correspond to a certain class of common band-edges of the spectrum of the individual species composing the wire. Notice that not all common band-edges will satisfy the above requirements. If the individual potentials are parity invariant, then only equation (4.31a) has to be imposed, since the off-diagonal elements of the transmission matrices are pure imaginary (see appendix A) and hence condition (4.31b) is identically satisfied. In the most general case both equations (4.31) must be fulfilled.

Now in the case of a disordered binary Pöschl-Teller wire, one could choose the values of the parameters of the potentials so that there exists an energy ϵ_c for which the matrices of both species take the form (4.29). From (4.10) it follows that the conditions for ϵ_c to exist are

$$\sqrt{1 + w_j^2}\,\sin\left[k(d_j^R + d_j^L) + \varphi_j\right] = -w_j \cos\left[k(d_j^R - d_j^L)\right], \tag{4.32a}$$

$$w_j \sin\left[k(d_j^R - d_j^L)\right] = 0, \qquad j = 1, 2. \tag{4.32b}$$

For the sake of clarity let us restrict to the default case of symmetric cut-off $d = 4/\alpha$, and the same α for both species. In this case the only constraint is

$$\sqrt{1 + w_j^2}\,\sin(8\epsilon_c + \varphi_j) + w_j = 0, \qquad j = 1, 2, \tag{4.33}$$

or $K_j = 0$, using the canonical equation function (4.15). Therefore for a fixed V_1 one chooses one of the infinite roots of $K_1(\epsilon)$ to place the extended state, namely ϵ_c, and then equation $K_2(\epsilon_c) = 0$ is solved in terms of V_2. In some cases several solutions exist for the latter equation. Then the Lyapunov exponent will vanish at ϵ_c for the disordered binary chain independently of the concentrations. A couple of examples are shown in figure 4.11 where the Lyapunov exponent for two binary chains is plotted. Notice that the existence of this kind of extended states is compatible with the presence of commuting-resonances. In fact the matrices (4.29) constitute an abelian subgroup of $\mathcal{SU}(1,1)$ as can be straightforwardly checked, which means that the resonances arising from the common band-edges are in fact particular cases of commuting-resonances arising from a very precise fit of the parameters of the different species. These extended states are exactly of the same type as the π-resonances for the delta model, since the multiples of π are always band edges of the periodic delta chain independently of the delta coupling. Although these critical energies are also commuting-resonances we shall refer to them using a different label, let us call them CBE-resonances (common band-edge resonances). The CBE-resonances and the rest of commuting-resonances exhibit very different features as we shall see.
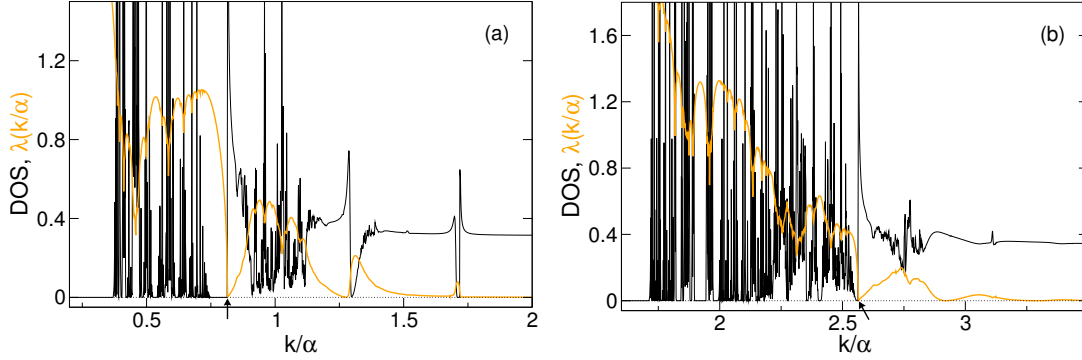
Figure 4.11. DOS and Lyapunov exponent for binary chains with parameters (a) $V_1 = -4$, $V_2 = 1.571051$ and (b) $V_1 = 4$, $V_2 = 7.217957$ with equal concentrations in both cases. The CBE-resonances are located at $\epsilon_c = 0.814459$ and $\epsilon_c = 2.56389$ respectively.

Let us check the functional dependence of the Lyapunov exponent and the density of states near the resonant energies. In the case of CBE-resonances a careful inspection reveals an asymmetric behaviour of the Lyapunov exponent around the critical energy. Seemingly it can be well described by

$$\lambda(\epsilon) \sim \begin{cases} |\epsilon - \epsilon_c|, \\ |\epsilon - \epsilon_c|^{1/2}, \end{cases} \tag{4.34}$$

on the different sides, as can be observed in figure 4.12(a). The DOS apparently behaves in the same way as for a periodic chain near a band-edge: gap on the side where the critical exponent for $\lambda(\epsilon)$ is $1/2$ and dependence of the type $g(\epsilon) \sim |\epsilon - \epsilon_c|^{-1/2}$ on the side with the linear change of the Lyapunov exponent. In summary the behaviour near the CBE-resonances is apparently the same as for the π-resonances in most of the delta chains. These resonances are of the same nature and exhibit similar features independently of the potential model. Therefore from the analysis made in chapter 3, the number of states around the CBE-resonance whose localization length is larger than the system size, in a finite chain, scales as $\sqrt{N}$ where N is the number of atoms.

On the other hand the behaviour of the distribution of states and the localization length in the vicinity of a commuting-resonance is completely different. In all cases studied the Lyapunov exponent seems to fit a quadratic dependence around the critical energy $\lambda(\epsilon) \sim (\epsilon - \epsilon_c)^2$, where the coefficients for $\epsilon < \epsilon_c$ and $\epsilon > \epsilon_c$ can differ. The DOS around these resonances evolves linearly $g(\epsilon) \sim g_0 + (\epsilon - \epsilon_c)$. It all can be observed in figure 4.12(b). With the dependence described for $\lambda(\epsilon)$ and $g(\epsilon)$, it follows that in a finite system the number of states near the commuting critical energy with a localization length larger than the system size scales as $\sqrt{N}$, the same as for
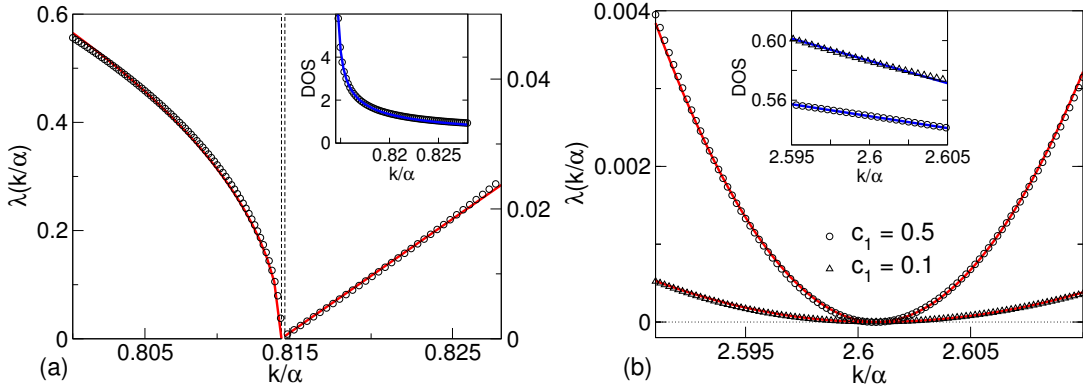
Figure 4.12. Behaviour of DOS and Lyapunov exponent near critical energies for binary wires. Symbols mark numerical results. (a) $V_1 = -4$ and $V_2 = 1.571051$ with equal concentrations. CBE-resonance located at $\epsilon_c = 0.814459$. Notice that for the Lyapunov exponent the vertical scales are different before and after the resonance to ensure an optimal visualization. Solid lines correspond to fits according to expression (4.34) for $\lambda(\epsilon)$ and $g(\epsilon) \sim |\epsilon - \epsilon_c|^{-1/2}$. (b) $V_1 = 5$ and $V_2 = 7$ with different concentrations. Commuting-resonance located at $\epsilon_c = 2.601$. Solid lines correspond to quadratic fits for $\lambda(\epsilon)$ and linear fits for DOS.

the CBE-resonances. As mentioned in the previous chapter, this scaling is exhibited by very different models with isolated extended states in their spectra [29, 161, 68], and it is probably a general feature of isolated resonances in one-dimensional disordered systems. The DOS and the Lyapunov exponent seem to balance their functional dependence near the critical energies to ensure the $\sqrt{N}$ scaling.

The different characters of the two types of extended states described also manifest themselves in the way that transmission resonances appear close to the critical energies for finite chains. As expected, within a small scale of energies near the CBE-resonances one finds exactly the same behaviour for the Lyapunov exponent and the IPR as for the π-resonances in the delta model, as can be seen in figure 4.13. The longer the system the higher the number of transmission resonances lying beside the critical energy is. The inverse participation ratio reaches its minimum value N^{-1} at ϵ_c for all lengths, and the spatial distributions of the wave functions inside the system show the same aspect as the ones in figures 3.14(c) on page 53. Within this energy scale near the CBE-resonances the system is mainly determined by its length and not by the atomic sequence, since all the individual transmission matrices behaves essentially in a similar manner independently of the species.

Let us see what happens in the vicinity of a general commuting-resonance. It is remarkable that the IPR for a finite system shows a characteristic *plateau* around the critical energy (figure 4.14(a)). This flat zone gets narrower as the length of the
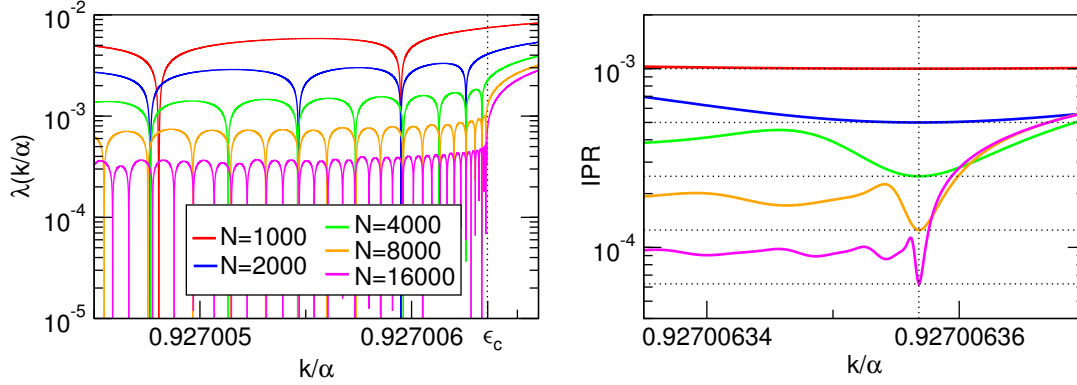
Figure 4.13. Lyapunov exponent and IPR near a CBE-resonance for a binary chain with parameters $V_1 = 2$ and $V_2 = -2.6422653344$ with equal concentrations. The critical energy is $\epsilon_c = 0.9270063568$. The horizontal dotted lines mark the inverse of the length of the system in the different cases considered.

system increases and it seems to be essentially symmetric around ϵ_c, which is in perfect agreement with the symmetric dependence of the Lyapunov exponent with the energy in this region in the thermodynamic limit. However in figures 4.14(a) and 4.14(b) it can be noticed that the IPR does not reach its minimum value N^{-1} for any energy. Nevertheless the inverse participation ratio for different lengths takes a value at ϵ_c that seems to scale roughly as $\mathrm{IPR}(\epsilon_c) \sim \frac{3}{2} N^{-1}$. Inspecting the Lyapunov exponent at a very small energetic scale near ϵ_c, it can be observed how as the length of the chain grows the number of transmission resonances increases following a symmetrical arrangement around the critical energy (figure 4.14(b)). This is in great contrast to the CBE critical energies for which the transmission resonances are only located on one of the sides of ϵ_c. In figures 4.14(c) one can have look at the appearance of the envelope of the electronic states with open boundary conditions near the critical energy for a chain with 1000 atoms. The states show a strongly fluctuating behaviour that seems to be modulated in a periodic manner. Apart from the differences in the global amplitude and the transmission, the three states shown exhibit essentially the same features. For cases 4.14(c.2) and (c.3), whose energy is not exactly the critical value, the periodic modulation starts to be subtly distorted. The spatial distribution of the states explains the behaviour of the IPR. First, all states near the critical energy have essentially the same structure leading to similar values of the IPR and therefore the *plateau*. And second, the fluctuating nature of the states prevents the IPR from reaching its minimum value N^{-1}, which requires of the envelope of the state to be flat. In figure 4.15 on page 96, one can observe how the state at the critical energy evolves as the concentration of the wire is changed for a finite binary system including 500
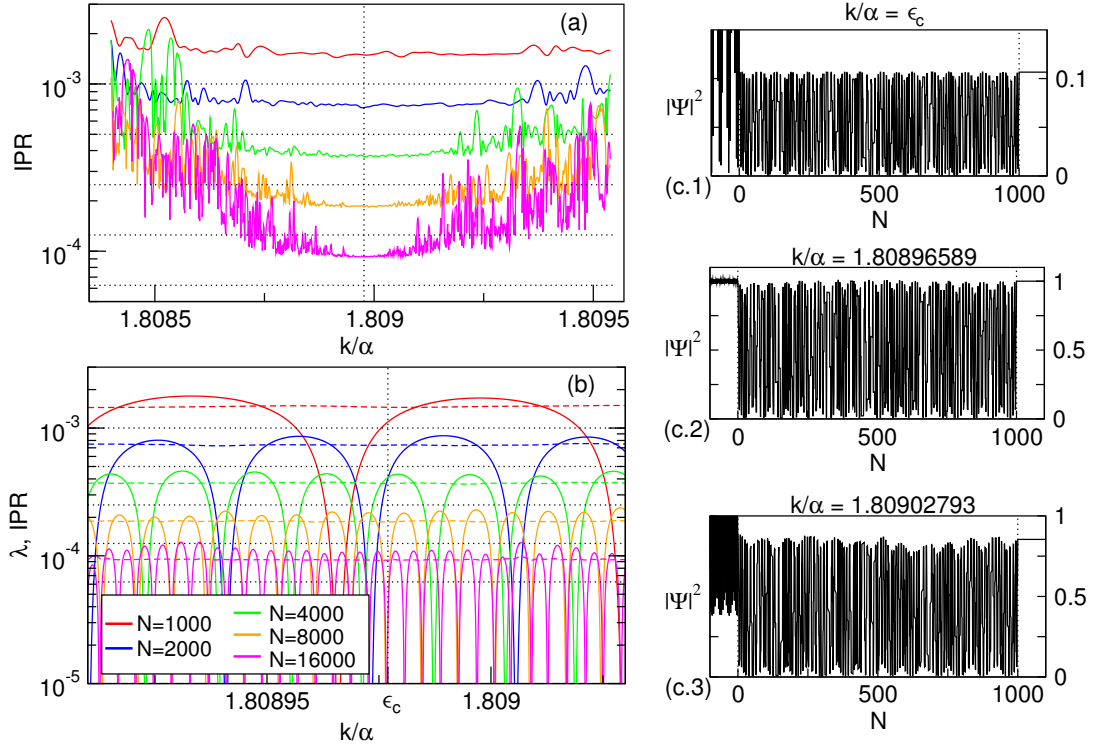
Figure 4.14. (a) IPR near the critical energy $\epsilon_c = 1.808977$ for a binary wire with parameters $V_1 = -2.5$ and $V_2 = 5$ with equal concentrations. (b) Lyapunov exponent (solid lines) and IPR (dashed lines) near the critical energy for different lengths. The horizontal dotted lines mark the inverse of the different lengths considered. For a given length, data of all figures correspond to the same disordered sequence. Only one realization of the disorder has been considered for each length. Graphics on the right column show the envelope of the electronic state for the chain with 1000 atoms for three different energies corresponding to transmissions: (c.1) $T = 0.1067$, (c.2) $T = 0.9999$, (c.3) $T = 0.8537$.

atoms. For pure one species chains the envelope shows a perfect periodic modulation, although the latter period sometimes can be larger than the size of the chain. The electronic state registers a morphing process through the disordered configurations between the two limiting pure cases and it always remains completely extended over the array.

Let us also comment that within this small scale of energies near the commuting-resonances, the influence of the atomic sequence is much more important than in the case of CBE-resonances, because the structure of the envelope of the wave function at a local level is fully determined by the atomic sequence. Of course this dependence on the realization of the disorder gets weaker as the system grows. This influence can be noticed in figure 4.14(b), where the arrangement of the hollows of the Lyapunov
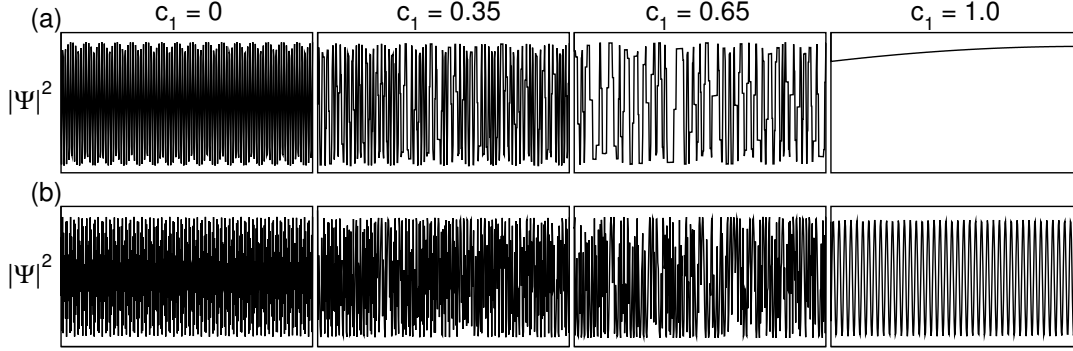
Figure 4.15. Evolution of the envelope of the electronic state at a commuting critical energy as a function of concentration, for binary disordered wires with open boundary conditions. (a) $V_1 = -2.5$, $V_2 = 5$ and $\epsilon_c = 1.808977$, (b) $V_1 = 5$, $V_2 = 7$ and $\epsilon_c = 2.600753$. In all cases the system includes 500 atoms and the states are properly normalized to make the comparison possible.

exponent (i.e. resonances of the transmission) for different N seems more irregular than in the case of a CBE-resonance (figure 4.13), although the length of the system is increased by the same factor in both cases. Only for the chain with 16000 atoms the self-similar pattern in the appearance of transmission resonances emerges, manifesting that the effect of the length of the system has become stronger than the effect of the particular sequence.

Finally, we carried out the multifractal analysis for states near the commuting critical energies. This is somehow motivated by the fluctuating structure of the wave functions and also as an additional check of their real extended character. The multifractal analysis was first introduced to characterize the structure of a fractal distribution at various spatial scales via a set of generalized fractal dimensions [94]. The applicability of this tool to the study of electronic states comes from critical wavefunctions, which exhibit an intricate oscillatory behaviour that may include self-similar fluctuations at different spatial scales (see reference [137] for a nice dissertation about critical states among many other things). Regarding electronic states, the multifractal analysis essentially studies the scaling of the different moments of the probability distribution of the state with the length of the system N. Those moments are defined as

$$\mu_q(N) \equiv \frac{\sum_j |\Psi_j|^{2q}}{\left(\sum_j |\Psi_j|^2\right)^q}. \tag{4.35}$$

And the corresponding generalized fractal dimensions D_q are obtained from the scaling law $\mu_q(N) \sim N^{-(q-1)D_q}$ for large N. Let us notice that the second order moment μ_2 is the inverse participation ratio. The multifractal analysis is useful in order to decide on the localized or extended character of a given state, since one finds $D_q = 0$
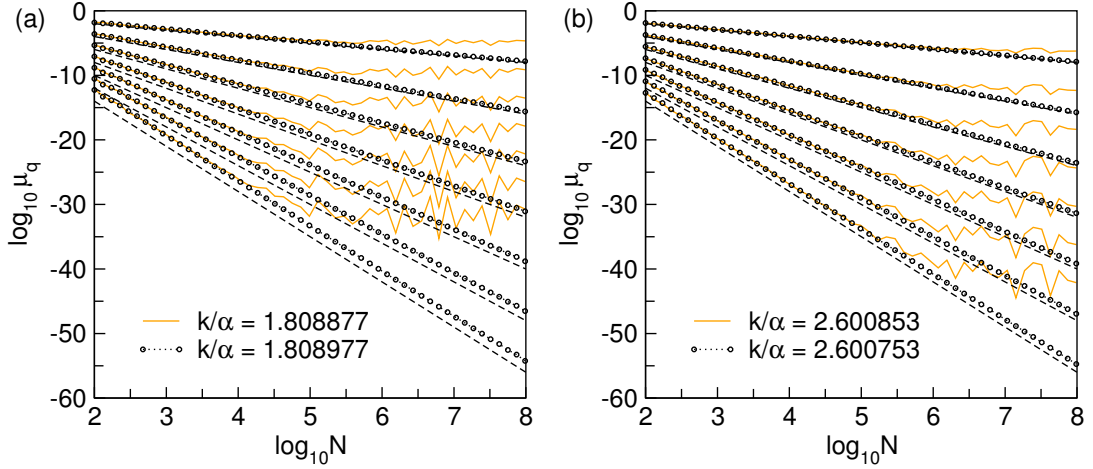
Figure 4.16. Multifractal analysis for binary wires with parameters: (a) $V_1 = -2.5$, $V_2 = 5$ and (b) $V_1 = 5$, $V_2 = 7$ with equal concentrations in both cases. The moments considered range from $q = 2$ to $q = 8$. Dashed lines correspond to equation $\mu_q(N) = N^{-(q-1)}$.

for all $q > 1$ for a localized state whereas in the case of extended states, which spread over the whole system and show no fractal structure at all, D_q equals the spatial dimension of the system for all $q > 1$. In figure 4.16 it can be seen for a couple of binary wires that at the critical energies the moments considered scale with the length of the system according to $D_q = 1$ confirming the extended character of the states, whereas for energies slightly deviated from the critical value the localized nature arises and the generalized dimensions go to zero.

To close this subsection the summarized characteristics of the different types of extended states described can be found on table 4.1 on the following page. Although those features correspond to the Pöschl-Teller model, we have seen how in the case of CBE-resonances the delta model exhibits the same behaviour, therefore it would be very interesting to study whether the features of a given resonance (critical exponents, behaviour of IPR, electronic envelope,...) are fully determined by the nature of the critical energy or on the contrary are also dependent upon the particular potential model.

4.3.3   Negative spectrum of the disordered wires

Let us have a look at the spectrum of bound states of the Pöschl-Teller wires. Most of the times the negative spectrum of disordered systems is not studied since it is not directly involved in the transport processes. The negative spectrum of our model exhibits interesting features very similar to those of the positive spectrum, that we shall

Table 4.1.   Summary of features of the different types of isolated resonances in the spectrum of a disordered Pöschl-Teller wire.

RESONANCE	CRITICAL EXPONENTS	IPR	ENVELOPE	STATES WITH $\lambda < N^{-1}$
Commuting	$\lambda \sim (\epsilon - \epsilon_c)^2$ $g(\epsilon) \sim g_0 + (\epsilon - \epsilon_c)$	$\mathrm{IPR}(\epsilon_c) \neq N^{-1}$ *plateau*	Fluctuating	$\sqrt{N}$
CBE	$\lambda(\epsilon) \begin{cases} \|\epsilon - \epsilon_c\|^{\frac{1}{2}} \\ \|\epsilon - \epsilon_c\| \end{cases}$ $g(\epsilon) \begin{cases} 0 \\ \|\epsilon - \epsilon_c\|^{-\frac{1}{2}} \end{cases}$	$\mathrm{IPR}(\epsilon_c) = N^{-1}$	Flat	$\sqrt{N}$

briefly describe. One can wonder about the degree of localization of the electronic bound states. For negative energies the localization can still be characterized via the Lyapunov exponent even though its physical meaning cannot be defined in terms of the rate of decreasing of the transmission with the length of the system. The well defined meaning of the Lyapunov exponent for negative energies is guaranteed by Oseledet's theorem (MET), as the quantity that measures the exponential divergence of an initial vector under the action of a product of random matrices. The continuous transmission matrices for negative energies are given in definition (4.6). The initial vector of amplitudes for the bound states must be $(A_1 = 0, B_1 = 1)$, where the amplitudes correspond respectively to the exponential solutions of the Schrödinger equation $\mathrm{e}^{-\eta x}, \mathrm{e}^{\eta x}$, where $\eta = \sqrt{2m|E|}/\hbar$. Then the MET implies that the Lyapunov exponent comes from

$$\lambda = \lim_{N \to \infty} \frac{1}{N} \log \sqrt{\mathbb{M}_{12}^2 + \mathbb{M}_{22}^2}, \tag{4.36}$$

where $\mathbb{M}$ is the global matrix of the system. Since the final condition for a state to be bound is $\mathbb{M}_{22} = 0$, one can characterize the electronic localization in a sufficiently large but finite system through

$$\lambda = \frac{1}{N} \log |\mathbb{M}_{12}|. \tag{4.37}$$

Then the Lyapunov exponent for bound states can only be understood as a measure of the inverse of their localization length, $\xi^{-1}(E) = \lambda(E)$, and the above expression is the natural extension for negative energies of expression (2.28). On the other hand the negative spectrum of the wire in the thermodynamic limit can be straightforwardly obtained by using the functional equation formalism —which is valid for the whole
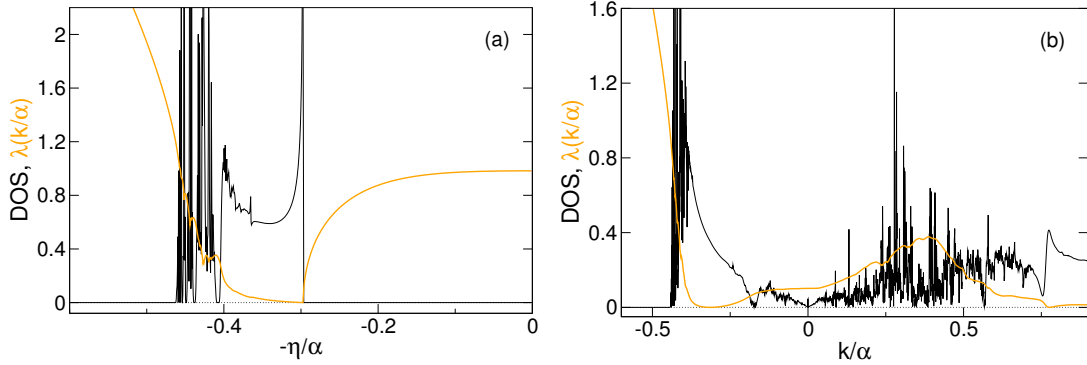
Figure 4.17. DOS and Lyapunov exponent for binary chains. (a) $V_1 = -0.5$, $V_2 = -3.399309$ with equal concentrations. The CBE extended state occurs at $\epsilon_c = -0.297183$. (b) $\alpha_1 = \alpha$, $V_1 = -3.1$, $d_1^L = 4.5/\alpha_1$, $d_1^R = 4/\alpha_1$ and $\alpha_2 = 2\alpha$, $V_2 = -2.5$, $d_2^L = 5.5/\alpha_2$, $d_2^R = 4.5/\alpha_2$ with equal concentrations. The commuting extended bound state is located at $\epsilon_c = -0.314670$. The negative part of the abscissa axis correspond to $-\eta/\alpha$.

spectrum— with the proper canonical functions (4.16)-(4.18). Then one can speak of extended bound states whenever $\lambda = 0$ and of exponentially localized bound states otherwise.

Extended bound states can generally be found using the same reasoning as for the positive spectrum. For example, imposing the condition $\Psi_{j+1} = \pm\Psi_j$ for all sites of the chain one can find the particular form the transmission matrices for negative energies must adopt to generate an extended state,

$$\mathbf{M} = \begin{pmatrix} \pm 1 - a(\eta) & -a(\eta) \\ a(\eta) & \pm 1 + a(\eta) \end{pmatrix}, \quad a(\eta) \in \mathbb{R}. \tag{4.38}$$

Imposing the proper equations to all species included in the chain one is led to the conclusion that this kind of extended bound states can only exist if all potential wells are symmetric ($d_j^R = d_j^L = d_j$), and in this case the following conditions must be satisfied,

$$q_j + \frac{1}{2}\left[f_j(-\eta)\mathrm{e}^{-2\eta d_j} - f_j(\eta)\mathrm{e}^{2\eta d_j} \right] = 0, \qquad \forall j, \tag{4.39}$$

in terms of q and $f(\eta)$ defined in (4.7) and (4.8). It can be checked that the above conditions imply that the energy is a common band-edge of the negative spectrum of the species. Therefore CBE extended bound states can be built as one can see in figure 4.17(a).

Extended bound states can also exist at commuting energies that belong to the permitted spectrum of all species of the wire. For negative energies the commutator

reads

$$[\mathbf{M}_1, \mathbf{M}_2] = \begin{pmatrix} F(-\eta) & H(\eta) \\ -H(-\eta) & F(\eta) \end{pmatrix}, \tag{4.40}$$

where

$$F(\eta) = 2q_1 q_2 \sinh\left[\eta(d_1^L - d_2^L - d_1^R + d_2^R)\right], \tag{4.41}$$

$$\begin{aligned} H(\eta) = & -\mathrm{e}^{-\eta(d_2^R - d_2^L)} q_2 \left[f_1(-\eta)\mathrm{e}^{-\eta(d_1^L + d_1^R)} - f_1(\eta)\mathrm{e}^{\eta(d_1^L + d_1^R)} \right] \\ & + \mathrm{e}^{-\eta(d_1^R - d_1^L)} q_1 \left[f_2(-\eta)\mathrm{e}^{-\eta(d_2^L + d_2^R)} - f_2(\eta)\mathrm{e}^{\eta(d_2^L + d_2^R)} \right]. \end{aligned} \tag{4.42}$$

Assuming that none of the species is a resonant well, then in general $q_1 \neq 0$ and $q_2 \neq 0$, although of course the critical energy could be fix from $q_1 = 0$ or $q_2 = 0$ but this would mean a much more restrictive fit of the parameters. Commuting extended bound states can be found for a really wide range of the parameters of the potentials as long as the asymmetry of the species is the same, $d_1^R - d_1^L = d_2^R - d_2^L$, since in this case $F(\eta)$ is identically zero and the only requirements to have a commuting energy are: $H(\eta) = 0$ and the condition of belonging to the permitted spectrum of both species, which can readily be obtained from the trace of the transmission matrix. An example is shown in figure 4.17(b).

A particular case that deserves a comment is the composition of wells for which b, defined in (4.5), is a half-integer (the case of integer b corresponds to the resonant well which will be treated in the next section). Let us remember that the dimensionless amplitude can be written as $V = -b(b-1)$. We already know from section 4.1 that the bound states of a well with a half-integer b correspond to half-integer values of η/α. It can easily be checked that the matrix of such a well at the eigenenergies reads

$$\mathbf{M} = \begin{pmatrix} 0 & \pm\mathrm{e}^{-\eta(d^R - d^L)} \\ \mp\mathrm{e}^{\eta(d^R - d^L)} & 0 \end{pmatrix}. \tag{4.43}$$

These matrices trivially commute with eachother provided the asymmetry is the same for all wells. Therefore a chain including different wells with different half-integer values of b_γ and values for α_γ such that the potentials exhibit common levels will show extended bound states precisely at those energy levels, as can be seen in figure 4.18(a).

Even when b is not a half-integer, due to the structure of the discrete spectrum of the Pöschl-Teller hole (figure 4.2 on page 77) is easy to choose a couple of different wells with common bound levels, however in this case the matrix of a general well for its eigenenergies reads

$$\mathbf{M} = \begin{pmatrix} f(-\eta)\mathrm{e}^{-\eta(d^R + d^L)} & \pm\mathrm{e}^{-\eta(d^R - d^L)} \\ \mp\mathrm{e}^{\eta(d^R - d^L)} & 0 \end{pmatrix}. \tag{4.44}$$
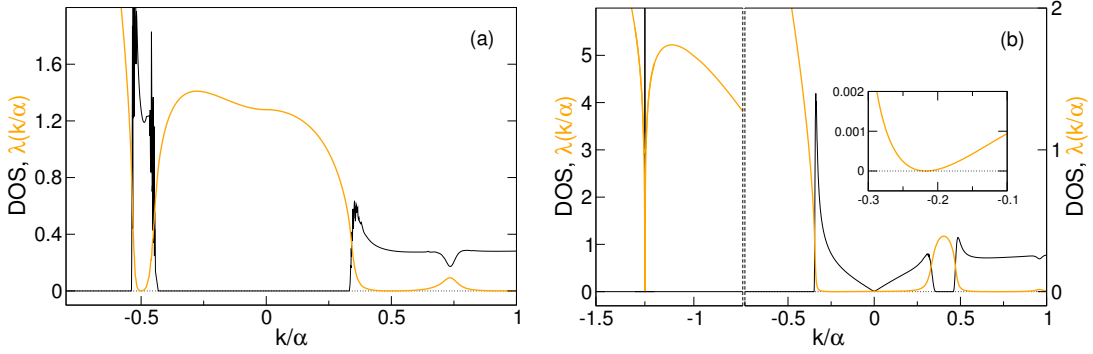
Figure 4.18. DOS and Lyapunov exponent for binary chains including wells in equal concentrations with parameters: (a) $b_1 = 3/2$, $b_2 = 5/2$ with a common eigenstate for $\eta/\alpha = 0.5$ and (b) $V_1 = -2.8125$ and $V_2 = -7.3125$ showing common eigenstates at $\eta/\alpha = 0.25, 1.25$. The commuting extended bound states are located at $\epsilon_c = -0.217142$ and $\epsilon_c = -1.25$. Notice the change in the vertical scale at -0.75 in the (b) example. The negative part of the abscissa axis represents $-\eta/\alpha$.

And these matrices do not commute. Therefore the composition of wells with common levels but with non half-integer (nor integer) values of b will not exhibit extended bound states at the energies of the common levels. Nevertheless since in this case all wells share common levels, a band of bound states is formed around these energies in the thermodynamic limit and we have checked that within these bands a commuting extended bound state always exists and it can be located quite near the common level depending on the width of the band, as can be seen in figure 4.18(b).

It must be emphasized that the behaviour of λ and DOS around the different types of negative critical energies is the same as for their counterparts in the positive spectrum described in table 4.1.

4.3.4 Including resonant wells in the disordered chain

Let us finally considered the interesting case of including resonant potential wells in the disordered system. The resonant wells correspond to potentials with an integer value of b greater than 1. From section 4.1 we know that the transmission for this kind of potentials is identically 1 for all positive energies. The transmission matrix (4.10) for a resonant well naturally reduces to

$$\mathbf{M} = \begin{pmatrix} e^{i[\varphi + k(d^L + d^R)]} & 0 \\ 0 & e^{-i[\varphi + k(d^L + d^R)]} \end{pmatrix}, \tag{4.45}$$

which is the transmission matrix of a zero potential. The resonant well for positive energies behaves as a zero potential with an effective length $L_{\mathrm{eff}}(k) = \varphi/k + (d^R + d^L)$

that depends on the energy. This definition of the effective length only makes sense if it appears multiplied by the energy, since otherwise a divergence appears as k goes to zero. A handy expression can be obtained for the effective length. For a resonant well described by parameters $\{d_\gamma^L, d_\gamma^R, \alpha_\gamma, b_\gamma\}$ it can be proved by induction using the properties of the Gamma function that the following expression is correct

$$kL_{\text{eff}_\gamma}(k) \equiv \epsilon L_{\text{eff}_\gamma}(\epsilon) = \epsilon \frac{\alpha_\gamma d_\gamma^R + \alpha_\gamma d_\gamma^R}{(\alpha_\gamma/\alpha)} + (b_\gamma - 1)\pi - 2 \sum_{j=1}^{b_\gamma - 1} \arctan\left(\frac{\epsilon}{j(\alpha_\gamma/\alpha)}\right), \quad (4.46)$$

where the variable $\epsilon \equiv k/\alpha$ has been introduced and α being the reference value for the parameters $\{\alpha_\gamma\}$.

Let us briefly analyse the appearance of critical energies for a binary chain in which one of the potentials is a resonant well. Since for the resonant well $w_\gamma = 0$ the conditions of positive commuting-resonance reduce simply to

$$\sin\left[kL_{\text{eff}_\gamma}(k)\right] = 0, \quad (4.47)$$

plus the condition of belonging to the permitted spectrum of the other species and without further restrictions on the parameters of the second potential. In the case of CBE-resonances, since the resonant well has no gaps in its positive spectrum it can easily be checked that the conditions (4.32) reduce also to equation (4.47) together with the energy being an appropriate band-edge of the spectrum of the second species. Therefore in a binary chain with one of the species being a resonant well, transmission resonances can only lie among the set of energies satisfying $\epsilon L_{\text{eff}_\gamma}(\epsilon) = n\pi$, $n \in \mathbb{Z}$. For the negative spectrum one similarly obtains that extended bound states must fulfill the equation

$$e^{-\eta(d_\gamma^L + d_\gamma^R)} f_\gamma(-\eta) - e^{\eta(d_\gamma^L + d_\gamma^R)} f_\gamma(\eta) = 0, \quad (4.48)$$

where $f_\gamma(\eta)$ for a resonant well can be expressed as

$$f_\gamma(\eta) = \prod_{j=1}^{b_\gamma - 1} \frac{\eta/\alpha_\gamma - j}{\eta/\alpha_\gamma + j}. \quad (4.49)$$

If such an energy lies in the permitted spectrum of the other species then a commuting extended bound state emerges without further requirements on the parameters of the second species. On the other hand if the energy coincides with a band-edge of the negative spectrum of the second species, which must be a symmetric well, then we have a CBE extended bound state.

Now let us consider a disordered chain entirely composed of different resonant wells. Regarding the negative spectrum of the chain, the matrix of a resonant well

for its eigenlevels is the same as for the case of half-integer b discussed previously (equation (4.43)). Let us remember that the well host $(b_\gamma - 1)$ bound states that correspond to integer values of η/α_γ. Therefore the common eigenlevels of all resonant wells, according to parameters $\{\alpha_\gamma\}$, will arise as extended bound states as long as the asymmetry of all wells is the same. For positive energies the canonical equation of the system (4.12) reduces to

$$\Psi_{j+1} = \left\{ \cos\left[kL_{\text{eff}_j}(k)\right] + \cot\left[kL_{\text{eff}_{j-1}}(k)\right] \sin\left[kL_{\text{eff}_j}(k)\right] \right\} \Psi_j - \frac{\sin\left[kL_{\text{eff}_j}(k)\right]}{\sin\left[kL_{\text{eff}_{j-1}}(k)\right]} \Psi_{j-1},$$
(4.50)

which is the canonical equation for the zero potential defined in (3.34) on page 49 where the wave function is evaluated at different distances corresponding to the effective length of each potential. It is then clear that the electronic states for all energies remain extended in the disordered system. The transmission of the whole structure is maximum for all energies since the system globally behaves as a zero potential. Let us remark that the fully resonant behaviour of the Pöschl-Teller hole provided b_γ is an integer is independent of d_γ^L, d_γ^R, and α_γ as long as the minimum value for the cut-off distances is preserved. In fact, the real dimensional depth of the well reads $\hbar^2\alpha_\gamma^2 V_\gamma/(2m)$, hence one can choose at will the depth of the resonant well by varying α_γ, although it also means a change in the width of the potential. Therefore, one can build a disordered chain of resonant wells with different widths and depths that even can be placed at arbitrary distances from one another with absolutely no correlations in the sequence, which can be completely random indeed, and the structure will behave as a transparent potential for all energies. To our knowledge this is the first theoretical model for which one can build totally random arrays that exhibit a full continuum of extended states and hence an interval of complete transparency, which is indeed the whole positive spectrum.

Let us see how it is possible to describe analytically the distribution of states of these disordered chains in the thermodynamic limit. For a zero potential of length L the integrated density of states is trivially $\mathcal{N}(k) = Lk/\pi$. From this fact one is led to the conclusion that a resonant well should provide the spectrum of the system with $kL_{\text{eff}_\gamma}(k)/\pi$ available states with energy less than k. Then the contribution of every resonant well to the integrated density of states (IDOS) of the chain per piece of length α^{-1} would be

$$\frac{(\alpha_\gamma/\alpha)}{\alpha_\gamma d_\gamma^R + \alpha_\gamma d_\gamma^L} \frac{\epsilon L_{\text{eff}_\gamma}(\epsilon)}{\pi}.$$
(4.51)

Since all species behave effectively as zero potentials, the IDOS of the chain per piece of length α^{-1} in the thermodynamic limit is just the composition of the contributions
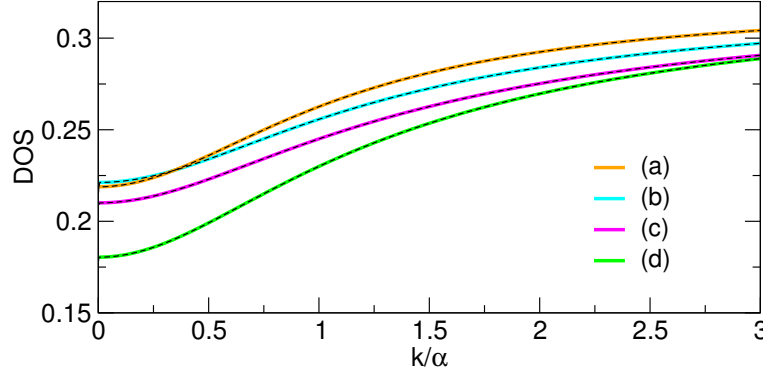
Figure 4.19. DOS for disordered chains composed of resonant Pöschl-Teller holes. Coloured lines correspond to definition (4.54) while black dashed lines are obtained by solving numerically the functional equation. (a) 2 species with $V_1 = -2$ and $V_2 = -6$ with equal concentrations (b) 3 species with $\{\alpha_\gamma, V_\gamma, d_\gamma^L, d_\gamma^R\}[c_\gamma]$: $\{\alpha, -2, 5/\alpha_1, 4/\alpha_1\}[0.5]$, $\{1.2\alpha, -6, 4/\alpha_2, 4/\alpha_2\}[0.3]$, $\{1.5\alpha, -12, 4.5/\alpha_3, 4.5/\alpha_3\}[0.2]$, (c) 2 species with $\{\alpha_\gamma, V_\gamma, d_\gamma^L, d_\gamma^R\}[c_\gamma]$: $\{\alpha, -6, 5/\alpha_1, 4/\alpha_1\}[0.7]$, $\{1.8\alpha, -12, 4.2/\alpha_2, 6.1/\alpha_2\}[0.3]$ and (d) 2 species with $V_1 = -6$, $c_1 = 0.3$ and $V_2 = -12$, $c_2 = 0.7$.

of the different species with their respective concentrations $\{c_\gamma\}$,

$$n(\epsilon) = \frac{1}{\pi} \sum_\gamma c_\gamma \frac{(\alpha_\gamma/\alpha)}{\alpha_\gamma d_\gamma^R + \alpha_\gamma d_\gamma^L} \epsilon L_{\text{eff}_\gamma}(\epsilon). \tag{4.52}$$

And the DOS would obey

$$g(\epsilon) = \frac{1}{\pi} \sum_\gamma c_\gamma \frac{(\alpha_\gamma/\alpha)}{\alpha_\gamma d_\gamma^R + \alpha_\gamma d_\gamma^L} \frac{\mathrm{d}}{\mathrm{d}\epsilon} \left[\epsilon L_{\text{eff}_\gamma}(\epsilon) \right]. \tag{4.53}$$

Inserting expression (4.46) into the latter definition one finally gets

$$g(\epsilon) = \frac{1}{\pi} - \frac{2}{\pi} \sum_\gamma c_\gamma \frac{(\alpha_\gamma/\alpha)}{\alpha_\gamma d_\gamma^R + \alpha_\gamma d_\gamma^L} \sum_{j=1}^{b_\gamma - 1} \frac{j(\alpha_\gamma/\alpha)}{j^2(\alpha_\gamma/\alpha)^2 + \epsilon^2}. \tag{4.54}$$

Using the same reasoning the analytical expression for the DOS can also be straightforwardly obtained when the parameters $\{\alpha_\gamma, d_\gamma^R, d_\gamma^L\}$ obey a continuous distribution. In figure 4.19 the DOS for several disordered chains composed of resonant wells is plotted. It can be seen how the analytical expression reproduces exactly the distribution of states calculated numerically via the functional equation formalism. The DOS for the resonant chains is a continuous and smooth function without gaps that does not vanish for zero energy, and it registers relatively small changes by varying the concentrations or the number of different resonant wells. In figure 4.20 the tolerance
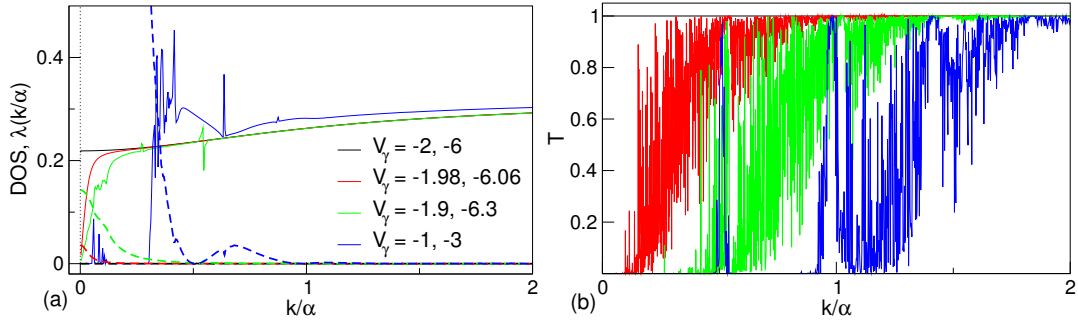
Figure 4.20. Tolerance of the properties of a binary resonant chain with their parameters. (a) DOS(solid line) and Lyapunov exponent(dashed line) in the thermodynamic limit. (b) Transmission patterns for a 1000-atom random sequence. Cases have been considered where both dimensionless amplitudes are deviated 1%, 5% and 50% from the resonant values $V_1 = -2$, $V_2 = -6$.

of the properties of a binary resonant chain are evaluated when their parameters are deviated from the resonant values. As can be seen, a small change of the parameters mean the lost of the full resonant behaviour for all energies. Nevertheless for deviations of order $1\% - 5\%$ in the dimensionless amplitudes, the efficiency of transmission is still much higher than for any other non-resonant binary chain composed of wells. Naturally, for the resonant chains the Lyapunov exponent in the thermodynamic limit calculated via the functional equation vanishes for all energies. It can also be checked that the IPR for finite resonant chains as a function of the energy is simply a straight line at the value N^{-1} where N is the number of potentials, as it must be for flat extended states.

One must not forget that the transmission matrix proposed for the Pöschl-Teller potential is an approximation, since we have assumed that at the cut-off distance the asymptotic form of the states can be used. In fact, this approximation is quite correct; the error that it entails is almost irrelevant for an individual potential and the larger the cut-off distance is the smaller the error becomes. However it might happen that when applying the composition procedure of the potentials to build a disordered array, these small individual deviations give rise to an error growing exponentially with the length of the chain. If it were true, then the behaviour of a real continuous composition of Pöschl-Teller units (i.e. the sum of all the contributions of the potentials centred at different positions) would be far from the results obtained using our techniques. In particular it would be dramatic for a resonant chain for which its resonant behaviour and the delocalization of the electronic states could disappear in the real continuous composition. To show that this exponential error does not occur, we have calculated the transmission probability of several random resonant chains with 100,
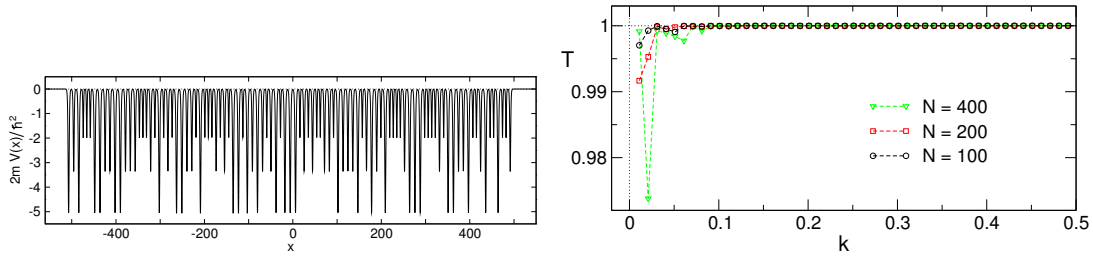
Figure 4.21. Transmission probability for random resonant chains of Pöschl-Teller holes, calculated by solving numerically the Schrödinger equation for the continuum spectrum. The left box shows the random potential profile for 100 potentials. For all lengths the chains include three different species with symmetric cut-off. The parameters are $\{\alpha_\gamma, V_\gamma, d_\gamma\}[c_\gamma]$: $\{1, -2, 4\}[0.4]$, $\{0.75, -6, 5.5\}[0.3]$, $\{0.65, -12, 6\}0.3]$.

200 and 400 potentials, by integrating numerically the Schrödinger equation[1] considering the whole continuous potential of the chain, that is taking into account the superposition of all potential holes centred at their respective positions. In figure 4.21 it can be observed how for very low energies ($k < 0.05$) a small deviation appears from $T = 1$, that for the longest chain is less than $3 \cdot 10^{-2}$. Although this deviation seems to increase slightly with the length of the chain, it apparently does not follow an exponential growing and its effect does not noticeably distort the resonant behaviour of the chain. Then, our composition procedure describes faithfully the properties of the real continuous composite potential profile.

As we have shown, the richness of the Pöschl-Teller potential gives rise to the emergence of new exciting effects in the disordered chains ranging from the appearance of different types of isolated extended states in the spectrum to the construction of resonant chains exhibiting a continuum of delocalized states.

4.4 Wires with correlated substitutional disorder

The Pöschl-Teller potential model is also studied under the effect of correlated substitutional disorder introduced in the same way as for the delta potential model, described in detail in section 3.6. The probability of appearance of different atomic groups is modified by the quantities $\{p_{\gamma\beta}\}$. We have the opportunity to check whether the influence of the model of correlations and their significant effects upon the transport properties of the one-dimensional systems are universal or on the contrary depend upon the atomic model.

---

[1]The numerical integration of the Schrödinger equation for the continuum spectrum must be understood as the numerical calculation of the scattering amplitudes via a spatial discretization of the global potential as described in chapter 2 (section 2.3).
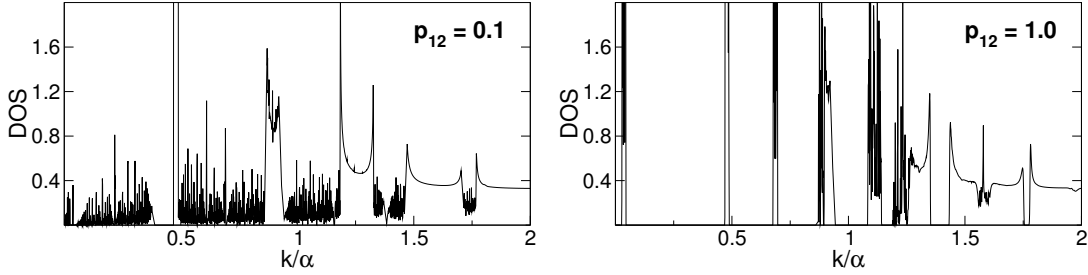
Figure 4.22. DOS for correlated configurations of a binary chain with parameters $V_1 = -2.5$ and $V_2 = 2$ with concentration $c_1 = 0.4$.
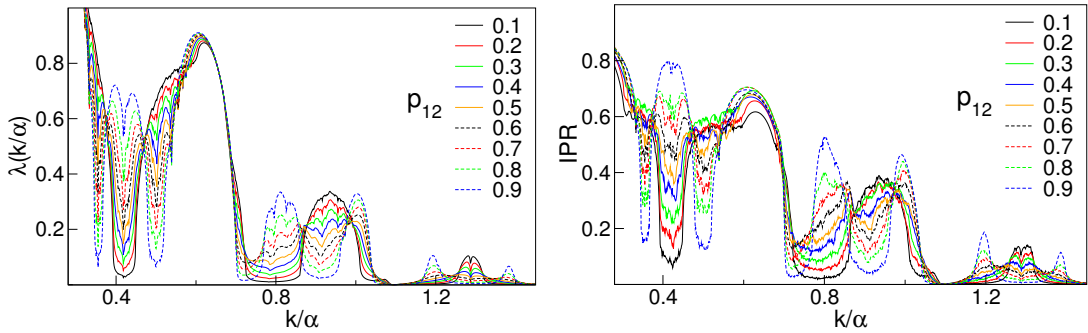

Figure 4.23. Evolution of the Lyapunov exponent and the IPR with the correlations for a binary chain. The IPR has been obtained after averaging 100 sequences of a 1000-atom array. The parameters are: $V_1 = -1$, $V_2 = 1$, $c_1 = 0.5$. Notice the presence of a critical energy at $\epsilon_c = 1.095$.

4.4.1 Effects of the correlations in the thermodynamic limit

As already known, the limiting distributions of the DOS and the Lyapunov exponent for the infinite system are obtained by solving numerically the most general form of the functional equations.

The density of states of a binary chain is altered by the effect of the correlations in a similar manner as for the delta model. In figure 4.22 the DOS is plotted for the two limiting correlated situations of a binary chain with fixed concentrations. The number of available states in certain ranges as well as the gaps can be changed by tuning p_{12}. It can also be checked that for the correlated configurations the fractal character of the distribution persists in different energy intervals.

The electronic localization is globally altered by the correlations in the whole energy spectrum, although as expected no new extended states emerge in the thermodynamic limit, as can be seen in the examples of figure 4.23. The evolution of the Lyapunov exponent for a fixed concentration with the probability p_{12} agrees perfectly with the behaviour of the inverse participation ratio calculated by averaging over
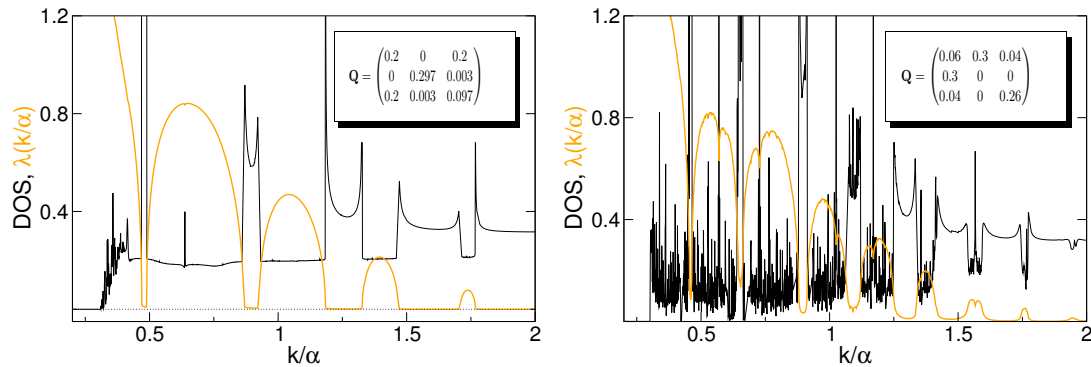
Figure 4.24. DOS and Lyapunov exponent for different correlated configurations of a ternary chain with fixed concentrations. The species are $V_1 = -3$, $V_2 = 2$ and $V_3 = -1$. The configuration for each case is included in the characteristic matrix **Q**.

many finite realizations of the disordered system. Let us notice that the critical energies of the spectrum corresponding to extended states are present in all the different correlated regimes. It is also remarkable the fact that as the correlations change, the value of the Lyapunov exponent can be strongly decreased for several energies. These energies for which the localization can be severely weakened are related to resonances of different atomic clusters whose concentration is modified by the correlations. For example, in a binary chain composed of a well (1) and a barrier (2), for the case $p_{12} = 1.0$ the wells are completely isolated so that they always appear in the cluster barrier-well-barrier. Therefore it seems reasonable that in this correlated situation the energies of transmission resonances of the latter cluster will tend to be more delocalized than for any other value of p_{12}. This effect is more noticeable in this model than for the delta model, since in that case the atomic potentials lack an internal structure.

When more species are included in the wire similar effects can be observed and the properties of the system can be considerably altered as can be seen in figure 4.24 for a ternary chain.

4.4.2 Effects of the correlations on finite wires

Although not truly extended states are included in the spectrum, the effects of these short-range correlations upon finite samples of the wires are able to improve noticeably the electronic transport. In figure 4.25 on the facing page several transmission patterns for finite binary chains composed of 1000 atoms are plotted. In the correlated configurations the transmission is improved with respect to the completely random situation. Let us notice that just like for the delta model the improvement can take place
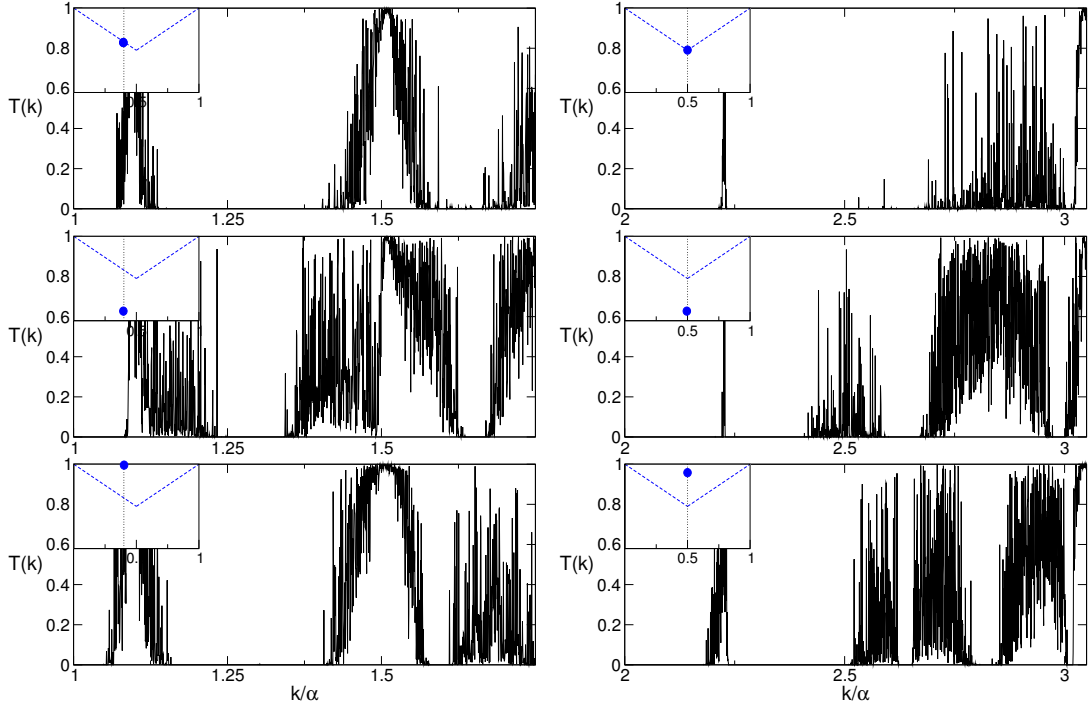
Figure 4.25. Transmission probability vs energy for 1000-atom binary disordered chains in different correlation regimes. The circular point inside the insets marks the configuration on the configurational space. Only one realization of the disorder has been considered for each case. Parameters: (left column) $V_1 = -1$, $V_2 = 1$, $c_1 = 0.4$ and correlation from top to bottom $p_{12} = 0.6, 0.1, 1.0$ and (right column) $V_1 = -2.5$, $V_2 = 5$, $c_1 = 0.5$ and correlation from top to bottom $p_{12} = 0.5, 0.1, 0.9$.

in different energy ranges and it is not restricted to the vicinity of the critical energies in the thermodynamic limit. As expected, the enhancement of transmission occurs in the whole configurational space of the binary wire as revealed by the transmission efficiency,

$$T_{\text{eff}} = \frac{1}{k_2 - k_1} \int_{k_1}^{k_2} T(k) \mathrm{d}k. \tag{4.55}$$

The minimum intensity of the transport is found around the completely random lines whereas the correlated configurations perform always better (figure 4.26 on the next page). The patterns of the enhancement are similar to those of the delta model although it must be emphasized that the transmission efficiency may adopt a strong asymmetric distribution over the configuration space, depending on the species amplitudes. This asymmetry is absolutely negligible in the delta model since the delta potential from the point of view of the transmission behaves essentially in the same way independently of the sign of the coupling. However provided the atomic potentials are non-punctual and have an internal structure, this asymmetry may be quite
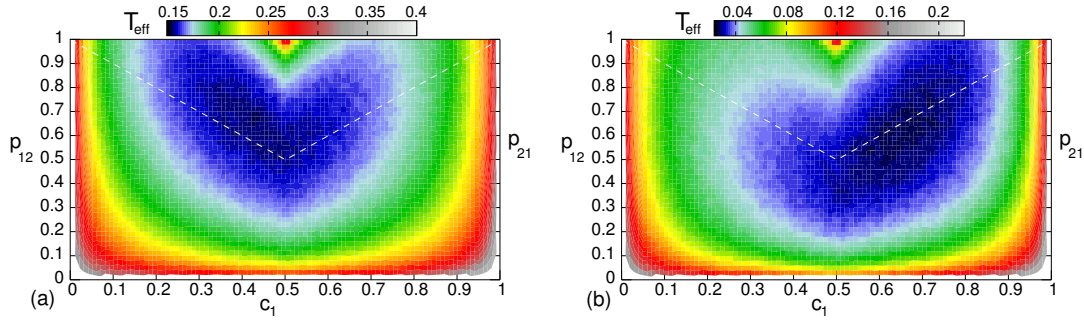
Figure 4.26. Transmission efficiency over correlation space for binary chains: (a) $V_1 = -2.5$, $V_2 = 5$ and integration interval $[0, 3.7]$, (b) $V_1 = 2.5$, $V_2 = 5$ and integration interval $[0, 3]$.

noticeable since a potential well performs a better transmission than a potential barrier, and the same thing happens comparing barriers of different heights. Therefore the transmission efficiency naturally registers a global lift or a global decrease depending on whether the concentration of the species that is more tolerant with the transmission process is larger or less than 0.5.

Then the enhancement of transmission in finite wires is a fact. And the reason is that the short-range correlations modify the localization in the thermodynamic limit in such a way that the fluctuations of the Lyapunov exponent for a finite system cause an important increase of the number of states whose localization length (ξ) is larger than the system size (L). This seems to be a universal effect of this sort of correlations independently of the atomic model. Additionally, once the compositional species and the concentrations of the wire are fixed, the correlations can be chosen to localize to a certain extent the improvement of transmission in a particular energy range. Let us also remember that the amplitude of the fluctuations of the Lyapunov exponent and therefore the number of states with $\xi > L$ only depends upon the length of the system. Hence in all the calculations only one realization of the disorder has been considered for each configuration.

As the length of the wire grows the completely random chain displays the fastest decay of T_{eff} whereas the correlated situations show higher efficiencies for all lengths, as can be seen in figure 4.27. The relative differences $\Delta T_{\text{eff}} = T_{\text{eff}} - T_{\text{eff}}(R)$ as a function of the length, where (R) means the completely random value, reveals that the effect of the correlations is generally maximized for short chains.

From the analysis made on the Pöschl-Teller wires and the delta wires, it must be remarked that the effects described of this type of correlated disorder are essentially independent of the potential model.
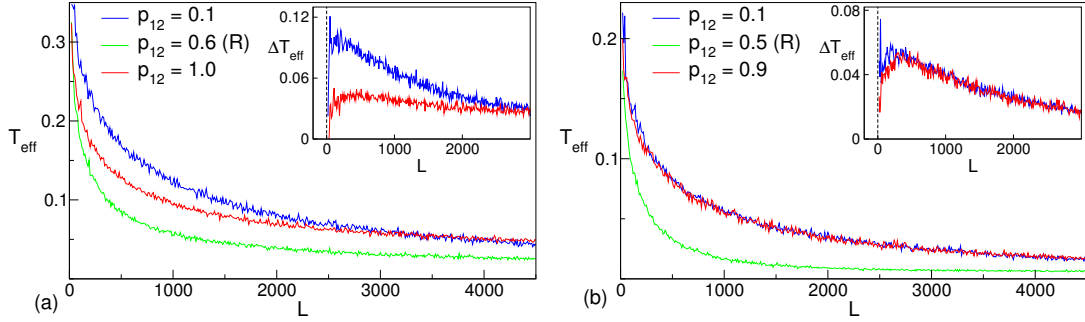
Figure 4.27. Transmission efficiency vs length for different configurations of a 1000-atom binary chain with parameters (a) $V_1 = -1$, $V_2 = 1$, $c_1 = 0.4$, integration interval $[0, 1.75]$ and (b) $V_1 = -2.5$, $V_2 = 5$, $c_1 = 0.5$, integration interval $[0, 3.05]$. (R) marks the completely random situation. The inset shows the relative differences $\Delta T_{\text{eff}} = T_{\text{eff}} - T_{\text{eff}}(R)$.

4.5 Concluding remarks

In this chapter the Pöschl-Teller potential has been considered to build one-dimensional quantum wires. Let us briefly summarize the results:

- The transmission matrix of the Pöschl-Teller potential has been constructed in its asymptotic as well as in its cut-off version. Using the former the peculiarities of the potential has been described whereas the latter has made it possible to assembly an arbitrary number of atoms to study different atomic potential profiles.

- The properties of the disordered wire in the thermodynamic limit have been thoroughly studied using the canonical equation and the functional equation formalism.

- Fractality of the density of states has manifested itself as a universal property of the spectra of disordered systems and it seems to be related to the discretized nature of the distributions of the parameters characterizing the disordered system.

- Different types of extended electronic states, defined as CBE-resonances and commuting-resonances, have been described for the disordered system. Their different features have been studied in detail in the thermodynamic limit and for finite realizations of the chains. The appearance of extended bound states belonging to the negative spectrum of the disordered wire has also been revealed.

- The building of a wire exhibiting a continuum of delocalized states for positive energies has been described. The array is composed of resonant wells and its implementation is quite versatile since many parameters of the system can be varied without any restrictions and of course its behaviour is absolutely independent of the random or correlated character of the sequence. The DOS for this system in the thermodynamic limit has been analytically obtained.

- Finally, short-range correlations have been introduced in the system, showing that the effects of the type of correlations proposed and its significant implications on the transmission efficiency of finite samples, are independent of the potential model.

Quantum wire with complex potentials

Non-Hermitian Hamiltonians and complex imaginary potentials are often used with different purposes. They lead to the appearance of new features in the behaviour of systems whose description can be sometimes related to dissipative processes. On the other hand the question of whether it is possible to define a less restrictive condition than Hermiticity to build Hamiltonians describing real physical situations is a subject of an intense research. The aim of this chapter is twofold. First a purely academic study on the characteristics of a periodic system under the requirement of $\mathcal{PT}$-symmetry is performed. More general non-Hermitian Hamiltonians are later on considered to try to describe electronic absorption in one-dimensional structures.

5.1 $\mathcal{PT}$-symmetric periodic wires

Several years ago, it was claimed that the reality of the spectrum of certain non-Hermitian Hamiltonians was due to $\mathcal{PT}$-symmetry [22]. That is the Hamiltonian is invariant under the joint action of parity ($\widehat{\mathcal{P}}$) and time-reversal ($\widehat{\mathcal{T}}$) operators. For a complex local potential, $\langle x| \widehat{V}(x) |x'\rangle = V(x)\delta(x - x')$, the requirement of $\mathcal{PT}$-symmetry imposes $V(x) = V^*(-x)$, which means that the real part of the potential must be symmetric and the imaginary part antisymmetric [150]. Different classes of $\mathcal{PT}$-symmetric Hamiltonians have been studied exhibiting a real and bounded below discrete spectrum [23], though in some cases for a range of parameters complex eigenvalues do occur which are associated with a spontaneous breaking of $\mathcal{PT}$-symmetry.

There have been various attempts to demonstrate that $\mathcal{PT}$-symmetry can be understood most conveniently using the theory of pseudo-Hermitian Hamiltonians (see reference [144] for a review about the physical aspects of pseudo-Hermitian quantum mechanics) and that a quantum system possessing $\mathcal{PT}$-symmetry is equivalent to a quantum system having a Hermitian Hamiltonian [146]. Nevertheless some controversial points are still part of the theory [145].

The examples of $\mathcal{PT}$-symmetric quantum Hamiltonians so far existing in the literature rely more on aspects concerning the discrete spectrum and bound states [191, 21, 20] although there has been some or other attempt to extend the discussion to states of the continuum spectrum [53].

Our aim is to perform band structure calculations by using $\mathcal{PT}$-symmetric Hamiltonians. As has been well known for years, a Hermitian periodic potential cannot alter its band spectrum just by fine tuning the parameters. The bands can indeed be made wider or narrower but their number and quality (forbidden or allowed) remain unchanged. The physical idea is indeed whether this behaviour would be maintained if a $\mathcal{PT}$-invariant potential is used. It was shown in an earlier work how for a certain $\mathcal{PT}$-symmetric periodic Hamiltonian the band condition remained real [24], however the results concerning the appearance of removal of bands were inconclusive.

To tackle the given problem we have the use of an analytical band condition for a simple one-dimensional model that can be easily extended to the $\mathcal{PT}$-symmetric domain.

5.1.1   The model

Let us begin with a brief remainder of the model presented in section 3.2 corresponding to an infinite periodic potential whose primitive cell is made out of N equally spaced deltas with different real couplings. If the spacing is a and $a_j = \hbar^2/m\alpha_j$ is the length associated to each coupling (α_j), the band structure can be written as

$$\cos(Nqa) = \mathcal{B}(\epsilon; a_1, \ldots, a_N), \tag{5.1}$$

where $q \in [-\pi/L, \pi/L]$ defines the first Brillouin zone (1BZ) in the reciprocal space, and the band condition $\mathcal{B}(\epsilon; a_1, \ldots, a_N)$ is defined in equations (3.12) in terms of the elementary functions $h_j(\epsilon) = \cos(\epsilon) + (a/a_j)\sin(\epsilon)/\epsilon$ and $\epsilon \equiv ka$ being a dimensionless representation of the energy. Let us list below, for the benefit of the reader, the first

three conditions for the cases $N = 2$, 3 and 4.

$$\cos(2qa) = 2\,h_1 h_2 - 1, \tag{5.2}$$

$$\cos(3qa) = 4\,h_1 h_2 h_3 - (h_1 + h_2 + h_3), \tag{5.3}$$

$$\cos(4qa) = 8\,h_1 h_2 h_3 h_4 - 2(h_1 h_2 + h_1 h_4 + h_2 h_3 + h_3 h_4) + 1. \tag{5.4}$$

The next step is to add $\mathcal{PT}$-symmetry to this model. In order to do so we include the following changes:

- Promote the couplings from real to complex: $\left(\frac{a}{a_j}\right) \to r_j + \mathrm{i}s_j$.

- Order the potential in a $\mathcal{PT}$-invariant form, that allows us to choose a $\mathcal{PT}$-symmetric primitive cell. This leads to the following identifications (* means complex conjugation):

$$h_N = h_1^*,$$
$$h_{N-1} = h_2^*,$$
$$\vdots$$
$$\begin{cases} h_{\frac{N}{2}+1} = h_{\frac{N}{2}}^*, & \text{even } N \\ h_{\frac{N+1}{2}} = h_{\frac{N+1}{2}}^*, & \text{odd } N. \end{cases}$$

It is easy to check that equation (5.1) remains real under these identifications, which make obviously the periodic potential complex but $\mathcal{PT}$-invariant. In order to analyse the band structure, one has to assert whether the band condition $\mathcal{B}(\epsilon; a_1, \ldots, a_N)$ is above (below) $+1$ (-1). In the model of reference [24] this appears a very hard task indeed as the authors do not have at their disposal an analytical band condition, so they must carry out various kinds of approximations. In our case several analytical and numerical analysis can be performed in order to check the dependence of the band width and the band number on the key parameter that arises in the model: the imaginary part of the complex couplings.

5.1.2 The band condition for couplings with non-vanishing imaginary part

In order to understand the effect of the imaginary part of the couplings on the band spectrum, one must analyse in detail the behaviour of the band condition. Let us begin with the simplest $\mathcal{PT}$-symmetric chain including 2 deltas in the primitive cell characterized by the parameters $(a/a_1) = r_1 + \mathrm{i}s_1$ and $(a/a_1)^* = r_1 - \mathrm{i}s_1$. This case has

been also studied considering different distances between the deltas [6]. The band structure is entirely determined by the function $\mathcal{B} = 2\,h_1 h_1^* - 1$, which can written as

$$\mathcal{B} = \mathcal{B}(s_1 = 0) + \frac{2s_1^2 \sin^2(\epsilon)}{\epsilon^2}. \tag{5.5}$$

The term due to the imaginary part is always positive and it has the effect of lifting up the band condition for all values of r_1. The position and width of the allowed (forbidden) bands come from the intersections at $\mathcal{B} = 1, -1$, which depend strongly on the position of the maxima and minima of the band condition. The changes on these limiting points can be analytically described in this case.

From the equation $\mathrm{d}\mathcal{B}/\mathrm{d}\epsilon = 0$ one can find the value of the oscillatory part of the band condition (i.e. the trigonometric functions) as a function of ϵ and substituting into $\mathcal{B}$ with a properly choice of signs will result in an analytical form for the curves crossing the extremal points of the band condition,

$$C_\pm = 2\,f_\pm f_\pm^* - 1, \tag{5.6}$$

where $C_+(C_-)$ lies on the maxima(minima) and the functions $f_\pm$ are defined as follows:

$$f_\pm = \frac{1}{\sqrt{F_\pm}} \left[\sqrt{2} r_1 (r_1 - \mathrm{i} s_1) \pm \left(F_\pm - 2 r_1^2 \epsilon^2 \right)^{\frac{1}{2}} \right], \tag{5.7}$$

$$F_\pm = r_1^2 + (r_1^2 + s_1^2)^2 + 2(r_1 + r_1^2 - s_1^2)\epsilon^2 + \epsilon^4 \\ \pm (r_1 - r_1^2 - s_1^2 + \epsilon^2) \left[(r_1 + r_1^2 + s_1^2)^2 + 2(r_1 + r_1^2 - s_1^2)\epsilon^2 + \epsilon^4 \right]^{\frac{1}{2}}. \tag{5.8}$$

Hence, the behaviour of the band condition can be studied through the evolution of $C_\pm$. Taking the limit $s_1 \to 0$ we obtain

$$\lim_{s_1 \to 0} C_+ = 1 + \frac{2r_1^2}{\epsilon^2} \frac{r_1(2 + r_1) + \epsilon^2}{r_1(2 + r_1) + \epsilon^2 + \frac{r_1^2}{\epsilon^2}}, \tag{5.9}$$

$$\lim_{s_1 \to 0} C_- = -1. \tag{5.10}$$

The real part of the couplings controls the amplitude of the oscillations (and therefore the distance between C_+ and C_-) but the minima will always lean on $\mathcal{B} = -1$ unless the imaginary part is non-zero. Thus as we increase s_1 the minima will rise, as can be seen in figure 5.1(a), and they never touch -1 since $\lim_{\epsilon \to \infty} C_- = -1$. On the other hand, considering $r_1 \to 0$, after some algebra one obtains

$$\lim_{r_1 \to 0} C_+ = \begin{cases} -1 + \dfrac{2s_1^2}{\epsilon^2} \dfrac{s_1^4 + \epsilon^4 + s_1^2(1 - 2\epsilon^2)}{s_1^4 + \epsilon^4 + s_1^2(\frac{s_1^2}{\epsilon^2} - 2\epsilon^2)} & \text{for } \epsilon \leqslant s_1, \\ 1 & \text{for } \epsilon > s_1, \end{cases} \tag{5.11}$$
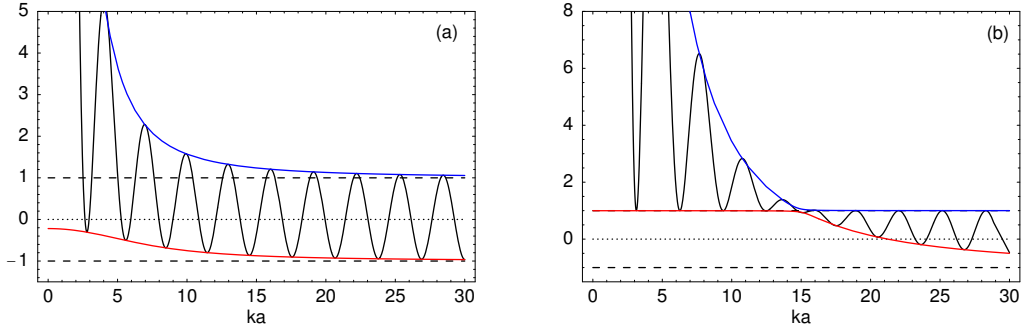
Figure 5.1. Band condition for $N = 2$ when $s \sim r$ in (a) $r_1 = 5$, $s_1 = 4$ and $s \gg r$ in (b) $r_1 = 0.5$, $s_1 = 15$. The coloured lines correspond to $C_{\pm}$.

and for C_- the limit is the same as for C_+ but interchanging with respect to the intervals in ϵ. Thus for an imaginary part of the coupling large enough compared to the real one the band condition goes above $+1$ for energies below the value s_1. Figure 5.1(b) shows this last configuration. In fact the situation $s_1 \gg r_1$ can be easily understood from the form of the band condition that can be written in this limit as

$$\mathcal{B} \simeq -1 + \frac{2s_1^2}{\epsilon^2} + 2\cos^2(x)\left(1 - \frac{s_1^2}{\epsilon^2}\right), \tag{5.12}$$

which shows clearly the boundaries when $\epsilon \leqslant s_1 : 1 \leqslant \mathcal{B} \leqslant -1 + 2s_1^2/\epsilon^2$ saturated at $\epsilon = n\pi$ and $\epsilon = (2n+1)\frac{\pi}{2}$, $n \in \mathbb{Z}$, respectively. For $\epsilon > s_1$ the boundaries simply interchange among them. Due to the nature of the functions $h_j(\epsilon)$ the band condition is always tied up to the value $+1$ at every multiple of π for all r_1, s_1, as figure 5.1(b) clearly shows. Several configurations of the spectrum such as those in figure 5.1 can be built for different values of the complex coupling.

Let us now consider a $\mathcal{PT}$-symmetric chain whose primitive cell includes 3 atoms characterized by the parameters $(a/a_1) = r_1 + is_1$, $(a/a_2) = r_2$ and $(a/a_1)^*$. The band condition function reads $\mathcal{B} = 4\,h_1 h_1^* h_2 - (h_1 + h_1^* + h_2)$. This can be arranged as

$$\mathcal{B} = \mathcal{B}(s_1 = 0) + \frac{4s_1^2 \sin^2(\epsilon)\left[\epsilon\cos(\epsilon) + r_2\sin(\epsilon)\right]}{\epsilon^3}. \tag{5.13}$$

The extra term arising from the imaginary part of the coupling can be either positive or negative depending on the value of r_2 and the energy. The effect of s_1 is different compared to the previous case although there is only one imaginary parameter. The structure of the band condition seems to be composed by pieces each one including 3 different types of extremal points, as figure 5.2(a) shows, each type apparently following a given pattern. The curves crossing the extremal points of the band condition can also be analytically calculated in the $N = 3$ case but the expressions are
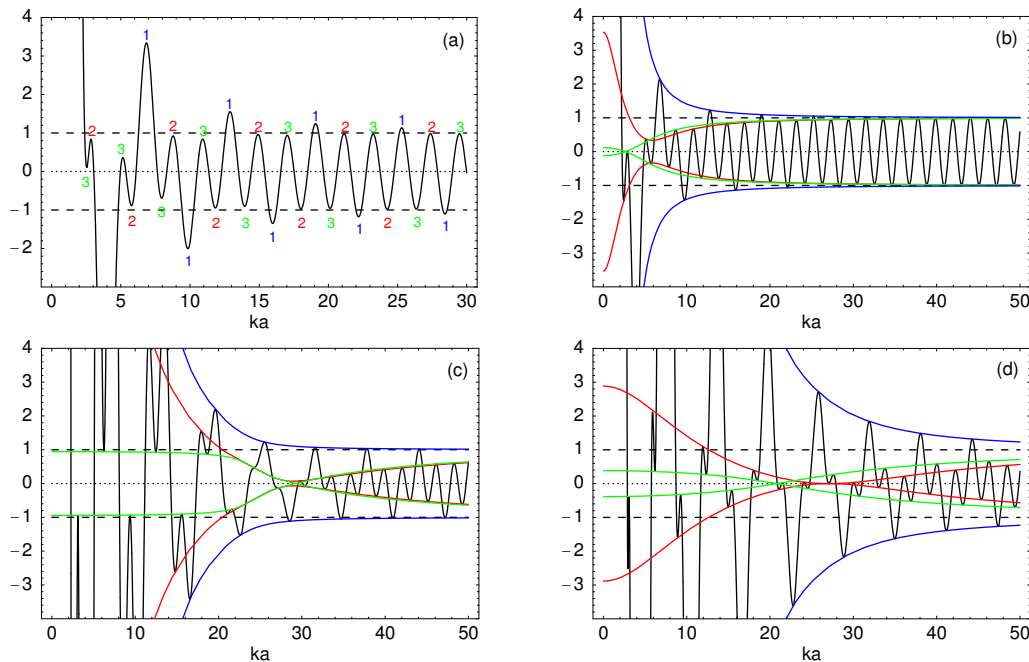
Figure 5.2. Band condition for $N = 3$ for different values of the couplings. Each type of extremal point is labelled with a different colour. (a) $r_1 = 4$, $r_2 = 5$, $s_1 = 3$, (b) $r_1 = 3$, $r_2 = 2$, $s_1 = 5$, (c) $r_1 = 3$, $r_2 = 2$, $s_1 = 25$, (d) $r_1 = 10$, $r_2 = 10$, $s_1 = 25$.

quite hard to simplify and therefore we do not provide the explicit form of the equations. Three curves are obtained, one for each type of extremal point. Initially when $s_1 = 0$ all the extremal points are outside or on the borders of the range $[-1, 1]$. As we increase the imaginary part, the amplitudes of two of the three types of extremal points begin to decrease (green and red in figure 5.2(b)). At the same time as s_1 becomes larger the green and red curves get narrower with decreasing energy until $\epsilon \sim s_1$. Below this value the curves broaden trying to expel the extremal points of the band condition outside the target range (figure 5.2(c)). From the form of $\mathcal{B}$ it is clear that the even(odd) multiples of π will remain fixed to $1(-1)$. The efficiency of this expelling process depends upon the values of the real couplings as they control the amplitudes of the oscillations. One can stretch the maxima and minima (up and down respectively) increasing r_1, r_2, as shown in figure 5.2(d).

Several configurations can be obtained among those shown in figure 5.2 and one important feature must be emphasized: the band condition always changes 'symmetrically' with respect to the abscissa axis. That is, there is the same amount of positive and negative function whatever the values of the couplings are. In fact the curves lying on the extremal points show an exact reflection symmetry around the energy axis. This is in great contrast to the $N = 2$ case where the band condition can be pushed
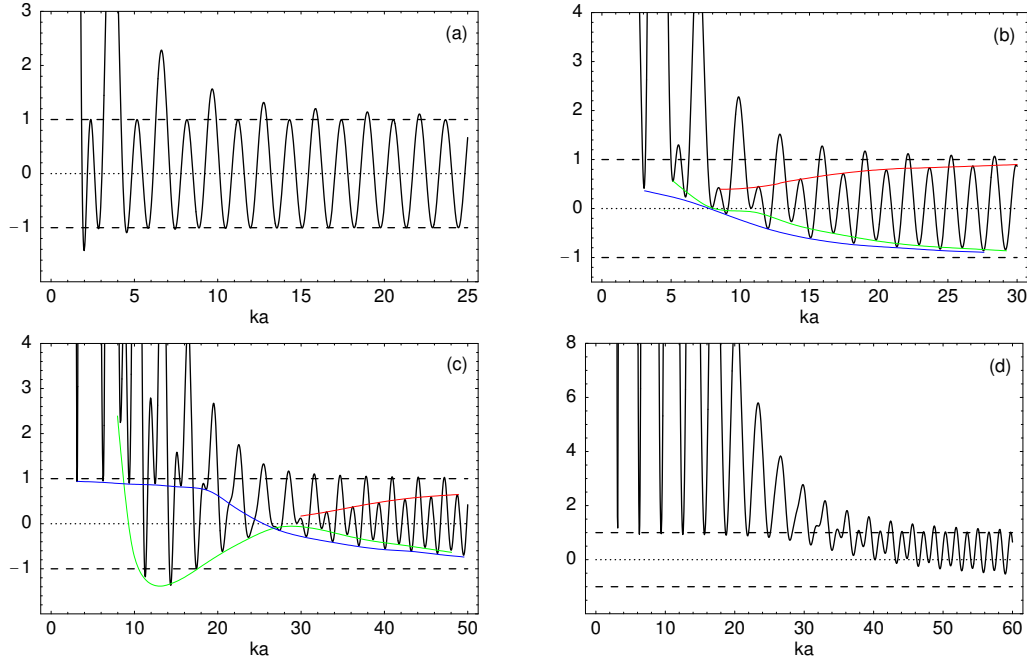
Figure 5.3. Band condition for $N = 4$ with different values of the couplings. The coloured lines are intended to clarify the behaviour of different groups of extremal points. (a) $r_1 = 3$, $r_2 = 2$, $s_1 = 0$, $s_2 = 0$, (b) $r_1 = 3$, $r_2 = 2$, $s_1 = 9$, $s_2 = 2$, (c) $r_1 = 3$, $r_2 = 2$, $s_1 = 4$, $s_2 = 25$, (d) $r_1 = 3$, $r_2 = 2$, $s_1 = 20$, $s_2 = 21$.

up above $+1$ for certain couplings. Thus when $s_1 \gg r_1, r_2$ there will always remain a trace of the original permitted energy ranges in the form of 'flat' bands.

The first chain for which two different imaginary couplings can be manipulated is the one with $N = 4$ atoms inside the primitive cell: $(a/a_1) = r_1 + \mathrm{i} s_1$, $(a/a_2) = r_2 + \mathrm{i} s_2$, $(a/a_2)^*$ and $(a/a_1)^*$. In this case we have not calculated analytically the curves crossing the extremal points. Nevertheless a pictorial approach for some of the curves has been included in the graphics for a better understanding of the tendencies of change. The initial situation ($s_1 = s_2 = 0$) is a common one for a periodic chain (figure 5.3(a)) and two different group of extremal points can be distinguished. As we increase the imaginary part of the couplings one group of extremal points starts to decrease and the band condition lifts up globally (figure 5.3(b)). The effect of the two imaginary parts is quite similar. When both of them have comparable values the two groups of minima follow the same tendency moving the band condition upwards. However if one imaginary part grows much more than the other one, several minima stretch down in a region of energy roughly included in $s_{small} < \epsilon < s_{large}$ (figure 5.3(c)). Finally when $s_1, s_2 \gg r_1, r_2$ one can force the band condition to go above $+1$ (keeping our well known knots at $\epsilon = n\pi$) in a certain energy range which depends on the val-
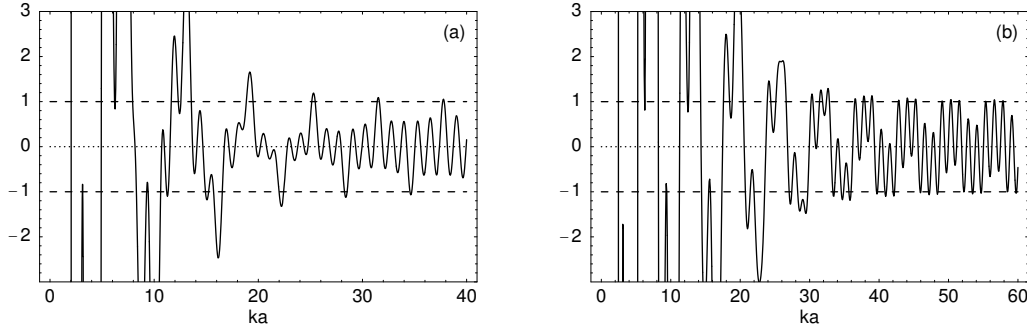
Figure 5.4. Band condition for a $\mathcal{PT}$-symmetric chain with $N = 5$. (a) $r_1 = 4$, $r_2 = 1$, $r_3 = 1$, $s_1 = 20$, $s_2 = 5$, (b) $r_1 = 4$, $r_2 = 2$, $r_3 = 3$, $s_1 = 10$, $s_2 = 20$.
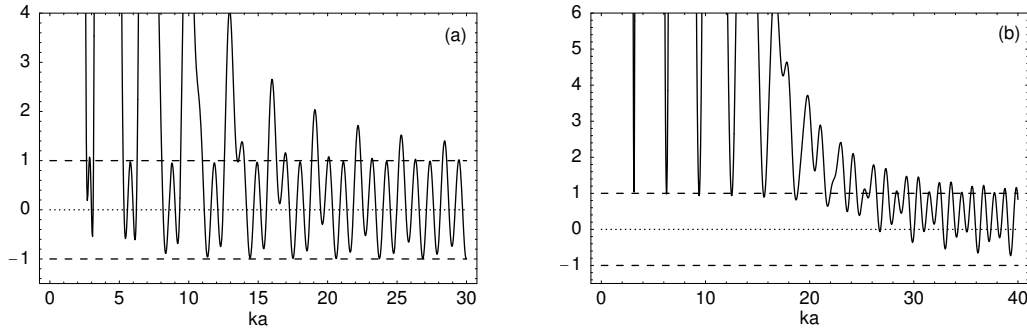
Figure 5.5. Band condition for a $\mathcal{PT}$-symmetric chain with $N = 6$. (a) $r_1 = 5$, $r_2 = 3$, $r_3 = 4$, $s_1 = 2$, $s_2 = 5$, $s_3 = 4$, (b) $r_1 = 1$, $r_2 = 2$, $r_3 = 0.5$, $s_1 = 10$, $s_2 = 11$, $s_3 = 12$.

ues of the imaginary parts of the couplings (figure 5.3(d)), approximately the same way as for the $N = 2$ case. Unlike the $N = 3$ example the band condition can be unbalanced to positive values with a proper choice of the parameters.

The band condition has been also studied in detail for $N = 5$ and $N = 6$. Its behaviour gets really complex as the number of atoms grows. In figures 5.4 and 5.5 some characteristic examples are shown. For $N = 5$ the band condition shows five types of extremal points that evolve 'symmetrically' around the abscissa axis as we change the imaginary couplings. For $N = 6$ three types of maxima and minima appear and for large enough values of the imaginary couplings the band condition is greater than $+1$.

To summarize this mathematical analysis of the band condition let us now list some of the most salient features:

- The band condition is composed of pieces integrated by $N(N/2)$ extremal points for odd(even) N. Each extremal point belongs to a group that evolves differently according to the values of the imaginary parts of the couplings.

- For odd N the band condition is 'symmetric' around the abscissa axis for all values of the couplings. Therefore, some permitted levels always remain as a part of the spectrum.

- For even N the band condition can be expelled out of the target range for certain values of the couplings, so removing the allowed bands.

- For $\epsilon = n\pi$ the band condition is fixed to $+1$ or -1 depending on the parity of N and n for all values of the couplings.

- The real parts of the couplings are always proportional to the amplitude of the oscillations.

Even with all the included figures, it is hard to make a complete explanation of the behaviour of the band condition that otherwise can only be fully understood watching some proper animations of the function. This is the procedure we have followed to support the results.

5.1.3 The band structure and the electronic states

Let us now make some comments about the band structure. One important feature that stands out from the above examples is the presence of maxima(minima) inside the target range $(-1, 1)$. This fact involves the presence of points in the reciprocal space where the gradient of the energy diverges, that makes the physical interpretation of the Hamiltonian not so straightforward. Probably some additional restrictions have to be imposed on the $\mathcal{PT}$-symmetric Hamiltonian. These special points also cause some changes on the form of the bands, which are always understood as the ensembles of states and energies labelled with a certain index (n for the n-th band). Every point of the Brillouin zone must represent a physical state on every band. Therefore for a certain value qa let us label the eigenenergies of the Hamiltonian following an increasing order ($\epsilon_1(qa) < \epsilon_2(qa) < \ldots$). This procedure leads unavoidably to the definition of bands whose dispersion relations are not continuous over the reciprocal space, as seen in figure 5.6(a). Of course the choice of the band indices is not unique but none of them will be free of these discontinuities.

On the other hand those pathologies can be avoided if one restricts one's working scenario to a small range of energies. In that case the imaginary parts of the couplings can be tuned to modify essentially the spectrum of the system removing or decreasing gaps to change virtually its response to transport phenomena (figures 5.6(b) and 5.6(c)).
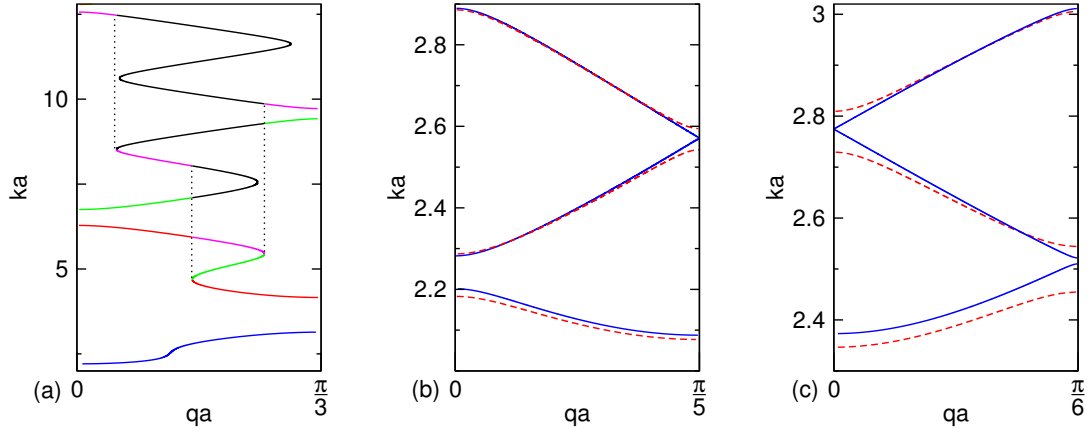
Figure 5.6. Band structure in the irreducible part of the first Brillouin zone for different chains: (a) $N = 3$ with $r_1 = 1$, $r_2 = 2$, $s_1 = 3$. Different colours show the first four bands. (b) $N = 5$ with $r_1 = 4$, $r_2 = 2$, $r_3 = 1$, $s_1 = s_2 = 0$ (red) and $s_1 = 0.775$, $s_2 = 0.1$ (blue). (c) $N = 6$ with $r_1 = 5$, $r_2 = 2$, $r_3 = 3$, $s_1 = s_2 = s_3 = 0$ (red) and $s_1 = 1.613$, $s_2 = 0.12$, $s_3 = 0.3$ (blue).

One can also wonder about the form of an electronic state belonging to such a characteristic spectrum. It is not hard to calculate analytically the wave function inside the primitive cell as a function of the position and the energy with the help of the computer for low N. To our surprise we have found that the imaginary parts of the couplings behave as control parameters of the distribution of probability of the electronic states inside the primitive cell. Thus one could tune these parameters to decrease the probability of presence in several sectors almost to zero or distribute it more homogeneously over the primitive cell, as shown in figure 5.7(a). Also for non-vanishing imaginary parts of the couplings the dependence of the state on the energy seems quite strong as a small variation of this energy can involve an important change in the shape of the state (figure 5.7(b)).

5.1.4 Concluding remarks

In this section the band structure of a periodic delta model with complex couplings exhibiting $\mathcal{PT}$-symmetry has been analysed:

- The band condition of the non-Hermitian Hamiltonian remains real under the requirement of $\mathcal{PT}$-symmetry .

- Appearance and removal of bands, impossible in the robust Hermitian models, have been clearly described analytically and graphically for a low number of deltas (N) in the primitive cell. For arbitrary N the band condition seems to
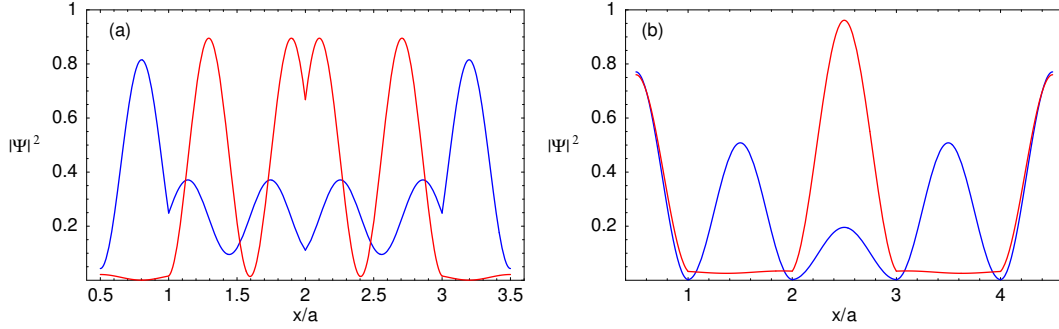
Figure 5.7. Electronic wave functions normalized to 1 inside the primitive cell of different $\mathcal{PT}$-symmetric chains. (a) $N = 3$ with $r_1 = 5$, $r_2 = 3$. $s_1 = 0$(blue) and $s_1 = 19$(red) at $\epsilon = 5.2$. (b) $N = 4$ with $r_1 = 3$, $r_2 = 4$, $s_1 = 5$, $s_2 = 8.1$ for different energies: $\epsilon = 2.95$(red) and $\epsilon = 3.13$(blue). The deltas are placed at the integer multiples of a.

evolve with the imaginary couplings according to a well-defined set of rules.

- The imaginary parts of the couplings play an important role in the way the band structure gets distorted and also have a significant effect on the form of the electronic states.

5.2 Absorption in atomic wires with non-Hermitian Hamiltonians

The inelastic scattering processes occurring in mesoscopic samples as a consequence of a finite non-zero temperature can noticeably change the coherent transport fingerprints of these structures. The worsening of electronic transmission due to such effects is expected but in some situations the competition between the phase-breaking mechanisms and the quantum coherent interferences can improve conductance in certain energetic regimes. This is the case, for example, of disordered structures. This fact has attracted much attention in the study and modelling of dissipative transport in one-dimensional structures. Interest is also prompted by experiments currently being carried out on real atomic chains [5].

A model of parametrized scatterers coupled through additional side channels to electron reservoirs incorporating inelastic scattering events was initially proposed by Büttiker [30, 32], and much work has been done along this line [119, 139, 140, 102]. On the other hand, inelastic processes can be modelled by small absorptions which in turn can be described by extending the nature of the quantum potentials to the complex domain. In this section we shall include absorptive processes by performing

these complex extensions on different quantum wire models.

In the framework of one-dimensional atomic chains, non-Hermitian Hamiltonians have been introduced for example in the study of electronic conductivity, using complex site energies and frequencies [39, 181, 41, 101], or also to design composite potentials behaving as perfect absorbers for certain energies [153]. But non-Hermitian Hamiltonians have also been used to account for a large variety of phenomena, such as wave transport in absorbing media [85, 54], violation of the single parameter scaling in one-dimensional absorbing systems [61], appearance of exceptional points in scattering theory [100, 56], description of vortex delocalization in superconductors with a transverse Meissner effect [96, 97] or more phenomenologically with nuclear optical potentials. Imaginary potentials also play a significant role for modelling time observables [149]. In fact a model of time-of-arrival measurement by fluorescence from a two-level atom excited by a laser beam has been recently proposed [42, 152, 43, 151] that in certain regimes can be exactly and rigorously described by local complex potentials [158]. An interesting modern review on complex potentials and absorption in quantum mechanics has appeared recently [150] and we address the interested reader to this publication and references therein.

5.2.1 The Schrödinger equation for a complex potential

Let us consider a one-dimensional complex potential of finite support $V(x) = V_r(x) + iV_i(x)$ ($V(\pm\infty) = 0$). For the stationary scattering states, the density of the current flux is proportional to the imaginary part of the potential

$$\frac{\mathrm{d}J}{\mathrm{d}x} = \frac{2}{\hbar}V_i(x)|\Psi(x)|^2, \tag{5.14}$$

where $J(x)$ is defined as

$$J(x) = \frac{\hbar}{2m\mathrm{i}} \left(\Psi^*(x)\frac{\mathrm{d}\Psi(x)}{\mathrm{d}x} - \Psi(x)\frac{\mathrm{d}\Psi^*(x)}{\mathrm{d}x} \right). \tag{5.15}$$

Therefore, in the presence of a non-vanishing $V_i(x)$ the unitarity relation regarding the transmission and reflection probabilities $T(E) + R(E) = 1$ is no longer valid. One can still recover a pseudounitarity relation by defining a quantity that accounts for the loss of flux in the scattering process. Dealing with the asymptotic state $\Psi_k^L(-\infty) = \mathrm{e}^{ikx} + r^L(k)\mathrm{e}^{-ikx}$, $\Psi_k^L(+\infty) = t(k)\mathrm{e}^{ikx}$, one can write the asymptotic values of the flux as

$$J_{-\infty} = \frac{\hbar k}{m} \left(1 - R^L(k) \right), \tag{5.16}$$

$$J_\infty = \frac{\hbar k}{m}T(k), \tag{5.17}$$

yielding the relation

$$T(k) + R^L(k) + \frac{m}{\hbar k}\left(J_{-\infty} - J_{\infty}\right) = 1. \tag{5.18}$$

This latter equation remains the same for the right incidence case (with $R^R(k)$) when the asymptotic state takes the form $\Psi_k^R(-\infty) = t(k)\mathrm{e}^{-ikx}$, $\Psi_k^R(+\infty) = \mathrm{e}^{-ikx} + r^R(k)\mathrm{e}^{ikx}$. Using equation (5.14) the flux term reads

$$A^{L,R}(k) \equiv -\frac{2m}{\hbar^2 k}\int_{-\infty}^{\infty} V_i(x)|\Psi_k^{L,R}(x)|^2 \mathrm{d}x = 1 - R^{L,R}(k) - T(k), \tag{5.19}$$

and it is usually understood as the probability of absorption [7]. But $A(k)$ must be a positive defined quantity in order to be strictly considered as a probability and this is not ensured by the definition (unless $V_i(x) < 0$ for all x). The sign of $A(k)$ depends on both the changes in sign of the imaginary part of the potential and the spatial distribution of the state. Although a negative value for $A(k)$ could be viewed as emission (because it means a gain in the flux current) it also leads the transmittivity and the reflectivity to attain anomalous values $T(k) > 1, R(k) > 1$, which are difficult to interpret. Let us also note that the integral representation of the absorption term is useless for practical purposes, because to build the correct expression of the state $\Psi_k^{L,R}(x)$ one needs to impose the given asymptotic forms to the general solution of the Schrödinger equation, therefore obtaining the scattering amplitudes, so one cannot calculate the absorption probability without knowing $R(k)$ and $T(k)$.

5.2.2   Chain of delta potentials

Let us first consider the delta model extensively described in chapter 3 and let us now incorporate the dissipative processes that are always present in real wires, causing energy losses. We model that effect by including an imaginary part in the potential. In this case the natural complex extension of our system consists in promoting the delta couplings from real to complex, thus writing $(a/a_j) = r_j - is_j$. We also take $s_j > 0$ for all j in order to avoid anomalous scattering. The effect of ordering the complex couplings in a $\mathcal{PT}$-symmetric manner on the spectrum of an infinite periodic delta chain has been studied in the previous section, now let us see what happens in a chain with open boundaries. In figure 5.8 the usual scattering diagram is shown for a short periodic chain with real potentials. Including a small imaginary part in the couplings we see how the transmission pattern is altered with a non-negligible absorption that peaks at the incoming band edges while the reflectivity is not noticeably changed. This tendency of the absorption term also appears when several species are included in the periodic array, and its pattern does not change much if only some of the couplings are complexified.
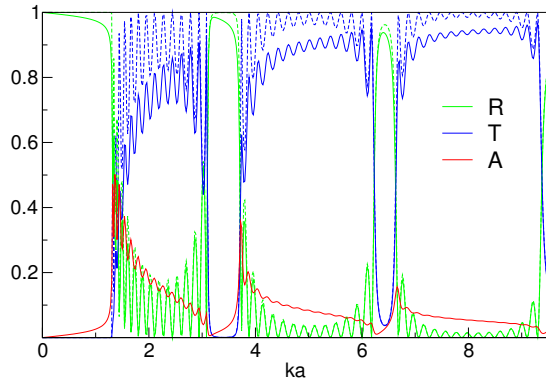
Figure 5.8. Scattering and absorption probabilities for one-species delta chains with length $N = 15$ and parameters $(a/a_1) = 1.0$ (dashed lines) and $(a/a_1) = 1.0 - 0.015\mathrm{i}$ (solid lines).
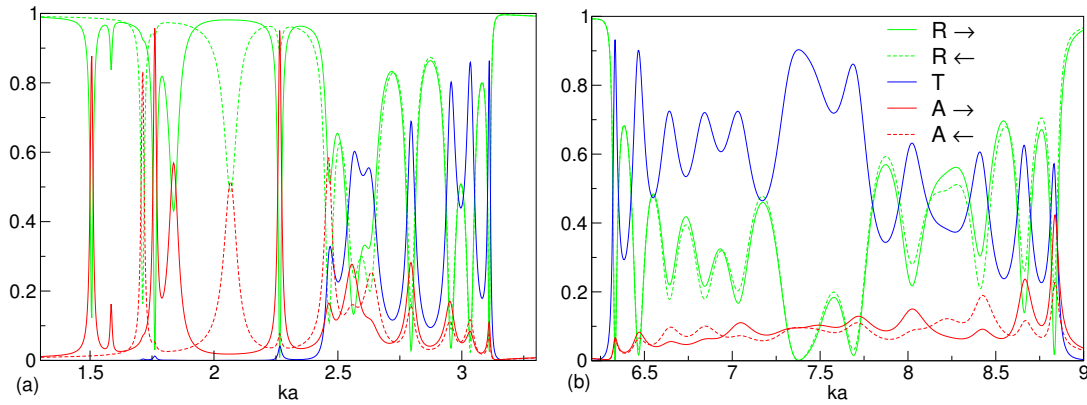
Figure 5.9. Scattering process for disordered arrays of 15 deltas with complex couplings. The sequences of the real parts of the characteristic parameters are: (a) $\mathrm{Re}\,(a/a_j)$: 3, 1, 2, 0.5, 3, 2, 1, 3, 0.5, 4, 5, 1, 2, 2, 3, (b) $\mathrm{Re}\,(a/a_j)$: -1, -4, -3, -1, -2, -3, -4, -1, -2, -3, -1, -4, -4, -2 ,-3. The imaginary part of each coupling has been chosen as $\mathrm{Im}\,(a/a_j) = -0.01|\mathrm{Re}\,(a/a_j)|$. The arrows in the legends mark the direction of incidence.

When the array presents no ordering at all, the graph is quite unpredictable and different configurations can be obtained. In figure 5.9(a) a peaky spectrum with very sharp absorption resonances is shown. The scattering process in this case is strongly dependent on the incidence direction, as can be seen. On the other hand, smoother diagrams are also possible in which the effect of the complex potential manifests through an almost constant absorption background and a small change depending upon the colliding side, like the one in figure 5.9(b). This naive model, apart from being exactly solvable, is powerful enough to account for very different physical schemes, which makes it a very useful bench-proof structure.
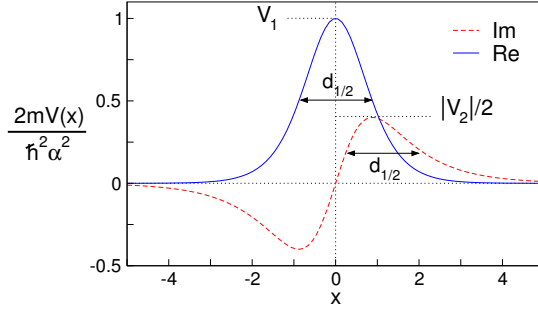
Figure 5.10.   Real and imaginary parts of the complex Scarf potential.

5.2.3   Dissipative atomic quantum wells/barriers

Let us go one step further and consider a potential that resembles the profile of an atomic well or barrier. We shall consider the extension of the Pöschl-Teller potential given by the complexified Scarf potential,

$$ V(x) = \frac{\hbar^2 \alpha^2}{2m} \left(\frac{V_1}{\cosh^2(\alpha x)} + i\, V_2 \frac{\sinh(\alpha x)}{\cosh^2(\alpha x)} \right), \tag{5.20} $$

with $V_1, V_2 \in \mathbb{R}$. It is a proper complex extension for two reasons: it admits analytical solutions [118, 40] and its imaginary part is somehow proportional to the derivative of the real part of the potential. This latter criterion has been considered in nuclear optical potentials to choose adequate complex extensions. It seems reasonable to measure the strength of the dissipation processes in terms of the 'density' of the real interaction and therefore writing an imaginary potential that is proportional to the spatial derivative of the real one. The potential profile is shown in figure 5.10.

The Scarf potential has been extensively considered in the literature, mainly dealing with its discrete spectrum, either in its real and complex forms, from the point of view of SUSY Quantum Mechanics [36, 134] or focusing on its $\mathcal{PT}$-symmetric form [8].

First, a detailed mathematical analysis of the potential, regarding its scattering properties, must be made to discuss some new features and some assertions that have been made.

The left scattering amplitudes of the real Scarf potential have been obtained in terms of complex Gamma functions [118]. Recently, a considerable simplification has been pointed out [8]. In fact, the asymptotic transmittivity and reflectivity for the

complex Scarf can be written as

$$T(k) = \frac{\sinh^2\left(2\pi\frac{k}{\alpha}\right)}{\sinh^2\left(2\pi\frac{k}{\alpha}\right) + 2\cosh\left(2\pi\frac{k}{\alpha}\right)\cosh(\pi g_+)\cosh(\pi g_-) + \cosh^2(\pi g_+) + \cosh^2(\pi g_-)}$$
(5.21)

$$R^L(k) = \frac{\cosh^2(\pi g_+)\mathrm{e}^{-2\pi k/\alpha} + \cosh^2(\pi g_-)\mathrm{e}^{2\pi k/\alpha} + 2\cosh(\pi g_+)\cosh(\pi g_-)}{\sinh^2\left(2\pi\frac{k}{\alpha}\right) + 2\cosh\left(2\pi\frac{k}{\alpha}\right)\cosh(\pi g_+)\cosh(\pi g_-) + \cosh^2(\pi g_+) + \cosh^2(\pi g_-)}$$
(5.22)

where $g_\pm = \sqrt{V_1 \pm V_2 - 1/4}$ and $R^R(k)$ is recovered from $R^L(k)$ by interchanging g_+ and g_- (which is equivalent to substituting $V_2 \to -V_2$ and therefore changing the direction of incidence). These expressions of course can be derived from the asymptotic transmission matrix, which we have obtained from the asymptotic form of the solutions of the Schrödinger equation (appendix E),

$$\mathcal{M} = \begin{pmatrix} e^{\mathrm{i}\phi}\sqrt{1+s\overline{s}} & -\mathrm{i}s \\ \mathrm{i}\overline{s} & e^{-\mathrm{i}\phi}\sqrt{1+s\overline{s}} \end{pmatrix},$$
(5.23)

where

$$\phi = \frac{\pi}{2} + \arg\left\{ \frac{\Gamma^2\left(\mathrm{i}\frac{k}{\alpha}\right)\Gamma^2\left(\frac{1}{2}+\mathrm{i}\frac{k}{\alpha}\right)}{\Gamma\left(c+\mathrm{i}\frac{k}{\alpha}\right)\Gamma\left(b+\mathrm{i}\frac{k}{\alpha}\right)\Gamma\left(1-c+\mathrm{i}\frac{k}{\alpha}\right)\Gamma\left(1-b+\mathrm{i}\frac{k}{\alpha}\right)} \right\},$$
(5.24)

$$s = \frac{\cosh(\pi g_+)e^{\pi k/\alpha} + \cosh(\pi g_-)e^{-\pi k/\alpha}}{\sinh(2\pi k/\alpha)},$$
(5.25)

$$\overline{s} = s(g_+ \rightleftarrows g_-),$$
(5.26)

with the definitions

$$c = \frac{1}{2} - \frac{\mathrm{i}}{2}(g_+ - g_-), \quad b = \frac{1}{2} - \frac{\mathrm{i}}{2}(g_+ + g_-).$$
(5.27)

It immediately follows from the transmission matrix that the absorption probabilities read

$$A^L(k) = \frac{s\overline{s} - \overline{s}^2}{1 + s\overline{s}}, \quad A^R(k) = \frac{s\overline{s} - s^2}{1 + s\overline{s}}.$$
(5.28)

Unlike the complex delta potentials example, this potential has some drawbacks that must be carefully solved. Its imaginary part is non-negative defined in its domain, which might cause anomalous scattering. Only some values of V_2 will be physically acceptable. To ensure that $T(k) \leqslant 1$ for all k, it is clear from equation (5.21) that the necessary and sufficient condition is $\cosh(\pi g_+)\cosh(\pi g_-) \geqslant 0$. The functions g_+, g_-, can be real or pure imaginary depending on the values of V_1 and V_2. A detailed analysis of the conditions for physical transmission is presented in appendix E. As

Table 5.1. Ranges of V_2 compatible with the condition $T(k) \leqslant 1$ for all k for the complex Scarf potential for certain negative values of V_1. The last column includes the intervals providing physical scattering from the emissive side of the potential.

V_1	$|V_2|$	$|V_2|$ emissive
-0.5	$[0, 0.5] \cup [1.5, 5.5] \cup [11.5, 19.5] \cdots$	$[0, 0.5]$
-1	$[0, 5] \cup [11, 19] \cup [29, 41] \cdots$	$\varnothing$
-2.4	$[0, 0.4] \cup [2.4, 3.6] \cup [9.6, 17.6] \cdots$	$[0, 0.4] \cup [2.4, 2.569]$
-3	$[0, 1] \cup \{3\} \cup [9, 17] \cdots$	$[0, 1]$
-4	$[0, 4] \cup [8, 16] \cup [26, 38] \cdots$	$[3.606, 4]$
-5	$[0, 1] \cup [3, 5] \cup [7, 15] \cdots$	$[3, 4.123] \cup [4.472, 5]$

a summary, let us say that for $V_1 > 0$ (barriers) , the evaluation of the condition translates into

$$|V_2| \in [0, V_1] \cup [2n(2n - 1) + V_1, 2n(2n + 1) + V_1], \quad n \in \mathbb{Z}^+. \tag{5.29}$$

For $V_1 < 0$ (wells) the situation becomes more complicated and the result can only be expressed through several inequalities, each one adding a certain allowed range for V_2 (see appendix E). As an example, in table 5.1 we show the compatible ranges of V_2 for a few negative values of V_1. One can trivially check the compatibility of the intervals presented for V_2 with the condition $T(k) \leqslant 1$ for all k by plotting equation (5.21). In a two dimensional plot of $|V_2|$ versus V_1, the physical ranges for the transmission distribute as alternating fringes and a funny chessboard like pattern (figure 5.11 on the following page).

One feature to emphasize according to the conditions given for acceptable transmission is the fact that the number of permitted intervals for V_2 is infinite for any V_1, either positive(barrier) or negative(well), and therefore there is no mathematical upper bound on $|V_2|(|V_2^{\text{critical}}|)$ above which the transmission probability always becomes unphysical, contrary to what has been reported recently [8]. From a physical viewpoint of course, a sensible limitation must also be imposed on V_2, usually $|V_2| \ll |V_1|$.

Let us see now what happens with the reflectivity. We assert that for the values of V_1 and V_2 preserving a physical transmission, one of the reflectivities of the system remains physical (i.e. $R(k) \leqslant 1 - T(k)$ for all k), left or right, depending on the particular values of the dimensionless amplitudes (or equivalently, one of the absorptions takes positive values for all k). The statement is easy to prove from equations (5.28) and more specifically reads: when $T(k) \leqslant 1$ for all k (i.e. $\cosh(\pi g_+) \cosh(\pi g_-) \geqslant 0$),
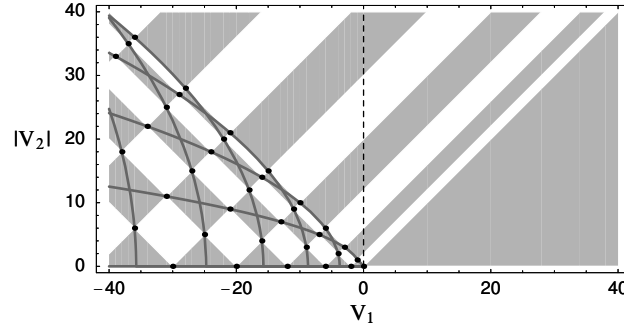
Figure 5.11. Scattering diagram for the complex Scarf potential in terms of the potential amplitudes. The physically acceptable ranges for V_1, V_2, correspond to the shaded zones. The curves are the inversion lines given by equation (5.33). The black points mark the correlated values of the amplitudes (equations (5.32)) generating a fully transparent behaviour.

then

$$|\cosh(\pi g_-)| < |\cosh(\pi g_+)| \Rightarrow A^L(k) \geqslant 0, \quad \forall \, k, \tag{5.30a}$$

$$|\cosh(\pi g_-)| > |\cosh(\pi g_+)| \Rightarrow A^R(k) \geqslant 0, \quad \forall \, k. \tag{5.30b}$$

Considering $V_1 > 0$ and $V_2 > 0$ it is not hard to see that the first of the above inequalities always holds. Therefore, in the case of a potential barrier the scattering is always physical from the absorptive side (trough of the imaginary part), as has already been stressed [8]. More interesting is the fact that this conclusion cannot be extended to the case $V_1 < 0$ (well). In this case the physical scattering sometimes occurs from the emissive side (peak of the imaginary part), producing smaller absorption terms. In table 5.1 a few examples of V_2 intervals providing physical scattering from the emissive side for some potential wells are shown.

Another interesting feature that must be observed is that there exists a set of correlated values of V_1, V_2 for which the complex Scarf potential behaves as fully transparent (i.e. $T(k) = 1$ for all k). The condition for this to happen is from equation (5.21) $\cosh(\pi g_+) = \cosh(\pi g_-) = 0$. Thus, the main requirement is that g_+ and g_- must be pure imaginary, yielding in this case the transparency equations

$$\cos\left(\pi\sqrt{\frac{1}{4} - V_1 \pm V_2}\right) = 0, \tag{5.31}$$

whose solutions are

$$V_1 = \frac{1}{4} - \frac{1}{8}\left[(2m+1)^2 + (2n+1)^2\right], \tag{5.32a}$$

$$V_2 = \frac{1}{8}\left[(2m+1)^2 - (2n+1)^2\right], \quad m, n \in \mathbb{Z}. \tag{5.32b}$$

Table 5.2. Some correlated values of V_1, V_2, producing the fully resonant behaviour of the complex Scarf potential. The particular Pöschl-Teller resonances are in square brackets.

$(-V_1,|V_2|)$				
$(1,1)$	$(3,3)$	$(6,6)$	$(10,10)$	$(15,15)$
$[2,0]$	$(4,2)$	$(7,5)$	$(11,9)$	$(16,14)$
$[6,0]$	$(9,3)$	$(13,7)$	$(18,12)$	$(24,18)$
$[12,0]$	$(16,4)$	$(21,9)$	$(27,15)$	$(34,22)$

It is worth noting that the transparencies only appear for potential wells ($V_1 < 0$). Considering the particular case $n = m$ one recovers the Pöschl-Teller resonances. In table 5.2 the first values of equations (5.32) are listed explicitly.

The absorption obviously vanishes for all energies when considering these special resonant values of the potential amplitudes. Surprisingly, there also exists another set of non-trivial correlated values of V_1, V_2 for which the potential is non-dissipative ($A(k) = 0$ for all energies) without being fully transparent. This set of values satisfies $\cosh(\pi g_+) = \cosh(\pi g_-) \neq 0$, as can be seen from equations (5.28). Non-trivial solutions exist when $g_+, g_- \in \mathbb{C}$, yielding

$$|V_2| = n\sqrt{1 - 4V_1 - 4n^2}, \quad n \in \mathbb{Z}^+. \tag{5.33}$$

Let us also notice from equations (5.30) that the latter points are also the borders where the physical scattering changes from the absorptive side to the emissive side or vice versa. We shall refer to these borders as inversion points (IP). Therefore, whenever we encounter an IP we can say $A(k) = 0$ for all k without a fully transparent behaviour, and hence a non-dissipative scattering process for all energies with a non-vanishing imaginary part of the potential. Let us note that from equation (5.33) the IPs only appear in the case of Scarf potential wells and only for $|V_2| \leqslant 1/4 - V_1$. In figure 5.12 the characteristic scattering probabilities are shown for a Scarf barrier and a Scarf well, and in figure 5.13 the maximum value of the physical absorption is plotted versus $|V_2|$ for different values of V_1. When V_1 is positive the absorption grows with the amplitude of the imaginary part of the potential. On the other hand, for negative V_1 a strikingly different pattern arises, with transparency points (TP) and inversion points (IP) and the absorption does not increase monotonically with $|V_2|$.

The whole behaviour of the scattering can be clearly understood by building a two dimensional diagram $|V_2|$ versus V_1 (figure 5.11 on the preceding page), including physically permitted ranges, inversion lines and the points of transmission resonance.
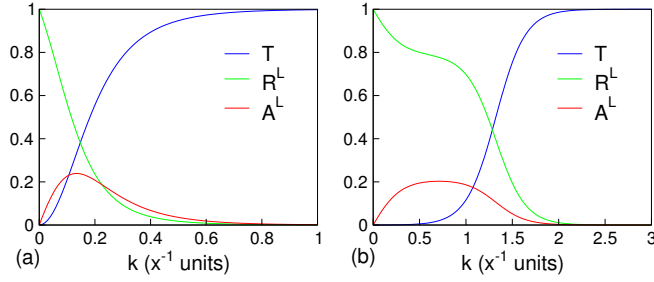
Figure 5.12. Scattering patterns for (a) a complex Scarf well $\alpha = 1(x^{-1}$ units), $V_1 = -0.5$, $V_2 = -0.4$ and (b) a complex Scarf barrier $\alpha = 1(x^{-1}$ units), $V_1 = 2$, $V_2 = 0.1$.
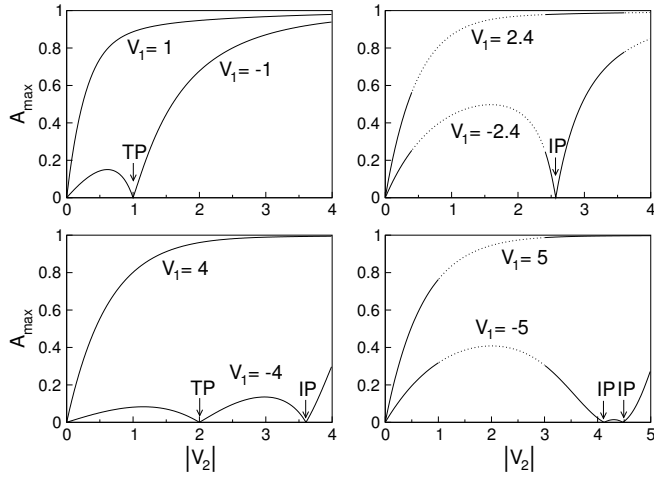

Figure 5.13. Maximum value of the absorption probability A_{max} vs $|V_2|$ for different values of V_1. For each graph the upper(lower) curve corresponds to a barrier(well). A dotted line is used in the forbidden values of $|V_2|$, nevertheless the whole curve is shown for continuity. The allowed ranges of $|V_2|$ and the position of the IPs can be compared with the values in table 5.1.

The complex Scarf potential shows two opposite faces to scattering, namely barrier and well, and a much richer structure in the latter case.

After this detailed analysis of the peculiarities of the complex Scarf, let us continue with our work on connecting several potentials to model dissipative atomic chains. The procedure is the same as the one described for the Pöschl-Teller potential in chapter 4. In this case a symmetric cut-off of the potential is taken, the portion included in the interval $[-d, d]$. Then from the asymptotic matrix it follows that the cut-off matrix reads, according to equation (2.10),

$$\mathbf{M} = \begin{pmatrix} e^{i(\phi+2kd)}\sqrt{1+s\overline{s}} & -is \\ i\overline{s} & e^{-i(\phi+2kd)}\sqrt{1+s\overline{s}} \end{pmatrix}, \tag{5.34}$$

in terms of the previously defined quantities ϕ, s and $\overline{s}$. It can be checked that the half-widths $d_{1/2}$ of both the real and imaginary parts of the potential coincide and that the decay of the imaginary part is always slower than that of the real part (figure 5.10). This causes an increase in the minimum value of the cut-off distance d_0 with regard to the Pöschl-Teller case. For a sensible wide range of the potential amplitudes we have found that considering $d_0 \simeq 3d_{1/2} = 5.3/\alpha$ is enough in most cases. In fact, this minimum value can be relaxed in the case of potential barriers ($V_1 > 0$), whereas for potential wells taking d below this value to apply the connection equations may
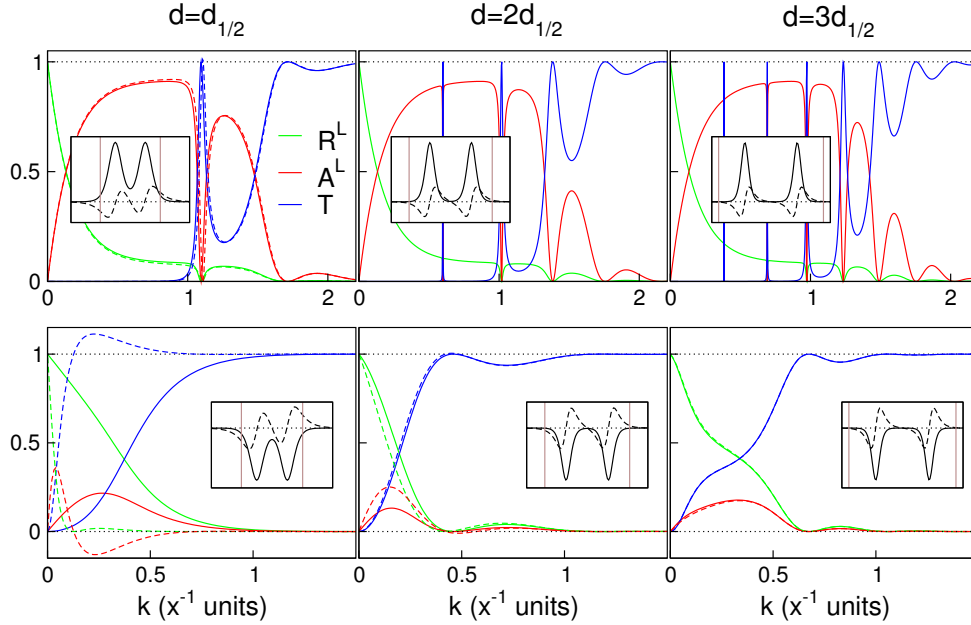
Figure 5.14. Scattering probabilities for double Scarf potentials with parameters $\alpha = 1(x^{-1}$ units), $V_1 = 2$, $V_2 = 1$ for barriers and $\alpha = 1(x^{-1}$ units), $V_1 = -4$, $V_2 = 3.1$ for wells. The solid lines were obtained from the analytical composition technique and the dashed lines correspond to the exact numerical integration of the Schrödinger equation for the global potential. The insets show the potential profile (in arbitrary units) for each case: solid line for the real part and dashed line for the imaginary part. The vertical lines limit the portion of the potential that the composition technique takes into account. Notice that for low d the exact integration may lead to unphysical scattering. As d is increased an acceptable scattering is recovered and both methods give the same result. In the case of potential barriers the analytical composition technique works impressively well even for very low values of d.

sometimes distort the results. The correct behaviour of the connection procedure for $d \geqslant d_0$ can be observed in figure 5.14, where the scattering probabilities obtained upon integrating the Schrödinger equation numerically for the global potential are compared with those given by the analytical composition technique, for two potential barriers and two potential wells with different choices of the cut-off distance and with high values for $|V_2|$. Notice how in the barrier example the agreement between both methods is completely reached for $d \simeq 2d_{1/2}$ whereas for potential wells a further step is needed since the minimum value of the cut-off is more critical.

Once the connection of potentials has been successfully made, one should ask which are the ranges of the potential amplitudes that provide an acceptable physical scattering in this new framework. Analysis of this issue is very non-trivial and quite complex analytically, but also very important because it determines whether this

model remains useful when considering atomic chains. First, in the case of two potentials we have observed that choosing each individual pair of amplitudes (V_1, V_2)
belonging to a physical range, and selecting the signs of the imaginary parts so that the
physical faces of both potentials point in the same direction, then an acceptable scattering for the composite potential can always be recovered at least from one of the two
possible orientations (both physical faces to the right or to the left). In other words,
considering that the incident particle always collides with the left side (it comes from
$-\infty$) and therefore orientating the individual physical faces to the left, then at least
one of the sequences $V_I(x) - V_{II}(x)$ or $V_{II}(x) - V_I(x)$ gives an acceptable scattering for
all energies. We have checked this assertion for a broad variety of Scarf couples. For
a higher number of potentials the situation becomes more complex but a few pseudo-
rules to obtain physical scattering can be deduced. For an arbitrary chain we have
found that in many cases the left scattering remains physical as long as: the left scattering of each individual potential is physical and the left scattering of each couple of
contiguous potentials is physical. This recipe seems completely true when composing
potential barriers only, whereas when wells are included it fails in some situations,
especially when several contiguous wells are surrounded by barriers. Although at the
beginning it may appear almost random to recover a physical scattering from a large
composition of Scarfs, following the given advices it turns out to be more systematic.

Let us remember that the composition procedure, apart from being a powerful tool
for numerical calculations also provides analytical expressions for the scattering probabilities, which of course adopt cumbersome forms for a large number of potentials
but are useful for obtaining simple expansions for certain energetic regimes. Just as
an example, the transmittivity and left reflectivity for the double Scarf read

$$T(k) = \frac{1}{s_1^2 \overline{s}_2^2 + (1 + s_1 \overline{s}_1)(1 + s_2 \overline{s}_2) - 2 s_1 \overline{s}_2 \sqrt{1 + s_1 \overline{s}_1} \sqrt{1 + s_2 \overline{s}_2} \cos(\Phi)}, \quad (5.35)$$

$$R^L(k) = \frac{\overline{s}_1^2 (1 + s_2 \overline{s}_2) + \overline{s}_2^2 (1 + s_1 \overline{s}_1) - 2 \overline{s}_1 \overline{s}_2 \sqrt{1 + s_1 \overline{s}_1} \sqrt{1 + s_2 \overline{s}_2} \cos(\Phi)}{s_1^2 \overline{s}_2^2 + (1 + s_1 \overline{s}_1)(1 + s_2 \overline{s}_2) - 2 s_1 \overline{s}_2 \sqrt{1 + s_1 \overline{s}_1} \sqrt{1 + s_2 \overline{s}_2} \cos(\Phi)}, \quad (5.36)$$

where $\Phi = \phi_1 + \phi_2 + 2k(d_1 + d_2)$ and making use of the previously defined terms
s, $\overline{s}$ and ϕ. Just like for the Pöschl-Teller potential, the formulae for the composite scattering probabilities analytically account for the fully transparent behaviour of
the whole structure as long as there is resonant forward scattering of the individual
potential units. Another curious feature arises when composing different potentials
whose amplitudes describe an inversion point. In this case the whole structure remains non-dissipative as can be seen in figure 5.15. Moreover, the complex Scarfs at
these points behave completely as real potentials, providing an acceptable scattering
for the composition that is independent of the incidence direction for any sequence of
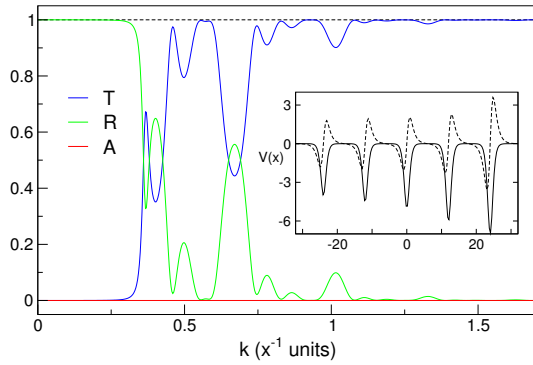
Figure 5.15. Composition of Scarfs with different pair amplitudes describing IPs. Sequence with $\alpha = 1(x^{-1}$ units) and cut-off distance $d = 6(x$ units) equal for all potentials, and (V_1, V_2): $(-4, \sqrt{13})$, $(-4.5, \sqrt{15})$, $(-5, \sqrt{17})$, $(-6, \sqrt{21})$, $(-7, 2\sqrt{13})$. The inset shows the potential profile with solid(dashed) line for the real(imaginary) part in arbitrary units.
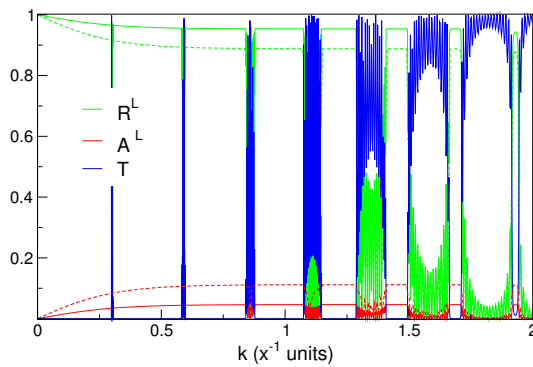
Figure 5.16. Periodic chain of 20 complex Scarfs with parameters $\alpha = 1(x^{-1}$ units), $V_1 = 2$, $V_2 = 0.02$ (solid lines) and $V_2 = 0.05$ (dashed lines) and cut-off distance $d = 6(x$ units).

the individual Scarfs.

Considering larger Scarf chains with small imaginary parts of the potentials, in the case of a periodic array we observe that the absorption term remains flat over a wide range of forbidden bands and oscillates inside the permitted ones. The variations in the absorption are entirely balanced by the reflectivity while the transmittivity is surprisingly not affected by the presence of a small complex potential, as can be seen in figure 5.16. This behaviour contrasts strongly with the periodic chain of complex delta potentials, where the absorption was completely different and it was the reflectivity that was little affected by the dissipation (figure 5.8 on page 126). For an aperiodic sequence the situation is quite different, as expected. In figure 5.17(a) a type of molecular aggregate is modelled with complex Scarfs. It exhibits a peaky absorption spectrum and a strongly oscillating transmittivity with sharp resonances. In figure 5.17(b) a symmetric atomic cluster has been considered in which the dissipation only occurs at both ends. The model is quite versatile since very different transmission and absorption configurations can be obtained by building different structures.

As a final exercise, two examples are included in figure 5.18 on page 137 showing the evolution of the transmittivity of two different Scarf compositions as a function of the imaginary part of the potential. The transmission patterns are plotted for different values of the parameter $\varepsilon = |V_2|/|V_1|$, which measures the strength of the imag-
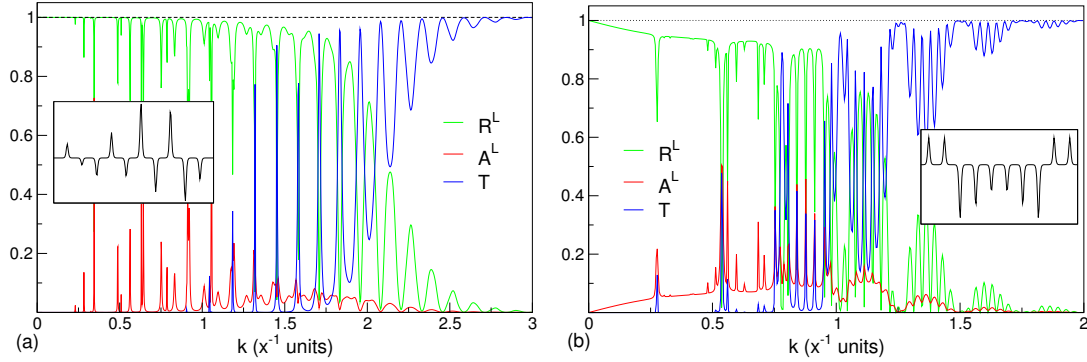
Figure 5.17. Scattering probabilities for a couple of 10-Scarf structures with parameters $\alpha = 1(x^{-1}$ units) and $d = 6(x$ units) equal for all potentials and amplitudes (a) (V_1, V_2): $(1, 0)$, $(-0.5, -0.005)$, $(-1.3, 0.013)$, $(1.8, 0.01)$, $(-1.3, 0.013)$, $(4, 0.04)$, $(-2.4, -0.024)$, $(3.5, 0.04)$, $(-3.1, 0.031)$, $(-1.5, 0.04)$ and (b) (V_1, V_2): $(1, 0.04)$, $(1, 0.05)$, $(-2, 0)$, $(-1.5, 0)$, $(-1, 0)$, $(-1, 0)$, $(-1.5, 0)$, $(-2, 0)$, $(1, 0.1)$, $(1, 0.1)$. The inset shows the real part of the potential profile (arbitrary units).

inary part. The transmission efficiency $T_{\text{eff}} = \int_{k_1}^{k_2} T(k)\, dk / (k_2 - k_1)$, corresponding to the area enclosed by $T(k)$ per energy unit, is evaluated in a characteristic energy range, generally the zone where T evolves until it becomes saturated. The imaginary potential tends to smooth the transmission pattern in the first example (figure 5.18(a), corresponding to a sequence of barriers), causing a slight decrease in the transmission efficiency for low ε, although it is finally improved. For a double well a different effect occurs (figure 5.18(b)). T_{eff} is always enhanced with increasing ε until it reaches a maximum, after which the transmittivity falls with the strength of the imaginary potential. These effects are very similar to those obtained for the conductivity of a disordered chain in which inelastic processes are included by means of parametrized scatterers [140, 102] or incorporating imaginary corrections to the Hamiltonians [41, 181, 101]. As we have seen, complex potentials are useful to model the effects of dissipative mechanisms in atomic chains. Then it would be specially interesting to implement these complex potentials in long disordered arrays where the break of the electronic localization regime could arise as a result of the loss of coherence due to phase-breaking mechanisms [66, 82, 78, 93], but this task demands a deeper analysis.

5.2.4 Concluding remarks

In this section dissipative scattering processes have been modelled in various types of atomic chains using complex potentials. In particular:
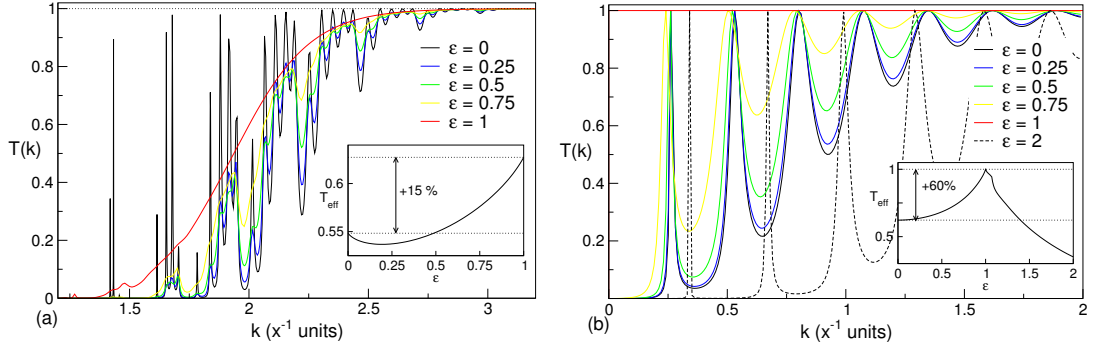
Figure 5.18. Transmittivity for different strengths of the imaginary part of the potentials in (a) a chain with 6 Scarf barriers $V_1 = 4, 2, 2.5, 3, 3.5, 4$ and $\alpha = 1(x^{-1}$ units), (b) a double Scarf well with $V_1 = -1, -1$ and $\alpha = 2(x^{-1}$ units). The cut-off distance in all cases is equal to $d = 6(x$ units). Each imaginary amplitude reads $V_2 = \varepsilon|V_1|$, except the first barrier in example (a) which is maintained real. The insets show the evolution of T_{eff} vs the strength of the imaginary amplitudes.

- The absorption probability has been rigorously included to recover unitarity for the non-Hermitian Hamiltonians.

- The asymptotic transmission matrix of the complex Scarf potential has been obtained. Using the cut-off version of the matrix, the linear composition of several potential units has been realized for which exact analytical expressions of the scattering amplitudes can be written.

- A profound mathematical analysis of the scattering properties of the complex Scarf potential has been carried out. The ranges of physical transmission have been analytically obtained and a group of interesting novel features have arisen such as the existence of parameters for which the potential becomes transparent for all energies or the presence of inversion points which are the borders where the acceptable scattering changes from the emissive side to the absorptive side or vice versa.

- The models proposed are able to include dissipation in the system in a tractable way. The versatility and richness of the different possible configurations may have direct applicability for considering molecular aggregates and other structures with explicit potential profiles. The results suggest that the models might also be able to account for the loss of coherence in the electronic localization regime due to phase-randomization events.

Final discussion

The generalization of some parts of the existing methodology together with the development of new tools to treat one-dimensional disordered systems have made it possible to carry out a thorough analysis of several models of quantum wires. A detailed study of the properties of their spectra and the nature of their electronic states has been made, and some novel and interesting features have arisen. An itemized list with the main results is included after each chapter.

We believe that the results presented can contribute to understand better some of the properties of disordered 1-D systems, but at the same time they require us to ask new questions (probably more than we had at the beginning!) about the physics of these structures. Therefore, it is worth to comment on the significance of several results and discuss future perspectives.

At the present time the theory of disordered systems does not include a unifying mathematical principle comparable to the Bloch theorem for the case of periodic structures. We would like to believe that the derivation of the **universal functional equations** for disordered systems in one dimension may mean a little advance in this direction. The fact that independently of the potential model it is possible to write a general set of functional equations which only depend on the distributions defining the disorder and that characterize the thermodynamic limit of the systems, is to our minds a result that must be taken into account. And physical relevant quantities such as the DOS or the localization length can be directly calculated in the thermodynamic limit from the functional equations. In spite of their formidable aspect the equations may have analytical solutions in certain cases or they may be useful to extract analytically information of the systems in the thermodynamic limit. Work along this line will probably require the use of a tough mathematical formalism but it also could be very

fruitful.

In the analysis of the different disordered models, it has been found that the distribution of states in the thermodynamic limit shows a **fractal behaviour** in certain energy ranges. Fractality of the DOS seems to be a universal feature of disordered systems in 1-D, independent of the potential model, and that apparently manifests itself whenever the distributions of the parameters of the system defining the disorder are discretized. This assertion has been checked for the delta model and the Pöschl-Teller model, for which fractality of the DOS always appears when the distribution of the different species is discretized, whereas if one allows one of the configurational parameters, for example the interatomic distances, to be governed by a continuous distribution, fractality disappears. The fractal character of the DOS has been confirmed numerically by studying the change of the distribution of the energy spacings between adjacent eigenlevels with the length of the system, as well as via the semi-variance analysis of the DOS which has been used to quantify the fractal dimension. It is also remarkable the fact that fractal energy ranges of the DOS are related to strong localization while extended states always occur, without exception, in smooth regions of the distribution of states. This fact establishes a link between localization of states at a given energy and the infinitesimal distribution of available levels around that energy. A homogeneous infinitesimal distribution of levels facilitates delocalization, while if homogeneity at the infinitesimal scale cannot be reached (i.e. a fractal distribution) then electrons have no chances to be extended. Then, one can wonder whether it is possible to characterize localization in terms of the nature of the distribution of states, or if a direct relationship exists between the mean value of the localization length in an energy range and the fractal dimension of the DOS within that range. On the contrary it may also happen that fractal dimensions of the distribution follow more general rules which could be determined by the potential model or the type of disorder. It would be interesting also to study whether fractality in the DOS of disordered systems also appears in 2-D and 3-D structures, or on the contrary is a fingerprint of one-dimensional physics. Further research is then needed to study in depth these topological features of the DOS, their connection if any with localization properties and their dependence upon disorder and dimensionality.

The analysis of the quantum wire models has also revealed the existence of isolated extended states exhibiting very dissimilar characteristics: different critical exponents for λ and DOS, different behaviour of the IPR and different aspect of the envelope of the state. However they share some common features, like the fact that the number of states near the resonance with a localization length larger than the system size scales as the square root of the length of the chain. But the most interesting thing

is that all extended states found are located at **commuting-energies**, that ensures the commutativity of the transmission matrices composing the array. Then one can conjecture that all extended states in 1-D systems may be commuting-energies of the spectrum. As we have seen, this common origin is compatible with very different features of the extended states, and if it were true it would mean to have a very simple condition to find all possible resonances that can occur in a one-dimensional disordered system. Of course we must not forget that the additional condition of belonging to the permitted spectrum of all species of the chain has also to be satisfied by the commuting-energy. In order to support this conjecture let us see that even when short-range correlations are included in the disorder, the extended states occur at commuting-energies. Let us consider for example the famous binary random-dimer model. One of the atomic species appears always in pairs (dimers), then the matrix of the dimer reads

$$\begin{pmatrix} \alpha & \beta \\ \beta^* & \alpha^* \end{pmatrix} \begin{pmatrix} \alpha & \beta \\ \beta^* & \alpha^* \end{pmatrix} = \begin{pmatrix} \alpha^2 + |\alpha|^2 - 1 & 2\beta \mathrm{Re}\,(\alpha) \\ 2\beta^* \mathrm{Re}\,(\alpha) & (\alpha^*)^2 + |\alpha|^2 - 1 \end{pmatrix}, \tag{6.1}$$

where we have used $|\alpha|^2 - |\beta|^2 = 1$. Then, due to the dimeric structure of the matrix it is possible that new resonant states emerge in the spectrum at energies for which the dimer matrix commutes with the matrix of the other species. The simplest case corresponds to the situation when the dimer matrix reduces to a multiple of the identity matrix, and that occurs whenever $\mathrm{Re}\,(\alpha) = 0$ as can be seen in the above expression. Then the only left condition to have a resonance is that the energy belongs to the permitted spectrum of the non-dimerized species. This is the most simple way to write the condition of the dimer resonance and it is independent of the potential model. Additionally the discrete transfer matrix can also be used instead of the continuous transmission matrix to deduce the commuting-energies. Moreover, other commuting-energies can exist for which the dimer matrix does not reduce to the identity, since it suffices that the dimer matrix ($\mathbf{M}_{\mathrm{dimer}}$) can be written as a combination of the identity and powers of the matrix of the non-dimerized species ($\overline{\mathbf{M}}$),

$$\mathbf{M}_{\mathrm{dimer}} = a_0 \mathbf{I} + \sum_{n>0} a_n \overline{\mathbf{M}}^n. \tag{6.2}$$

And the same reasoning can be applied to other types of impurities that can be included inside a periodic chain. In fact, it has been found that if the impurities are symmetric then extended states can exist at energies for which the impurity matrix reduces to a linear combination of the identity and the matrix of the other species of the chain [188, 108], hence they are commuting-resonances. Therefore, this kind of short-range correlations are able to include new extended states in the spectrum because there exist energies for which the matrices of the new compositional units (i.e.

the dimer matrix or the impurity matrix and the matrices of the other species) can commute. And some of these commuting-energies will not be commuting energies of the individual matrices of the system and that is the reason why these extended states do not exist in the uncorrelated model. Let us consider another correlated model supporting extended states, for example the simplest case of the diluted Anderson model [104, 68]. It consists of a one-dimensional tight-binding Hamiltonian for which the self-energies ε_j of the odd sites are random, whereas they are all equal for the even sites that can be set to zero without loss of generality. This model is known to support an extended state for $E = 0$. Let us see that it is a commuting-resonance. The discrete transfer matrix for the diagonal tight-binding model reads from equation (2.42) on page 26

$$\begin{pmatrix} E - \varepsilon_j & -1 \\ 1 & 0 \end{pmatrix}. \tag{6.3}$$

We can define a new compositional unit in the system including an odd and an even site, which can be described by the product of the individual matrices,

$$\mathbf{M}_j = \begin{pmatrix} E^2 - \varepsilon_j E - 1 & \varepsilon_j - E \\ E & -1 \end{pmatrix}, \tag{6.4}$$

and the commutator of these compositional units can be readily calculated,

$$[\mathbf{M}_j, \mathbf{M}_i] = \begin{pmatrix} (\varepsilon_j - \varepsilon_i)E & 0 \\ (\varepsilon_j - \varepsilon_i)E^2 & (\varepsilon_i - \varepsilon_j)E \end{pmatrix}, \tag{6.5}$$

that obviously vanishes for $E = 0$ independently of the values of the site-energies. It can be easily seen that $E = 0$ belongs to the permitted spectrum of the periodic chain of matrices (6.4) for all values of ε_j, and therefore a commuting-resonance emerges at that energy whatever the distribution of the site-energies for the odd sites is. It can be shown that the extended states appearing in more complex configurations of the diluted Anderson model are also commuting-resonances. It must then be clear that not all kind of short-range correlations will be able to include new extended states in the spectrum (in the thermodynamic limit). The correlations must be such that new compositional units can be defined in the system, so that new commuting-energies for the matrices of the new compositional units can exist. This reasoning explains why the model of correlations proposed in this work is not able to include new extended states, since the probability of appearance of certain binary clusters is modified but the compositional units of the system remain the same as for the completely random case, and they are the individual matrices of the atomic species. Then, although the localization and the transport properties can be modified by the correlations, as it has

been shown, however no additional truly extended states emerge in the spectrum. And, what about long-range correlations? Certainly the situation is quite more complex with long-range correlations, however at the present time, to our knowledge, there does not exist in the literature any proof that long-range correlations are able to include in the spectrum of disordered systems strictly extended states, that is with a divergent localization length. Only numerical proofs and also analytical calculations up to fourth-order in perturbation theory exist that have proved that qualitatively a MIT happens due to long-range correlations. However the states of the 'delocalized' phase are strictly speaking still exponentially localized, as we discussed in the first chapter of the present work. Hence, it seems that a large variety of models existing so far in the literature are compatible with the conjecture that all extended states in the thermodynamic limit of one-dimensional disordered structures occur at commuting-energies of the transmission matrices of the compositional units of the system. Nevertheless, further research is needed to confirm the validity of such hypothesis.

Among all the interesting features exhibited by the Pöschl-Teller model, such as the presence of isolated extended states in uncorrelated disordered sequences in which the parameters of the different species satisfy certain properties, one of them deserves a special remark: the building of random resonant chains with a **continuum of delocalized states**. The composition of resonant Pöschl-Teller wells behaves as a transparent potential for all positive energies. As described in chapter 4, as long as the dimensionless amplitude of the well belongs to an infinite set of discrete values that provide the resonant behaviour, the rest of the parameters of the well can be varied randomly, therefore the configuration of the resonant chain is quite versatile. And of course the delocalization of the electronic states for positive energies is absolutely independent of the random or correlated character of the disordered sequence. Then, at least it is possible to find a theoretical model for which disordered arrays of potentials exhibits a full continuum of extended states which is independent of the length of the system. It is in principle a pure academic model whose properties are tightly bound to the functional dependence of the potentials. Hence, its real importance depends up to a point on the possibility to reproduce experimentally such a structure. Semiconductor heterostructures may be considered as applicants for this task. Advances in the epitaxial growing techniques have made it possible to manipulate the profiles of the band conduction inside the heterostructure in order to build for example confining parabolic wells. Then if not now, perhaps in the future it might be possible to control the growing process of semiconductor samples in such a manner that the spatial profile of the band conduction follows the functional dependence of the Pöschl-Teller hole and therefore having the possibility to check experimentally the predicted behaviour.

The Pöschl-Teller potential has shown an ensemble of very interesting properties and also a completely new behaviour not expected from a disordered system. From our point of view, it is important to build new models of one-dimensional disordered systems using other potentials, in order to analyse their properties and decide on the validity of our conjectures.

Regarding complex potentials, let us say that their real importance lies on the fact that they can model very easily dissipative processes, as we have studied in chapter 5. Nevertheless the utility of the models proposed in this work to account for delocalization due to decoherence in long disordered wires has not been fully studied already, and certain additional problems such as the presence of anomalous scattering needs to be solved when considering large systems. Much work needs to be done in order to build general complex extensions of the potentials, based on physical grounds, so that they can be used to incorporate successfully decoherence processes and dissipation in the systems.

To conclude let us finally say that there is still a lot to be learned about one-dimensional systems and the effects of disorder. The physics underlying localization phenomena have turned out to be enormously rich and long after Anderson made the first description it is still possible to find surprising results. We hope that our little contribution to the field stimulates other people to face interesting questions that remain to be answered, some of which have been formulated in this final discussion.

The transmission matrix

A.1 Properties and symmetries of the transmission matrix

Let be $V(x)$ a finite range potential appreciable only inside the region $[-d, d]$, so that the wave function can be written as

$$\Psi(x) = \begin{cases} A_1 e^{ik(x+d)} + B_1 e^{-ik(x+d)}, & x \leqslant -d, \\ A_2 u(x) + B_2 v(x), & -d < x \leqslant d, \\ A_3 e^{ik(x-d)} + B_3 e^{-ik(x-d)}, & x > d. \end{cases} \tag{A.1}$$

$u(x), v(x)$ being the linearly independent elementary solutions for each k of the continuum spectrum of the potential. By applying the continuity conditions of the state and its derivative at $x = \pm d$, it is possible to reach an expression of the form

$$\begin{pmatrix} A_3 \\ B_3 \end{pmatrix} = \begin{pmatrix} M_{11} & M_{12} \\ M_{21} & M_{22} \end{pmatrix} \begin{pmatrix} A_1 \\ B_1 \end{pmatrix} \equiv \mathbf{M} \begin{pmatrix} A_1 \\ B_1 \end{pmatrix}, \tag{A.2}$$

relating the amplitudes of the free particle states on the right and left sides of the potential. $\mathbf{M}$ is the continuous transmission matrix of the potential and its elements

read in a general form:

$$
\begin{aligned}
\mathrm{M}_{11} =& \frac{v(d)u'(-d) + v(-d)u'(d) - u(d)v'(-d) - u(-d)v'(d)}{2\mathcal{W}} \\
& + \mathrm{i}\,\frac{k^2u(d)v(-d) - k^2u(-d)v(d) + u'(d)v'(-d) - u'(-d)v'(d)}{2k\mathcal{W}},
\end{aligned}
\tag{A.3a}
$$

$$
\begin{aligned}
\mathrm{M}_{12} =& \frac{v(d)u'(-d) - v(-d)u'(d) - u(d)v'(-d) + u(-d)v'(d)}{2\mathcal{W}} \\
& + \mathrm{i}\,\frac{k^2u(-d)v(d) - k^2u(d)v(-d) + u'(d)v'(-d) - u'(-d)v'(d)}{2k\mathcal{W}},
\end{aligned}
\tag{A.3b}
$$

$$
\begin{aligned}
\mathrm{M}_{21} =& \frac{v(d)u'(-d) - v(-d)u'(d) - u(d)v'(-d) + u(-d)v'(d)}{2\mathcal{W}} \\
& + \mathrm{i}\,\frac{k^2u(d)v(-d) - k^2u(-d)v(d) - u'(d)v'(-d) + u'(-d)v'(d)}{2k\mathcal{W}},
\end{aligned}
\tag{A.3c}
$$

$$
\begin{aligned}
\mathrm{M}_{22} =& \frac{v(d)u'(-d) + v(-d)u'(d) - u(d)v'(-d) - u(-d)v'(d)}{2\mathcal{W}} \\
& + \mathrm{i}\,\frac{k^2u(-d)v(d) - k^2u(d)v(-d) - u'(d)v'(-d) + u'(-d)v'(d)}{2k\mathcal{W}},
\end{aligned}
\tag{A.3d}
$$

where $\mathcal{W} = v(x)u'(x) - u(x)v'(x)$ is the Wronskian of the solutions and it must be independent of x. A straightforward calculation of the determinant of the transmission matrix leads to

$$
\det \mathbf{M} = \frac{v(d)u'(d) - u(d)v'(d)}{v(-d)u'(-d) - u(-d)v'(-d)}.
\tag{A.4}
$$

Therefore $\det \mathbf{M} = 1$ for all kind of potentials, since no specific assumptions have been made regarding $V(x)$. Let us remark that this property is not a consequence of the time reversal symmetry of the Hamiltonian as it is usually stated. Let us study now the symmetries of the elements of the matrix in different special cases.

A.1.1 $V(x) \in \mathbb{R}$

If the potential is real it is always possible to find real linearly independent solutions $u(x), v(x)$ for each value of the energy k. And from equations (A.3) the following relations hold,

$$
\mathrm{M}_{22} = \mathrm{M}_{11}^*, \qquad \mathrm{M}_{21} = \mathrm{M}_{12}^*.
\tag{A.5}
$$

Therefore in the case of a real potential the transmission matrix can be written as

$$
\mathbf{M} = \begin{pmatrix} \alpha & \beta \\ \beta^* & \alpha^* \end{pmatrix}, \quad |\alpha|^2 - |\beta|^2 = 1.
\tag{A.6}
$$

It is easy to check that these matrices satisfy

$$
\mathbf{M} \begin{pmatrix} 1 & 0 \\ 0 & -1 \end{pmatrix} \mathbf{M}^\dagger = \begin{pmatrix} 1 & 0 \\ 0 & -1 \end{pmatrix}.
\tag{A.7}
$$

The latter equation together with $\det \mathbf{M} = 1$ define the group $\mathcal{SU}(1,1)$.

$V(x)$ **with parity symmetry**

If the potential is real such that $V(-x) = V(x)$, then it is possible to find elementary solutions with parity symmetry. Let us suppose $u(x)$ to be even and $v(x)$ to be odd, then

$$u(-x) = u(x), \qquad\qquad v(-x) = -v(x), \qquad\qquad \text{(A.8)}$$
$$u'(-x) = -u'(x), \qquad\qquad v'(-x) = v'(x). \qquad\qquad \text{(A.9)}$$

Using this symmetry in (A.3) one finds

$$\mathrm{M}_{21} = -\mathrm{M}_{12}. \qquad\qquad \text{(A.10)}$$

And together with (A.5) it yields a matrix of the form

$$\mathbf{M} = \begin{pmatrix} \alpha & ib \\ -ib & \alpha^* \end{pmatrix}, \quad b \in \mathbb{R}, \, |\alpha|^2 - b^2 = 1. \qquad\qquad \text{(A.11)}$$

A.1.2 $V(x) \in \mathbb{C}$

If the potential is complex, it is not possible generally to build functions $u(x), v(x)$ being real, therefore the conjugation relations (A.5) are not satisfied. There are no special symmetries among the matrix elements.

$$\mathbf{M} = \begin{pmatrix} \alpha & \beta \\ \delta & \gamma \end{pmatrix}, \quad \alpha\gamma - \beta\delta = 1. \qquad\qquad \text{(A.12)}$$

$V(x)$ **with parity symmetry**

In the case of a complex potential with parity symmetry, the same analysis as for a real potential can be applied, and equation (A.10) is obtained, since it does not depend on the elementary solutions being real or complex but only on their symmetries.

$$\mathbf{M} = \begin{pmatrix} \alpha & \beta \\ -\beta & \gamma \end{pmatrix}, \quad \alpha\gamma + \beta^2 = 1. \qquad\qquad \text{(A.13)}$$

$V(x)$ **with $\mathcal{PT}$-symmetry**

Let us consider a complex local potential invariant under the joint action of parity and time-reversal operations $V^*(-x) = V(x)$ [150]. Then it is possible to find $u(x), v(x)$ satisfying

$$u^*(-x) = u(x), \qquad\qquad v^*(-x) = -v(x), \qquad\qquad \text{(A.14)}$$
$$(u^*)'(-x) = -(u^*)'(x), \qquad\qquad (v^*)'(-x) = (v^*)'(x). \qquad\qquad \text{(A.15)}$$

Using the above symmetries in (A.3) one is led to

$$M_{22} = M_{11}^*, \qquad M_{12}^* = -M_{12}, \qquad M_{21}^* = -M_{21}. \tag{A.16}$$

Thus the matrix can be written as

$$\mathbf{M} = \begin{pmatrix} \alpha & ib \\ ic & \alpha^* \end{pmatrix}, \quad b, c \in \mathbb{R}, \ |\alpha|^2 + bc = 1. \tag{A.17}$$

A.2   Scattering amplitudes

The scattering amplitudes are directly calculated from the transmission matrix. Figure A.1 is a pictorial representation of equation (A.2). Considering left incidence then

$A_1 e^{ikx}$ $B_2 e^{-ikx}$

$B_1 e^{-ikx}$ V(x) $A_2 e^{ikx}$
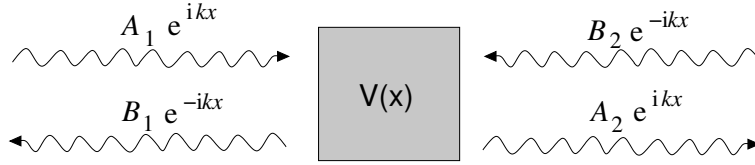
Figure A.1.

$A_1 = 1$, $B_1 = r^L$, $A_2 = t^L$, $B_2 = 0$. And it follows

$$t^L = \frac{1}{M_{22}}, \qquad r^L = -\frac{M_{21}}{M_{22}}. \tag{A.18}$$

In the case of right incidence $A_1 = 0$, $B_1 = t^R$, $A_2 = r^R$, $B_2 = 1$. And the equations yield

$$t^R = \frac{1}{M_{22}}, \qquad r^R = \frac{M_{12}}{M_{22}}. \tag{A.19}$$

The insensitivity of the complex transmission amplitude to the incidence direction is trivially proved. Using the properties of the transmission matrix for particular cases of the potential is easy to see that for parity invariant potentials (real or complex) $r^L = r^R$, for generic real potentials $r^L = e^{i\varphi} r^R$ and for generic complex ones both amplitudes differ.

In table A.1 a summary of the symmetries of the transmission matrices and scattering amplitudes is given for the different type of potentials described.

Table A.1. Symmetries of the transmission matrix and scattering amplitudes for different potentials. Greek letters mean complex elements of the matrix while Latin ones represent real coefficients. $\widehat{\mathcal{P}}$ and $\widehat{\mathcal{T}}$ denote the parity and time reversal operators respectively.

$\widehat{V}(x)\left[\langle x|\,\widehat{V}\,|x'\rangle = V(x)\delta(x-x')\right]$	Transmission Matrix	Scattering Amplitudes
All	$\det \mathbf{M} = 1$	$t^R = t^L$
Real	$\begin{pmatrix} \alpha & \beta \\ \beta^* & \alpha^* \end{pmatrix} \in \mathcal{SU}(1,1)$	$r^L = \mathrm{e}^{\mathrm{i}\varphi}r^R$
Real, $\left[\widehat{V},\widehat{\mathcal{P}}\right] = 0$	$\begin{pmatrix} \alpha & \mathrm{i}b \\ -\mathrm{i}b & \alpha^* \end{pmatrix} \in \mathcal{SU}(1,1)$	$r^L = r^R$
Complex	$\begin{pmatrix} \alpha & \beta \\ \delta & \gamma \end{pmatrix}$	$r^L \neq r^R$
Complex, $\left[\widehat{V},\widehat{\mathcal{P}}\right] = 0$	$\begin{pmatrix} \alpha & \beta \\ -\beta & \gamma \end{pmatrix}$	$r^L = r^R$
Complex, $\left[\widehat{V},\widehat{\mathcal{P}}\widehat{\mathcal{T}}\right] = 0$	$\begin{pmatrix} \alpha & \mathrm{i}b \\ \mathrm{i}c & \alpha^* \end{pmatrix}$	$r^L \neq r^R$

A.3 Transmission matrix for a continuous potential

For the most general continuous potential, equation (A.2) is only satisfied asymptotically, that is the amplitudes of the asymptotic states

$$\Psi(-\infty) = A_1\mathrm{e}^{\mathrm{i}kx} + B_1\mathrm{e}^{-\mathrm{i}kx}, \tag{A.20a}$$

$$\Psi(\infty) = A_3\mathrm{e}^{\mathrm{i}kx} + B_3\mathrm{e}^{-\mathrm{i}kx}, \tag{A.20b}$$

can be related via the asymptotic transmission matrix $\mathcal{M}$,

$$\begin{pmatrix} A_3 \\ B_3 \end{pmatrix} = \mathcal{M} \begin{pmatrix} A_1 \\ B_1 \end{pmatrix}. \tag{A.21}$$

The procedure to obtain this asymptotic matrix is the following. First is solving the Schrödinger equation for positive energies so that the more general state reads

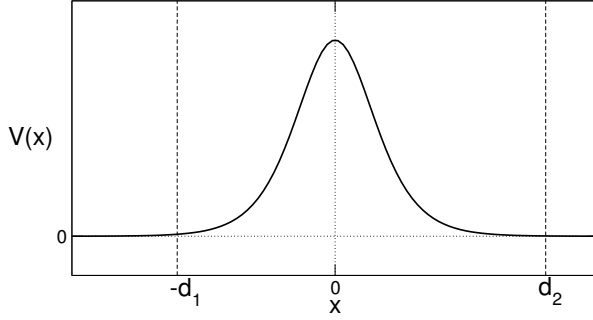$$\Psi(x) = A_2 u(x) + B_2 v(x), \tag{A.22}$$

Figure A.2. A continuous potential

in terms of the elementary solutions $u(x)$, $v(x)$. Now one needs to build the asymptotic form of the elementary solutions,

$$u(\pm\infty) = U_1^{\pm}e^{ikx} + U_2^{\pm}e^{-ikx}, \tag{A.23a}$$

$$v(\pm\infty) = V_1^{\pm}e^{ikx} + V_2^{\pm}e^{-ikx}. \tag{A.23b}$$

Therefore the more general asymptotic state becomes

$$\Psi(\pm\infty) = \left(A_2 U_1^{\pm} + B_2 V_1^{\pm}\right)e^{ikx} + \left(A_2 U_2^{\pm} + B_2 V_2^{\pm}\right)e^{-ikx}. \tag{A.24}$$

Equating the coefficients with those corresponding to the asymptotic forms (A.20) yields

$$A_1 = A_2 U_1^- + B_2 V_1^-, \qquad A_3 = A_2 U_1^+ + B_2 V_1^+, \tag{A.25}$$

$$B_1 = A_2 U_2^- + B_2 V_2^-, \qquad B_3 = A_2 U_2^+ + B_2 V_2^+. \tag{A.26}$$

Solving (A_3, B_3) in terms of (A_1, B_1) one obtains for the elements of the asymptotic matrix

$$\mathcal{M} = \frac{2ik}{\mathcal{W}}\begin{pmatrix} U_1^+ V_2^- - V_1^+ U_2^- & V_1^+ U_1^- - U_1^+ V_1^- \\ U_2^+ V_2^- - V_2^+ U_2^- & V_2^+ U_1^- - U_2^+ V_1^- \end{pmatrix}, \tag{A.27}$$

where $\mathcal{W} = vu' - v'u$ is the Wronskian of the solutions.

A.3.1 Including a cut-off in the potential

Let us suppose that due to the nature of the potential, it is only appreciable inside the region $[-d_1, d_2]$ (figure A.2). Then the transfer matrix for the potential with the cut-off relates the amplitudes of the plane waves at $x = d_2$ and $x = -d_1$, which can be written from the asymptotic forms (A.20), yielding the relation

$$\begin{pmatrix} A_3 e^{ikd_2} \\ B_3 e^{-ikd_2} \end{pmatrix} = \mathbf{M}_{\text{cut}} \begin{pmatrix} A_1 e^{-ikd_1} \\ B_1 e^{ikd_1} \end{pmatrix}, \tag{A.28}$$

which implies

$$\mathbf{M}_{\text{cut}} = \begin{pmatrix} \mathrm{e}^{\mathrm{i}kd_2} & 0 \\ 0 & \mathrm{e}^{-\mathrm{i}kd_2} \end{pmatrix} \mathcal{M} \begin{pmatrix} \mathrm{e}^{\mathrm{i}kd_1} & 0 \\ 0 & \mathrm{e}^{-\mathrm{i}kd_1} \end{pmatrix}, \tag{A.29}$$

leading to

$$\mathbf{M}_{\text{cut}} = \begin{pmatrix} \mathcal{M}_{11}\,\mathrm{e}^{\mathrm{i}k(d_2+d_1)} & \mathcal{M}_{12}\,\mathrm{e}^{\mathrm{i}k(d_2-d_1)} \\ \mathcal{M}_{21}\,\mathrm{e}^{-\mathrm{i}k(d_2-d_1)} & \mathcal{M}_{22}\,\mathrm{e}^{-\mathrm{i}k(d_2+d_1)} \end{pmatrix}. \tag{A.30}$$

Once the asymptotic transmission matrix is known, the cut-off matrix is straightforwardly built. And for a given potential it is usually easier to calculate the asymptotic matrix than to construct directly the cut-off version using the continuity conditions at the cut-off points.

A.4   Canonical equation from the transmission matrix

Let us consider a linear composition of potentials. All of them are formally described by the same transmission matrix with different parameters. And let be $\mathbf{M}_j$ the transmission matrix of the jth potential,

$$\begin{pmatrix} A_{j+1} \\ B_{j+1} \end{pmatrix} = \mathbf{M}_j \begin{pmatrix} A_j \\ B_j \end{pmatrix}, \tag{A.31}$$

where the coordinates of the electronic wave function in the different sectors of the chain are chosen to satisfy that the amplitude of the state at all sites is simply given by the sum of the complex amplitudes of the travelling plane waves, that is $\Psi_j = A_j + B_j$ for all j. To build the canonical equation one simply calculates the quantity $\Psi_{j+1} + \chi\Psi_{j-1}$, using $\mathbf{M}_j$ and $\mathbf{M}_{j-1}^{-1}$ to write the amplitudes $(A_{j\pm1}, B_{j\pm1})$ in terms of (A_j, B_j). Then χ is solved by imposing the coefficients of A_j and B_j to be the same. Following this procedure one concludes that the canonical equation for the most general potential can be written as,

$$\Psi_{j+1} = \left(\overline{S}_j + S_{j-1}\frac{K_j}{K_{j-1}} \right) \Psi_j - \frac{K_j}{K_{j-1}}\Psi_{j-1}, \tag{A.32}$$

where

$$\overline{S}_j = \frac{1}{2}\left[(\mathbf{M}_j)_{11} + (\mathbf{M}_j)_{12} + (\mathbf{M}_j)_{21} + (\mathbf{M}_j)_{22} \right], \tag{A.33a}$$

$$S_j = \frac{1}{2}\left[(\mathbf{M}_j)_{11} - (\mathbf{M}_j)_{12} - (\mathbf{M}_j)_{21} + (\mathbf{M}_j)_{22} \right], \tag{A.33b}$$

$$K_j = \frac{1}{2}\left[(\mathbf{M}_j)_{11} - (\mathbf{M}_j)_{22} + (\mathbf{M}_j)_{21} - (\mathbf{M}_j)_{12} \right]. \tag{A.33c}$$

In the case of a real potential, using the symmetries of the transmission matrix described previously, one finds

$$\overline{S}_j = \mathrm{Re}\,[(\mathbf{M}_j)_{11}] + \mathrm{Re}\,[(\mathbf{M}_j)_{12}]\,, \tag{A.34a}$$

$$S_j = \mathrm{Re}\,[(\mathbf{M}_j)_{11}] - \mathrm{Re}\,[(\mathbf{M}_j)_{12}]\,, \tag{A.34b}$$

$$K_j = \mathrm{Im}\,[(\mathbf{M}_j)_{11}] - \mathrm{Im}\,[(\mathbf{M}_j)_{12}]\,. \tag{A.34c}$$

And it also can be observed that for real and parity invariant potentials the functions $\overline{S}_j$ and S_j coincide because the off-diagonal elements of the matrix are pure imaginary.

The Lyapunov exponents

Let us prove that for a one-dimensional Hamiltonian system, suitable to be described in terms of products of random matrices, the two Lyapunov characteristic exponents (LCE) come in a pair of the form $\{\lambda, -\lambda\}$.

Let us consider our system within the discrete transmission matrix formalism. If the Hamiltonian of the system can be written in terms of a potential $V(x)$ then it can be shown that the canonical equation takes always the form

$$\Psi_{j+1} = J(\gamma_{j-1}, \gamma_j)\Psi_j - \frac{K(\gamma_j)}{K(\gamma_{j-1})}\Psi_{j-1}, \tag{B.1}$$

where γ_j denotes the parameters of the potential at the jth site of the system and J, K are functions depending on these parameters and the energy. Hence the discrete transmission matrix reads

$$\mathbf{P}_j(\gamma_{j-1}, \gamma_j) = \begin{pmatrix} J(\gamma_{j-1}, \gamma_j) & -\frac{K(\gamma_j)}{K(\gamma_{j-1})} \\ 1 & 0 \end{pmatrix}. \tag{B.2}$$

The above matrix becomes a symplectic transformation if $K(\gamma_j)/K(\gamma_{j-1}) = 1$ but in general $\det \mathbf{P}_j \neq 1$. The necessary and sufficient condition to ensure that the LCE of the asymptotic product $\mathbb{P}_N = \mathbf{P}_N \ldots \mathbf{P}_1$ ($N \to \infty$) are $\{\lambda, -\lambda\}$ is that the determinant of Oseledet's matrix Γ equals 1. Let us remember that $\Gamma = \lim_{N\to\infty} \left(\mathbb{P}_N^t \mathbb{P}_N\right)^{\frac{1}{2N}}$. Thus we only need to prove that $\lim_{N\to\infty}(\det \mathbb{P}_N)^{1/N} = 1$ which is trivial if the individual transfer matrices are symplectic, like for example in the tight-binding model with constant transfer integrals or for the delta potential model, but it may not be so obvious in the most general case. For the proof let us suppose that our system is composed of two different kind of potentials 1, 2, in a random sequence. Then the product matrix $\mathbb{P}_N$ will contain four different types of matrices, namely $\mathbf{P}(1,1)$, $\mathbf{P}(1,2)$, $\mathbf{P}(2,1)$,

$\mathbf{P}(2,2)$ according to the different pairs of potentials occurring in the sequence and participating in the canonical equation. Then,

$$\lim_{N\to\infty} (\det \mathbb{P}_N)^{\frac{1}{N}} =$$
$$\lim_{N\to\infty} \left[(\det \mathbf{P}(1,1))^{N_{11}} (\det \mathbf{P}(1,2))^{N_{12}} (\det \mathbf{P}(2,1))^{N_{21}} (\det \mathbf{P}(2,2))^{N_{22}} \right]^{\frac{1}{N}} =$$
$$(\det \mathbf{P}(1,1))^{C_{11}} (\det \mathbf{P}(1,2))^{C_{12}} (\det \mathbf{P}(2,1))^{C_{21}} (\det \mathbf{P}(2,2))^{C_{22}}, \quad \text{(B.3)}$$

N_{ij} being the number of times that $\mathbf{P}(i,j)$ appears, and C_{ij} the frequencies of appearance of the pairs $-ij-$ in the thermodynamic limit. From (B.2) it readily follows

$$\lim_{N\to\infty} (\det \mathbb{P}_N)^{\frac{1}{N}} = \left[\frac{K(2)}{K(1)} \right]^{C_{12}} \left[\frac{K(1)}{K(2)} \right]^{C_{21}}. \quad \text{(B.4)}$$

A simple reflection symmetry argument requires that $C_{12} = C_{21}$ so the above expression equals 1. And finally the eigenvalues of Γ must be of the form e^{λ}, $\mathrm{e}^{-\lambda}$.

This proof can be straightforwardly extended for a case considering k different potentials or for a continuous model with parameters inside a certain range with a given probability distribution.

This result about the Lyapunov exponent for a one-dimensional system must be naturally expected, by the fact that the same physical problem can be treated through the continuous transmission matrix formalism and it must lead to the same results. Therefore considering the latter matrices which have always determinant unity, it is obvious that $\det \Gamma = 1$. Nevertheless it is interesting to see how the discrete transfer matrices, although not symplectic individually, lead to a global symplectic transformation in the canonical sense, provided they describe a Hamiltonian system.

DOS from node counting

James and Ginzbarg obtained the expression of the integrated density of states (IDOS) of a linear chain of potentials in terms of the changes of sign of the wave function inside the different sectors of the system [115]. Their reasoning is the following. Let us consider a binary wire composed of two types of potentials β_1 and β_2. And let be $[x_j, x_{j+1}]$ the jth sector of the chain including a β_1 potential. Then the elementary solutions for positive energy in this cell $f_1(x)$, $g_1(x)$, can be chosen to satisfy

$$f_1(x_j) = 1, \qquad f_1'(x_j) = 0, \tag{C.1a}$$

$$g_1(x_j) = 0, \qquad g_1'(x_j) = 1. \tag{C.1b}$$

Now let us consider a certain energy E for which $g_1(x)$ has p_1 nodes inside the given sector (the first one at x_j). Then for this energy, possible states include $\psi(x) = g_1(x) + \mu f_1(x)$ with $(p_1 - 1)$ zeros and $\psi(x) = g_1(x) - \mu f_1(x)$ with p_1 zeros in the cell (for sufficiently small μ). For low E, $p_1 = 1$ and as the energy grows the index p_1 increases by one whenever $g_1(x_{j+1}) = 0$. Thus the energy spectrum can be divided in intervals according to the value of the index p_1, so that if E lies in the interval labelled with p_1 then the solution $\psi(x)$ will have p_1 or $(p_1 - 1)$ nodes in every sector of type β_1. To determine whether the number of zeros is p_1 or $(p_1 - 1)$, one has to check if $\psi(x_j)$ and $\psi(x_{j+1})$ have the same signs (even number of nodes) or opposite signs (odd number of nodes). Thus for that energy the number of nodes in a β_1 sector can be written as

$$p_1 - \frac{1}{2} + (-1)^{p_1} \frac{z}{2}, \tag{C.2}$$

where $z = 1$ if $\psi(x_j)$ and $\psi(x_{j+1})$ have the same signs and $z = -1$ otherwise. The same reasoning can be used for the species β_2. And for an energy E with the labels

p_1 for the species β_1 and p_2 for β_2, the total number of nodes inside the mixed system and therefore the IDOS per atom reads

$$n(E) = c_1\left(p_1 + \frac{(-1)^{p_1}-1}{2}\right) + c_2\left(p_2 + \frac{(-1)^{p_2}-1}{2}\right)$$
$$- (-1)^{p_1}\mathcal{N}_1(E) - (-1)^{p_2}\mathcal{N}_2(E), \tag{C.3}$$

where c_1, c_2, are the concentrations of the species and $\mathcal{N}_1(E)$, $\mathcal{N}_2(E)$, are the concentrations of changes of sign for each species, that is the number of cells containing a certain species in which the state changes sign (i.e. $\psi(x)$ has opposite signs at the beginning and at the end of the sector) divided by the total number of potentials of the system. To obtain the density of states one needs to evaluate $n(E)$ in the interval $(E, E + \mathrm{d}E)$ in which the indices p_1, p_2, can be considered to remain fixed. Therefore the only quantities that can vary in the differential interval are the concentrations of changes of sign. Hence,

$$g(E) = \left|(-1)^{p_1}\frac{\mathrm{d}\mathcal{N}_1(E)}{\mathrm{d}E} + (-1)^{p_2}\frac{\mathrm{d}\mathcal{N}_2(E)}{\mathrm{d}E}\right|. \tag{C.4}$$

And this expression is straightforwardly generalized for an arbitrary number of species. The main result is that to determine the DOS correctly, depending on the energy range one has to sum or subtract the changes of sign of the wave function at sectors corresponding to different species.

Now let us see how one can know the indices p_1, p_2, in a practical way. The system is completely determined by the canonical equation

$$\Psi_{j+1} = J(\gamma_{j-1}, \gamma_j)\Psi_j - \frac{K(\gamma_j)}{K(\gamma_{j-1})}\Psi_{j-1}. \tag{C.5}$$

The functions J, K, can be obtained in terms of the elementary solutions of the Schrödinger equation in each sector of the chain. According to reference [161], $K(\gamma_j)$ can be written as

$$K(\gamma_j) = \frac{f_{\gamma_j}(x_{j+1})g_{\gamma_j}(x_j) - f_{\gamma_j}(x_j)g_{\gamma_j}(x_{j+1})}{f'_{\gamma_j}(x_j)g_{\gamma_j}(x_j) - f_{\gamma_j}(x_j)g'_{\gamma_j}(x_j)}, \tag{C.6}$$

where $f_{\gamma_j}(x), g_{\gamma_j}(x)$ are the elementary solutions in the jth sector $[x_j, x_{j+1}]$ with a potential of type γ_j. Imposing the additional conditions (C.1) it follows for the case $\gamma_j = \beta_1$ that $K(\beta_1) = -g_1(x_{j+1})$. That is, the function $-K(\beta_1)$ takes the same values that the elementary solution $g_1(x)$, verifying equations (C.1), would reach at the end of every β_1 sector. Thus, whenever $g_1(x_{j+1})$ as a function of the energy changes its sign, and therefore the index p_1 increases by 1, $K(\beta_1)$ also registers a change of sign.

What is more, it is not hard to see that in equation (C.4) the terms $(-1)^{p_1}$, $(-1)^{p_2}$, can be directly identified with the signs of $K(\beta_1)$, $K(\beta_2)$. And finally, one can write

$$g(E) = \left| \mathrm{sgn}[K(\beta_1)]\frac{\mathrm{d}\mathcal{N}_1(E)}{\mathrm{d}E} + \mathrm{sgn}[K(\beta_2)]\frac{\mathrm{d}\mathcal{N}_2(E)}{\mathrm{d}E} \right|. \tag{C.7}$$

From a numerical viewpoint one must do the transmission of the state through the system using the functional equation and count the number of changes of sign from site to site for the different atomic species, to perform finally a numerical differentiation with respect to the energy and sum or subtract the different contributions of the species according to the sign of the function $K(\beta)$ for the energy considered.

The Functional Equation

Let us begin with the canonical equation describing our one-dimensional problem,

$$\Psi_{j+1} = J(\gamma_{j-1}, \gamma_j)\Psi_j - \frac{K(\gamma_j)}{K(\gamma_{j-1})}\Psi_{j-1}, \tag{D.1}$$

where Ψ_j means the real amplitude of the electronic state at the jth site of the wire and γ_j denotes the set of parameters characterizing the potential at the jth site (jth sector). The functions $J(\gamma, \beta)$ and $K(\gamma)$ which depend on the potential and the energy, rule the spreading of the state from one site to its neighbours. From now on Greek letters are used to label the parameters of the different types of potentials composing the chain, while Latin letters always mean site indices. The above equation can be casted as a two-dimensional mapping defining $x_{j+1} = \Psi_{j+1}$, $y_{j+1} = \Psi_j$,

$$\begin{pmatrix} x_{j+1} \\ y_{j+1} \end{pmatrix} = \begin{pmatrix} J(\gamma_{j-1}, \gamma_j) & -\frac{K(\gamma_j)}{K(\gamma_{j-1})} \\ 1 & 0 \end{pmatrix} \begin{pmatrix} x_j \\ y_j \end{pmatrix}, \tag{D.2}$$

which in polar coordinates $x_j = \rho_j \cos\theta_j$, $y_j = \rho_j \sin\theta_j$ leads to the following transmission relations for the phase and the moduli

$$\theta_{j+1} \equiv \mathfrak{T}(\theta_j; \gamma_{j-1}, \gamma_j) = \arctan\left\{\left(J(\gamma_{j-1}, \gamma_j) - \frac{K(\gamma_j)}{K(\gamma_{j-1})}\tan\theta_j\right)^{-1}\right\}, \tag{D.3}$$

$$\left(\frac{\rho_{j+1}}{\rho_j}\right)^2 \equiv \mathfrak{F}(\theta_j; \gamma_{j-1}, \gamma_j) = \cos^2\theta_j + \left(J(\gamma_{j-1}, \gamma_j)\cos\theta_j - \frac{K(\gamma_j)}{K(\gamma_{j-1})}\sin\theta_j\right)^2. \tag{D.4}$$

In order to ensure the continuity of the phase transmission for a given energy we work
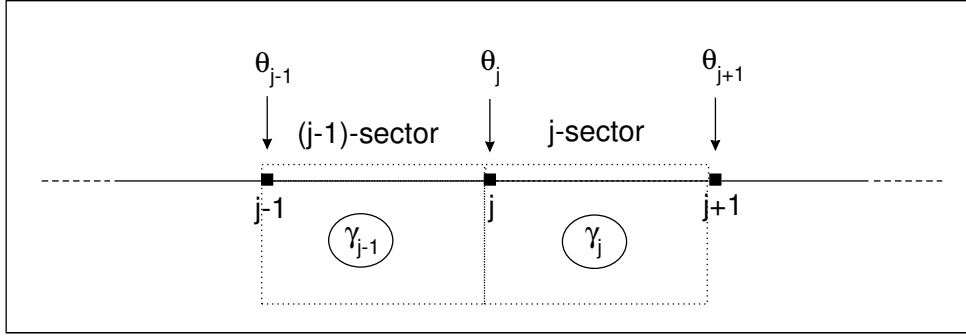
Figure D.1.   Sites and sectors of the one-dimensional system.

with the inverse function defined as

$$\mathcal{T}^{-1}(\theta_{j+1}; \gamma_{j-1}, \gamma_j) = \arctan\left\{ \frac{K(\gamma_{j-1})}{K(\gamma_j)} \left(J(\gamma_{j-1}, \gamma_j) - \frac{1}{\tan\theta_{j+1}} \right) \right\}, \quad \text{(D.5a)}$$

$$\mathcal{T}^{-1}(\theta_{j+1} + n\pi; \gamma_{j-1}, \gamma_j) = \mathcal{T}^{-1}(\theta_{j+1}; \gamma_{j-1}, \gamma_j) \pm n\pi, \qquad \theta_{j+1} \in [0, \pi), \ n \in \mathbb{Z}, \tag{D.5b}$$

where the plus (minus) sign in (D.5b) must be taken when $\frac{K(\gamma_j)}{K(\gamma_{j-1})} > 0 \left(\frac{K(\gamma_j)}{K(\gamma_{j-1})} < 0 \right)$ corresponding to an increasing (decreasing) behaviour of the phase transmission.

The goal is to calculate a distribution function for the phase θ, valid in the thermodynamic limit, so that the differential form of such a function acts as a natural measure of the phase in that limit. In this way one then would be able to obtain the thermodynamic average of any quantity of the system that could be written in terms of the phase.

The first step is to define the functions $W_j(\theta)$ with $\theta \in [0, \pi)$, that means the probability for $\theta_j(\bmod \pi)$ to be included in the interval $[0, \theta)$, that is $\mathrm{d}W_j(\theta)$ means the probability that $\theta_j(\bmod \pi)$ belongs to $(\theta, \theta + \mathrm{d}\theta)$, for a given energy. Therefore it follows that $W_j(\theta)$ are monotonically increasing functions with θ such that $W_j(0) = 0$, $W_j(\pi) = 1$ for all j. And we impose

$$W_j(\theta + n\pi) = W_j(\theta) + n, \qquad \theta \in [0, \pi), \ n \in \mathbb{Z}, \quad \forall\, j. \tag{D.6}$$

According to the meaning of these distribution functions for the individual phases, it is clear that they must satisfy the relation

$$\mathrm{d}W_{j+1}(\theta) = \mathrm{d}W_j\left(\mathcal{T}^{-1}(\theta; \gamma_{j-1}, \gamma_j) \right), \tag{D.7}$$

that is, the probability for $\theta_{j+1}(\bmod \pi)$ of being included in $(\theta, \theta + \mathrm{d}\theta)$ must be the probability for $\theta_j(\bmod \pi)$ of appearing in $\left(\mathcal{T}^{-1}(\theta), \mathcal{T}^{-1}(\theta) + \mathrm{d}\mathcal{T}^{-1}(\theta) \right) (\bmod \pi)$. Integrating the above equation leads us to

$$W_{j+1}(\theta) = \left| W_j\left(\mathcal{T}^{-1}(\theta; \gamma_{j-1}, \gamma_j) \right) - W_j\left(\mathcal{T}^{-1}(0; \gamma_{j-1}, \gamma_j) \right) \right|, \tag{D.8}$$

where the absolute value is necessary for the cases when $\mathcal{T}^{-1}(\theta)$ decreases with θ (i.e. $[K(\gamma_j)/K(\gamma_{j-1})] < 0$), because the distribution functions must be positive. Since the inverse transmission function of the phase gives a value in the interval $[-\pi/2, \pi/2]$, the additional condition (D.6) is used to ensure that the argument of W_j is always included in the interval $[0, \pi)$. And from the definition of the inverse transmission function it follows

$$\mathcal{T}^{-1}(0; \gamma_{j-1}, \gamma_j) = \begin{cases} -\frac{\pi}{2} & \text{if } \frac{K(\gamma_j)}{K(\gamma_{j-1})} > 0, \\ \frac{\pi}{2} & \text{if } \frac{K(\gamma_j)}{K(\gamma_{j-1})} < 0. \end{cases} \tag{D.9}$$

The equations relating the distributions for the phase at the different sites of the system clearly show that in fact those distributions only depend on the atomic species composing the chain. Thus the functions can be properly redefined in terms of the compositional species. $W_{j+1}(\theta)$ is the distribution for the phase at the site $(j+1)$, generated after a potential of type γ_j (see figure D.1), therefore we relabel the function as $W_{j+1}(\theta) \equiv W_{\gamma_j}(\theta)$, that is the distribution function for the phase after a γ_j potential. And it is defined by

$$W_{\gamma_j}(\theta) = \left| W_{\gamma_{j-1}} \left(\mathcal{T}^{-1}(\theta; \gamma_{j-1}, \gamma_j) \right) - W_{\gamma_{j-1}} \left(\frac{\pi}{2} \right) + \delta(\gamma_{j-1}, \gamma_j) \right|, \tag{D.10a}$$

$$W_{\gamma_j}(\theta + n\pi) = W_{\gamma_j}(\theta) + n, \qquad \theta \in [0, \pi), \ n \in \mathbb{Z}, \quad \forall j, \tag{D.10b}$$

where

$$\delta(\gamma_{j-1}, \gamma_j) = \begin{cases} 1 & \text{if } \frac{K(\gamma_j)}{K(\gamma_{j-1})} > 0, \\ 0 & \text{if } \frac{K(\gamma_j)}{K(\gamma_{j-1})} < 0, \end{cases} \tag{D.11}$$

due to (D.6) and (D.9). Now it is straightforward to carry out a thermodynamical average of the probabilities $W_{\gamma_j}(\theta)$. We only have to sum over all the atomic species and binary clusters taking into account their respective concentrations,

$$\sum_\gamma c_\gamma W_\gamma(\theta) = \sum_{\gamma, \beta} C_{\beta\gamma} \left| W_\beta \left(\mathcal{T}^{-1}(\theta; \beta, \gamma) \right) - W_\beta \left(\frac{\pi}{2} \right) + \delta(\beta, \gamma) \right|, \tag{D.12}$$

where c_γ is the concentration of the γ species and $C_{\gamma\beta} = C_{\beta\gamma}$ is the frequency of appearance of the cluster $-\gamma\beta-$ or $-\beta\gamma-$. Writing $C_{\gamma\beta} = c_\gamma p_{\gamma\beta}$, where $p_{\gamma\beta}$ is the probability of finding a β atom besides a γ atom, one can obtain an individual equation for each species,

$$W_\gamma(\theta) = \sum_\beta p_{\gamma\beta} \left| W_\beta \left(\mathcal{T}^{-1}(\theta; \beta, \gamma) \right) - W_\beta \left(\frac{\pi}{2} \right) + \delta(\beta, \gamma) \right|, \tag{D.13a}$$

$$W_\gamma(\theta + n\pi) = W_\gamma(\theta) + n, \qquad \theta \in [0, \pi), \ n \in \mathbb{Z}. \tag{D.13b}$$

So that in the thermodynamic limit there exists a phase distribution function for each species composing the chain, and binary statistical correlations naturally appear in their definitions. Although we have supposed a discrete composition of the system, the same reasoning can be used for a continuous model in which the compositional parameters belong to a certain interval with a given probability distribution.

Therefore solving equations (D.13), one would be able to calculate the average in the thermodynamic limit of any quantity of the system that can be written in terms of the phase θ as long as it is a periodic function with period π. The latter expressions are the most general functional equations valid for all one-dimensional systems for which a canonical equation of the form (D.1) can be obtained.

D.1 Calculating the localization length and the DOS in the thermodynamic limit

Let us consider the Lyapunov exponent given by

$$\lambda = \lim_{N \to \infty} \frac{1}{N} \sum_j \log \left(\frac{\Psi_{j+1}}{\Psi_j} \right) = \left\langle \log \left(\frac{\Psi_{j+1}}{\Psi_j} \right) \right\rangle, \tag{D.14}$$

where $\langle \cdots \rangle$ denotes the average in the thermodynamic limit and the amplitudes of the state at the different sites are considered to be real. Using the two-dimensional mapping defined in the previous section,

$$\lambda = \left\langle \frac{1}{2} \log \left(\frac{\rho_{j+1}}{\rho_j} \right)^2 \right\rangle + \left\langle \log \left| \frac{\cos \theta_{j+1}}{\cos \theta_j} \right| \right\rangle + \left\langle \log \left[\frac{\cos \theta_{j+1} \, | \cos \theta_j |}{| \cos \theta_{j+1} | \, \cos \theta_j} \right] \right\rangle. \tag{D.15}$$

The middle term vanishes because the cosine is a bounded function that does not diverge as the length of the system grows. On the other hand the argument of the logarithm in the last term takes only the values ± 1. Since $\log(1) = 0$ and $\log(-1) = \mathrm{i}\pi$ it readily follows

$$\mathrm{Re} \, (\lambda) = \left\langle \frac{1}{2} \log \left(\frac{\rho_{j+1}}{\rho_j} \right)^2 \right\rangle, \tag{D.16}$$

$$\mathrm{Im} \, (\lambda) = -\mathrm{i} \left\langle \log \left[\frac{\cos \theta_{j+1} | \cos \theta_j |}{| \cos \theta_{j+1} | \cos \theta_j} \right] \right\rangle. \tag{D.17}$$

From equation (D.4) the average of the real part can be easily written using the distribution functions for the phase and therefore obtaining the inverse of the localization length $\xi(E)$,

$$\xi(E)^{-1} \equiv \mathrm{Re} \, (\lambda(E)) = \frac{1}{2} \sum_{\gamma, \beta} C_{\gamma\beta} \int_0^\pi \mathrm{d}W_\gamma(\theta) \log \mathcal{F}(\theta; \gamma, \beta), \tag{D.18}$$

which integrated by parts can also be written as

$$\xi(E)^{-1} = \frac{1}{2}\sum_{\gamma,\beta} C_{\gamma\beta} \log \mathcal{F}(\pi;\gamma,\beta) - \frac{1}{2}\sum_{\gamma,\beta} C_{\gamma\beta} \int_0^\pi W_\gamma(\theta)\frac{\mathcal{F}'(\theta;\gamma,\beta)}{\mathcal{F}(\theta;\gamma,\beta)}\mathrm{d}\theta. \qquad \text{(D.19)}$$

Let us remember that $C_{\gamma\beta} = C_{\beta\gamma}$ is the probability for the cluster $-\gamma\beta-$ or $-\beta\gamma-$ to appear at any position of the chain.

On the other hand the imaginary part of the Lyapunov exponent increases by $\mathrm{i}\pi$ every time the wave function changes sign from one site to the next one. Therefore by averaging equation (D.17) over all possible species at the site $(j+1)$ when the jth species is a γ atom, and dividing by π, one obtains the fraction of γ atoms after which the state changes its sign.

$$-\frac{\mathrm{i}}{\pi}\left\langle \log\left[\frac{\cos\theta_{j+1}|\cos\theta_j|}{|\cos\theta_{j+1}|\cos\theta_j}\right]\right\rangle_{j+1} = -\frac{\mathrm{i}}{\pi}\sum_\beta c_\beta \int_0^\pi \mathrm{d}W_\gamma(\theta)\log\left[\frac{\cos\mathcal{T}(\theta;\gamma,\beta)\,|\cos\theta|}{|\cos\mathcal{T}(\theta;\gamma,\beta)|\cos\theta}\right]$$

$$= \int_{\pi/2}^\pi \mathrm{d}W_\gamma(\theta) = 1 - W_\gamma\left(\frac{\pi}{2}\right), \qquad \text{(D.20)}$$

since the transmission function always returns a value in the interval $[-\pi/2, \pi/2]$, where the cosine is positive. Thus it follows that $c_\gamma\left[1 - W_\gamma(\pi/2)\right]$ is the concentration of changes of sign for the γ species, $\mathcal{N}_\gamma(E)$ as denoted in appendix C. And from the results of the appendix cited the density of states per atom reads

$$g(E) = \left|\sum_\gamma \mathrm{sgn}[K(\gamma)]c_\gamma\frac{\mathrm{d}W_\gamma\left(\frac{\pi}{2}\right)}{\mathrm{d}E}\right|. \qquad \text{(D.21)}$$

D.2   Particular cases

The functional equations can be considerably simplified depending on the particular model of the one-dimensional system. Let us consider a couple of examples appearing in this work.

D.2.1   The canonical equation reads $\Psi_{j+1} = J(\gamma_j)\Psi_j - \Psi_{j-1}$

This is one of the simplest forms for the canonical equation, appearing for example in the diagonal tight-binding model or the delta potential model with substitutional disorder. In this case the function $J(\gamma)$ depends only on the parameters of one potential and one can take $K(\gamma) = 1$ for all the species. Therefore the problems concerning the changes of sign of the latter function are completely avoided and the inverse transmission function for the phase is an increasing function for all energies which depends
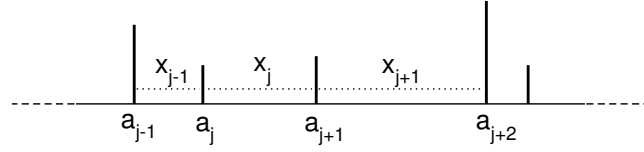
Figure D.2.   Delta chain with structural and substitutional disorder.

only on one atomic species, $\mathfrak{T}^{-1}(\theta; \gamma)$. Then equations (D.13) read

$$W_\gamma(\theta) = \sum_\beta p_{\gamma\beta} \left\{ W_\beta \left(\mathfrak{T}^{-1}(\theta; \gamma) \right) - W_\beta \left(\frac{\pi}{2} \right) \right\} + 1, \tag{D.22a}$$

$$W_\gamma(\theta + n\pi) = W_\gamma(\theta) + n, \qquad \theta \in [0, \pi),\ n \in \mathbb{Z}. \tag{D.22b}$$

If one further considers the case of uncorrelated disorder, that is $p_{\gamma\beta} = c_\beta$ for all γ, β, then a global distribution function for the phase can be defined $W(\theta) \equiv \sum_\gamma c_\gamma W_\gamma(\theta)$ being the solution of

$$W(\theta) = \sum_\gamma c_\gamma W \left(\mathfrak{T}^{-1}(\theta; \gamma) \right) - W \left(\frac{\pi}{2} \right) + 1, \tag{D.23a}$$

$$W(\theta + n\pi) = W(\theta) + n, \qquad \theta \in [0, \pi),\ n \in \mathbb{Z}. \tag{D.23b}$$

In this particular case only one functional equation needs to be solved and the localization length as well as the density of states per atom can be calculated respectively from

$$\xi(E)^{-1} \equiv \operatorname{Re}\left(\lambda(E)\right) = \frac{1}{2} \sum_\gamma c_\gamma \int_0^\pi \mathrm{d}W(\theta) \log \mathfrak{F}(\theta; \gamma), \tag{D.24}$$

$$g(E) = \left| \frac{\mathrm{d}W\left(\frac{\pi}{2}\right)}{\mathrm{d}E} \right|. \tag{D.25}$$

D.2.2   The delta potential model with uncorrelated structural and substitutional disorder

Let us consider a very specific model treated in chapter 3: the delta chain with uncorrelated structural and substitutional disorder. The system is composed of different atomic species following a random sequence and whose positions are not equally spaced, as shown in figure D.2. The potential at each sector is determined by two parameters: the delta coupling and the distance right after the delta. For this particular setup the canonical equation takes the general form (D.1) with functions

$$J(x_{j-1}, x_j, a_j) = \cos(kx_j) + \cot(kx_{j-1})\sin(kx_j) + \frac{2}{ka_j}\sin(kx_j), \tag{D.26}$$

$$K(x_j) = \sin(kx_j). \tag{D.27}$$

The function J depends on the coupling and the distance of the j sector and the distance of the $(j-1)$ sector, while K is determined by the distance of each sector. The spacing between neighbouring atoms is determined by a certain probability distribution depending on one free parameter σ that quantifies the degree of structural disorder. This distribution is chosen to satisfy the following requirements:

- It is the same for all atomic species.

- It maximizes at $x_j = a$ for all j. a being the interatomic distance of the regular lattice.

- It is symmetric around the value a and therefore its domain is the interval $(0, 2a]$ in which it must be correctly normalized.

Our distribution for the distances shall be denoted by $P(l, \sigma)$, where $l = x/a$ is a dimensionless variable and σ measures the degree of disorder. According to the above requirements $P(l, \sigma \to 0) = \delta(l-1)$ and $\int_0^2 P(l, \sigma) \mathrm{d}l = 1$. $P(l, \sigma)$ is the probability density for the values of l for the spacings of the chain. Defining a dimensionless energy variable $\epsilon \equiv ka$ the functions of the canonical equation read

$$J\left(\bar{l}, l, a_\gamma\right) = \cos(l\epsilon) + \cot\left(\bar{l}\epsilon\right)\sin(l\epsilon) + \frac{2(a/a_\gamma)}{\epsilon}\sin(l\epsilon), \tag{D.28}$$

$$K(l) = \sin(l\epsilon). \tag{D.29}$$

And the relevant functions $\mathcal{T}^{-1}\left(\theta; \bar{l}, l, a_\gamma\right)$ and $\mathcal{F}\left(\theta; \bar{l}, l, a_\gamma\right)$ are built from definitions (D.4) and (D.5).

The derivation of the functional equation is naturally followed until equations (D.10). Now for taking the average in the thermodynamic limit one must also include the distribution for the distances. Let us remember that in this situation each potential is characterized by two parameters: the atomic species and the distance. Therefore the equation for the phase distributions is

$$\sum_\gamma c_\gamma \int_0^2 P(l, \sigma) \mathrm{d}l \, W_{(\gamma, l)}(\theta) =$$

$$\sum_{\gamma, \beta} c_\gamma c_\beta \int_0^2 P(l, \sigma)\mathrm{d}l \int_0^2 P\left(\bar{l}, \sigma\right) \mathrm{d}\bar{l} \left| W_{(\beta, \bar{l})}\left(\mathcal{T}^{-1}\left(\theta; \bar{l}, l, \gamma\right)\right) - W_{(\beta, \bar{l})}\left(\frac{\pi}{2}\right) + \delta\left(\bar{l}, l\right) \right|, \tag{D.30}$$

where the uncorrelated case $p_{\gamma\beta} = c_\beta$ has been considered. The situation can be slightly simplified defining the phase distribution functions in terms only of the distances, $W_l(\theta) \equiv \sum_\gamma c_\gamma W_{(\gamma, l)}(\theta)$. And considering a discretization of the continuous

distribution for the distances, one is finally led to an equation for each value of l,

$$W_l(\theta) = \sum_\gamma c_\gamma \int_0^2 P\left(\bar{l}, \sigma\right) \mathrm{d}\bar{l} \left| W_{\bar{l}} \left(\mathcal{T}^{-1}\left(\theta; \bar{l}, l, \gamma\right)\right) - W_{\bar{l}}\left(\frac{\pi}{2}\right) + \delta\left(\bar{l}, l\right) \right|, \quad \text{(D.31a)}$$

$$W_l(\theta + n\pi) = W_l(\theta) + n, \qquad \theta \in [0, \pi),\ n \in \mathbb{Z}. \tag{D.31b}$$

Finally the localization length and the DOS per atom can be obtained from

$$\lambda(\epsilon) = \frac{1}{2} \int_0^2 P\left(\bar{l}, \sigma\right) \mathrm{d}\bar{l} \int_0^\pi \mathrm{d}W_{\bar{l}}(\theta) \left[\sum_\gamma c_\gamma \int_0^2 P(l, \sigma) \mathrm{d}l \, \log \mathcal{F}\left(\theta; \bar{l}, l, a_\gamma\right) \right], \quad \text{(D.32)}$$

$$g(\epsilon) = \left| \int_0^2 P(l, \sigma) \mathrm{d}l \, \mathrm{sgn}\left[K(l)\right] \frac{\mathrm{d}W_l\left(\frac{\pi}{2}\right)}{\mathrm{d}\epsilon} \right|. \tag{D.33}$$

Pöschl-Teller and complex Scarf potentials

E.1 Solutions of the Pöschl-Teller potential

The elementary positive energy solutions of the Schrödinger equation for the potential

$$V(x) = \frac{\hbar^2 \alpha^2}{2m} \frac{V}{\cosh^2(\alpha x)}, \quad V \in \mathbb{R}, \tag{E.1}$$

read

$$u(x) = \cosh^b(\alpha x) \, {}_2F_1 \left(\frac{b}{2} + i\frac{k}{2\alpha}, \frac{b}{2} - i\frac{k}{2\alpha}, \frac{1}{2}; -\sinh^2(\alpha x) \right), \tag{E.2a}$$

$$v(x) = \sinh(\alpha x) \cosh^b(\alpha x) \, {}_2F_1 \left(\frac{b+1}{2} + i\frac{k}{2\alpha}, \frac{b+1}{2} - i\frac{k}{2\alpha}, \frac{3}{2}; -\sinh^2(\alpha x) \right). \tag{E.2b}$$

where $b = \frac{1}{2} + \sqrt{\frac{1}{4} - V}$ and $_2F_1(a_1, a_2, a_3; z)$ is the Hypergeometric function. And their asymptotic forms can be written as [2]

$$u(x) \to m e^{ik|x|} + m^* e^{-ik|x|}, \tag{E.3a}$$

$$v(x) \to \operatorname{sgn}(x) \left(n e^{ik|x|} + n^* e^{-ik|x|} \right), \tag{E.3b}$$

where

$$m = \frac{\sqrt{\pi} \, \Gamma\left(i\frac{k}{\alpha}\right) 2^{-ik/\alpha}}{\Gamma\left(\frac{b}{2} + i\frac{k}{2\alpha}\right) \Gamma\left(\frac{1-b}{2} + i\frac{k}{2\alpha}\right)}, \tag{E.4a}$$

$$n = \frac{\sqrt{\pi} \, \Gamma\left(i\frac{k}{\alpha}\right) 2^{-ik/\alpha}}{2 \, \Gamma\left(\frac{b+1}{2} + i\frac{k}{2\alpha}\right) \Gamma\left(1 - \frac{b}{2} + i\frac{k}{2\alpha}\right)}. \tag{E.4b}$$

E.2 Complex Scarf potential

E.2.1 Scattering states

The elementary positive energy solutions of the Schrödinger equation for the complex potential

$$V(x) = \frac{\hbar^2 \alpha^2}{2m} \left(\frac{V_1}{\cosh^2(\alpha x)} + i \, V_2 \frac{\sinh(\alpha x)}{\cosh^2(\alpha x)} \right), \quad V_1, V_2 \in \mathbb{R}, \tag{E.5}$$

are

$$\begin{aligned} u(x) =& e^{-i(b-1/2)\arctan[\sinh(\alpha x)]} \cosh^c(\alpha x) \\ & \times {}_2F_1 \left(c + i\frac{k}{\alpha}, c - i\frac{k}{\alpha}, 1 - b + c; \frac{1}{2} + \frac{i}{2}\sinh(\alpha x) \right), \end{aligned} \tag{E.6a}$$

$$\begin{aligned} v(x) =& e^{-i(b-1/2)\arctan[\sinh(\alpha x)]} \cosh^c(\alpha x) \left(\frac{1}{2} + \frac{i}{2}\sinh(\alpha x) \right)^{b-c} \\ & \times {}_2F_1 \left(b + i\frac{k}{\alpha}, b - i\frac{k}{\alpha}, 1 + b - c; \frac{1}{2} + \frac{i}{2}\sinh(\alpha x) \right), \end{aligned} \tag{E.6b}$$

where

$$c = \frac{1}{2} - \frac{i}{2}(g_+ - g_-), \quad b = \frac{1}{2} - \frac{i}{2}(g_+ + g_-), \tag{E.7}$$

$g_\pm = \sqrt{V_1 \pm V_2 - 1/4}$ and ${}_2F_1(a_1, a_1, a_3; z)$ is the Hypergeometric function. The asymptotic limit $x \to \pm\infty$ yields [2]

$$u(x) \to 2^c \left(m_1 e^{ik|x|} + m_2 e^{-ik|x|} \right), \tag{E.8a}$$

$$v(x) \to 2^c \left(n_1 e^{ik|x|} + n_2 e^{-ik|x|} \right), \tag{E.8b}$$

where

$$m_1 = \frac{i^{\text{sgn}(x)[1/2-b+c]} 2^{-2ik/\alpha} \Gamma\left(1 - b + c\right) \Gamma\left(2i\frac{k}{\alpha}\right) e^{\text{sgn}(x)\pi k/(2\alpha)}}{\Gamma\left(c + i\frac{k}{\alpha}\right) \Gamma\left(1 - b + i\frac{k}{\alpha}\right)}, \tag{E.9a}$$

$$m_2 = \frac{i^{\text{sgn}(x)[1/2-b+c]} 2^{2ik/\alpha} \Gamma\left(1 - b + c\right) \Gamma\left(-2i\frac{k}{\alpha}\right) e^{-\text{sgn}(x)\pi k/(2\alpha)}}{\Gamma\left(c - i\frac{k}{\alpha}\right) \Gamma\left(1 - b - i\frac{k}{\alpha}\right)}, \tag{E.9b}$$

$$n_1 = m_1 \left(b \rightleftarrows c \right), \tag{E.9c}$$

$$n_2 = m_2 \left(b \rightleftarrows c \right). \tag{E.9d}$$

E.2.2 Ranges of physical transmission

The condition for physical transmission reads $\cosh(\pi g_+) \cosh(\pi g_-) \geqslant 0$ as can be seen from equation (5.21) on page 128. V_2 can be considered positive without loss of

generality since its change in sign (which is equivalent to changing the side of incidence) does not affect the transmission. With the definitions $X = |V_1| - V_2$ and $Y = |V_1| + V_2$, the study can be easily carried out. Considering $V_1 > 0$ the inequality translates into the permitted regions

$$\forall \quad Y \begin{cases} X > 0, \\ -2n(2n+1) \leqslant X \leqslant -2n(2n-1), \quad n \in \mathbb{Z}^+, \end{cases} \tag{E.10}$$

which is clearly a sequence of allowed vertical fringes in the negative X quadrant and the whole positive X quadrant. This pattern will be same but rotated $\pi/4$ clockwise when the change of variables is undone. More specifically, in terms of the potential amplitudes the allowed intervals can be written as

$$|V_2| \in [0, V_1] \cup [2n(2n-1) + V_1, 2n(2n+1) + V_1], \quad n \in \mathbb{Z}^+. \tag{E.11}$$

In the case of $V_1 < 0$ a careful analysis leads to the following cumbersome allowed ranges:

$$X < 0 \Rightarrow 2n(2n-1) \leqslant Y \leqslant 2n(2n+1), \quad n = 1, 2, 3, \ldots, \tag{E.12}$$

$$X > 0 \Rightarrow \begin{cases} \{2n(2n-1) \leqslant X \leqslant 2n(2n+1)\} \bigcap \{2m(2m-1) \leqslant Y \leqslant 2m(2m+1)\}, \\ \{2j(2j+1) \leqslant X \leqslant 2j(2j+3) + 2\} \bigcap \{2k(2k+1) \leqslant Y \leqslant 2k(2k+3) + 2\}, \end{cases} \tag{E.13}$$

for $n, m \in \mathbb{Z}^+$ and $k, j = 0, 1, 2, \ldots$. In this case the permitted zones are a set of allowed horizontal fringes in the negative X quadrant and a chessboard like structure for positive X. Undoing the change of variables will mean a $\pi/4$ clockwise rotation followed by a reflection around the vertical axis of this pattern to recover the negative axis of V_1. Solving these inequalities in terms of the potential amplitudes gives rise to the following group of inequalities, each one assigning a certain allowed interval for $|V_2|$ when fulfilled:

for $n \in \mathbb{Z}^+$,

$$|V_1| \leqslant n(2n-1) \Rightarrow \big[2n(2n-1) - |V_1|, 2n(2n+1) - |V_1|\big], \tag{E.14a}$$

$$n(2n-1) \leqslant |V_1| \leqslant n(2n+1) \Rightarrow \big[|V_1|, 2n(2n+1) - |V_1|\big], \tag{E.14b}$$

for $m, n \in \mathbb{Z}^+ \quad (m \geqslant n)$,

$$m(2m-1) + n(2n-1) \leqslant |V_1| \leqslant m(2m-1) + n(2n+1)$$
$$\Rightarrow \big[2m(2m-1) - |V_1|, -2n(2n-1) + |V_1|\big], \tag{E.15a}$$

$$m(2m - 1) + n(2n + 1) \leqslant |V_1| \leqslant m(2m + 1) + n(2n - 1)$$
$$\Rightarrow \big[- 2n(2n + 1) + |V_1|, -2n(2n - 1) + |V_1| \big], \quad \text{(E.15b)}$$

$$m(2m + 1) + n(2n - 1) \leqslant |V_1| \leqslant m(2m + 1) + n(2n + 1)$$
$$\Rightarrow \big[- 2n(2n + 1) + |V_1|, 2m(2m + 1) - |V_1| \big], \quad \text{(E.15c)}$$

and for $j, k = 0, 1, 2, \ldots$ $(k \geqslant j)$,

$$k(2k + 1) + j(2j + 1) \leqslant |V_1| \leqslant k(2k + 1) + j(2j + 3) + 1$$
$$\Rightarrow \big[2k(2k + 1) - |V_1|, -2j(2j + 1) + |V_1| \big], \quad \text{(E.16a)}$$

$$k(2k + 1) + j(2j + 3) + 1 \leqslant |V_1| \leqslant k(2k + 3) + 1 + j(2j + 1)$$
$$\Rightarrow \big[- 2 - 2j(2j + 3) + |V_1|, -2j(2j + 1) + |V_1| \big], \quad \text{(E.16b)}$$

$$k(2k + 3) + 1 + j(2j + 1) \leqslant |V_1| \leqslant k(2k + 3) + j(2j + 3) + 2$$
$$\Rightarrow \big[- 2 - 2j(2j + 3) + |V_1|, 2 + 2k(2k + 3) - |V_1| \big]. \quad \text{(E.16c)}$$

In the particular cases $m = n$ for inequalities (E.15) and $k = j$ for (E.16) only the positive part of the allowed intervals must be considered. The total physical range for $|V_2|$ comes from the union of the different permitted intervals.

Collection of 1-D models

This appendix includes a collection of different models of 1-D potentials which can be used and combined to build one-dimensional quantum wires. The tables in the following pages gather their transmission matrices and the canonical equations applying to their compositions, so that they can be used as a quick reference handbook. One remark to keep in mind: for the calculation of the transmission matrix the coordinates of the electronic wave function at the right and at the left of the potential are chosen to satisfy that the state right before and right after the potential is simply given by the sum of the complex amplitudes of the travelling plane waves, that is if the potential ranges in the interval $[x_1, x_2]$ then one considers $\Psi^L(x) = A^L e^{ik(x-x_1)} + B^L e^{-ik(x-x_1)}$ and $\Psi^R(x) = A^R e^{ik(x-x_2)} + B^R e^{-ik(x-x_2)}$ for the states at the left and the right side of the potential respectively. In this way one obtains the more general form of the transmission matrix and removes any dependence on the relative coordinates of the potential. Let us also remember that the canonical equation can generally be written as

$$\Psi_{j+1} = \left(\overline{S}_j + S_{j-1}\frac{K_j}{K_{j-1}}\right)\Psi_j - \frac{K_j}{K_{j-1}}\Psi_{j-1}, \tag{F.1}$$

where the jth sector of the chain is the one between the sites j and $j+1$.

The matrices and functions given in the following tables are valid for positive energies in principle. The extension to negative energies is straightforward for some models but it is not trivial for the potentials of table F.2 for which several simplifications have been carried out that are not true for negative energies.
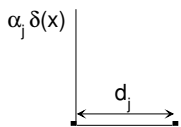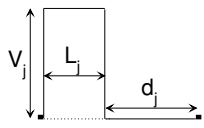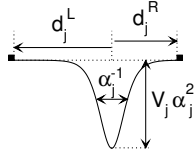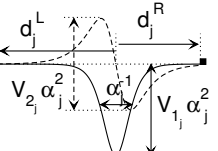
Table F.1.

POTENTIAL	TRANSMISSION MATRIX		CANONICAL EQUATION
Zero potential of length d_j	$\begin{pmatrix} \mathrm{e}^{\mathrm{i}kd_j} & 0 \\ 0 & \mathrm{e}^{-\mathrm{i}kd_j} \end{pmatrix}$		$\overline{S}_j = S_j = \sin(kd_j)$ $K_j = \cos(kd_j)$
Delta potential $\alpha_j\,\delta(x)$ d_j	$\begin{pmatrix} \left[1 - \frac{\mathrm{i}}{ka_j}\right]\mathrm{e}^{\mathrm{i}kd_j} & -\frac{\mathrm{i}}{ka_j}\mathrm{e}^{\mathrm{i}kd_j} \\ \frac{\mathrm{i}}{ka_j}\mathrm{e}^{-\mathrm{i}kd_j} & \left[1 + \frac{\mathrm{i}}{ka_j}\right]\mathrm{e}^{-\mathrm{i}kd_j} \end{pmatrix}$	$a_j = \dfrac{\hbar^2}{m\alpha_j}$	$\overline{S}_j = \cos(kd_j) + \dfrac{2}{ka_j}\sin(kd_j)$ $S_j = \cos(kd_j)$ $K_j = \sin(kd_j)$
Square barrier V_j L_j d_j	$\begin{pmatrix} \mu_j\,\mathrm{e}^{\mathrm{i}kd_j} & \beta_j\,\mathrm{e}^{\mathrm{i}kd_j} \\ \beta_j^*\,\mathrm{e}^{-\mathrm{i}kd_j} & \mu_j^*\,\mathrm{e}^{-\mathrm{i}kd_j} \end{pmatrix}$	$\mu_j = \cos(L_j\kappa_j) + \mathrm{i}\dfrac{k^2 + \kappa_j^2}{2k\kappa_j}\sin(L_j\kappa_j)$ $\beta_j = -\mathrm{i}\dfrac{k^2 - \kappa_j^2}{2k\kappa_j}\sin(L_j\kappa_j)$ $\kappa_j = \sqrt{k^2 - \dfrac{2mV_j}{\hbar^2}}$	$\overline{S}_j = \cos(L_j\kappa_j)\cos(kd_j) - \dfrac{\kappa_j}{k}\sin(L_j\kappa_j)\sin(kd_j)$ $S_j = \cos(L_j\kappa_j)\cos(kd_j) - \dfrac{k}{\kappa_j}\sin(L_j\kappa_j)\sin(kd_j)$ $K_j = \cos(L_j\kappa_j)\sin(kd_j) + \dfrac{k}{\kappa_j}\sin(L_j\kappa_j)\cos(kd_j)$
	These expressions are valid for $E > V_j$. In the case $0 < E < V_j$ the equations are formally the same with the substitution $\kappa_j = \mathrm{i}\eta_j = \mathrm{i}\sqrt{\frac{2mV_j}{\hbar^2} - k^2}$		

Table F.2.

POTENTIAL	TRANSMISSION MATRIX	CANONICAL EQUATION
Pöschl-Teller potential $$\frac{\hbar^2\alpha^2}{2m}\frac{V}{\cosh(\alpha x)^2}$$	$$\begin{pmatrix} \mathrm{e}^{\mathrm{i}\left[\varphi_j+k(d_j^R+d_j^L)\right]}\sqrt{1+w_j^2} & -\mathrm{i}w_j\mathrm{e}^{\mathrm{i}k(d_j^R-d_j^L)} \\ \mathrm{i}w_j\mathrm{e}^{-\mathrm{i}k(d_j^R-d_j^L)} & \mathrm{e}^{-\mathrm{i}\left[\varphi_j+k(d_j^R+d_j^L)\right]}\sqrt{1+w_j^2} \end{pmatrix}$$ $$w_j=\frac{\sin(\pi b_j)}{\sinh(\pi k/\alpha_j)}\quad,\quad b_j=1/2+\sqrt{1/4-V_j}$$ $$\varphi_j=\arg\left\{\frac{\mathrm{i}\,\Gamma^2(\mathrm{i}k/\alpha_j)}{\Gamma(b_j+\mathrm{i}k/\alpha_j)\Gamma(1-b_j+\mathrm{i}k/\alpha_j)}\right\}$$	$$\overline{S}_j=-w_j\sin\left[k(d_j^L-d_j^R)\right]+\sqrt{1+w_j^2}\cos\left[k(d_j^L+d_j^R)+\varphi_j\right]$$ $$S_j=w_j\sin\left[k(d_j^L-d_j^R)\right]+\sqrt{1+w_j^2}\cos\left[k(d_j^L+d_j^R)+\varphi_j\right]$$ $$K_j=w_j\cos\left[k(d_j^L-d_j^R)\right]+\sqrt{1+w_j^2}\sin\left[k(d_j^L+d_j^R)+\varphi_j\right]$$
Complex Scarf $$\frac{\hbar^2\alpha^2}{2m\cosh(\alpha x)^2}\times$$ $$[V_1+\mathrm{i}V_2\sinh(\alpha x)]$$	$$\begin{pmatrix} \mathrm{e}^{\mathrm{i}\left[\phi_j+k(d_j^R+d_j^L)\right]}\sqrt{1+s_j\overline{s}_j} & -\mathrm{i}s_j\mathrm{e}^{\mathrm{i}k(d_j^R-d_j^L)} \\ \mathrm{i}\overline{s}_j\mathrm{e}^{-\mathrm{i}k(d_j^R-d_j^L)} & \mathrm{e}^{-\mathrm{i}\left[\phi_j+k(d_j^R+d_j^L)\right]}\sqrt{1+s_j\overline{s}_j} \end{pmatrix}$$ $$\phi_j=\arg\left\{\frac{\mathrm{i}\,\Gamma^2(\mathrm{i}k/\alpha_j)\Gamma^2(1/2+\mathrm{i}k/\alpha_j)}{\Gamma\left(c_j+\mathrm{i}\frac{k}{\alpha_j}\right)\Gamma\left(b_j+\mathrm{i}\frac{k}{\alpha_j}\right)\Gamma\left(1-c_j+\mathrm{i}\frac{k}{\alpha_j}\right)\Gamma\left(1-b_j+\mathrm{i}\frac{k}{\alpha_j}\right)}\right\}$$ $$s_j=\frac{\cosh(\pi g_j^+)e^{\pi k/\alpha_j}+\cosh(\pi g_j^-)e^{-\pi k/\alpha_j}}{\sinh(2\pi k/\alpha_j)}\;,\;\overline{s}_j=s_j(g_j^+\rightleftarrows g_j^-)$$ $$c_j=\frac{1}{2}-\frac{\mathrm{i}}{2}(g_j^+-g_j^-)\;,\;b_j=\frac{1}{2}-\frac{\mathrm{i}}{2}(g_j^++g_j^-)\;,\;g_j^\pm=\sqrt{V_{1_j}\pm V_{2_j}-\frac{1}{4}}$$	$$\overline{S}_j=-\mathrm{i}\left[s_j\mathrm{e}^{\mathrm{i}k(d_j^R-d_j^L)}-\overline{s}_j\mathrm{e}^{-\mathrm{i}k(d_j^R-d_j^L)}\right]+\sqrt{1+s_j\overline{s}_j}\cos\left[k(d_j^L+d_j^R)+\phi_j\right]$$ $$S_j=\mathrm{i}\left[s_j\mathrm{e}^{\mathrm{i}k(d_j^R-d_j^L)}-\overline{s}_j\mathrm{e}^{-\mathrm{i}k(d_j^R-d_j^L)}\right]+\sqrt{1+s_j\overline{s}_j}\cos\left[k(d_j^L+d_j^R)+\phi_j\right]$$ $$K_j=s_j\mathrm{e}^{\mathrm{i}k(d_j^R-d_j^L)}+\overline{s}_j\mathrm{e}^{-\mathrm{i}k(d_j^R-d_j^L)}+\sqrt{1+s_j\overline{s}_j}\sin\left[k(d_j^L+d_j^R)+\phi_j\right]$$

Publications

Some of the results presented in this work are collected in the following publications:

1. *Infinite chain of N different deltas: a simple model for a quantum wire*
   J. M. Cerveró and A. Rodríguez, Eur. Phys. J. B **30**, 239-251 (2002)

2. *Simple model for a quantum wire II. Statistically correlated disoder*
   J. M. Cerveró and A. Rodríguez, Eur. Phys. J. B **32**, 537-543 (2003)

3. *The band spectrum of periodic potentials with $\mathcal{PT}$-symmetry*
   J. M. Cerveró and A. Rodríguez, J. Phys. A: Math. Gen. **37**, 10167-10177 (2004)

4. *Absorption in atomic wires*
   J. M. Cerveró and A. Rodríguez, Phys. Rev. A **70**, 052705 (2004)

5. *Simple model for a quantum wire III. Transmission in finite samples with correlated disorder*
   J. M. Cerveró and A. Rodríguez, Eur. Phys. J. B **43**, 543-548 (2005)

Publications of the author not directly related to this work:

1. *Squeezing and quantum canonical transformations*
   J. M. Cerveró and A. Rodríguez, Int. J. Theor. Phys. **41**, 503-510 (2002)

2. *Collective versus local measurements in a qubit mixed-state stimation*
   E. Bagán. R. Muñoz-Tapia, M. Baig and A. Rodríguez, Phys. Rev. A **69**, 010304(R) (2004)

Bibliography

[1] E. Abrahams, P. W. Anderson, D. C. Liciardello, and T. V. Ramakrishnan, *Scaling theory of localization: absence of quantum diffusion in two dimensions*, Phys. Rev. Lett. **42** (1979), 673–676. (Cited in sections 1.1.2, 1.1.4, and 3.6.2)

[2] M. Abramowitz and I. A. Stegun (eds.), *Handbook of mathematical functions*, ninth ed., Dover Publications, inc., New York, 1970. (Cited in sections E.1 and E.2.1)

[3] R. L. Agacy, *The vibrational spectrum of a disordered linear system*, Proc. Phys. Soc. **83** (1964), 591–596. (Cited in section 2.6)

[4] R. L. Agacy and R. E. Borland, *The electronic structure of a one dimensional random alloy*, Proc. Phys. Soc. **84** (1964), 1017–1026. (Cited in sections 2.6, 3.4.1, and 3.4.2)

[5] N. Agraït, C. Untiedt, G. Rubio-Bollinger, and S. Vieira, *Onset of energy dissipation in ballistic atomic wires*, Phys. Rev. Lett. **88** (2002), 216803. (Cited in section 5.2)

[6] Z. Ahmed, *Energy band structure due to a complex, periodic, $\mathcal{PT}$-invariant potential*, Phys. Lett. A **286** (2001), 231–235. (Cited in section 5.1.2)

[7] Z. Ahmed, *Schrödinger transmission through one-dimensional complex potentials*, Phys. Rev. A **64** (2001), 042716. (Cited in sections 2.2 and 5.2.1)

[8] Z. Ahmed, *Handedness of complex $\mathcal{PT}$-symmetric potential barriers*, Phys. Lett. A **324** (2004), 152–158. (Cited in section 5.2.3)

[9] P. W. Anderson, *Absence of diffusion in certain random lattices*, Phys. Rev. **109** (1958), 1492–1505. (Cited in section 1.1.2)

[10] P. W. Anderson, *New method for a scaling theory of localization. II. Multichannel theory of a "wire" and possible extension to higher dimensionality*, Phys. Rev. B **23** (1981), 4828–4836. (Cited in section 1.1.4)

[11] P. W. Anderson, D. J. Thouless, E. Abrahams, and D. S. Fisher, *New method for a scaling theory of localization*, Phys. Rev. B **22** (1980), 3519–3526. (Cited in sections 1.1.2, 1.1.4, and 3.6.2)

[12] L. Arnold, *Random dynamical systems*, Springer Verlag, 1998. (Cited in section 2.4.1)

[13] M. Y. Azbel, *Eigenstates and properties of random systems in one dimension at zero temperature*, Phys. Rev. B **28** (1983), 4106–4125. (Cited in section 3.4.2)

[14] M. Y. Azbel, *Impurities in semimetals*, Solid State Commun. **46** (1983), 113–115. (Cited in section 3.4.2)

[15] M. Y. Azbel and P. Soven, *Analytical and numerical study of the Anderson localization length and residual resistivity*, Phys. Rev. Lett. **49** (1982), 751–754. (Cited in section 3.4.2)

[16] A. L. Barabási and H. E. Stanley, *Fractal concepts in surface growth*, Cambridge University Press, 1995. (Cited in section 3.4.1)

[17] J. E. Beam, *Multiple reflection in potential-barrier scattering*, Am. J. Phys. **38** (1970), 1395–1401. (Cited in section 2.2)

[18] V. Bellani, E. Diez, R. Hey, L. Tony, L. Tarricone, G. B. Parravicini, F. Domínguez-Adame, and R. Gómez-Alcalá, *Experimental evidence of delocalized states in random dimer superlattices*, Phys. Rev. Lett. **82** (1999), 2159–2162. (Cited in sections 1.1.2, 3.6, and 3.6.2)

[19] J. Bellissard, A. Formoso, R. Lima, and D. Testard, *Quasiperiodic interaction with a metal-insulator transition*, Phys. Rev. B **26** (1982), 3024–3030. (Cited in section 1.1.2)

[20] C. Bender and S. Boettcher, *Quasi-exactly solvable quartic potential*, J. Phys. A: Math. Gen. **31** (1998), L273–L277. (Cited in section 5.1)

[21] C. M. Bender, M. V. Berry, and A. Mandilara, *Generalized $\mathcal{PT}$-symmetry and real spectra*, J. Phys. A: Math. Gen. **35** (2002), L467–L471. (Cited in section 5.1)

[22] C. M. Bender and S. Boettcher, *Real spectra in non-Hermitian Hamiltonians having $\mathcal{PT}$-symmetry*, Phys. Rev. Lett. **80** (1998), 5243–5246. (Cited in section 5.1)

[23] C. M. Bender, S. Boettcher, and P. N. Meisinger, *$\mathcal{PT}$-symmetric quantum mechanics*, J. Math. Phys. **40** (1999), 2201–2229. (Cited in section 5.1)

[24] C. M. Bender, G. V. Dunne, and P. N. Meisinger, *Complex periodic potentials with real band spectra*, Phys. Lett. A **252** (1999), 272–276. (Cited in sections 5.1 and 5.1.1)

[25] R. E. Borland, *Existence of energy gaps in one dimensional liquids*, Proc. Phys. Soc. **78** (1961), 926–931. (Cited in section 3.5)

[26] R. E. Borland, *One-dimensional chains with random spacing between atoms*, Proc. Phys. Soc. **77** (1961), 705–711. (Cited in section 3.5)

[27] R. E. Borland, *The nature of the electronic states in disordered one-dimensional systems*, Proc. Roy. Soc. A **274** (1963), 529–545. (Cited in section 1.1.2)

[28] R. E. Borland and N. F. Bird, *A calculation of the density of electron states and degree of localization in a one-dimensional liquid model*, Proc. Phys. Soc. **83** (1964), 23–29. (Cited in sections 2.6 and 3.5)

[29] A. Bovier, *Perturbation theory for the random dimer model*, J. Phys. A: Math. Gen. **25** (1992), 1021–1029. (Cited in sections 1.1.2, 3.4.2, and 4.3.2)

[30] M. Büttiker, *Small normal-metal loop coupled to an electron reservoir*, Phys. Rev. B **32** (1985), 1846–1849. (Cited in section 5.2)

[31] M. Büttiker, *Four-terminal phase-coherent conductance*, Phys. Rev. Lett. **57** (1986), 1761–1764. (Cited in section 1.1.3)

[32] M. Büttiker, *Role of quantum coherence in series resistors*, Phys. Rev. B **33** (1986), 3020–3026. (Cited in section 5.2)

[33] M. Büttiker, *Coherent and sequential tunneling in series barriers*, IBM J. Red. Dev. **32** (1988), 63–75. (Cited in section 1.1.5)

[34] M. Büttiker, *Symmetry of electrical conduction*, IBM J. Res. Dev. **32** (1988), 317–334. (Cited in section 1.1.3)

[35] J. Canisius and J. L. van Hemmen, *Localisation of phonons*, J. Phys. C **18** (1985), 4873–4884. (Cited in section 2.4.2)

[36] J. M. Cerveró, *Supersymmetric quantum mechanics: another nontrivial quantum superpotential*, Phys. Lett. A **153** (1991), 1–4. (Cited in section 5.2.3)

[37] A. Cohen, Y. Roth, and B. Shapiro, *Universal distributions and scaling in disordered systems*, Phys. Rev. B **38** (1988), 12125–12132. (Cited in section 1.1.4)

[38] A. Crisanti, G. Paladin, and A. Vulpiani, *Products of random matrices in statistical physics*, Springer-Verlag, 1993. (Cited in section 2.4.1)

[39] G. Czycholl and B. Kramer, *Nonvanishing zero temperature static conductivity in one dimensional disordered systems*, Solid State Commun. **32** (1979), 945–951. (Cited in section 5.2)

[40] J. W. Dabrowska, A. Khare, and U. P. Sukhatme, *Explicit wavefunctions for shape-invariant potentials by operator techniques*, J. Phys. A: Math. Gen. **21** (1988), L195–L200. (Cited in sections 4.1 and 5.2.3)

[41] J. L. D'Amato and H. M. Pastawski, *Conductance of a disordered linear chain including inelastic scattering events*, Phys. Rev. B **41** (1990), 7411–7420. (Cited in sections 1.1.5, 5.2, and 5.2.3)

[42] J. A. Damborenea, I. L. Egusquiza, G. C. Hegerfeldt, and J. G. Muga, *Measurement-based approach to quantum arrival times*, Phys. Rev. A **66** (2002), 052104. (Cited in section 5.2)

[43] J. A. Damborenea, I. L. Egusquiza, G. C. Hegerfeldt, and J. G. Muga, *On atomic time-of-arrival measurements with a laser of finite beam width*, J. Phys. B: At. Mol. Opt. Phys. **36** (2003), 2657–2669. (Cited in section 5.2)

[44] R. de L. Kronig and W. G. Penney, *Quantum mechanics of electrons in crystal lattices*, Proc. Roy. Soc. A **130** (1931), 499–513. (Cited in section 3.1)

[45] F. A. B. F. de Moura, M. D. Coutinho-Filho, E. R. Raposo, and M. L. Lyra, *Delocalization in harmonic chains with long-range correlated random masses*, Phys. Rev. B **68** (2003), 012202. (Cited in section 1.1.2)

[46] F. A. B. F. de Moura and M. L. Lyra, *Delocalization in the 1D Anderson model with long-range correlated disorder*, Phys. Rev. Lett. **81** (1998), 3735–3738, See also comment by J. K. Kantelhardt *et al.*, Phys. Rev. Lett. **84**, 198 (2000) and reply Phys. Rev. Lett. **84**, 199 (2000). (Cited in section 1.1.2)

[47] F. A. B. F. de Moura and M. L. Lyra, *Correlation-induced metal-insulator transition in the one-dimensional Anderson model*, Physica A **266** (1999), 465–470. (Cited in section 1.1.2)

[48] F. A. B. F. de Moura, M. L. Lyra, F. Domínguez-Adame, and V. A. Malyshev, *Bloch oscillations in an aperiodic one-dimensional potential*, Phys. Rev. B **71** (2005), 104303. (Cited in section 1.1.2)

[49] F. A. B. F. de Moura, A. V. Malyshev, M. L. Lyra, V. A. Malyshev, and F. Domínguez-Adame, *Localization properties of a one-dimensional tight-binding model with nonrandom long-range intersite interactions*, Phys. Rev. B **71** (2005), 174203. (Cited in section 1.1.2)

[50] F. A. B. F. de Moura, M. N. B. Santos, U. L. Fulco, M. L. Lyra, E. Lazo, and M. E. Onell, *Delocalization and wave-packet dynamics in one-dimensional diluted Anderson model*, Eur. Phys. J. B **36** (2003), 81–86. (Cited in section 1.1.2)

[51] P. Dean, *Vibrations of glass-like disordered chains*, Proc. Phys. Soc. **84** (1964), 727–744. (Cited in section 2.6)

[52] P. Dean, *The vibrational properties of disordered systems: numerical studies*, Rev. Mod. Phys. **44** (1972), 127–168. (Cited in section 2.5)

[53] R. N. Deb, A. Khare, and B. D. Roy, *Complex optical potentials and pseudo-Hermitian Hamiltonians*, Phys. Lett. A **307** (2003), 215–221. (Cited in section 5.1)

[54] F. Delgado, J. G. Muga, and A. Ruschhaupt, *Ultrafast propagation of Schrödinger waves in absorbing media*, Phys. Rev. A **69** (2004), 022106. (Cited in section 5.2)

[55] F. Delyon, H. Kunz, and B. Souillard, *One-dimensional wave equations in disordered media*, J. Phys. A: Math. Gen. **16** (1983), 25–42. (Cited in section 1.1.2)

[56] C. Dembowski, H. D. Gräf, H. L. Harney, A. Heine, W. D. Heiss, H. Rehfeld, and A. Richter, *Experimental observation of the topological structure of exceptional points*, Phys. Rev. Lett. **86** (2001), 787–790. (Cited in section 5.2)

[57] L. I. Deych, M. V. Erementchouk, and A. A. Lisyansky, *Scaling in one-dimensional Anderson localization problem in the region of fluctuation states*, Phys. Rev. Lett. **90** (2003), 126601. (Cited in sections 1.1.4 and 3.6.2)

[58] L. I. Deych, M. V. Erementchouk, and A. A. Lisyansky, *Scaling properties of the one-dimensional Anderson model with correlated diagonal disorder*, Phys. Rev. B **67** (2003), 024205. (Cited in sections 1.1.4 and 3.6.2)

[59] L. I. Deych, A. A. Lisyansky, and B. L. Altshuler, *Single parameter scaling in one-dimensional localization revisited*, Phys. Rev. Lett. **84** (2000), 2678–2681. (Cited in sections 1.1.4 and 3.6.2)

[60] L. I. Deych, A. A. Lisyansky, and B. L. Altshuler, *Single-parameter scaling in one-dimensional Anderson localization: exact analytical solution*, Phys. Rev. B **64** (2001), 224202. (Cited in section 1.1.4)

[61] L. I. Deych, A. Yamilov, and A. A. Lisyansky, *Scaling in one-dimensional localized absorbing systems*, Phys. Rev. B **64** (2001), 024201. (Cited in section 5.2)

[62] L. I. Deych, D. Zaslavsky, and A. A. Lisyansky, *Statistics of the Lyapunov exponents in 1D random periodic-on-average systems*, Phys. Rev. Lett. **81** (1998), 5390–5393. (Cited in section 1.1.4)

[63] E. Diez, F. Domínguez-Adame, and A. Sánchez, *Nonlinear resonant tunnelling through double-barrier structures*, Phys. Lett. A **198** (1995), 403–406. (Cited in section 1.1.5)

[64] E. Diez, A. Sánchez, and F. Domínguez-Adame, *Absence of localization and large dc conductance in random superlattices with correlated disorder*, Phys. Rev. B **50** (1994), 14359–14367. (Cited in sections 1.1.2 and 3.6)

[65] E. Diez, A. Sánchez, and F. Domínguez-Adame, *Intentionally disordered superlattices with high-dc conductance*, IEEE Journal of Quantum electronics **31** (1995), 1919–1926. (Cited in section 1.1.2)

[66] T. Dittrich and R. Graham, *Continuous quantum measurement and chaos*, Phys. Rev. A **42** (1990), 4647–4660. (Cited in section 5.2.3)

[67] F. Domínguez-Adame, E. Diez, and J. Devís, *Time-dependent phenomena in unintentionally disordered superlattices*, Recent Res. Devel. Quantum Electronics **1** (1999), 137–164. (Cited in section 1.1.5)

[68] F. Domínguez-Adame, I. Gómez, A. Avakyan, D. Sedrakyan, and A. Sedrakyan, *Electron states in a class of one-dimensional random binary alloys*, phys. stat. sol. (b) **221** (2000), 633–639. (Cited in sections 1.1.2, 3.4.2, 4.3.2, and 6)

[69] F. Domínguez-Adame, V. Malyshev, F. A. B. F. de Moura, and M. L. Lyra, *Bloch-like oscillations in a one-dimensional lattice with long-range correlated disorder*, Phys. Rev. Lett. **91** (2003), 197402. (Cited in section 1.1.2)

[70] F. Domínguez-Adame and V. A. Malyshev, *A simple approach to Anderson localization in one-dimensional disordered superlattices*, Am. J. Phys. **72** (2004), 226–230. (Cited in section 1.1.2)

[71] F. Domínguez-Adame, A. Sánchez, and E. Diez, *Quasi-ballistic-electron transport in random superlattices*, Phys. Rev. B **50** (1994), 17736–17739. (Cited in section 1.1.2)

[72] V. Dossetti-Romero, F. M. Izrailev, and A. A. Krokhin, *Transport properties of 1D tight-binding disordered models: the Hamiltonian map approach*, Physica E **25** (2004), 13–22. (Cited in section 3.6.2)

[73] D. H. Dunlap, H-L. Wu, and P. W. Phillips, *Absence of localization in a random-dimer model*, Phys. Rev. Lett. **65** (1990), 88–91. (Cited in sections 1.1.2 and 3.4.2)

[74] F. J. Dyson, *The dynamics of a disordered linear chain*, Phys. Rev. **92** (1953), 1331–1338. (Cited in section 2.6)

[75] E. N. Economou and C. M. Soukoulis, *Static conductance and scaling theory of localization in one dimension*, Phys. Rev. Lett. **46** (1981), 618–621. (Cited in section 1.1.3)

[76] H. L. Engquist and P. W. Anderson, *Definition and measurement of the electrical and thermal resistances*, Phys. Rev. B **24** (1981), 1151–1154. (Cited in section 1.1.3)

[77] S. N. Evangelou and E. N. Economou, *Reflecionless modes in chains with large-size homogeneous impurities*, J. Phys. A: Math. Gen. **26** (1993), 2803–2813. (Cited in section 1.1.2)

[78] P. Facchi, S. Pascazio, and A. Scardicchio, *Measurement-induced quantum diffusion*, Phys. Rev. Lett. **83** (1999), 61–64. (Cited in section 5.2.3)

[79] D. S. Fisher and P. A. Lee, *Relation between conductivity and transmission matrix*, Phys. Rev. B **23** (1981), 6851–6854. (Cited in section 1.1.3)

[80] J. Flores, P. A. Mello, and G. Monsiváis, *Statistical distribution of the resistance in a one-dimensional disordered electrified chain*, Phys. Rev. B **35** (1987), 2144–2150. (Cited in section 1.1.4)

[81] J. C. Flores, *Transport in models with correlated diagonal and off-diagonal disorder*, J. Phys.: Condens. Matter **1** (1989), 8471–8479. (Cited in section 1.1.2)

[82] J. C. Flores, *Iterative quantum local measurements and Anderson localization inhibition*, Phys. Rev. B **69** (2004), 012201. (Cited in sections 1.1.5 and 5.2.3)

[83] J. C. Flores and M. Hilke, *Absence of localization in disordered systems with local correlation*, J. Phys. A: Math. Gen. **26** (1993), L1255–L1259. (Cited in section 1.1.2)

[84] S. Flügge, *Practical quantum mechanics*, Springer-Verlag, Berlin, 1970. (Cited in section 4.1)

[85] V. Freilikher, M. Pustilnik, and I. Yurkevich, *Effect of absorption on the wave transport in the strong localization regime*, Phys. Rev. Lett. **73** (1994), 810–813. (Cited in section 5.2)

[86] H. L. Frisch and S. P. Lloyd, *Electron levels in a one dimensional random lattice*, Phys. Rev. **120** (1960), 1175–1189. (Cited in section 3.5)

[87] S. Gangopadhyay and A. K. Sen, *The resonance structure in a random dimer model*, J. Phys.: Condens. Matter **4** (1992), 9939–9954. (Cited in section 1.1.2)

[88] I. Gómez, F. Domínguez-Adame, and E.Diez, *Nature of the extended states in random dimer-barrier superlattices*, Physica B **324** (2002), 235–239. (Cited in section 4.3.2)

[89] D. J. Griffiths and C. A. Steinke, *Waves in locally periodic media*, Am. J. Phys. **69** (2000), 137–154. (Cited in section 3.2)

[90] M. Griniasty and S. Fishman, *Localization by pseudorandom potentials in one dimension*, Phys. Rev. Lett. **60** (1988), 1334–1337. (Cited in section 1.1.2)

[91] J. E. Gubernatis and P. L. Taylor, *Special aspects of the electronic structure of a onedimensional random alloy*, J. Phys. C **4** (1971), L94–L96. (Cited in sections 2.6 and 3.4.1)

[92] J. E. Gubernatis and P. L. Taylor, *Some details of the density of states of a disordered alloy*, J. Phys. C **6** (1973), 1889–1895. (Cited in section 3.4.1)

[93] S. A. Gurvitz, *Delocalization in the Anderson model due to a local measurement*, Phys. Rev. Lett. **85** (2000), 812–815. (Cited in sections 1.1.5 and 5.2.3)

[94] T. C. Halsey, M. H. Jensen, L. P. Kadanoff, I. Procaccia, and B. I. Shraiman, *Fractal measures and their singularities: the characterization of strange sets*, Phys. Rev. A **33** (1986), 1141–1151. (Cited in section 4.3.2)

[95] P. Harrison, *Quantum wells, wires and dots*, John Wiley & Sons, 2000. (Cited in section 1)

[96] N. Hatano and D. R. Nelson, *Localization transitions in non-Hermitian quantum mechanics*, Phys. Rev. Lett. **77** (1996), 570–573. (Cited in section 5.2)

[97] N. Hatano and D. R. Nelson, *Vortex pinning and non-Hermitian quantum mechanics*, Phys. Rev. B **56** (1997), 8651–8673. (Cited in section 5.2)

[98] H. Hegger, B. Huckestein, et al., *Fractal conductance fluctuations in gold nanowires*, Phys. Rev. Lett. **77** (1996), 3885–3888. (Cited in section 1.1.3)

[99] T. Heinzel, R. Jäggi, E. Ribeiro, M. v. Waldkirch, K. Ensslin, S. E. Ulloa, G. Medeiros Ribeiro, and P. M. Petroff, *Transport signatures of correlated disorder in a two-dimensional electron gas*, Europhys. Lett. **61** (2003), 674–680. (Cited in section 1.1.2)

[100] W. D. Heiss, *Repulsion of resonance states and exceptional points*, Phys. Rev. E **61** (2000), 929–932. (Cited in section 5.2)

[101] R. Hey, F. Gagel, M. Schreiber, and K. Maschke, *Coherent and dissipative dc transport in quasi-one-dimensional systems of coupled polyaniline chains*, Phys. Rev. B **55** (1997), 4231–4237. (Cited in sections 5.2 and 5.2.3)

[102] R. Hey, K. Maschke, and M. Schreiber, *dc transport in dissipative disordered one-dimensional systems*, Phys. Rev. B **52** (1995), 8184–8190. (Cited in sections 1.1.5, 5.2, and 5.2.3)

[103] M. Hilke, *Local correlations in one- and two-dimensional disordered systems*, J. Phys. A: Math. Gen. **27** (1994), 4773–4782. (Cited in section 1.1.2)

[104] M. Hilke, *Localization properties of the periodic random Anderson model*, J. Phys. A: Math. Gen. **30** (1997), L367–L371. (Cited in sections 1.1.2 and 6)

[105] M. Hilke, *Noninteracting electrons and the metal-insulator transition in two dimensions with correlated impurities*, Phys. Rev. Lett. **91** (2003), 226403. (Cited in section 1.1.2)

[106] M. Hilke and J. C. Flores, *Delocalization in continuous disordered systems*, Phys. Rev. B **55** (1997), 10625–10630. (Cited in section 4.3.2)

[107] X. Huang, X. Wu, and C. Gong, *Periodic wave functions and number of extended states in random dimer systems*, Phys. Rev. B **55** (1997), 11018–11021, See comment by M. Hilke, J. C. Flores and F. Domínguez-Adame, Phys. Rev. B **58** (1998), 8837-8838. (Cited in section 1.1.2)

[108] X. Q. Huang, R. W. Peng, F. Qiu, S. S. Jiang, and A. Hu, *Delocalization in disordered chains with random symmetrical impurities*, Eur. Phys. J. B **23** (2001), 275–281. (Cited in sections 1.1.2 and 6)

[109] K. Ishii, *Localization of eigenstates and transport phenomena in the one-dimensional disordered system*, Prog. Theor. Phys. Suppl. **53** (1974), 77–138, This is the correct reference although in the original article the year reads 1973. (Cited in sections 1.1.2 and 3.4.2)

[110] F. M. Izrailev, T. Kottos, and G. P. Tsironis, *Hamiltonian map approach to resonant states in paired correlated binary alloys*, Phys. Rev. B **52** (1995), 3274–3279. (Cited in sections 1.1.2 and 2.1)

[111] F. M. Izrailev, T. Kottos, and G. P. Tsironis, *Scaling properties of the localization length in one-dimensional paired correlated binary alloys of finite size*, J. Phys.: Condens. Matter **8** (1996), 2823–2834. (Cited in section 1.1.2)

[112] F. M. Izrailev and A. A. Krokhin, *Localization and the mobility edge in one-dimensional potentials with correlated disorder*, Phys. Rev. Lett. **82** (1999), 4062–4065. (Cited in sections 1.1.2 and 3.6)

[113] F. M. Izrailev, A. A. Krokhin, and S. E. Ulloa, *Mobility edge in aperiodic Kronig-Penney potentials with correlated disorder: perturbative approach*, Phys. Rev. B **63** (2001), 041102. (Cited in sections 3.5 and 3.6)

[114] F. M. Izrailev, S. Ruffo, and L. Tessieri, *Classical representation of the one-dimensional Anderson model*, J. Phys. A: Math. Gen. **31** (1998), 5263–5270. (Cited in sections 1.1.2 and 2.1)

[115] H. James and A. Ginzbarg, *Band structure in disordered alloys and impurity semiconductors*, J. Phys. Chem. **57** (1953), 840–848. (Cited in section C)

[116] M. Janssen, *Fluctuations and localizations in mesoscopic electron systems*, World Scientific, 2001. (Cited in section 1.1.5)

[117] R. Johnson and H. Kunz, *The conductance of a disordered wire*, J. Phys. C **16** (1983), 3895–3912. (Cited in sections 1.1.4 and 2.4.1)

[118] A. Khare and U. P. Sukhatme, *Scattering amplitudes for supersymmetric shape-invariant potentials by operator methods*, J. Phys. A: Math. Gen. **21** (1988), L501–L508. (Cited in sections 4.1 and 5.2.3)

[119] A. N. Khonder and M. A. Alam, *Büttiker-Landauer conductance formulas in the presence of inelastic scattering*, Phys. Rev. B **44** (1991), 5444–5452. (Cited in section 5.2)

[120] P. D. Kirkman and J. B. Pendry, *The statistics of one-dimensional resistances*, J. Phys. C **17** (1984), 4327–4344. (Cited in sections 1.1.4 and 2.4.1)

[121] T. Kottos, G. P. Tsironis, and F. M. Izrailev, *Transport properties of one-dimensional Kronig-Penney models with correlated disorder*, J. Phys.: Condens. Matter **9** (1997), 1777–1791. (Cited in section 1.1.2)

[122] B. Kramer and A. MacKinnon, *Localization: theory and experiment*, Rep. Prog. Phys. **56** (1993), 1469–1564. (Cited in sections 2.4 and 2.4.1)

[123] S. V. Kravchenko, G. V. Kravchenko, and J. E. Furneaux, *Possible metal-insulator transition at B=0 in two dimensions*, Phys. Rev. B **50** (1994), 8039–8042. (Cited in section 1.1.2)

[124] A. Krokhin, F. Izrailev, U. Kuhl, H. J. Stöckmann, and S. E. Ulloa, *Random 1D structures as filters for electrical and optical signals*, Physica E **13** (2002), 695–698. (Cited in sections 1.1.2 and 3.6)

[125] U. Kuhl, F. M. Izrailev, A. A. Krokhin, and H. J. Stöckmann, *Experimental observation of the mobility edge in a waveguide with correlated disorder*, Appl. Phys. Lett. **77** (2000), 633–635. (Cited in sections 1.1.2 and 3.6)

[126] R. Landauer, *Spatial variation of currents and fields due to localized scatterers in metallic conduction*, IBM J. Res. Dev. **1** (1957), 223–231. (Cited in section 1.1.3)

[127] R. Landauer, *Electrical resistance of disordered one-dimensional lattices*, Philos. Mag. **21** (1970), 863–867. (Cited in section 1.1.3)

[128] R. Landauer, *Spatial variation of currents and fields due to localized scatterers in metallic conduction*, IBM J. Res. Dev. **32** (1988), 306–316. (Cited in section 1.1.3)

[129] D. C. Langreth and E. Abrahams, *Derivation of the Landauer conductance formula*, Phys. Rev. B **24** (1981), 2978–2984. (Cited in section 1.1.3)

[130] E. Lazo and M. E. Onell, *Existence of delocalized states in two interpenetrated 1-D diluted Anderson chains*, Phys. Lett. A **283** (2001), 376–381. (Cited in section 1.1.2)

[131] E. Lazo and M. E. Onell, *Extended states in 1-D Anderson chain diluted by periodic disorder*, Physica B **299** (2001), 173–179. (Cited in section 1.1.2)

[132] P. A. Lee and T. V. Ramakrishnan, *Disordered electronic system*, Rev. Mod. Phys. **57** (1985), 287–337. (Cited in section 1.1.4)

[133] P. A. Lee and A. D. Stone, *Universal conductance fluctuations in metals*, Phys. Rev. Lett. **55** (1985), 1622–1625. (Cited in section 1.1.3)

[134] G. Lévai and M. Znojil, *The interplay of supersymmetry and $\mathcal{PT}$-symmetry in quantum mechanics: a case study for the scarf II potential*, J. Phys. A: Math. Gen. **35** (2002), 8793–8804. (Cited in section 5.2.3)

[135] Elliot H. Lieb and Daniel C. Mattis (eds.), *Mathematical physics in one dimension*, Academic Press, 1966. (Cited in section 1.1.2)

[136] J. M. Luttinger, *Wave propagation in one dimensional structures*, Philips Res. Rep. **6** (1951), 303–310. (Cited in section 3.4)

[137] E. Maciá and F. Domínguez-Adame, *Electrons, phonons and excitons in low dimensional aperiodic systems*, Editorial Complutense, 2000. (Cited in sections 1.1.1, 2.1, 2.5, and 4.3.2)

[138] A. V. Malyshev, V. A. Malyshev, and F. Domínguez-Adame, *Monitoring the localization-delocalization transition within one-dimensional model with nonrandom long-range interaction*, Phys. Rev. B **70** (2004), 172202. (Cited in section 1.1.2)

[139] K. Maschke and M. Schreiber, *Unified description of coherent and dissipative electron transport*, Phys. Rev. B **44** (1991), 3835–3841. (Cited in section 5.2)

[140] K. Maschke and M. Schreiber, *Electron transport along a spatially disordered chain in the presence of dissipation*, Phys. Rev. B **49** (1994), 2295–2305. (Cited in sections 1.1.5, 5.2, and 5.2.3)

[141] P. A. Mello, *Central-limit theorem on groups*, J. Math. Phys. **27** (1986), 2876–2891. (Cited in section 1.1.4)

[142] P. Mohanty, *Of decoherent electrons and disordered conductors*, Lectures Notes for NATO ASI (2001), Published in *Complexity from microscopic to macroscopic scales: coherence and large deviations*, edited by A.T. Skjeltorp and T. Vicsek (Kluwer, Dordrecht, 2001). (Cited in section 1.1.5)

[143] M. Moško, P. Vagner, M. Bajdich, and T. Schäpers, *Coherent "metallic" resistance and medium localization in a disordered one-dimensional insulator*, Phys. Rev. Lett. **91** (2003), 136803. (Cited in section 3.5)

[144] A. Mostadazadeh and A. Batal, *Physical aspects of pseudo-Hermitian and $\mathcal{PT}$-symmetric quantum mechanics*, J. Phys. A: Math. Gen. **37** (2004), 11645–11679. (Cited in section 5.1)

[145] A. Mostafazadeh, *A critique of $\mathcal{PT}$-symmetric quantum mechanics*, quant-ph/0310164. (Cited in section 5.1)

[146] A. Mostafazadeh, *Exact $\mathcal{PT}$-symmetry is equivalent to Hermiticity*, J. Phys. A: Math. Gen. **36** (2003), 7081–7091. (Cited in section 5.1)

[147] N. F. Mott, *Electrons in disordered structures*, Adv. Phys. **50** (2001), 865–945, reprint of the article published in Adv. Phys. **16**, 49-144 (1967). (Cited in section 1.1.2)

[148] N. F. Mott and W. D. Twose, *The theory of impurity conduction*, Adv. Phys. **10** (1961), 107–163. (Cited in section 1.1.2)

[149] J. G. Muga, I. L. Egusquiza, and R. Sala (eds.), *Time in Quantum Mechanics*, Springer, Berlin, 2002. (Cited in section 5.2)

[150] J. G. Muga, J. P. Palao, B. Navarro, and I. L. Egusquiza, *Complex absorbing potentials*, Phys. Rep. **395** (2004), 357–426. (Cited in sections 5.1, 5.2, and A.1.2)

[151] B. Navarro, I. L. Egusquiza, J. G. Muga, and G. C. Hegerfeldt, *Optimal atomic detection of ultracold atoms by control of detuning and spatial dependence of laser intensity*, J. Phys. B: At. Mol. Opt. Phys. **36** (2003), 3899–3907. (Cited in section 5.2)

[152] B. Navarro, I. L. Egusquiza, J. G. Muga, and G. C. Hegerfeldt, *Suppression of Rabi oscillations for moving atoms*, Phys. Rev. A **67** (2003), 063819. (Cited in section 5.2)

[153] J. P. Palao, J. G. Muga, and R. Sala, *Composite absorbing potentials*, Phys. Rev. Lett. **80** (1998), 5469–5472. (Cited in section 5.2)

[154] P. Phillips and H. L. Wu, *Localization and its absence: a new metallic state for conducting polymers*, Science **252** (1991), 1805–1812. (Cited in section 1.1.2)

[155] J. L. Pichard and G. Sarma, *Finite size scaling approach to Anderson localisation*, J. Phys. C **14** (1981), L127–L132. (Cited in section 1.1.2)

[156] D. Porath, A. Bezryadin, S. de Vries, and C. Dekker, *Direct measurement of electrical transport through DNA molecules*, Nature **403** (2000), 635–638. (Cited in section 1)

[157] A. Rodríguez, V. A. Malyshev, G. Sierra, M. A. Martín-Delgado, J. Rodríguez-Laguna, and F. Domínguez-Adame, *Anderson transition in low-dimensional disordered systems driven by long-range nonrandom hopping*, Phys. Rev. Lett. **90** (2003), 027404. (Cited in section 1.1.2)

[158] A. Ruschhaupt, J. A. Damborenea, B. Navarro, J. G. Muga, and G. C. Hegerfeldt, *Exact and approximate complex potentials for modelling time observables*, Europhys. Lett. **67** (2004), 1–7. (Cited in section 5.2)

[159] S. Russ, J. W. Kantelhardt, A. Bunde, and S. Havlin, *Localization in self-affine landscapes*, Phys. Rev. B **64** (2001), 134209. (Cited in section 1.1.2)

[160] A. Sánchez, F. Domínguez-Adame, G. Berman, and F. Izrailev, *Explanation of delocalization in the continuous random-dimer model*, Phys. Rev. B **51** (1995), 6769–6772. (Cited in sections 1.1.2 and 3.6)

[161] A. Sánchez, E. Maciá, and F. Domínguez-Adame, *Suppression of localization in Kronig-Penney models with correlated disorder*, Phys. Rev. B **49** (1994), 147–157, Erratum, Phys. Rev. B **49**, 15428 (1994). (Cited in sections 1.1.2, 2.1, 2.5, 3.4.2, 3.6, 3.6.2, 4.3.2, and C)

[162] S. D. Sarma, S. He, and X. C. Xie, *Mobility edge in a model one-dimensional potential*, Phys. Rev. Lett. **61** (1988), 2144–2147. (Cited in section 1.1.2)

[163] D. Saxon and R. Hutner, *Some electronic properties of a one dimensional crystal model*, Philips Res. Rep. **4** (1949), 81–122. (Cited in section 3.4)

[164] H. Schmidt, *Disordered one dimensional crystals*, Phys. Rev. **105** (1957), 425–441. (Cited in section 2.6)

[165] H. Schomerus and M. Titov, *Short-distance wavefunction statistics in one-dimensional Anderson localization*, Eur. Phys. J. B **35** (2003), 421–427. (Cited in section 3.6.2)

[166] M. Schreiber, F. Epperlein, and T. Vojta, *Transport in disordered interacting systems: numerical results for one-dimensional spinless electrons*, Physica A **266** (1999), 443–449. (Cited in section 1.1.5)

[167] T. Sedrakyan, *Localization-delocalization transition in a presence of correlated disorder: the random dimer model*, Phys. Rev. B **69** (2004), 085109. (Cited in section 1.1.2)

[168] D. Shahar, M. Hilke, C. C. Li, D. C. Tsui, S. L. Sondhi, J. E. Cunningham, and M. Razeghi, *A new transport regime in the quantum Hall effect*, Solid State Commun. **107** (1998), 19–23. (Cited in section 1.1.2)

[169] B. Shapiro, *Probability distributions in the scaling theory of localization*, Phys. Rev. B **34** (1986), 4394–4397. (Cited in section 1.1.4)

[170] H. Shima, T. Nomura, and T. Nakayama, *Localization and delocalization transition in one-dimensional electron systems with long-range correlated disorder*, Phys. Rev. B **70** (2004), 075116. (Cited in section 1.1.2)

[171] J. Singleton, *Band theory and electronic properties of solids*, Oxford University Press, 2001. (Cited in section 3.2)

[172] S. L. Sondhi, S. M. Girvin, J. P. Carini, and D. Shahar, *Continuous quantum phase transitions*, Rev. Mod. Phys. **69** (1997), 315–333. (Cited in section 1.1.4)

[173] A. D. Stone and P. A. Lee, *Effect of inelastic processes on resonant tunneling in one dimension*, Phys. Rev. Lett. **54** (1985), 1196–1199. (Cited in section 1.1.5)

[174] A. D. Stone and A. Szafer, *What is measured when you measure a resistance?-The Landauer formula revisited*, IBM J. Res. Dev. **32** (1988), 384–413. (Cited in section 1.1.3)

[175] M. Tabor, *Chaos and integrability in nonlinear dynamics: an introduction*, John Wiley & Sons, 1989. (Cited in sections 2.1 and 2.4.1)

[176] L. Tessieri, *Delocalization phenomena in one-dimensional models with long-range correlated disorder: a perturbative approach*, J. Phys. A: Math. Gen. **35** (2002), 9585–9600. (Cited in section 1.1.2)

[177] L. Tessieri and F. M. Izrailev, *One-dimensional quantum models with correlated disorder versus classical oscillators with colored noise*, Phys. Rev. E **64** (2001), 066120. (Cited in section 1.1.2)

[178] L. Tessieri and F. M. Izrailev, *One-dimensional tight-binding models with correlated diagonal and off-diagonal disorder*, Physica E **9** (2001), 405–417. (Cited in section 1.1.2)

[179] D. J. Thouless, *A relation between the density of states and range of localization for one-dimensional random systems*, J. Phys. C **5** (1972), 77–81. (Cited in section 3.4.2)

[180] D. J. Thouless, *Electrons in disordered systems and the theory of localization*, Phys. Rep. **13** (1974), 93–142. (Cited in section 3.4.2)

[181] D. J. Thouless and S. Kirkpatrick, *Conductivity of the disordered linear chain*, J. Phys. C **14** (1981), 235–245. (Cited in sections 5.2 and 5.2.3)

[182] B. Y. Tong, *Localization of electronic states in one-dimensional disordered systems*, Phys. Rev. A **1** (1970), 52–58. (Cited in section 1.1.2)

[183] T. Schneider, M. P. Soerensen, A. Politi, and M. Zannetti, *Relationship between classical motion in random media and quantum localization*, Phys. Rev. Lett. **56** (1986), 2341–2343. (Cited in section 1.1.2)

[184] K. v. Klitzing, G. Dorda, and M. Pepper, *New method for high-accuracy determination of the fine-structure constant based on quantized Hall resistance*, Phys. Rev. Lett. **45** (1980), 494–497. (Cited in section 1.1.3)

[185] B. J. van Wees, H. van Houten, C. W. J. Beenakker, J. G. Williamson, L. P. Kouwenhoven, D. van der Marel, and C. T. Foxon, *Quantized conductance of point contacts in a two-dimensional electron gas*, Phys. Rev. Lett. **60** (1988), 848–850. (Cited in section 1.1.3)

[186] T. Vojta, F. Epperlein, and M. Schreiber, *Do interactions increase or reduce the conductance of disordered electrons? It depends!*, Phys. Rev. Lett. **81** (1998), 4212–4215. (Cited in section 1.1.5)

[187] J. W. G. Wildöer, L. C. Venema, et al., *Electronic structure of atomically resolved carbon nanotubes*, Nature **391** (1998), 59–62. (Cited in section 1)

[188] H. L. Wu, W. Goff, and P. Phillips, *Insulator-metal transitions in random lattices containing symmetrical defects*, Phys. Rev. B **45** (1992), 1623–1628. (Cited in sections 1.1.2 and 6)

[189] J. Yoon, C. C. Li, D. Shahar, D. C. Tsui, and M. Shayegan, *Parallel magnetic field induced transition in transport in the dilute two-dimensional hole system in GaAs*, Phys. Rev. Lett. **84** (2000), 4421–4424. (Cited in section 1.1.2)

[190] W. Zhang and S. E. Ulloa, *Extended states in disordered systems: role of off-diagonal correlations*, Phys. Rev. B **69** (2004), 153203. (Cited in section 1.1.2)

[191] M. Znojil, *Solvable simulation of a double-well problem in $\mathcal{PT}$-symmetric quantum mechanics*, J. Phys. A: Math. Gen. **36** (2003), 7639–7648. (Cited in section 5.1)